Dual Roles for NBR1 in Bone Remodelling and Autophagosomal Protein Degradation

Marchbank, Katie

Awarding institution:
King's College London

Title: Dual Roles for NBR1 in Bone Remodelling and Autophagosomal Protein Degradation

Author: Katie Marchbank

Dual Roles for NBR1 in Bone Remodelling and Autophagosomal Protein Degradation

Katie Elizabeth Marchbank

Thesis submitted to King's College London for the degree of Doctor of Philosophy

Department of Medical & Molecular Genetics
Division of Genetics & Molecular Medicine
King's College London
School of Medicine

2011

Abstract

NBR1 (Neighbour of BRCA1) is a ubiquitously expressed scaffold protein that mediates intracellular functions through protein-protein interactions. The C-terminal UBA domain of Nbr1 binds mono- and polyubiquitinated chains whilst the N-terminal PB1 domain interacts with the structurally similar protein p62. The aims of this thesis were to further characterise the biological functions of Nbr1 by identifying novel protein interactors. A yeast-2-hybrid screen revealed a direct interaction between Nbr1 and the autophagic effector protein LC3. This suggested a role for Nbr1 in the autophagic degradation of polyubiquitinated proteins. A further yeast-2-hybrid screen identified a direct interaction between Nbr1 and the microtubule associated protein MAP1B. It is hypothesised that via its interaction with MAP1B and LC3, Nbr1 targets ubiquitinated proteins to the microtubule network where they can be transported to sites of autophagosomal formation. Further putative interactors were identified for Nbr1 including the ubiquitin conjugating enzyme, UBE20 and the eukaryotic translation elongation factor eEF1A. These suggested a role for Nbr1 as a scaffold to facilitate protein ubiquitination and degradation by the proteasome as eEF1A is involved in the cotranslational degradation of polyubiquitinated proteins.

In bone, Nbr1 was previously identified as a key regulator of osteoblast differentiation and activity. The work described in this thesis strengthened these observations and highlighted that the interaction between Nbr1 and p62 is also important for the maintenance of bone. Mice with the $Nbr1^{D50R}$ point mutation which inhibits the interaction between Nbr1 and p62 displayed an early osteoporotic phenotype due to altered osteoblast function and osteoclast size and nucleation that was subsequently resolved with age. Additionally, Nbr1 was demonstrated to interact with osteocalcin, a protein secreted by osteoblasts. Finally, sequence analysis of idiopathic high bone mass cases determined that sequence variation in the coding regions of *NBR1* was unlikely to be the major contributor to the observed phenotype.

This thesis is dedicated to my Mum and Dad and especially to Rob for their love and constant support.

Acknowledgements

I would first like to thank my two supervisors Ellen Solomon and Caroline Whitehouse for giving me the opportunity to undertake this PhD. They have provided me with guidance, advice and support over the last four years for which I am very grateful.

My whole PhD experience both in and out of the lab would not have been the same without my very good friend Sarah. She provided me with my main source of knowledge in the first three months of my PhD and has continued to give me invaluable scientific support and advice throughout the last four years, for which I am forever grateful. Sarah has always been there as a shoulder to cry on or for those nights out of which I don't remember much! Her sound fashion and beauty advice will also never be forgotten. I would also like to thank the other members of the cancer genetics lab, past and present for their constant help and advice whenever needed, with particular mention to Melanie for always being there with chocolate, tissues and hugs whenever I have need them and to Adam for permanently being happy and so laid back, I wish I had those qualities too!

Next, I would like to express my thanks to all those who have helped me with my experiments along the way. Tim Skerry at the Mellanby Centre for bone research in Sheffield provided me with the opportunity to carry out the microCT bone analysis which has formed a major chapter of my thesis. Also to his colleagues, Gareth for providing me with a place to stay and engaging in stimulating discussion, Susana and Suruchi for teaching me all I know about microCT and to the rest of the lab for making me feel so welcome. I am very grateful to Agi for providing me with the equipment and knowledge to carry out the *in vitro* bone assays required for my thesis and to Isabel Orriss for her help with microCT analysis back in London. Also to Natalie Prescott who has always been happy to answer all my genetics based questions and has provided me with valuable and helpful feedback. Finally, I am extremely appreciative to Prof. Gordon-Weekes who provided me with antibodies and tips on MAP1B, Prof. Ikramuddin Aukhil who gave me with the yeast-2-hybrid

library and Dr Celia Gregson who provided me with genomic DNA for the patient sequencing.

Lastly, and most importantly, I would like to thank my family and partner Rob. I owe it to my parents, especially my Mum for always being on the end of the phone in times of need and never failing to believe that I would succeed. However, the most important person is Rob who has been my rock over the last four years. His constant love, support and down-to-earth advice has pulled me through.

Table of Contents

List of Figures

Chapter 1

Chapter 2

Chapter 3

Chapter 4

Chapter 5

Chapter 6

List of Tables

Chapter 2

Chapter 3

Chapter 4

Chapter 5

Chapter 6

Appendix

List of Abbreviations

3-AT	3-amino-1,2,4-triazole
Ade	Adenine
ALFY	FYVE domain containing protein
ALP	Alkaline phosphatase
AP1	Activator protein 1
ApoE	Apolipoprotein E
ATF4	Activating transcription factor 4
Atg	Autophagy-related gene
ATP	Adenosine triphosphate
Atp6v0d2	d2 isoform of vacuolar (H^+) ATPase (v-ATPase) V_0 domain
Baf	Bafilomycin A_1
BMD	Bone mineral density
BMI	Body mass index
BMP	Bone morphogenic protein
Bmpr1a	Type 1A receptor for BMPs
BMU	Basic Multicellular units
BRC	Bone remodelling compartment
CC	Coiled coil domain
CEU	Caucasian European
CFU	Colony forming unit
CIB	Calcium and integrin binding protein
ClC-7	Chloride ion channel 7
COPI	Coat protein complex I
Ct.BMD	Cortical bone mineral density
Ct.BV	Cortical bone volume
Ct.Th	Cortical thickness
CYLD	Cylondromatosis deubiquitinating enzyme
DC-STAMP	Dendritic cell-specific transmembrane protein
DMEM	Dulbecco's Modified Eagle's Medium
DMP-1	Dentin matrix protein 1
DMSO	Dimethyl sulfoxide

DUB	Deubiquitinating enzyme
DXA	Dual energy x-ray absorptiometry
ECL	Enhanced chemiluminescence
ECM	Extracellular matrix
EDTA	Ethylenediaminetetracetic acid
eEF1A	Eukaryotic translation elongation factor 1A
eEF2	Eukaryotic elongation factor 2
EGFR	Epidermal growth factor receptor
ePDB	Early onset Paget's disease of bone
ERAD	Endoplasmic reticulum-associated protein degradation
ERK	Extracellular signal-related kinases
ES cells	Embryonic stem cells
ESCRT	Endosomal sorting complex required for transport
FCS	Fetal calf serum
FEO	Familial expansile osteolysis
FEZ1	Fasciculation and elongation protein zeta-1
FGF	fibroblast growth factor
FGFR3	Fibroblast growth factor receptor 3
FIP200	Focal adhesion kinase interacting protein of 200 kDa
FOXO	Forkhead box class O
FRT	Flp recombinase target sequence
FYCO1	FYVE and coiled-coil (CC) domain–containing protein
GABARAP	γ-Aminobutyric-acid-type-A($GABA_A$)-receptor-associated protein
GATA 3	GATA binding protein 3
GATE-16	Golgi associated ATPase enhancer of 16kDa
GFP	Green fluorescent protein
GST	Glutathione-S-transferase
GWAS	Genome-wide association study
H&E stain	Haematoxylin and eosin stain
HA	Haemagglutinin
HBM	High bone mass
HDAC	Histone deacetylase
HIF-1	Hypoxia inducible factor-1

HIPK2	Homeodomain interacting protein kinase 2
His	Histidine
HMERF	Hereditary Myopathy with Early Respiratory Failure
IBMPFD	Inclusion body myopathy with Paget's disease and frontotemporal dementia
IBSP	Integrin-binding bone sialoprotein
IGF	Insulin-like growth factor
Ihh	Indian hedgehog
IL-1	Interleukin-1
IM	Isolation membrane
IPTG	Isopropyl β-D-thiogalactopyranoside
JNK	Jun N-terminal Kinase
JPD	Juvenile Paget's disease
kDa	Kilodalton
Keap1	Kelch-like ECH-associated protein 1
LAMP2	Lysosomal-associated membrane protein 2
LC3	Microtubule-associated protein 1 light chain 3
LD	Linkage disequilibrium
LIR	LC3 interaction region
LRP5	low density lipoprotein receptor-related protein 5
MAP1B	Microtubule associated protein 1B
MAP1B-HC	Microtubule associated protein 1B heavy chain
MAP1B-LC1	Microtubule associated protein 1B light chain 1
MAPK	Mitogen-activated protein kinase
MCP-1	Monocyte chemoattractant protein-1
M-CSF	Macrophage colony-stimulating factor
MEFs	Mouse embryonic fibroblasts
MicroCT	Micro computer tomography
MMP	Matrix metalloproteinase
mTOR	Mammalian target of rapamycin kinase
MURF	Muscle specific RING finger protein
NBR1	Neighbour of BRCA1 (human)
Nbr1	Neighbour of BRCA1 (mouse)

NFATc1	Nuclear factor of activated T cells 1
NF-κB	Nuclear factor-κB
NGF	Nerve growth factor
NPC2	Niemann-Pick C2
OPG	Osteopotegerin
OPPG	Osteoporosis-pseudoglioma syndrome
Osx	Osterix
PAS	Pagophore assembly site
PB1	Phox and Bem1p
PBS	Phosphate buffered saline
PCR	Polymerase chain reaction
PDB	Paget's disease of bone
PDGF-bb	Platelet-derived growth factor bb
PE	Phosphatidylethanolamine
PEST	Proline, glutamine, serine, threonine
PFA	Paraformaldehyde
PI3K	Phosphatidylinositol 3 kinase
PI3P	Phosphatidylinositol-3-phosphate
PIAS	Protein inhibitor of activated STAT
PTH	Parathyroid hormone
PTHrP	Parathyroid hormone-related protein
RANK	Receptor activator of nuclear factor-κB
RANKL	Receptor activator of nuclear factor-κB ligand
Rnf26	Ring finger protein 26
ROA	Regulation of autophagy
ROI	Region of interest
S1P	Sphingosine 1-phosphate
S6K	Ribosomal kinase
SD	Synthetic dropout (yeast media)
SD	Standard deviation (statistics)
SDF-1	Stromal cell-derived factor-1
SDS PAGE	Sodium dodecyl sulphate polyacrylamide gel electrophoresis
SEM	Standard error of the mean

SAP	Shrimp Alkaline Phosphatase
SNP	Single nucleotide polymorphism
SOST	Sclerostin
SPRED2	Sprouty related with Ena/VASP homology 1 domain 2
SQSTM1	Sequestosome 1
SRF	Serum response factor
SUMO	Small ubiquitin-like modifier
Tb.BV/TV	Trabecular bone volume/tissue volume
Tb.N	Trabecular number
Tb.Sp	Trabecular separation
Tb.Th	Trabecular thickness
TENS	Tris, EDTA, NaOH, SDS
TGFβ	Transforming growth factor β
Th2	T helper 2
TK	Thymidine kinase
TNF	Tumour necrosis factor
TNFR2	Tumour necrosis factor receptor 2
TRAF	TNF receptor-associated factor
TRAP	Tartrate-resistant acid phosphatase
Trp	Tryptophan
TXAS	Thromboxane synthase
UBA	Ubiquitin associated
UBC9	Ubiquitin-like protein SUMO-1 conjugating enzyme
ULK1	Unc-51-like kinase 1
UPS	Ubiquitin proteasome system
USP	Ubiquitin specific protease
VCP	Valosin-containing protein
WB	Western blot
WIPI1	WD repeat domain phosphoinositide interacting 1
Wnt	Wingless and Int proteins
WT	Wild type
YFP	yellow fluorescent protein

Chapter 1. Introduction

1.1. Bone

The vertebrate skeleton is largely comprised of two distinct tissue types; cartilage and bone (Karsenty, 1999). Bone has many functions including providing mechanical support to soft tissues, serving as levers for muscle action, supporting haematopoiesis and housing the brain and spinal cord (Harada and Rodan, 2003). It forms a highly ordered structure which enables it to carry out its functions.

1.1.1. Bone structure

Bone tissue is comprised of an outer layer of cortical (compact) bone which surrounds the inner trabecular (spongy) bone. Both bone types have the same matrix composition however cortical bone has a greater mass to volume ratio which provides maximum resistance to tension and bending whilst trabecular bone is a more loosely organised porous matrix, and has a greater metabolic function (Figure 1.1). The cortex constitutes 80% of mature bone and is lined on the outside by the periosteum whilst the inner marrow cavity is lined by the endosteum; both of which are thin layers of fibrous tissue. The embryonic skeleton and regions of rapid bone turnover in the adult skeleton consist of woven bone that is subsequently resorbed and replaced by slower forming lamellar bone. Woven bone consists of an irregular pattern of collagen fibres and hydroxyapatite crystals whilst lamellar bone is more uniform in structure composed of collagen fibres arranged in parallel sheets around blood vessels to form osteons or Haversian systems (the primary structural unit of cortical bone). (Bilezikian, 2002; Buckwalter, 1995; Ng et al., 1997). Micro Computer Tomography (MicroCT) is a widely used technique for the study of bone morphology and microarchitecture and has been instrumental in aiding the bone phenotypic analysis of mutant mouse models. It was first pioneered by Feldkamp et al. (Feldkamp et al., 1989) and uses X-ray attenuation data from multiple angles to reconstruct a 3D representation of the bone in question (Bouxsein et al., 2010).

The bone extracellular matrix (ECM) constitutes 90% of the volume of bone tissue, and consists of an organic and an inorganic component. The organic phase is primarily comprised of type I collagen fibres (90%) and noncollagenous proteins (10%) such as osteonectin, osteopontin, osteocalcin and glycoproteins. The inorganic phase consists of hydroxyapatite crystals and serves as an ion reservoir. Approximately 99% of bodily calcium and 85% of phosphorus are associated with bone mineral crystals. The ECM is rich in growth factors such as fibroblast growth factor-2 (FGF2) (Montero et al., 2000), cell adhesion molecules and proteolytic enzymes and provides a structural framework for bone cells to adhere to (Buckwalter, 1995; Camozzi et al., 2010).

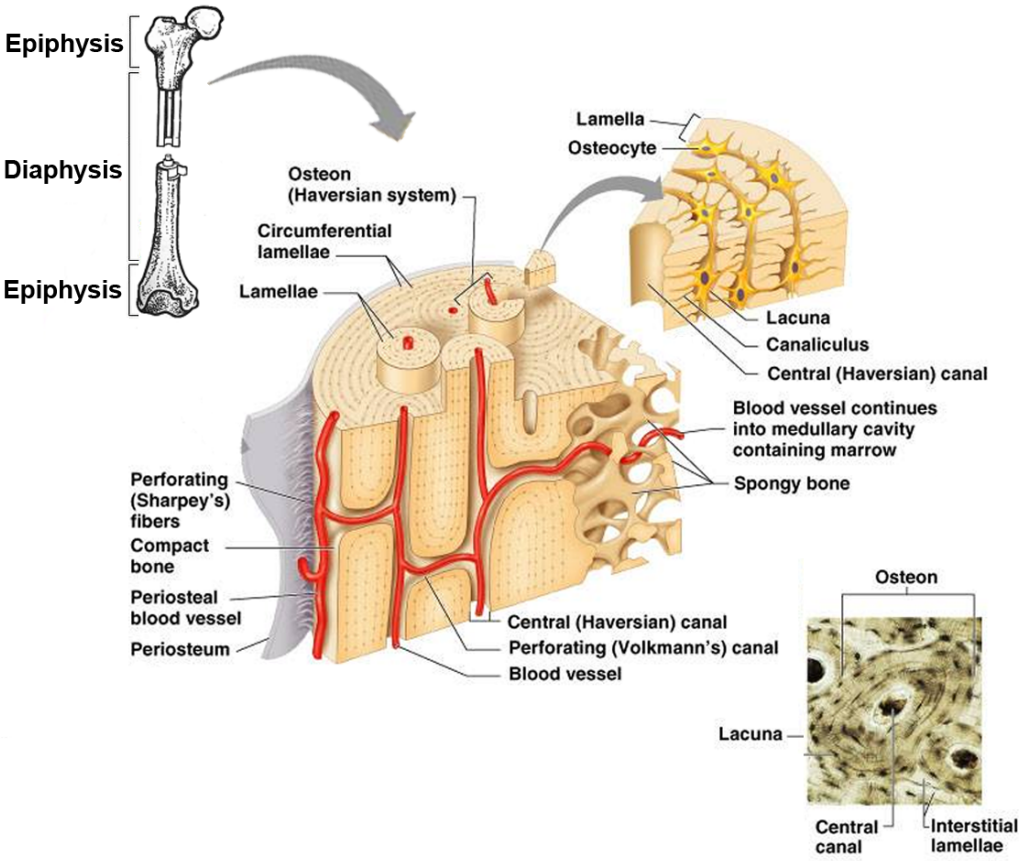

Figure 1.1. Long bone structure. The mature skeleton is comprised of two types of bone tissue, the cortical (compact) bone and the trabecular (spongy) bone. Both have the same matrix composition which consists of collagen fibres interlaced with hydroxyapaptite crystals. These are arranged into uniform parallel sheets termed lamellae and form around blood vessels (Haversian system or osteon). Cortical bone has a greater mass to volume ratio providing resistance to tension and bending whilst the trabecular bone has a more loosely organised porous matrix. The cortical bone is surrounded by a thin layer of fibrous tissue call the periosteum (modified from Fischer 2011).

24

1.1.2. Cell types present in bone

There are three main cell types that are found within bone; osteoblasts, osteoclasts and osteocytes. The osteoblast is derived from mesenchymal stem cells and its primary function is to synthesize and release type I collagen and noncollagenous bone matrix proteins including osteocalcin and osteonectin. Osteoblasts subsequently regulate the mineralisation of the organic matrix (Buckwalter, 1995; Sommerfeldt and Rubin, 2001). Following the synthesis and mineralisation of the bone matrix, osteoblasts can undergo cell death, decrease their activity and form bone lining cells that cover the bone surface or they differentiate into osteocytes. Osteocytes embed into the bone matrix and regulate bone formation.

Osteoclasts are the third main cell type found in bone. They originate from the hematopoietic stem cell population (Walker, 1975) and develop through the fusion of mononuclear myeloid precursors. Once fully differentiated, osteoclasts function to resorb the fully mineralised bone matrix (Edwards and Mundy, 2011).

The formation and maintenance of bone is a tightly coupled process mediated by the bone forming activity of osteoblasts and the bone resorbing activity of osteoclasts (discussed in section 1.3). In early human life, osteoblast activity predominates over osteoclast activity until peak bone density is reached between the ages of 25-35 years. After these initial years, the adult skeleton is maintained by removing and replacing tissue. Throughout this time, bone formation rate is equal to resorption. Later in life, resorption starts to accede formation resulting in a net loss of bone tissue and reduced bone mass and skeletal strength (Bilezikian, 2002).

1.1.3. Bone development

There are two distinct mechanisms that contribute to the formation of the skeleton; intramembranous and endochondral ossification. During intramembranous ossification (Figure 1.2), mesenchymal cells develop directly into osteoblasts giving rise to the flat bones of the skull, the clavicle and the pectoral girdle (Franz-Odendaal, 2011; Hartmann, 2009). The majority of bones however (including the appendicular skeleton, facial bones and vertebrae), are formed by endochondral ossification whereby cells at the centre of mesenchymal condensations differentiate into chondrocytes creating the template for future bone (Figure 1.3). The transcription factor Sox9, is expressed by chondroprogenitor cells and is essential for chondrogenesis (Hargus et al., 2008). Differentiated chondrocytes undergo unidirectional proliferation and form a columnar layer of dividing cells that express cartilaginous matrix genes such as *type II collagen, aggrecan and chonromodulin-1*. After proliferation, chondrocytes become prehypertrophic, exit the cell cycle and differentiate into post-mitotic hypertrophic chondrocytes. They synthesize type X collagen and mineralize their surrounding matrix before undergoing cell death. Following this, perichondrial cells surrounding the cartilage begin to differentiate into osteoblasts and form the bone collar, which will eventually become the cortical bone. Blood vessel invasion from the bone collar into zones of hypertrophic chondrocytes occurs, resulting in the infiltration of osteoblasts and osteoclasts into the cartilaginous extracellular matrix (ECM). The ECM is then degraded and replaced with primary spongiosa (the precursor of trabecular bone and bone marrow) (de Crombrugghe et al., 2001; Hojo et al., 2010; Karsenty and Wagner, 2002; Provot and Schipani, 2005). The replacement of chondrocytes by osteoblasts leads to the development of organised growth plates at each end of the expanding bone which are separated by an internal space containing the bone marrow. At the growth plate, new chondrocytes are generated and their proliferation enables longitudinal bone growth to occur during post-natal life (Karsenty, 1999; Provot and Schipani, 2005) (Figure 1.3).

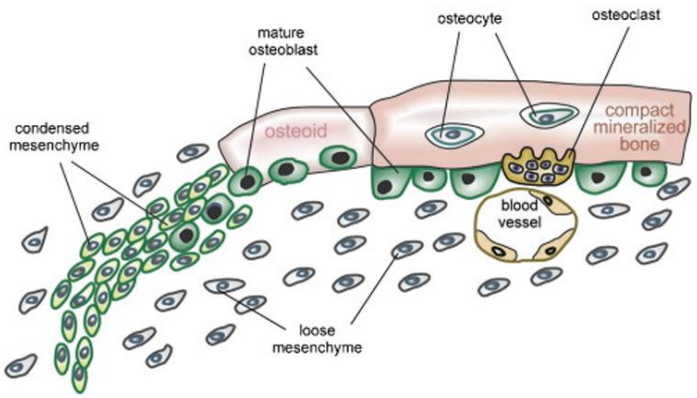

Figure 1.2. Intramembranous bone formation. Mesenchymal cells condense and osteoblast progenitors differentiate without the prior formation of cartilage. Osteoblasts are retained in the compact bone and differentiate into osteocytes. This occurs in the bones of the skull, clavicle and pectoral girdle (taken from Hartmann,2009).

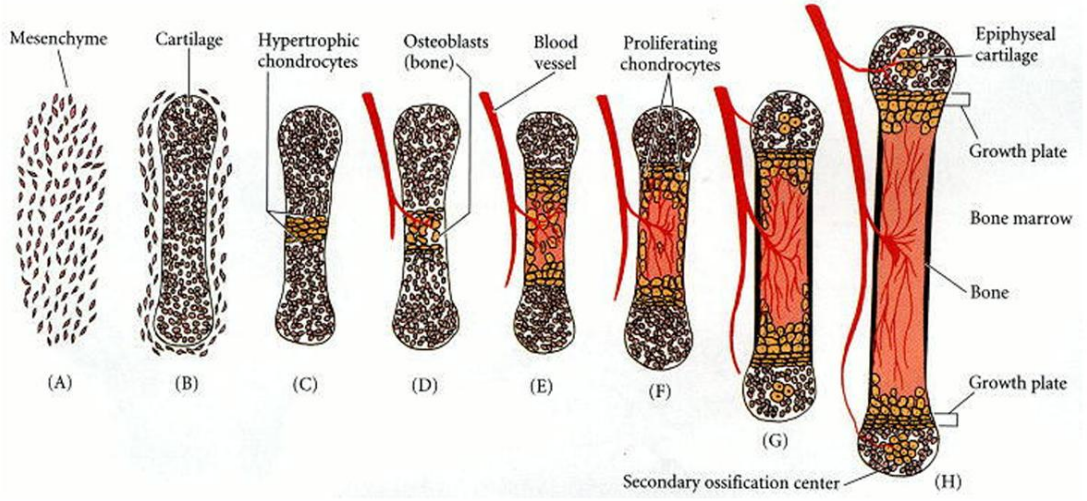

Figure 1.3. Endochondral bone formation
A, B. Mesenchymal stem cells condense and differentiate into chondrocytes.
C. Chondrocytes differentiate into large hypertrophic cells that synthesise and mineralise their extracellular matrix.
D, E. Blood vessels invade enabling osteoblasts to enter and deposit bone matrix where the cartilagenous matrix is being degraded.
F-H. The replacement of chondrocytes by osteoblasts becomes an organised growth plate at each end of the expanding bone. Secondary ossification centers also form as blood vessels enter near the tips of the bone.
(taken from Gilbert 2000).

1.2. Molecular regulation of bone cell differentiation

Skeletogenesis occurs during both embryonic development and postnatal life. The differentiation and activity of osteoblasts, osteoclasts and osteocytes is tightly controlled both spatially and temporally in order to maintain bone integrity.

1.2.1. Osteoblasts

Osteoblasts are cuboidal in shape and their cytoplasmic processes extend through the osteoid matrix and come into contact with osteocytes (Sommerfeldt and Rubin, 2001). The differentiation of mesenchymal stem cells into osteoblasts requires a specific set of transcription factors and growth factors and results in the fully functioning bone forming cell (Figure 1.4).

1.2.1.1. Transcription factors

The earliest and most specific marker of the osteoblast lineage is the transcription factor Runx2 (Cbfa1) whose expression is restricted to cells of the mesenchymal condensations and precedes osteoblast differentiation (Ducy et al., 1997). The absolute requirement of Runx2 for the differentiation of mesenchymal progenitors into osteoblasts was demonstrated with the generation of a Runx2 deficient mouse model (Komori et al., 1997). Affected mice died shortly after birth with a skeleton completely lacking in bone. Osterix (Osx), a zinc finger-containing transcription factor is also essential for osteogenesis. Mice deficient in osterix also died soon after birth due to lack of bone formation and the arrest of osteoblast differentiation downstream of Runx2 (Nakashima et al., 2002). Through its interaction with nuclear factor of activated T cells c1 (NFATc1), osterix activates the *Col1a1* (encoding type 1 collagen) promoter and controls osteoblastic bone formation. In NFATc1 deficient cells, nodule formation assays demonstrated that bone formation was severely impaired (Koga et al., 2005). The actions of both Runx2, osterix and NFATc1 result in cells of the early osteoblast lineage expressing the bone specific markers alkaline phosphatase (ALP) and type 1 collagen (Candeliere et al., 1999).

The transcription factor ATF4 is required for osteoblast terminal differentiation. Mice lacking ATF4 exhibit delayed skeletal development, a decrease in bone formation and a failure to reach normal bone mass. This has been attributed to a decrease in the synthesis of type I collagen by osteoblasts (Yang et al., 2004). ATF4 mRNA expression is not restricted to osteoblasts however there is a selective accumulation of the ATF4 protein in these cells resulting in the expression of osteoblast specific proteins such as osteocalcin (Yang and Karsenty, 2004).

The activator proteins 1 (AP1) are a group of transcription factors that have a variety of functions in different cell types, however a subset are specifically involved in bone formation. Mice overexpressing Fra-1 showed a progressive increase in bone mass (manifested by an increase in cortical thickness and trabecular number and diameter), first observed at four weeks of age. This was due to a cell-autonomous increase in the number of mature osteoblasts (Jochum et al., 2000). Mice overexpressing another osteoblast specific AP1 family protein ΔFosB have increased bone formation throughout the skeleton and a continuous post-developmental increase in bone mass (Sabatakos et al., 2000).

1.2.1.2. Indian hedgehog and Wnt Signalling

Along with transcription factors, a number of signalling pathways and extracellular molecules are important for osteoblast differentiation and maturation. Indian hedgehog (Ihh) is essential for osteoblast differentiation. When the transmembrane protein smoothened, which is essential for Ihh signal transduction was knocked out specifically from perichondrial cells, mice displayed impaired bone collar formation and lacked the development of primary spongiosa (Long et al., 2004)

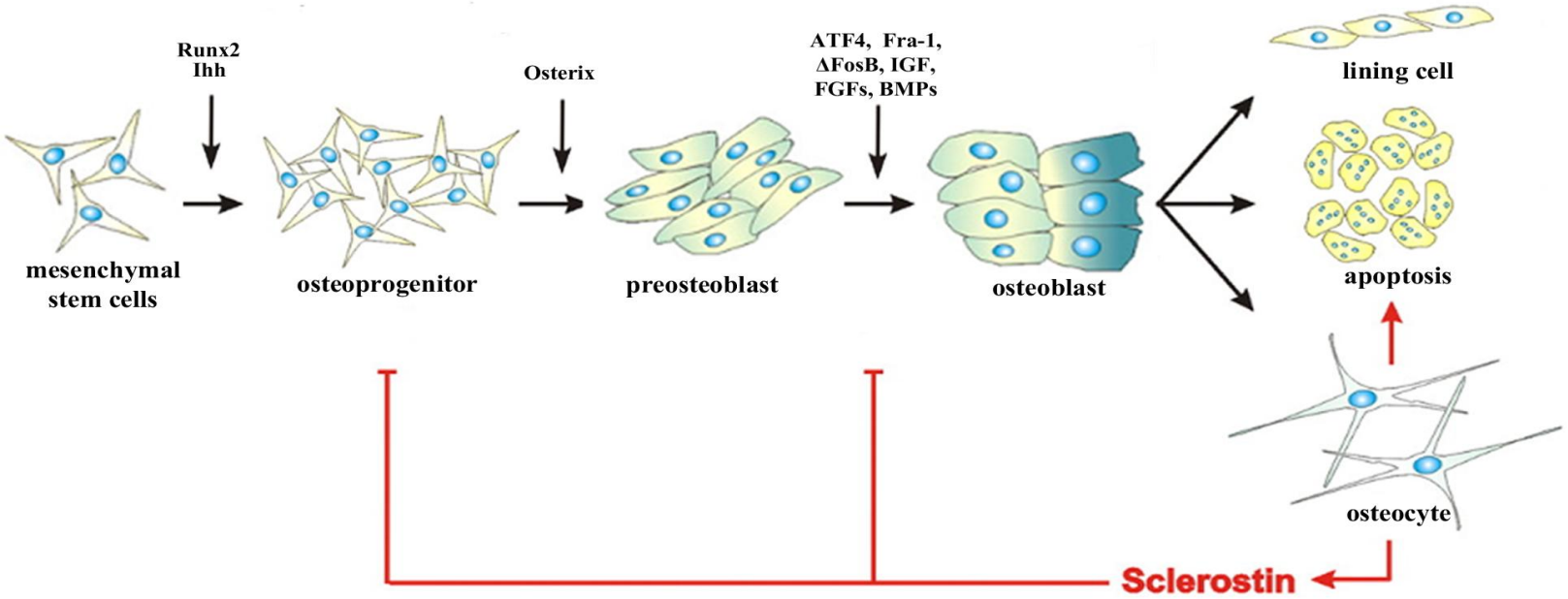

Figure 1.4. Osteoblast differentiation. Osteoblast differentiation requires the transcription factors Runx2, osterix and ATF4 and a number of growth factors including FGFs, BMPs and IGF. Mature osteoblasts secrete components of the bone extracellular matrix. Following bone formation, osteoblasts either undergo cell death, become inactive bone lining cells or embed into the bone matrix and differentiate into osteocytes. Osteocytes secrete sclerostin which inhibits osteoblast differentiation (modified from Dijke et al. 2008).

The Wnt signalling pathway is also important for osteoblast differentiation and a number of key proteins in this pathway have been extensively studied. Genetic disruption of β-catenin (a central player in the Wnt signalling pathway) in mice lead to a complete absence of intramembranous and endochondral skeleton. Osteoblast development was arrested after Runx2 expression but before the expression of osterix, suggesting a key role for Wnt signalling in early bone formation (Hu et al., 2005). LRP5 (low density lipoprotein receptor-related protein 5) is also part of the Wnt signalling pathway and targeted disruption in mice lead to a decrease in quantity of mineralised bone in the primary spongiosa and a lower bone mass throughout life. Affected mice also had a decrease in bone formation rate and a decrease in total osteoblast number (Kato et al., 2002). Activation of Wnt signalling in cell culture models can also induce osteoblast differentiation (Bain et al., 2003). Altered expression of Wnt ligands in mice can also result in a range of skeletal phenotypes (Glass Ii and Karsenty, 2006). For example, overexpression of Wnt10b in osteoblasts causes an increase in bone formation, bone mineral density and trabecular number (Bennett et al., 2007).

1.2.1.3. Growth factors

Growth factors present in the bone ECM and systemic circulation can also influence bone formation. A number of fibroblast growth factors (FGFs) are important for intramembranous and endochondral ossification and are differentially expressed in both bone and cartilage. Deletion of any one of these ligands or their receptors cause a variety of skeletal malformations (Ornitz and Marie, 2002). Binding of FGFs to their receptors leads to activation of a number of downstream signalling pathways including mitogen-activated protein kinase (MAPK) and phosphatidylinositol 3 kinase (PI3K) (Miraoui and Marie, 2010). FGF-2 is expressed in osteoblasts and is important for bone formation and the maintenance of bone mass. Genetic ablation of FGF-2 in mice results in reduced trabecular bone volume and number due to a decrease in bone formation rate, and osteoblast differentiation and proliferation (Montero et al., 2000). Furthermore, mice lacking the fibroblast growth factor receptor 3 (FGFR3) display an array of skeletal abnormalities including kyphosis, bowed femurs that were thicker and longer and an expansion of the hypertrophic chondrocytes in the growth plate (Deng et al., 1996).

Insulin-like growth factor-I and –II (IGF-I and -II) are the most abundant growth factors present in skeletal tissue and are important in the paracrine and autocrine regulation of bone. IGF-I utilises the PI3K pathway which induces the activation of downstream effectors including Akt, MAPK and ERK1/2 (Qiang et al., 2002; Sakata et al., 2004). IGF-I maintains appropriate levels of bone matrix by upregulating type 1 collagen transcription and downregulating the expression of collagenase 3. However, a decline in IGF-I expression is required for the terminal differentiation of osteoblasts (Canalis, 2009). Systemic IGF-I is important for regulating cortical bone as mice exhibiting a 75% decrease in serum IGF-1 levels have a decreased cortical bone volume and thickness, bone mineral density and periosteal circumference (Yakar et al., 2002). In contrast, overexpression of skeletal IGF-1 using the osteocalcin promoter caused an overall increase in trabecular bone volume and thickness but no difference in cortical bone volume (Zhao et al., 2000). This suggests that IGF-I exerts site specific actions on bone formation.

Bone morphogenetic proteins (BMPs) are members of the transforming growth factor β (TGFβ) super-family and were first identified for their ability to induce endochondral bone formation through a Smad dependent signalling pathway (Canalis et al., 2003). *In vitro* studies have shown that BMP-2 is able to convert myoblastic cell lines into the osteoblastic lineage and induce the expression of osteoblast specific markers such as ALP, osteocalcin and Runx2 (Katagiri et al., 1994). Postnatal osteoblast specific disruption of Bmpr1a (type 1A receptor for BMPs) in mice and overexpression of the BMP agonist noggin under the control of the osteocalcin promoter demonstrated essential roles for BMP signalling. Both mouse models displayed a decrease in bone mass with no change in the number of osteoblasts suggesting impaired osteoblast function (Devlin et al., 2003; Mishina et al., 2004). Disruption of Bmpr1a also highlighted the potential of BMP signalling molecules to regulate osteoblast function in different ways as aged mice showed an increase in bone mass due to reduced bone resorption (Mishina et al., 2004).

1.2.1.4. Crosstalk between signalling pathways in osteoblasts

The signalling pathways involved in osteoblast differentiation and function are interconnected and highly complex. Runx2 appears to link some of the signalling

pathways as BMP signalling increases Runx2 expression (described above) whilst β-catenin can bind to and activate the transcription of *Runx2* (Gaur et al., 2005). Using luciferase assays, it was demonstrated that FGF signalling can antagonise the Wnt signalling pathway (Ambrosetti et al., 2008) therefore influencing osteoblastogenesis. Furthermore, BMP-2 treatment can induce the expression of Wnt signalling family members in a dose-dependent manner in primary calvarial cultures (Chen et al., 2007). These are just a few examples of how signalling pathways may be interlinked (Lin and Hankenson, 2011) and serve to illustrate the complexity of osteoblastogenesis.

1.2.2. Osteocytes

Following the synthesis and mineralisation of the bone matrix, approximately 10-30% of osteoblasts differentiate into osteocytes which are the longest lived bone cell and form between 90 and 95% of all cells in adult bone (Franz-Odendaal et al., 2006). During the transition of osteoblasts into osteocytes, cells embed into the mineralised bone matrix, show a reduction in the expression of bone markers such as ALP and an upregulation of osteocyte markers including dentin matrix protein 1 (DMP-1), FGF 23 and sclerostin (Bonewald, 2011). Sclerostin acts to impair osteoblast activity by inhibiting the Wnt signalling pathway (Lin et al., 2009). Furthermore, DMP-1 is important for osteocyte differentiation as DMP-1 deficient mice display aberrant osteocyte maturation, and hypomineralised bone accompanied by an increase in FGF 23 expression. This also results in a reduction in circulating phosphate and an osteomalacia phenotype illustrating that osteocytes have an endocrine function (Feng et al., 2006).

Differentiating osteocytes undergo significant morphological changes. They become smaller in size, contain less cell organelles (e.g. ribosomes and endoplasmic reticulum), have an increased nucleus to cytoplasmic ratio and form dendritic processes. Osteocyte morphology is controlled by podoplanin (E11/gp38), the earliest osteocyte specific protein and knock-down of expression in an osteocyte cell line blocked the elongation of dendrites (Zhang et al., 2006). Morphological changes

are also accompanied by redistribution of cytoskeletal proteins such as filamin and actin binding proteins (Kamioka et al., 2004).

Osteocytes are able to respond to changes in mechanical loading. Upon mechanical stimulation, they modulate the expression of IGF-I, osteocalcin, and sclerostin which can influence the activity of osteoblasts and osteoclasts (Kawata and Mikuni-Takagaki, 1998; Mikuni-Takagaki et al., 1996; Robling et al., 2008). The importance of osteocytes to the maintenance of bone has been further illustrated by the generation of osteocyte deficient mice that display fragile bone, osteoblast dysfunction, trabecular bone loss and are resistant to mechanical unloading-induced bone loss (Tatsumi et al., 2007). There is also a high correlation between bone remodelling sites and osteocyte apoptosis (Hedgecock et al., 2007). Furthermore, proapoptotic molecules can be found in osteocytes that are close to microcracks, these can be transmitted to the bone surface to initiate osteoclast differentiation and bone repair (Verborgt et al., 2002). Collectively, these data suggest that osteocytes have important functions in regulating bone mass and maintaining skeletal integrity.

1.2.3. Osteoclasts

Osteoclasts develop through the fusion of mononuclear myeloid precursors and are located on trabeculae and endosteal cortical bone surfaces, usually in a resorption pit. Osteoclast differentiation is a multistep process that eventually leads to a fully functioning cell that acts to resorb bone matrix proteins (Edwards and Mundy, 2011) (Figure 1.5).

1.2.3.1 Transcription factors and signalling molecules

The molecule known to initially influence the differentiation of the osteoclast from its myeloid precursor is the transcription factor PU.1. Mice deficient in PU.1 died within 24-48 hours of birth, showed an osteopetrotic phenotype and completely lacked both osteoclasts and macrophages suggesting that PU.1 regulates the initial stages of myeloid differentiation (Tondravi et al., 1997). Transplantation of normal bone marrow into PU.1 deficient mice rescued this phenotype which confirmed the origins of the osteoclast (Tondravi et al., 1997). Micro-ophthalmia-associated

transcription factor (MITF) is also essential for osteoclast differentiation. Mutations in the *Mitf* locus result in bone resorption defects and an inactivation of MITF target genes such as *tartrate-resistant acid phosphatase* (*TRAP*) (Hodgkinson et al., 1993; Luchin et al., 2001). Furthermore, the macrophage colony-stimulating factor (M-CSF) is important for the maturation and commitment of osteoclast precursor cells. Mice lacking functional M-CSF display osteoclast-deficient osteopetrosis (Wiktor-Jedrzejczak et al., 1982; Yoshida et al., 1990). M-CSF binds directly to its receptor c-fms on the surface of early osteoclast progenitors and activates downstream signalling pathways including ERK 1/2 to promote osteoclast proliferation and differentiation (Faccio et al., 2003). Additionally, the oncoprotein, c-Fos, which is a member of the AP-1 transcription factor complex is important for osteoclast-macrophage lineage determination. Mice lacking c-Fos develop osteopetrosis, display a block in the differentiation of osteoclasts and an increase in the bone marrow macrophage numbers (Grigoriadis et al., 1994) (Figure 1.5).

The requirement of marrow stromal cells for the differentiation of osteoclasts *in vitro* led to the discovery of the key osteoclastogenic cytokine, receptor activator of nuclear factor-κB ligand (RANKL) (Yasuda et al., 1998). RANKL is expressed on the surface of osteoblasts and signals through the transmembrane signalling receptor RANK (a member of the TNF receptor family), present on the osteoclast surface (Nakagawa et al., 1998). Downstream of the RANK receptor, TNF receptor-associated factor (TRAF) proteins initiate a signalling cascade that results in the activation of nuclear factor-κB (NF-κB) and the expression of osteoclastogenic genes (Darnay et al., 1998; Jimi et al., 1999a; Lamothe et al., 2008). Mice lacking subunits of the NF-κB complex display an osteopetrotic phenotype due to a reduction in osteoclast numbers (Iotsova et al., 1997). Additionally, the NFATc1 transcription factor could be seen as a master regulator of osteoclastogenesis as without it, embryonic stem cells fail to differentiate into osteoclasts on stimulation with RANKL (Takayanagi et al., 2002). RANKL is negatively regulated by the decoy receptor osteopotegerin (OPG) that is produced by osteoblasts. There is a careful balance between RANKL and OPG levels to ensure the correct differentiation of osteoblasts and osteoclasts and to control the rate of bone resorption (Gori et al., 2000). The inhibitory action of OPG was confirmed in mice lacking the protein as

they displayed an age dependent decrease in bone mass, lack of trabecular bone and decreased bone strength due to enhanced osteoclastogenesis (Mizuno et al., 1998).

A number of inflammatory cytokines have also been identified as stimulators of osteoclast differentiation. In the presence of M-CSF, TNFα induces the formation of osteoclasts (Azuma et al., 2000). This is important for the osteoclast formation and activation in inflammatory arthritis which is characterised by the eroding of periarticular bone by osteoclasts (Kitaura et al., 2005). Interleukin-1 (IL-1) also stimulates the multinucleation and function of osteoclasts (Jimi et al., 1999b). Upon binding to their receptors, these molecules can initiate a cascade of signalling events leading to the activation of the NF-κB and Jnk pathways (Katagiri and Takahashi, 2002).

1.2.3.2 Osteoclast fusion

Osteoclastogenesis requires the fusion of mononuclear preosteoclasts to form large multinucleated mature osteoclasts. A number of molecules have been implicated in this process. Osteoclast cell fusion was completely abrogated in mice deficient in the dendritic cell-specific transmembrane protein (DC-STAMP) however, the expression of osteoclast markers such as tartrate-resistant acid phosphatase (TRAP) were unaltered suggesting that DC-STAMP is not important for osteoclastogenesis but is important for cellular fusion (Yagi et al., 2005). The d2 isoform of vacuolar (H^+) ATPase (v-ATPase) V_0 domain (Atp6v0d2) deficient mice also display a reduction in osteoclast fusion and an increase in bone mass due to defective osteoclast resorption activity (Lee et al., 2006). NFATc1 induces the expression of both DC-STAMP and Atp6v0d2 demonstrating that it is also important in the regulation of osteoclast fusion (Kim et al., 2008a).

1.2.3.3. Formation of the osteoclast ruffled border

Once differentiated, the mature osteoclast must create an isolated microenvironment to carry out its function of resorbing the bone matrix. Osteoclasts undergo significant cytoskeletal rearrangement to form a distinct actin complex termed the podosome and together with adhesion-associated proteins such as integrin αVβ3 this mediates

osteoclast attachment to the bone matrix creating the 'sealing zone' (Novack and Faccio, 2011; Pfaff and Jurdic, 2001). The highly specialised ruffled border is then formed by fusion of secretory vesicles with the plasma membrane within the sealing zone and the delivery of H^+/ATPase and the chloride channel ClC-7 to the cell surface. This enables the acidification of the sealed extracellular space between the osteoclast and the bone (Blair et al., 1989; Kornak et al., 2001). The resulting acidity and the secretion of proteases and enzymes such as cathepsin K, matrix metalloproteinases (MMPs) and TRAP results in the degradation of the bone matrix. The digested components are subsequently transcytosed and secreted at the side of the cell furthest away from the bone matrix (Salo et al., 1997).

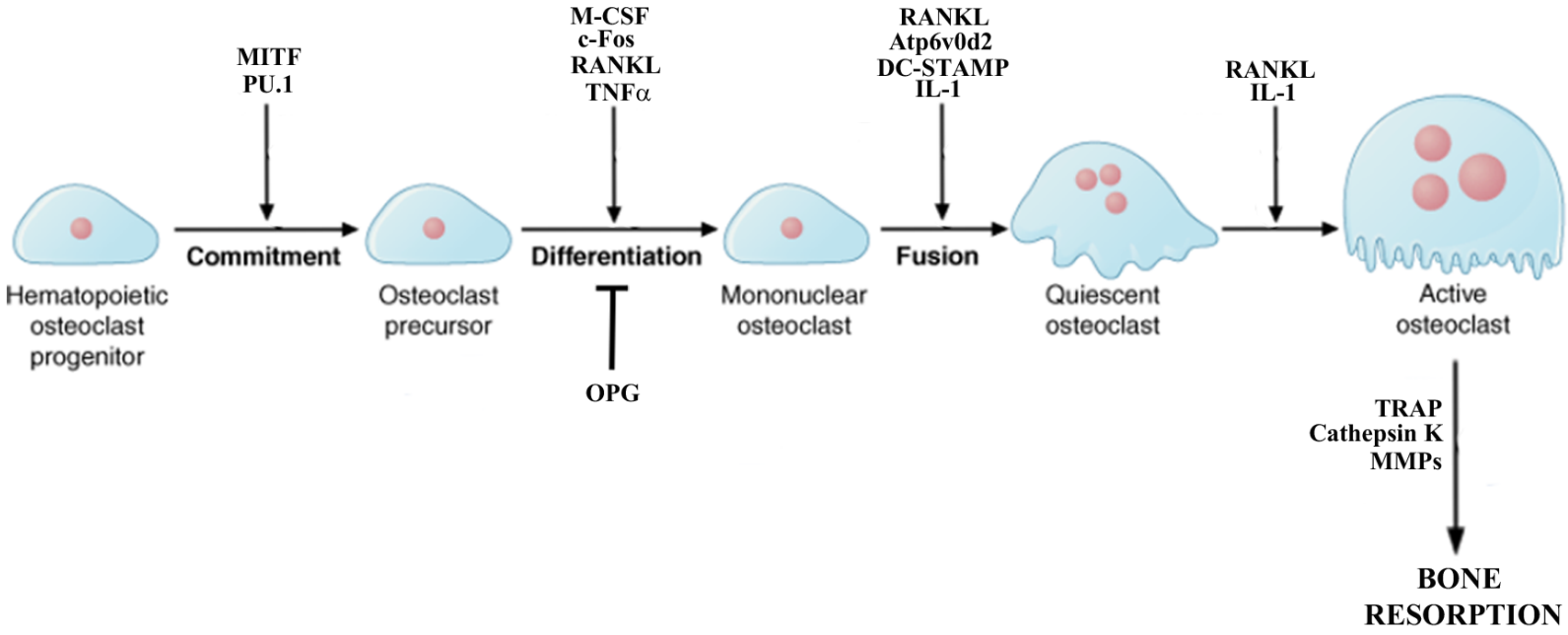

Figure 1.5. Osteoclast differentiation. Early osteoclast differentiation requires the transcription factor PU.1 and the macrophage-colony stimulating factor M-CSF. The transcription factor c-Fos is also required for osteoclasts lineage determination. RANKL (secreted by osteoblasts) and other factors such as IL-1 and TNFα stimulate preosteoclasts to become mature osteoclasts. Atp6v0d2 and DC-STAMP are required for fusion of mononuclear osteoclasts. Mature osteoclasts secrete enzymes and proteases that resorb bone matrix. OPG competes with RANKL and acts as a decoy molecule to inhibit osteoclastogenesis (modified from Suda et al. 1999)

1.3. Bone remodelling

To maintain stability and integrity, bone undergoes constant renewal. It is estimated that as much as 25% of trabecular and 3% of cortical bone is resorbed and replaced each year (Ng et al., 1997). Bone remodelling occurs in Basic Multicellular Units (BMU) (Frost, 1969) where bone lining cells prepare the endosteal membrane by exposing the mineralised matrix. They then form a canopy over the bone to be remodelled creating a temporary bone remodelling compartment (BRC) (Hauge et al., 2001) (figure 1.6).

The remodelling cycle consists of three main phases; resorption, reversal or transition and formation. Resorption is initiated with the recruitment of osteoclast precursors to the remodelling site where they differentiate and attach to the bone matrix. A reversal or transition phase subsequently takes place when mononuclear cells are recruited to the site of resorption. These cells prepare the freshly resorbed bone surface for subsequent bone formation by osteoblasts. The formation phase proceeds and osteoblasts deposit bone matrix (osteoid) to replace what has been resorbed by osteoclasts. The resulting matrix is then mineralised and the surface is covered with bone lining cells which marks the termination phase. A resting period then follows before a new cycle is initiated (Feng and McDonald, 2011; Hadjidakis and Androulakis, 2006). This cycle of removal and formation requires the intricate coordination of signals and communication between cells of the osteoblast and osteoclast lineages.

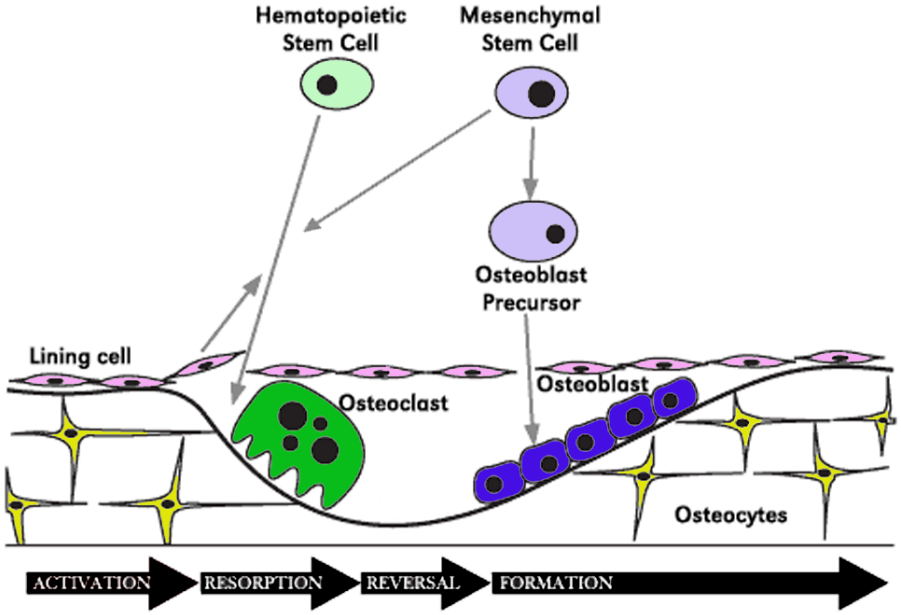

Figure 1.6. Phases of Bone Remodelling. Bone remodelling is activated by a variety of stimuli including mechanical strain, microcracks, blood calcium levels, inflammation and hormone levels. Bone lining cells create the bone remodelling compartment (BRC) which is followed by the recruitment of osteoclast precursors to the sites of remodelling where they differentiate and resorb the bone matrix. Osteoblast precursors are also recruited, differentiate and establish links with the osteoclasts. Osteoclasts then die through apoptosis and osteoblasts enter to start the process of bone formation. Once completed, bone lining cells cover the newly formed bone and the cycle is complete (modified from Carmona, 2004).

1.3.1 Initiation and resorption phases

Bone remodelling is initiated by a number of stimuli including hormones, inflammation, mechanical loading or inactivity and low blood calcium. Osteocytes are thought to be the main sensors of microcracks and mechanical loading. They express RANKL on their dendritic processes which results in osteoclast formation and resorption activity (Zhao et al., 2002). Hormones are important for the systemic control of bone remodelling. Parathyroid hormone (PTH) is secreted in response to changes in blood calcium and when administered continuously to rats, it increases RANKL expression and decreases OPG expression in osteoblasts and results in an increase in osteoclast number and resorption and a decrease in bone formation related genes (Ma et al., 2001). In contrast, when administered intermittently, PTH can increase bone formation, mineral density and strength (Ejersted et al., 1995). Collectively, this suggests that PTH can exert different effects on bone remodelling. Oestrogen is also critical for maintaining bone mass as it can promote osteoclast apoptosis. Ablation of the osteoclastic oestrogen receptor in female mice resulted in trabecular bone loss and an increase in osteoclast number (Nakamura et al., 2007).

Chemokines or chemotactic cytokines secreted by stromal cells or bone lining cells can recruit osteoclast precursors to areas of bone remodelling. Monocyte chemoattractant protein-1 (MCP-1) is a member of the CC chemokine subfamily expressed by osteoblasts in the presence of PTH and is thought to recruit osteoclast precursors to sites of bone remodelling and promote their fusion (Li et al., 2007). Stromal cell-derived factor (SDF-1) is another chemokine produced by marrow stromal cells that binds to osteoclast precursors and induces the osteoclast expression of matrix metalloproteinase-9 (MMP-9), contributing to their chemotactic migration to sites of remodelling (Yu et al., 2003).

1.3.2. Transition phase

The transition phase of bone remodelling succeeds resorption of the bone matrix and requires carefully regulated cross-talk between osteoblasts and osteoclasts. Bone lining cells are thought to clean the resorbed pit and prepare it for bone formation (Everts et al., 2002). The recruitment of osteoblasts to the site of bone formation is

regulated in part by factors such as IGF-I and –II, FGF, and BMPs that are all released from the bone matrix during resorption (Sims and Gooi, 2008). Factors secreted by osteoclasts have been demonstrated to activate the bone formation phase. For example, sphingosine 1-phosphate (S1P) enhances the migration and survival of osteoblasts (Ryu et al., 2006) whilst the platelet-derived growth factor bb (PDGF-bb) is secreted by osteoclasts and acts as a chemotactic factor to which osteoblasts respond (Sanchez-Fernandez et al., 2008). Membrane bound molecules also play a critical role in the communication between osteoblasts and osteoclasts during the transition phase. The ephrinB2 transmembrane ligand expressed on osteoclasts can interact with the tyrosine kinase receptor EphB4 expressed on osteoblasts. This enhances osteoblast differentiation by reducing RhoA activity and suppresses osteoclast function by reducing c-Fos and NFATc1 activities (Zhao et al., 2006). Extracellular calcium released as a result of bone resorption also functions in the transition phase as it acts as a negative feedback loop and induces osteoclast apoptosis and the termination of resorption by osteoclasts (Lorget et al., 2000).

1.3.3 Formation and termination phases

The end result of the many factors regulating bone remodelling discussed above is the formation of new bone matrix by osteoblasts. Bone matrix deposition is then negatively regulated by the secretion of sclerostin by osteocytes. Sclerostin is transported to the bone surface where it inhibits the late stages of bone formation by osteoblasts (van Bezooijen et al., 2004).

Bone resorption within a BRC is estimated to take 2-3 weeks and is much faster than bone formation as osteoblasts take approximately three months to replace the equivalent amount of bone (Harada and Rodan, 2003). In spongy bone, remodelling occurs on the surface of the trabeculae. In cortical bone however, remodelling occurs in tunnels where osteoclasts form ‘cutting zones’, removing bone whilst osteoblasts follow and fill in the tunnels in the ‘closing cone’. The mechanisms controlling bone remodelling in trabecular and cortical bone are largely the same (Eriksen, 2010).

1.4. Bone disease

Maintaining the balance between bone formation and resorption is critical for the correct functioning of bone tissue. A deviation from this balance can result in a broad spectrum of skeletal pathologies (Janssens and Van Hul, 2002). These can be caused by primary defects in osteoblasts and osteoclasts or can be a consequence of immunological or endocrinological abnormalities (Lazner et al., 1999). Mouse models have been instrumental in identifying genes and molecular mechanisms involved in skeletal development and remodelling (as described above). However, the identification of genetic mutations in individuals with skeletal disorders is also an important step to identifying causes of disease and therapeutic targets. In addition, genome-wide association studies (GWAS) are crucial for identifying genetic loci that may be contributing to disease. Although there are many idiopathic skeletal disorders, a large number of genes have been identified as contributing to bone disease and a selection of these will be discussed below.

1.4.1. Low bone mass diseases

When bone resorption exceeds bone formation, this can result in either a generalised or localised loss of bone mass. Osteogenesis imperfecta is characterised by low bone mass and although they do not account for all cases, various mutations in one of the two chains that encode type I collagen (*COL1A1* and *COL1A2*) have been identified. This leads to abnormalities in the structure of the bone matrix and reduced cortical and trabecular thickness (Rauch and Glorieux, 2004). Mutations in the *LRP5* gene have been identified in individuals with osteoporosis-pseudoglioma syndrome (OPPG) (Gong et al., 2001). LRP5 is part of the Wnt signalling pathway and reduced Wnt signalling in osteoblasts can result in decreased bone formation (Kato et al., 2002). Many genes including *OPG* (Ohmori et al., 2002), and *tumour necrosis factor receptor2* (*TNFR2*) (Spotila et al., 2000) have also been identified by association studies to be involved in low bone mass phenotypes.

1.4.2. High bone mass diseases

High bone mass (HBM) can be as deleterious to health as low bone mass and results in a reduction of the bone marrow cavity (Günther and Schinke, 2000). Van Buchem's disease, characterised by generalised bone overgrowth, has been attributed to a deletion downstream of the *SOST* gene (encoding sclerostin) that is likely to cause the suppression of *SOST* gene expression and therefore increase osteoblast activity (Balemans et al., 2002). Pycnodysostosis is the result of a mutation in the *CTSK* gene that encodes cathepsin K. This leads to the ablation of cathepsin K collagenase activity and therefore an increase in bone mass (Gelb et al., 1996). Mutations in the *TBXAS1* gene that encodes thromboxane synthase (TXAS) are thought to be responsible for Ghosal syndrome, a disorder of increased bone density. TXAS normally acts to regulate RANKL and OPG gene expression by osteoblasts and genetic inactivation decreased RANKL expression, and increased OPG expression and therefore an overall decrease in osteoclastogenesis was observed (Genevieve et al., 2008). Furthermore, activating mutations in the *LRP5* gene have been identified in individuals with high bone mass (Boyden et al., 2002). Association studies have identified the *Osterix* locus (Timpson et al., 2009) and the *IBSP* (integrin-binding bone sialoprotein) gene to be associated with bone mineral density in populations where extremes of high and low bone mineral densities were compared (Duncan et al., 2011). In addition to genetic factors, HBM can also be a secondary effect of other diseases such as myelofibrosis (Diamond et al., 2002) or hepatitis C infection (Manganelli et al., 2005).

1.4.3. Paget's disease of bone (PDB) and p62

Paget's disease of bone (PDB) is the second most common bone disorder in Caucasian populations and affects approximately 3% of individuals over 50 years of age (Goode and Layfield, 2010; Helfrich and Hocking, 2008). PDB can affect just one (monostotic) or multiple (polyostotic) bones and symptoms can range from asymptomatic to pain, bone deformity, fractures and neurological complications such as deafness and spinal cord compression (Falchetti et al., 2010). PDB is characterised by focal increases in osteoclastic bone resorption and increased formation of disorganised bone that is weak and prone to fracture. Affected osteoclasts are

enlarged, have an increased number of nuclei and also contain intranuclear inclusion bodies. Osteoclast precursors from Pagetic lesions display increased expression and responsiveness to RANKL (Menaa et al., 2000). The familial clustering and ethnic differences observed in the prevalence of the disease suggests a genetic predisposition however, environmental factors could also be involved as clinical severity has altered in areas such as the UK and New Zealand over the past few decades (Ralston, 2008). In addition to classical PDB, other, rarer forms have been described that include early onset Paget's disease (ePDB), juvenile Paget's disease (JPD), familial expansile osteolysis (FEO), expansile skeletal hyperphosphatasia and inclusion body myopathy with Paget's disease and frontotemporal dementia (IBMPFD) (Helfrich and Hocking, 2008; Ralston, 2008).

Mutations in the ubiquitously expressed scaffold protein p62/SQSTM1 are thought to be the primary cause of approximately 40% of all classical Paget's disease cases (Helfrich and Hocking, 2008). Through positional cloning studies, mutations in this gene were identified as having likely causal roles in the disease (Hocking et al., 2002; Laurin et al., 2002). Subsequently, over 20 mutations in p62 have been identified in individuals with PDB, most of these clustering in the ubiquitin-associated (UBA) domain (Goode and Layfield, 2010). The deletion of the UBA domain of p62 in osteoclast precursors enhances osteoclastogenesis (Yip et al., 2006). UBA domains are known to bind mono- and polyubiquitinated chains and facilitate protein degradation. Mutations observed in PDB individuals that cluster in the UBA domain of p62 are known to alter p62 ubiquitin binding ability (Cavey et al., 2006; Cavey et al., 2005; Garner et al., 2011). Several studies that have analysed transgenic mouse models harboring the common PDB mutation $p62^{P394L}$ have observed differing results. In one study, osteoclast precursors from $p62^{P394L}$ mutant mice displayed hyperresponsiveness to RANKL but bones from these mice were histologically normal (Hiruma et al., 2008). A separate study has shown that the $p62^{P394L}$ mutation does indeed cause a phenotype remarkably similar to PDB as mice displayed an age dependent increase in focal bone lesions with increased bone formation and resorption and the accumulation of woven bone (Daroszewska et al., 2011).

Mutations have also been identified in p62 that reside outside of the UBA domain. Some exert modest effects on ubiquitin binding (Najat et al., 2009) whilst others have no effect (Rea et al., 2009). One of these mutations is located in the LC3-binding region (discussed later) of p62 however, its effects on protein function are still unclear (Falchetti et al., 2009). Studies within families have shown reduced PDB clinical severity in offspring inheriting a p62 mutation (Bolland et al., 2007) which suggests that other factors such as common polymorphisms in other genes or environmental factors are likely to be involved. Additionally, it has been suggested that viral infection plays a role in the pathogenesis of PDB (Kurihara et al., 2011) however data is conflicting as some studies have found no evidence of viral nucleic acid sequences in Pagetic bone samples (Helfrich et al., 2000). While p62 is a ubiquitously expressed protein the mutations observed in PDB patients only affect the osteoclast. The mechanisms responsible for this apparent cell specificity are still unclear.

Whilst p62 mutations are a major cause of classical PDB, they only account for 40% of cases (Helfrich and Hocking, 2008), therefore other factors are likely to be involved. Both linkage and association studies have identified a number of susceptibility loci (Albagha, 2011; Albagha et al., 2010; Chung et al., 2010; Hocking et al., 2001). Additionally, mutations in other genes have been identified in individuals with the more severe forms of PDB. For example, complete deletion of the OPG gene was identified in patients with JPD (Whyte et al., 2002) whilst mutations affecting the signal peptide region of RANK have been found in patients with ePDB, FEO and Expansile skeletal hyperphosphatasia (ESH) (Hughes et al., 2000; Nakatsuka et al., 2003; Whyte and Hughes, 2002).

p62 is known to play an important role in the regulation and maintenance of bone tissue. Mice deficient in p62 did not initially display any skeletal phenotype suggesting that basal osteoclastogenesis is not affected by loss of p62 (Duran et al., 2004). However, on stimulation with parathyroid hormone-related protein (PTHrP), mice showed impaired osteoclastogenesis and inhibition of NF-κB activation (Duran et al., 2004). Later, it was revealed that p62 deficient mice have an age dependent increase in bone density and mature-onset obesity due to an increase in ERK activity

and adipocyte differentiation (Rodriguez et al., 2006). These mouse studies confirm the important role for p62 in NF-κB activation, osteoclastogenesis and the maintenance of bone. There are also multiple binding sites for AP-1 and NF-κB transcription factors in the promoter region of p62 suggesting p62 transcription may be regulated by these factors (Vadlamudi, 1998).

p62 was initially identified as a phosphotyrosine-independent ligand of the Src homology 2 (SH2) domain of $p56^{lck}$ (Joung et al., 1996). A number of biochemical studies have identified the mechanisms by which p62 modulates NF-κB signalling. Upon stimulation with IL-1 or nerve growth factor (NGF), p62 acts as a scaffold protein, binding to TRAF6 and ultimately resulting in the activation of NF-κB (Sanz et al., 2000; Wooten et al., 2001). Additionally, in response to TNFα, activation of NFκB can be achieved by the formation of a signalling complex that includes p62, RIP and aPKC. (Sanz et al., 1999). RANK is a member of the TNF receptor family and through its interaction with TRAF6 is important for NF-κB signalling (Darnay et al., 1998). Deletion of the UBA domain or TRAF6 binding domain of p62 abolishes TRAF6 polyubiquitination and NGF induced NF-κB signalling (Wooten et al., 2005). Furthermore, the deubiquitinating enzyme cylondromatosis (CYLD) binds to the UBA domain of p62 (but not the UBA mutant $p62^{P392L}$) in a ubiquitin-independent manner and negatively regulates NF-κB signalling (Jin et al., 2008; Sundaram, 2011). Collectively, these data suggest that p62 modulates NF-κB signalling through several of its interaction domains.

1.5. Autophagy

Autophagy (meaning ‘auto’ oneself, ‘phagy’ to eat) refers to the process that eukaryotic cells use to deliver long-lived proteins and organelles to the lysosome for degradation. There are three main types of autophagy; macroautophagy, microautophagy and chaperone-mediated autophagy, that differ in their physiological functions and the mode of cargo delivery to the lysosome (Levine and Kroemer, 2008; Yoshimori, 2004). Macroautophagy is the main process for bulk degradation of cytosolic proteins and organelles and will be referred to as autophagy from here on.

Autophagy commences with the formation of the preautophagosome structure or the phagophore assembly site (PAS), referred to as the isolation membrane (IM) or phagophore in mammals. This membrane subsequently expands and sequesters cytosolic components of the cell and eventually closes to form a double membrane bound vesicle termed the autophagosome. The autophagosome then fuses with the lysosome to become an amphisome or degradative autophagosome. This structure matures into an autolysosome and its contents are degraded (Tooze et al., 2010) (Figure 1.7).

The PAS has already been identified in the yeast *S. cerevisiae*, as the perivacuolar compartment where proteins required for autophagy are localised (Suzuki et al., 2001), however, the origin of autophagosomal formation in mammals is still under debate. Live cell imaging has been used to show that the autophagosome could form from the endoplasmic reticulum (Axe et al., 2008) or randomly in peripheral regions of the cell, a long way from the nucleus (Jahreiss et al., 2008). Recently, the plasma membrane has also been shown to contribute to autophagosomal formation (Ravikumar et al., 2010). Together, these data suggests that the membrane origins of the autophagosome may arise from multiple sources.

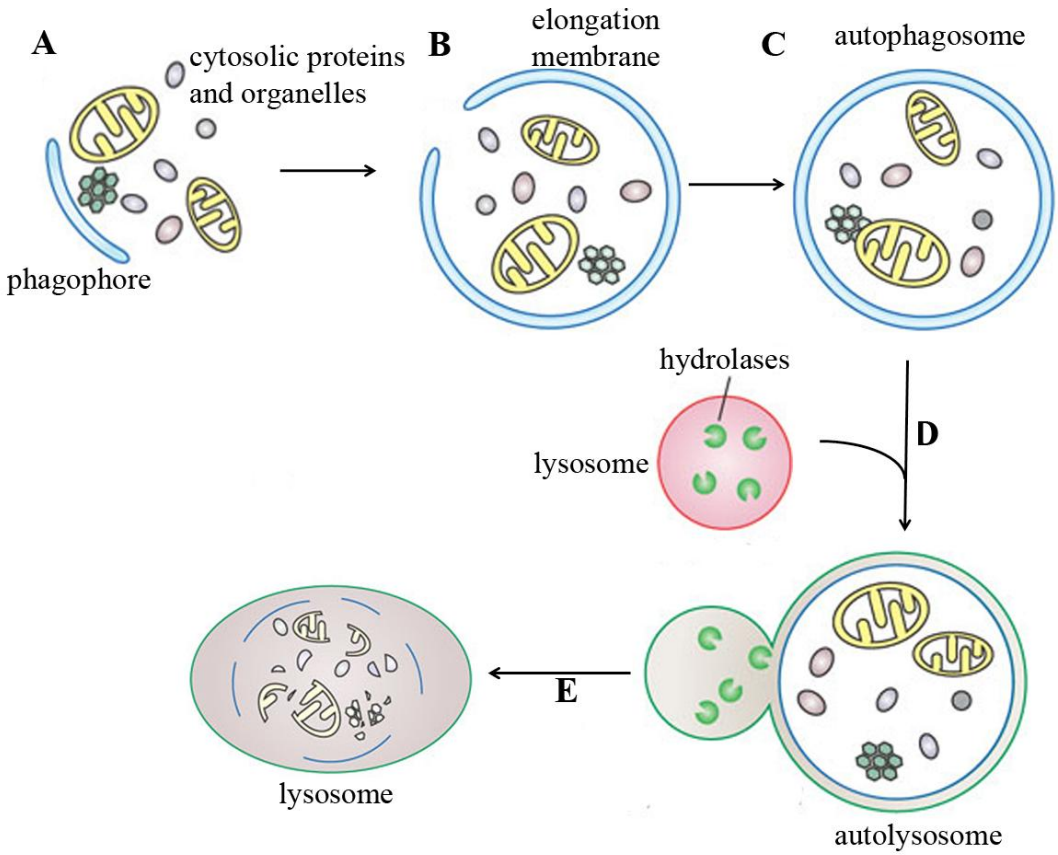

Figure 1.7. Autophagosome formation.
A. The isoloation membrane (IM)/phagophore forms within the cytosol.
B. The membrane expands and encloses cytosolic proteins and organelles.
C. The membrane closes forming a double membrane bound vesicle termed the autophagosome.
D. The autophagosome matures and fuses with the lysosome to form an autolysosome.
E. The contents of the autolysosome are degraded by lysosomal proteases.
(modified from Xie et al. 2007).

1.5.1. The molecular basis of autophagy

The initial breakthrough in the identification of the autophagic molecular machinery arose from yeast genetic studies. A total of 35 AuTophaGy-related genes (ATG) have now been identified (Mizushima et al., 2011) and many of these have mammalian homologues. The Atg proteins involved in autophagosome formation are composed of a number of functional groups; the ULK1 (Atg1) complex, the PI3K complex, Atg9, the Atg2-WIPI (Atg18) complex and finally the two ubiquitin conjugating systems (Mizushima et al., 2011). Each one of these complexes has a crucial role in the autophagic process (Figure 1.8).

Autophagy can be induced by a variety of stimuli including amino acid starvation, growth factor withdrawal and at times of structural remodelling (Levine and Kroemer, 2008). Upon autophagic induction, the number of autophagosomes increases by more than 10-fold (Mizushima et al., 2011). Amino acid and growth factor signals converge on the master regulator mammalian target of rapamycin (mTOR). Under starvation conditions, mTOR is inhibited resulting in the activation of ULK1 which phosphorylates both Atg13 and FIP200 to initiate autophagosomal formation (Hosokawa et al., 2009a). The transcription factor FoxO3 also induces the transcription of multiple autophagy genes and acts in parallel to the mTOR pathway (He and Klionsky, 2009; Zhao et al., 2007).

The ULK1 complex consists of ULK1, Atg13, FIP200 and Atg101 and each one of these components is essential for autophagosome formation (Hosokawa et al., 2009a; Hosokawa et al., 2009b). Using genetic knock-down studies, it has been demonstrated that the ULK1 complex is the most upstream step in autophagosomal formation (Itakura and Mizushima, 2010). The PI3K complex acts downstream of the ULK1 complex and consists of vacuolar sorting protein 34 (Vps34), Vps15, Beclin1 (Atg6 homolog) and Atg14L. This complex produces PI3P and is present on the IM and elongating membrane (Longatti and Tooze, 2009). PI3P is required for the recruitment of the Atg18-Atg2 complex to the autophagosomal membrane (Obara et al., 2008). The mammalian Atg18 homolog WIPI-1 accumulates in large vesicular and cup-shaped structures upon induction of autophagy which are blocked by

wortmannin treatment, an inhibitor of autophagy (Proikas-Cezanne et al., 2004). The only known transmembrane Atg protein is Atg9 and although its exact function is unclear, it is required for autophagosomal formation (Noda et al., 2000).

The two ubiquitin conjugating systems function at a later stage in autophagosomal elongation (Itakura and Mizushima, 2010). Atg12 conjugation is the first ubiquitination-like reaction, Atg12 is activated and transferred to Atg10 (an E2-like enzyme) by Atg7 (an E1-like enzyme) (Tanida et al., 2001). Atg10 then conjugates Atg12 to Atg5 to form the Atg12-Atg5 complex. A mutation in Atg10 that is essential for Atg12 conjugation severely reduced autophagic activity (Shintani et al., 1999). Atg16L interacts with Atg5 forming the Atg12-Atg5-Atg16L complex and dissociates from the membrane upon closure of the isolation membrane. This renders Atg16L a reliable marker to distinguish between the forming autophagosome and the mature autophagosome (Mizushima et al., 2003). The Atg12-Atg5-Atg16L complex is important for the elongation of the isolation membrane as demonstrated in Atg5-deficient embryonic stem cells that exhibited defects in autophagosomal formation (Mizushima et al., 2001).

The second ubiquitin-like conjugation system consists of the yeast protein Atg8 and functions downstream of the Atg12-Atg5 complex (Itakura and Mizushima, 2010). To date, four Atg8 homologues have been identified; microtubule associated protein 1 light chain 3 (LC3), GABARAP, GATE-16 and Atg8L (Tanida, 2011). All homologues are essential for the autophagic process however, they differ in their N-terminal structure which is required for tethering and membrane fusion (Shpilka et al., 2011). LC3 is involved in membrane elongation whereas GATE-16 family proteins are involved at a later stage, possibly in the sealing of the autophagosome (Weidberg et al., 2010). There are three human homologues of LC3; MAP1LC3A, MAP1LC3B and MAP1LC3C all of which are synthesised as proLC3 and subsequently cleaved by Atg4 to form LC3-1 (He et al., 2003; Kirisako et al., 2000). LC3-1 localises to the cytosol (Kabeya et al., 2000) and is activated by Atg7, transferred to Atg3 and conjugated to the phospholipid phosphatidylethanolamine (PE) (Tanida et al., 2002; Tanida et al., 2001) resulting in LC3-II which localises to the autophagosomal membrane (Kabeya et al., 2000). LC3-II on the cytosolic

surface can be delipidated by Atg4B and recycled for further autophagosome formation whereas LC3-II on the inner membrane of the autophagosome is degraded (Kabeya et al., 2004). The LC3 conjugation system is essential for autophagosomal formation as mice deficient in Atg3 are defective in elongation and closure of isolation membranes (Sou et al., 2008). The two conjugation systems functionally cooperate, as the Atg12-Atg5 complex is required for targeting LC3 to the isolation membrane (Mizushima et al., 2001) whilst Atg3 deficient mice display a defect Atg12-Atg5 conjugation (Sou et al., 2008). LC3 is a widely used marker of autophagosomes and autophagic activity and can be measured via Western blotting for LC3-I and –II levels (Mizushima et al., 2010).

Subsequent to the two ubiquitin-conjugating systems, the autophagosome elongates and fuses to form the autophagosome. During autophagosomal maturation, fusion with different endosomal populations occurs (Liou et al., 1997). Early endosomal fusion with autophagosomes is essential for autophagosomal maturation as demonstrated by the siRNA depletion of subunits of the coat protein complex I (COPI). Loss of COPI resulted in an accumulation of ubiquitin containing aggregates and LC3-II positive vesicles (Razi et al., 2009). Loss of components of the endosomal sorting complex required for transport (ESCRT) also leads to the accumulation of autophagosomes (Lee et al., 2007a). Furthermore, inhibition of early/late endosomal conversion by overexpression of the early endosomal marker Rab5 or knock-down of the late endosomal marker Rab7 inhibited downstream mTOR signalling measured by S6K1 phosphorylation (Flinn et al., 2010). This suggests that proteins involved in endosomal maturation are also involved in regulation of autophagy. Following maturation of the autophagosome and fusion with endosomes, the mature autophagosome fuses with the lysosome and its contents are degraded by hydrolytic enzymes (Lawrence and Brown, 1992).

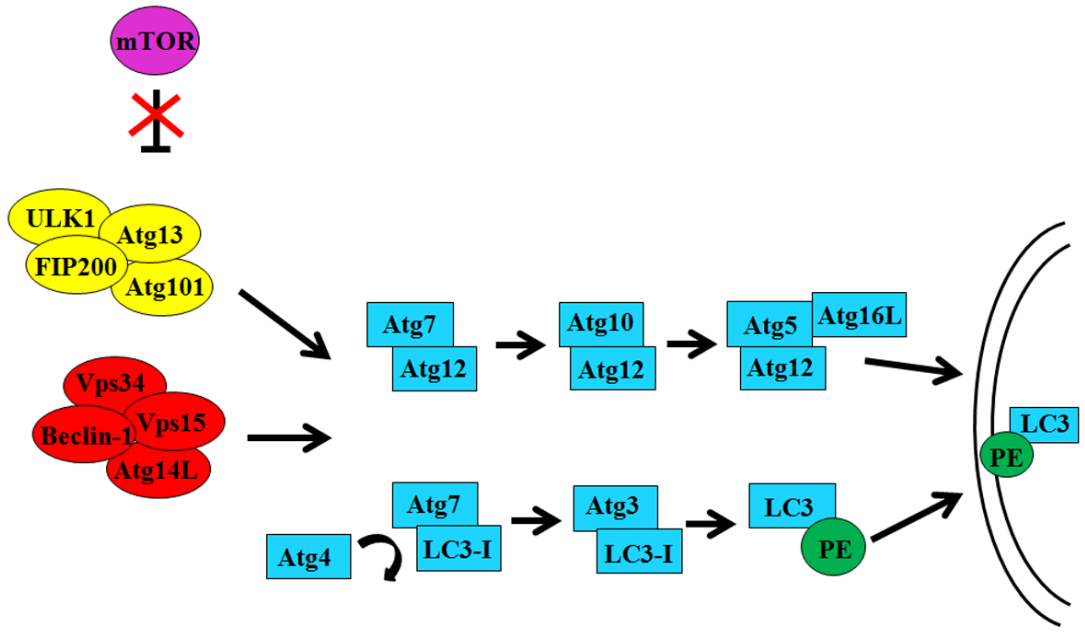

Figure 1.8. Autophagy molecular machinery. Under conditions of nutrient deprivation, the master regulator, mTOR is inactivated, resulting in the activation of the ULK1 complex (yellow). The PI3K complex (red) acts downstream of the ULK1 complex and is required for autophagosomal formation. Two ubiqutin conjugating-like systems are required for the formation of the membrane. Atg12 is activated by Atg7, transferred to Atg10 and conjugated to Atg5 which forms a complex with Atg16L. This complex is localised to the isolation membrane. ProLC3 is cleaved by Atg4 into LC3-I which is activated by Atg7 before transfer to Atg3 and conjugated to phospholipids (PE). LC3-PE is localised to the inner and outer isolation membrane (modified from Hill 2001).

1.5.2. The role of microtubules in autophagy

Microtubules form a complex, interconnected network within the cell and serve as tracks for intracellular movement of proteins and organelles. This movement is powered by the motor proteins kinesin which moves cargo towards the plus end of microtubules (the cell periphery) and dynein which moves cargo towards the minus end of microtubules (Monastyrska et al., 2009). It is widely accepted that microtubules play an important role in the autophagy process; however, the molecular mechanisms involved are still unclear.

The first connection between microtubules and autophagy-related genes was established with the identification of LC3 which can bind and stabilise microtubules (Faller et al., 2009; Mann and Hammarback, 1994) . Aplin *et al*. had previously demonstrated that disruption of the microtubule network, with drugs such as nocodazole, blocks fusion of autophagosomes with lysosomes but has no effect on the formation of autophagosomes (Aplin et al., 1992). However, Reunanen et al. found that nocodazole had no effect on autophagosome fusion with lysosomes (Reunanen et al., 1988). Subsequent studies have agreed that microtubules facilitate autophagosome formation (Fass et al., 2006; Köchl et al., 2006) but disagreed on whether microtubules are required for autophagosomal fusion with lysosomes (Fass et al., 2006; Köchl et al., 2006). Discrepancies could be explained by the different cell types used, the concentrations of drugs and the time-points studied. Additional studies have identified acetylated microtubules as being required for fusion of autophagosomes with lysosomes (Xie et al., 2010) and that the movement of mature autophagosomes towards lysosomes is dependent on the motor protein dynein (Jahreiss et al., 2008; Kimura et al., 2008).

Roles for distinct populations of microtubules have been proposed where labile microtubules specifically recruit markers of the autophagosome isolation membrane such as the Atg12-Atg5 conjugate and WIPI-I, whereas stable microtubules bind mature autophagosomes and facilitate their movement towards lysosomes (Geeraert et al., 2010). LC3 and Atg12 also bind the microtubule associated protein MAP1B, providing an additional mechanism for the targeting of autophagosomal structures to

the microtubule network (Behrends et al., 2010; Wang et al., 2006). Collectively, these data demonstrates that microtubules are required for different stages of autophagosome formation and maturation and that microtubule binding proteins provide a further mechanism for the recruitment of the autophagy machinery.

The tubulin deacetylase HDAC6 binds both polyubiquitinated protein aggregates and dynein motors, therefore coupling protein aggregates to the microtubule network (Kawaguchi et al., 2003). When the microtubule network is disrupted using nocodazole, colocalisation of LC3 and ubiquitin is abolished. Furthermore, inhibition of HDAC6 deacetylase activity impairs the recruitment of LC3 to sites of aggregated proteins (Iwata et al., 2005). This suggests that HDAC is required for the recruitment of autophagic machinery and protein aggregates to sites of autophagosomal formation and that this also requires the microtubule network.

1.5.3. Selective autophagy and p62

The aggregate forming ability of p62 was first identified by Shin et al. (Shin, 1998). Subsequently, p62 has been observed to accumulate in ubiquitin (Ub)-containing inclusions in a number of protein aggregation diseases including Parkinson's disease, Alzheimer's disease and tumourigenesis (Mathew et al., 2009; Wooten et al., 2006). Accumulation of p62 occurs in autophagy deficient mice and promotes tumourigenesis (Mathew et al., 2009). Additionally, p62 binds both mono- and polyubiquitinated chains (Seibenhener et al., 2004; Vadlamudi et al., 1996), and together with its ability to polymerize via its PB1 domain, p62 targets large ubiquitinated protein aggregates for autophagosomal degradation (Bjørkøy et al., 2006; Tan et al., 2008). p62 depletion causes a reduction in ubiquitin-positive inclusion bodies (Pankiv et al., 2007a), however the formation of LC3-labelled autophagosomes and their delivery to lysosomes is not affected (Shvets et al., 2008). Although autophagy had been thought of as a non-selective process, the binding of p62 to ubiquitinated proteins provides a mechanism by which specific cargo can be selectively degraded.

The autophagic marker LC3 localises to p62 containing subcellular structures and through its LC3 interaction region (LIR), p62 directly binds to LC3. This interaction is required for the degradation of p62 bodies (Pankiv et al., 2007a). An 11 amino acid motif in p62, which contains conserved acidic and hydrophobic residues, was identified as the LC3 recognition sequence (Ichimura et al., 2008). LC3 belongs to a ubiquitin-like protein family and its interaction with p62 is dependent on the N-terminal ten amino acids located within its ubiquitin core (Shvets et al., 2008). Structural studies revealed that the LIR region is highly conserved throughout LC3 interacting proteins and consists of a WXXL-like sequence (Noda et al., 2010). The LC3 interaction region functions in a number of autophagic receptors including Nix (Novak et al., 2010) and Atg32 (Noda et al., 2010) and this interaction is likely to serve as a mechanism through which autophagic receptors tether their cargo to the autophagic membrane (Noda et al., 2010). With respect to p62, it becomes possible to propose a model whereby misfolded proteins are identified by molecular chaperones and labeled with polyubiquitin chains which in turn are recognized by p62 and sequestered into larger aggregates. These aggregates are targeted to the forming autophagosome via the interaction between p62 and LC3 (Johansen and Lamark, 2011). p62 is itself degraded by autophagy and is often used as a marker of autophagic flux. Levels of p62 increase upon blockage of the autophagy pathway (Mizushima et al., 2010).

The autophagic degradation of invading bacteria has been termed xenophagy and p62 is recruited to ubiquitinated proteins localized to bacteria and targets them for degradation. These structures are also labeled with LC3. The LIR and UBA domains of p62 are required for autophagic degradation of the invading bacteria. Upon knock-down of p62 by siRNA, there was also a 50% reduction in bacteria targeted for autophagy, suggesting that p62 facilitates autophagic degradation of invading bacteria (Zheng et al., 2009). The removal of p62 by selective autophagy can also impact on intracellular signalling pathways. Hypoxia induced autophagy enhances degradation of p62 which results in increased activation of ERK 1/2 in carcinoma cells as p62 normally acts to inhibit ERK signalling (Pursiheimo et al., 2008). Additionally, p62 is known to interact with Keap1. Keap1 facilitates the degradation of the transcription factor Nrf2. Under conditions of impaired autophagy, p62

interacts with Keap1 and competitively inhibits its interaction with Nrf2. Nrf2 is therefore stabilised and this results in the abnormal accumulation of a variety of Nrf2 target proteins which are present in autophagy-deficient livers and may contribute to liver abnormality (Komatsu et al., 2010).

The role of p62 in autophagic degradation is largely thought to depend on the ubiquitination of target proteins however recently p62 has been identified in the clearance of non-ubiquitylated substrates. The non-ubiquitylated protein STAT5A_ΔE18, which is prone to aggregation, forms HDAC6 dependent aggresomes which are degraded by autophagy. This degradation is dependent on STAT5A_ΔE18 binding to the PB1 domain of p62 (Watanabe and Tanaka, 2011).

1.5.4. Autophagy and bone

There has been limited research with respect to autophagy and bone however, recent studies have demonstrated that autophagy is likely to be important for bone maintenance and cell survival.

Osteocytes reside deep within the mineralised bone matrix, often out of contact with the vascular supply, where oxygen levels are low. Low oxygen levels affect the osteogenic activity of pre-osteocyte cells through the transcription factor hypoxia-inducible factor-1 (HIF-1) (Zahm et al., 2008). As autophagy is activated under hypoxic conditions (Tracy et al., 2007) and is dependent on HIF-1 (Bellot et al., 2009), it is likely that autophagy may play a role in the differentiation and survival of osteocytes. Osteocytes located in cortical bone display a punctate distribution of LC3 as observed in longitudinal sections of rat tibiae. Furthermore, autophagy is upregulated in cultures of an osteocyte cell line under hypoxic and low calcium conditions and this was dependent on HIF-1 (Zahm et al., 2011). Hypoxic conditions have also been demonstrated in primary osteoblast cultures to decrease the formation of bone nodules and the expression of ALP and osteocalcin therefore suggesting that autophagy could be involved in the bone forming and mineralisation activity of osteoblasts (Utting et al., 2006). Additionally, an increase in osteoclast formation has been noted under hypoxic conditions (Arnett et al., 2003).

A genome-wide association study (GWAS) identified single nucleotide polymorphisms (SNPs) in a number of genes involved in the regulation of autophagy (ROA) including Atg12, Atg7 and Atg5. These SNPs were shown to be associated with wrist bone mineral density (Zhang et al., 2010). Furthermore, misfolded collagen accumulates in the ER and can be toxic to cells. Elimination of collagen is mediated by autophagy suggesting that in diseases such as osteogenesis imperfecta where misfolded collagen accumulates in cells, autophagy could provide a possible therapeutic target (Ishida et al., 2009).

Systemic factors could also influence the autophagic activity and survival of bone cells. Glucocorticoid therapy is known to cause osteoporosis and bone weakness and has recently been demonstrated to induce autophagy in osteocytes (Xia et al., 2010). Whilst autophagy is largely thought to be a cellular survival mechanism, prolonged activation causes the massive accumulation of autophagosomes and results in apoptosis (Eisenberg-Lerner et al., 2009). This suggests that long term treatment with glucocorticoid could lead to prolonged autophagic induction and ultimately cell death resulting in reduced bone strength and osteoporosis (Xia et al., 2010).

The multifunctional scaffold protein p62 is involved in the maintenance of bone (section 1.4.3) and is a key autophagic protein (section 1.5.3). Whilst p62 accumulates in large inclusions in numerous diseases, its role in autophagy in bone is largely unclear. Recently, p62 was identified as an interacting partner of the autophagy-linked FYVE domain-containing protein (ALFY) in osteoclasts. Upon starvation, p62 and ALFY translocate from the nucleus to the cytoplasm and colocalise in cytoplasmic aggregates. This translocation is faster in mature osteoclasts compared to osteoclast precursors (Hocking et al., 2010). The UBA domain of p62 is required for the formation of these aggregates (Clausen et al., 2010), however, their formation is not affected by the PDB-causing mutation P392L (Hocking et al., 2010). The mechanism by which mutated p62 could lead to over-activation of osteoclasts in PDB but have no affect on other cells could be attributable to the differences observed in response to starvation in osteoclasts and their precursors (Hocking et al., 2010). PDB is a late-onset disease and as the

efficiency of the autophagy pathway declines with age (Cuervo and Dice, 2000), this suggests that autophagy deficiency could be contributing to the PDB phenotype.

Inclusion body myopathy associated with Paget's disease of bone and fronto-temporal dementia (IBMPFD) is a disease that could also link autophagy to the regulation and maintenance of bone. IBMPFD is characterised by muscle myopathy, fronto-temporal lobar degeneration in the brain and late-onset PDB and is caused by mutations in the valosin-containing protein, p97/VCP (Ju and Weihl, 2010; Watts et al., 2004). p97 is an essential, ubiquitously expressed, member of the type II AAA (ATPase associated with various activities) ATPase family and its knockdown in mice is lethal (Müller et al., 2007). P97 mediates a wide variety of cellular processes including protein degradation via the ubiquitin proteasome system (UPS) (Wójcik et al., 2004) and the endoplasmic reticulum-associated protein degradation (ERAD) pathway (Rabinovich et al., 2002). One of the main pathological features of IBMPFD is the presence of ubiquitinated inclusions probably due to the role of p97 in autophagosomal protein degradation. Cells expressing the IBMPFD associated mutations in p97 display an increased level of autophagosome markers including LC3-II and p62 and an accumulation of non-degradative autophagosomes (Ju et al., 2009). Delivery of aggregates to the sites of autophagosome formation is also impaired and overexpression of HDAC6 can rescue this and reduce cell death (Ju et al., 2008). IBMPFD therefore demonstrates the importance of autophagy in the maintenance of bone.

1.6. The Ubiquitin proteasome system (UPS)

The ubiquitin proteasome system (UPS) is the major non-lysosomal mechanism utilised by the cell to degrade misfolded and damaged proteins. Proteins are ubiquitinated and subsequently targeted for degradation via the proteasome. Under normal conditions, unwanted proteins are removed promptly before any damage can be caused to the cell. However, many diseases such as Alzheimers, Parkinsons and myopathies can be caused by the accumulation of proteins that form aggregates due to the failure of parts of the UPS (Leroy et al., 1998; van Leeuwen et al., 1998; Zolk et al., 2006).

1.6.1. Ubiquitination

Proteins are tagged for degradation by the proteasome with chains of ubiquitin, a small, highly conserved, ubiquitously expressed, protein (Wilkinson et al., 1980). The process by which ubiquitin is added to target proteins is termed ubiquitination and is mediated by a cascade of enzymes. Ubiquitin is initially activated by an E1 ubiquitin activating enzyme in the presence of ATP, resulting in the formation of a thiol ester bond with the carboxyl group of glycine76 on ubiquitin. The activated ubiquitin molecule is subsequently transferred to the active site of an E2 ubiquitin conjugating enzyme through another thiol ester bond and attached to a lysine residue of the target protein, aided by an E3 ubiquitin ligase enzyme. The precise mechanisms of different E3s vary, however they all promote the transfer of ubiquitin either directly or indirectly. The ubiquitin conjugation cascade contains a large family of E2s and an even larger family of E3s that confer substrate specificity. (Nandi et al., 2006; Passmore and Barford, 2004) (Figure 1.9).

Additional ubiquitin molecules can be added to form polyubiquitin chains. The efficient multiubiquitination of a substrate requires an additional conjugation factor (E4) that catalyses the extension of the ubiquitin chain in collaboration with E1, E2 and E3 enzymes (Koegl et al., 1999). Ubiquitin can form chains at all seven of its lysine residues (K6, K11, K27, K29, K33, K48 and K63) of various lengths and therefore can create a range of molecular signals influencing DNA repair, ribosome function, the stress response and protein degradation (Wooten et al., 2006). Monoubiquitination can also provide signals for cellular functions such as histone regulation and endocytosis (Hicke, 2001) whilst the synthesis of mixed ubiquitin chains have been reported to prevent protein degradation by the proteasome (Kim et al., 2007a). K48- and K29-linked chains are thought to be the principle signal for degradation via the proteasome and a chain of at least four ubiquitin moieties are required for substrate recognition (Thrower et al., 2000).

The 26S proteasome is a large cytosolic protease complex that consists of a 20S proteolytic core particle and one or two 19S regulatory caps. The 19S cap has several functions including recognition of polyubiquitinated substrates, deubiquitination and translocation of substrates to the lumen of the core particle.

Protease enzymes are contained within the proteasome core and act to degrade targeted proteins (Ferrell et al., 2000). Many proteins also transiently associate with the 26S proteasome (Berke and Paulson, 2003).

1.6.2. Ubiquitin recognition and deubiquitinating enzymes (DUBs)

Ubiquitin binding domains (UBD) are diverse modules present in many proteins and can bind to mono- and polyubiquitinated chains. Over twenty different UBD families have been identified to date (Dikic et al., 2009) that diverge in both structure and the type of ubiquitin modification they recognise. The ubiquitin associated domain (UBA) is one such UBD.

The UBA domain was first identified in 1996 and is approximately 45 residues in length. It is structurally similar to ubiquitin itself (Hofmann and Bucher, 1996) and contains three α-helices and a hydrophobic core (Mueller and Feigon, 2002). UBA domains bind monoubiquitin and a number of different lysine-linked polyubiquitinated chains (Raasi et al., 2005). They also have lysine chain specificity, some only bind one polyubiquitinated chain type whereas others bind several different types and some do not bind ubiquitin at all (Raasi et al., 2005). Through binding to monoubiquitin and specific polyubiquitinated chains, UBA domains can modulate a variety of cellular functions. The UBA domain of p62 binds to the K48-linked polyubiquitinated chains on tau and thereby facilitates its degradation by the proteasome (Babu et al., 2005). The UBA domain of Rad-23 binds K48-linked multi-ubiquitin chains leading to the selective inhibition of chain assembly and disassembly, which prevents protein degradation by the proteasome (Raasi and Pickart, 2003). The dimerisation of UBA domains affects their ubiquitin binding ability. This has been illustrated by a study of the p62 UBA domain which was demonstrated to dimerise and this dimerisation inhibited its ability to bind ubiquitin (Long et al., 2010). In addition, destabilisation of the p62 UBA domain dimer interface affects NFκB signalling (Long et al., 2010). UBA domains have also been implicated in the direct interaction of proteins which do not involve ubiquitin. This has been illustrated by the interaction of the E3 ligase MURF2 with the UBA domain of p62 (Lange et al., 2005).

Ubiquitination is a reversible process and removal of ubiquitin from substrates is catalyzed by deubiquitinating enzymes (DUBs). In order for tagged proteins to be degraded, ubiquitin must be removed and recycled before the protein enters the proteolytic core (Yao and Cohen, 2002). DUBs can also rescue poorly ubiquitinated or slowly degraded ubiquitin conjugates from proteasomal degradation. UCH37 is a subunit of the 19s regulatory particle and achieves this function by disassembling the degradation signal from the distal end of Lys48-linked chains thereby releasing the protein before it is degraded (Lam et al., 1997). Furthermore, the endosomal degradation of membrane receptors is regulated by DUBs. USP10 acts to deubiquitinate the cystic fibrosis transmembrane conductance regulator (CFTR) chloride channel and therefore promote its endocytic recycling. Knock-down of USP10 increased the multi-ubiqutination of CFTR and therefore enhanced its degradation via the lysosome (Bomberger et al., 2009). Among their diverse functions, DUBs have been implicated in the regulation of osteoclastogenesis. Mice deficient in the DUB CYLD displayed an osteoporotic phenotype due to an increase in osteoclast response to RANKL. CYLD was shown to negatively regulate RANK signalling by inhibiting TRAF6 ubiquitination, and activation of downstream signalling events (Jin et al., 2008).

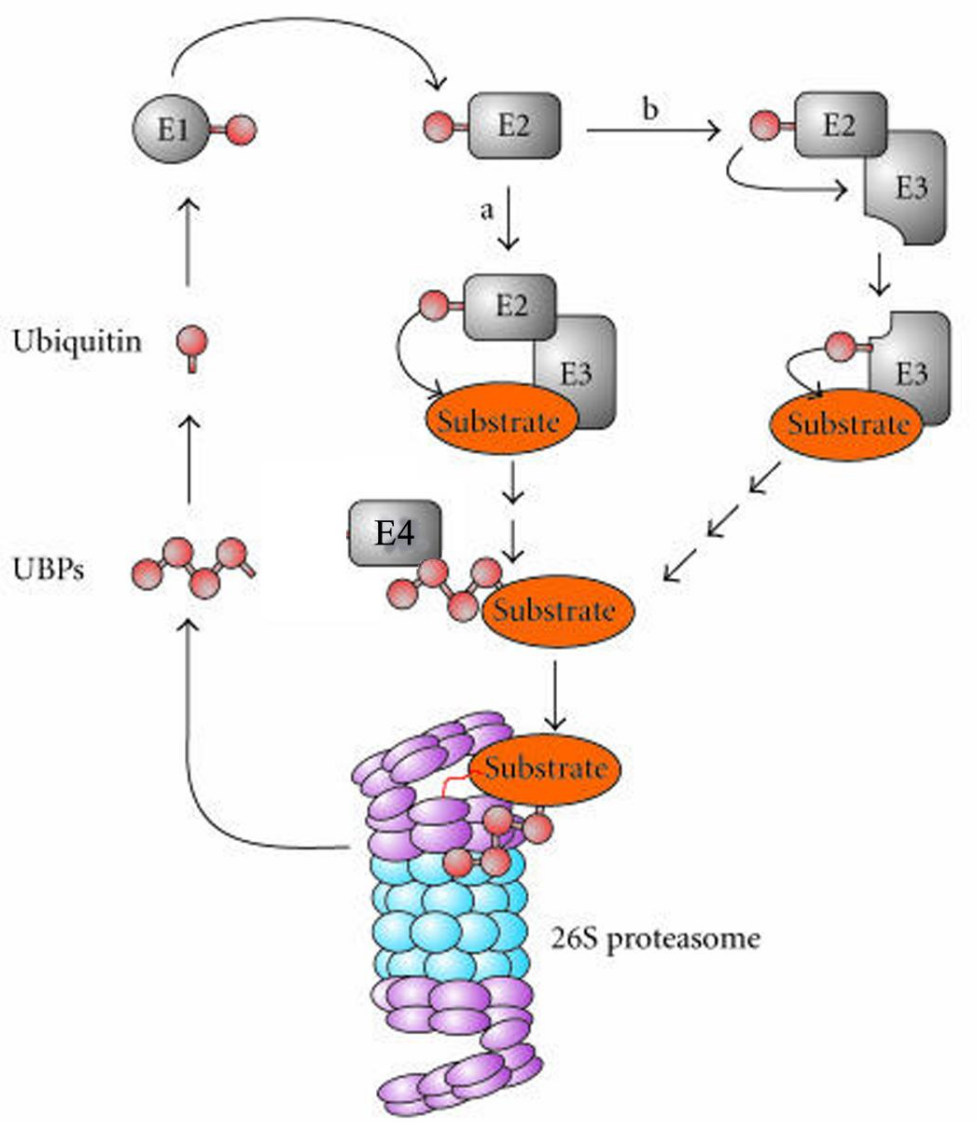

Figure 1.9. The ubiquitin proteasome system. Proteins are tagged for degradation with chains of ubiquitin. Ubiquitin is activated by a ubiquitin activating enzyme (E1), transferred to a ubiquitin conjugating enzyme (E2) and then, aided by a ubiquitin ligase (E3), is attached to a lysine residue on the target protein. The efficient multiubiquitylation of a substrate requires an additional conjugation factor (E4) that catalyses the extension of the ubiquitin chain in collaboration with E1, E2 and E3 enzymes. Ubiquitin specific proteases (UBPs) remove the polyubiquitin chain and the ubiquitin is recycled (modified from Wooten at al. 2006).

1.6.3. Autophagy and UPS Crosstalk

Selective autophagy and the UPS system both require the ubiquitination signal therefore, it is likely that they are functionally linked. Whilst K48-linked ubiquitin chains are generally a signal for degradation via the proteasome (Thrower et al., 2000), K63-linked chains are recognized by components of the autophagosome-lysosome pathway (Tan et al., 2008). However, specificity may overlap as proteins such as p62 are involved in the degradation of proteins via the proteasome and autophagy (Geetha et al., 2008; Pankiv et al., 2007a). Additionally, inhibition of autophagy increases the levels of proteasome substrates such as p53. This was largely found to be due to an increase in p62 levels which inhibits the clearance of ubiquitinated proteins by the proteasome (Korolchuk et al., 2009). Chemical inhibition of lysosome function also reduces proteasomal function, again suggesting a link between proteasomal and autophagic activity (Qiao and Zhang, 2009).

1.7. NBR1

Expression cloning with an antibody raised against CA125 (an ovarian tumour antigen) identified a novel peptide sequence which lacked the mucin-like membrane protein characteristics expected of CA125 (Campbell et al., 1994). The new gene was identified as *1a1.3b* which was later renamed *NBR1* (Neighbour of *BRCA1*). Analysis of the genomic sequence of *NBR1* in breast and ovarian cancer patients did not identify any mutations in its coding region. This suggests that mutations in this gene are not involved directly in causing breast or ovarian cancer in these patients (Campbell et al., 1994).

This thesis focuses on extending the current knowledge of Nbr1 as a scaffold protein involved in multiple protein-protein interactions. It also further investigates the involvement of Nbr1 in bone formation and remodelling.

1.7.1. The *NBR1*/*Nbr1* gene

NBR1 was mapped to chromosome 17 in humans (Campbell et al., 1994) and chromosome 11 in mice (Chambers and Solomon, 1996) and in both species lies in

close proximity to the breast cancer susceptibility gene *BRCA1* (Chambers and Solomon, 1996). Murine Nbr1 has two main transcripts, produced by alternative splicing; Nbr1 (1a), the testes predominant form (Dimitrov et al., 2001) and Nbr1 (1b) which is highly expressed in the neural tube during early embryonic stages (Whitehouse et al., 2002) but is widely expressed in all tissues later in development (Chambers and Solomon, 1996; Dimitrov et al., 2001). Expression of the Nbr1 1a and 1b transcripts are controlled by two different promoters, α and β respectively. Analysis of the 289 base pair region separating *Brca1* and *Nbr1* in a reporter transient transfection assay demonstrated that the α promoter is bidirectional and controls the expression of both *Nbr1* and *Brca1* (Whitehouse et al., 2004). The ATG start sites are located in exon 2 of *Nbr1*, therefore the protein coding sequence is unchanged between transcripts a and b (Chambers and Solomon, 1996).

1.7.2. The NBR1/Nbr1 protein

Nbr1 is 89% homologous between mouse and human and is highly conserved (Chambers and Solomon, 1996) with homologues identified throughout the eukaryotic kingdom (Svenning et al., 2011). Analysis of the structure of Nbr1 has shown that it is structurally similar to the scaffold protein p62 and possesses a number of common protein domains (Figure 1.10). The N-terminus contains a Phox and Bem1p (PB1) domain (Ito et al., 2001) that is evolutionarily conserved and found in many scaffold proteins involved in cellular signal transduction pathways (Moscat et al., 2006). PB1 domains display the topology of ubiquitin-like β-grasp folds and either contain an acidic OPCA motif (type I), an invariant lysine residue on the first β strand (type II) or both of these motifs (type I/II). Type I and type II PB1 domains interact in a front-to-back manner where acidic residues on the OPCA motif form salt bridges with the basic residues on the type II PB1 domain (Sumimoto et al., 2007). Analysis of the crystal structure of the PB1 domain of Nbr1 has revealed that it adopts a ubiquitin-like β-grasp fold containing two α-helices, a mixed β-sheet and an OPCA motif making it a type I PB1 domain (Müller et al., 2006). Two sequential folding transitions states in the PB1 domain of Nbr1 have also been identified and characterised (Chen et al., 2010).

The central region of the NBR1 protein contains a zinc-binding domain and two coiled-coil (CC) domains. The zinc binding domain is similar to that present in dystrophin-like proteins and CREB-binding proteins (Whitehouse et al., 2002) while CC domains are responsible for protein oligomerization (Beck and Brodsky, 1998). Through its first coiled-coiled domain, Nbr1 is able to homodimerise (Whitehouse et al., 2002).

The C-terminus of Nbr1 contains a UBA domain. As described above, UBA domains can bind both mono- and poly ubiquitin and using ubiquitin binding assays, it was shown that both human and mouse Nbr1 UBA domains can bind monoubiquitin and K48- and K63-linked polyubiquitin chains ranging from two to seven in length (Waters, 2009).

Figure 1.10. Schematic representation of Nbr1 and p62 proteins. Both proteins have a PB1 domain (red) ZZ domain (purple) and UBA domain (green). Nbr1 also contains two coiled coil (CC) domains (blue). Nbr1 and p62 interact via their PB1 domains.

1.7.3. Interacting partners of Nbr1

At the outset of this project, a number of proteins were known to interact with Nbr1 (Figure 1.11). Yeast-2-hybrid analysis showed that amino acids 451-597 of NBR1 interact with fasciculation and elongation protein zeta-1 (FEZ1) and calcium and integrin binding protein (CIB) (Whitehouse et al., 2002). FEZ1 is highly expressed in the developing brain and FEZ1 deficient mice show characteristics of schizophrenia and hypersensitivity to psychostimulant drugs (Sakae et al., 2008). FEZ1 also interacts with and is phosphorylated by PKCζ, which has been shown to stimulate the neuronal differentiation of PC12 cells and suggests a role in axonal guidance (Kuroda et al., 1999). Additionally, FEZ1 interacts with E4B (U-box-type ubiquitin-protein isopeptide ligase) which promotes its polyubiquitination however, this does not affect its degradation but does provide a signal for neurite extension in PC12 cells (Okumura et al., 2004). FEZ1 also interacts with the microtubule protein β-tubulin and facilitates the movement of mitochondria along the microtubule network towards extending neurites in PC12 cells (Fujita et al., 2007) and may play a role in the remodelling of microtubules through its interaction with PKCζ (Mori et al., 2009). FEZ1 and NBR1 colocalise in perinuclear compartments when overexpressed in COS-7 cells (Whitehouse et al., 2002).

CIB interacts with polo-like kinase 3 and regulates its activity during cell division. Altered expression of CIB results in multinucleated cells due to aberrant centrosomal segregation (Naik and Naik, 2011). Mice deficient in CIB display cardiac dysfunction and hypertrophy in response to pressure overload (Heineke et al., 2010). As Nbr1 plays a role in muscle function (see below), this could provide a further mechanism by which it exerts its function. Additionally, CIB interacts with the apoptosis signal-regulating kinase 1 (ASK1) and negatively regulated stress activated MAPK signalling pathways (Yoon et al., 2009). CIB is normally localised in the nucleus, however on coexpression with NBR1 in COS-7 cells it redistributes to perinuclear regions that colocalise with NBR1 (Whitehouse et al., 2002).

Yeast-2-hybrid studies also showed direct interactions between the N-terminus of Nbr1 and Ubc-9, PIASγ and HIPK2 (unpublished data). HIPK2 is a negative

regulator of Wnt signalling and functions to phosphorylate β-catenin, enhancing its degradation (Kim et al., 2010). Ubc-9 is an E2 SUMO conjugating enzyme that covalently modifies target proteins by the addition of the small ubiquitin-like modifier (SUMO) whilst PIASγ is a SUMO E3 ligase (Gareau and Lima, 2010). These two proteins link Nbr1 to the sumoylation pathway.

The type I PB1 domain of Nbr1 interacts with the type I/II PB1 domain of p62 (Lamark et al., 2003). The D50R mutation in NBR1 (a point mutation in exon three causing amino acid 50 to be changed from aspartic acid to arginine) can inhibit interaction with p62 whilst a corresponding mutation in p62 (K7A) also abrogates this interaction. This suggests that the PB1 domain of p62 utilises its basic cluster to interact with the OPCA motif of the PB1 domain of Nbr1 (Lamark et al., 2003). p62 also contains a ZZ domain, and two PEST sequences which are regions of the protein that are rich in the amino acids proline (P), glutamic acid (E), serine (S), and threonine (T) and act as proteolysis signals (Rechsteiner and Rogers, 1996). The C-terminus of p62 contains a UBA domain which binds polyubiquitinated chains, and this is important for degradation of proteins via autophagy and the UPS (discussed above) (Figure 1.11). p62 has been far more extensively studied than Nbr1 and as discussed is implicated in bone remodelling, obesity, signalling pathways such as NF-κB and protein degradation. Due to similarities with p62, it is likely that Nbr1 is involved in these biological processes, some of which have been identified and are discussed below.

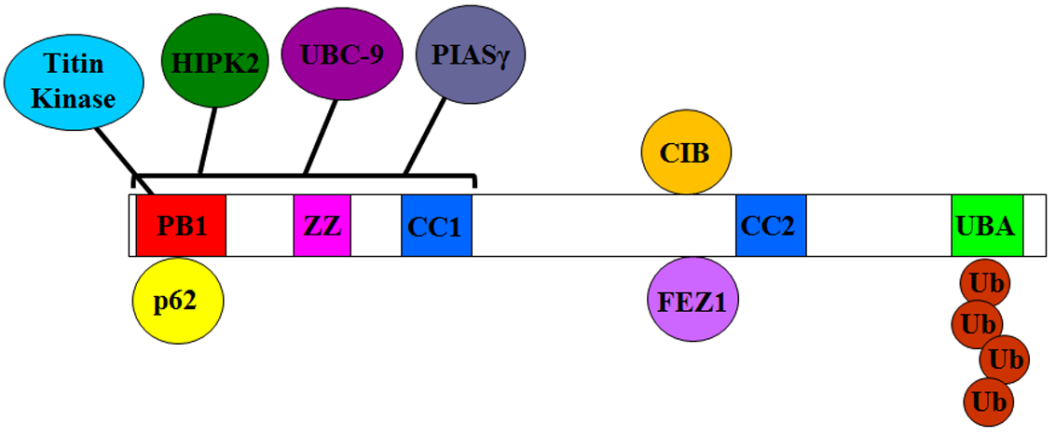

Figure 1.11. Nbr1 interacting partners. Nbr1 interacts with calcium and integrin binding protein (CIB) and fasciculation and elongation protein zeta-1 (FEZ1). Interaction with titin and p62 link Nbr1 to muscle signalling. Nbr1 is also linked to the sumoylation machinary via UBC-9 and PIASγ and to protein degradation via its interaction with poly ubiquitinated chains. Additionally, Nbr1 may be involved in the Wnt signalling pathway through its interaction with HIPK2.

1.7.4. The role of Nbr1 in bone

To elucidate a function for Nbr1, our laboratory generated a mouse model that expressed a truncated form of the protein. Exons 6, 7, and part of 8 were deleted causing a frameshift and premature stop codon resulting in mice expressing only amino acids 1-135 of the protein (trNbr1) (Whitehouse et al., 2010). The resulting protein lacked the UBA, ZZ and both CC domains but retained the PB1 domain. This strategy was used due to the close proximity of the *Brca1* gene, the bidirectionality of the promoter and the known lethality of the Brca1-deficient mice. When the trNbr1 mice were generated, there was also very little known about the structure of the Nbr1 protein and the PB1 domain had not been identified.

Mice homozygous for the truncated Nbr1 protein (trNbr1) displayed an age dependent increase in bone mass and bone mineral density that became apparent at three months of age (Whitehouse et al., 2010). Micro-quantitative computed tomography (μQCT) showed there were significant increases in trabecular bone volume (Tb.BV), trabecular number (Tb.N) and a decrease in trabecular separation (Tb.Sp) (Whitehouse et al., 2010). Calcein labelling identified an increase in bone formation rate in truncated mice compared with WT at two and seven months of age and an increase in serum osteocalcin levels was also identified (Figure 1.12). *In vitro* analysis of osteoblast precursors derived from neonatal calvaria displayed increased osteoblast differentiation and mineralisation as demonstrated by ALP and von Kossa staining however there was no difference in osteoblast proliferation rate (Whitehouse et al., 2010). Quantitative PCR also demonstrated an increase in the expression of osteoblast marker genes *ALP*, *osteocalcin* and *Atf4* whereas levels of *Runx2* were unaltered. These data established that truncation of Nbr1 causes an increase in bone formation due to an increase in osteoblast differentiation and activity (Whitehouse et al., 2010). The osteoclast phenotype of these mice was also analysed and whilst at two months of age, there was an increase in osteoclast activity *in vivo* (analysed by osteoclast surface and mean erosion depth) in mutant mice compared with WT, this was transient and there were no significant differences at either six or eleven months of age between the genotypes (Whitehouse et al., 2010). *In vitro* analysis of osteoclast function revealed a slight enhancement of osteoclast resorption activity

(Whitehouse et al., 2010). Collectively, these data suggests that there is an alteration in the homeostatic set point in trNbr1 mice, resulting in an increase in bone formation but no corresponding increase in bone resorption (Whitehouse et al., 2010).

Osteoblasts derived from trNbr1 mice also displayed enhanced and prolonged p38 MAPK activation but ERK signalling was not affected in this cell type (Whitehouse et al., 2010). Furthermore, full length Nbr1 but not trNbr1 can form a complex with phosphorylated p38 MAPK. Additionally, osteoclasts from trNbr1 mice, stimulated with RANKL displayed an increase in p38 MAPK and ERK1/2 activation compared to WT controls (Whitehouse et al., 2010). p38 MAPK is activated during osteoblast differentiation in response to BMPs (Guicheux et al., 2003) and regulates osteoblast differentiation through the activation of the transcription factor osterix (Wang et al., 2007). In addition, p38 MAPK-mediated signals are essential for RANKL induced osteoclast differentiation but not function (Li et al., 2002). p38 MAPK is also activated in osteoblasts stimulated with the proinflammatory cytokines IL-1 and TNFα and inhibition of p38 MAPK prevents bone resorption in the presence of IL-1 and TNFα (Kumar et al., 2001).

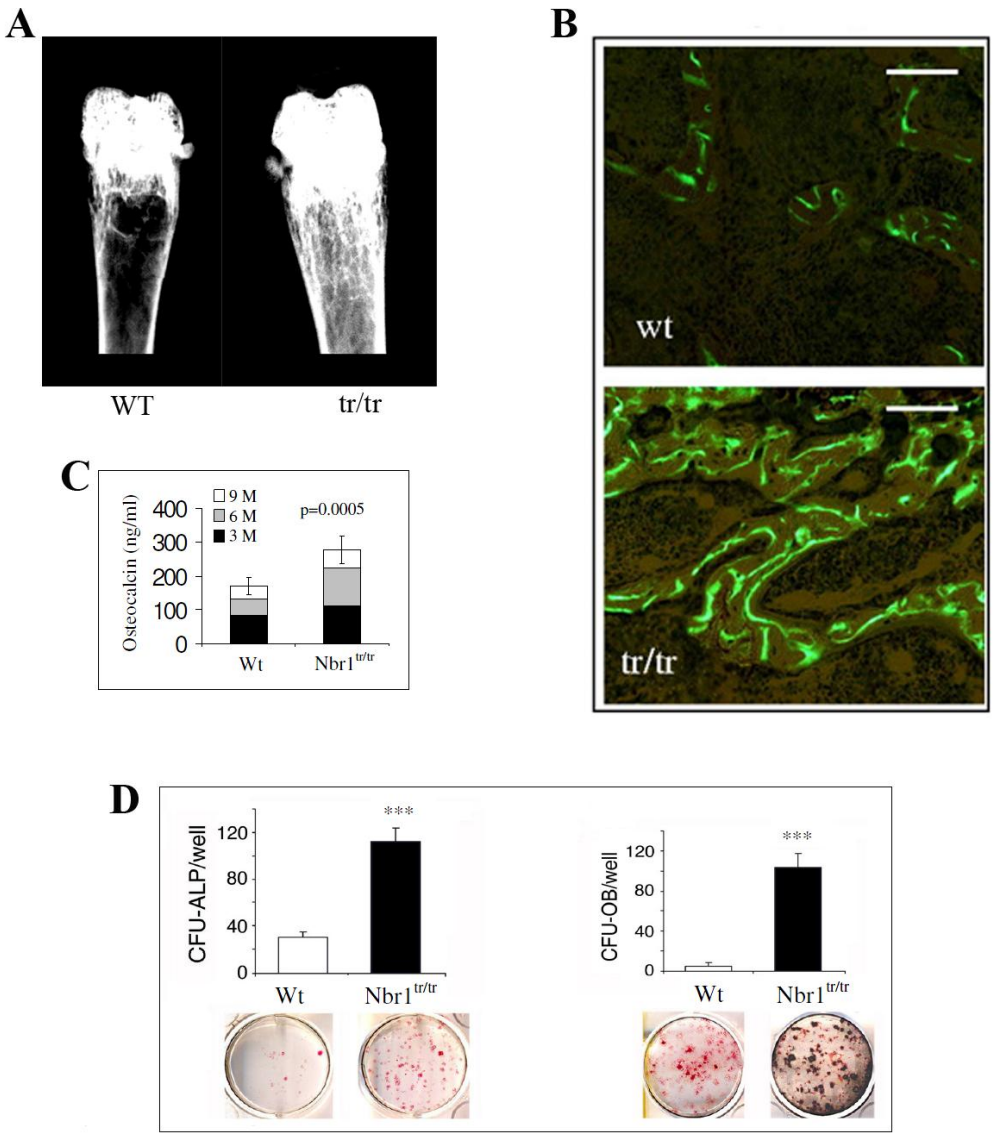

Figure 1.12. Increased bone mass and bone mineral density in truncated Nbr1 (trNbr1) mice compared to WT.
A. Radiographs of distal femurs from WT and trNbr1 mice (tr/tr).
B. Calcein double-labeled mineralization fronts in femoral cortex of 8-wk-old mice by fluorescent micrography. (Scale bar, 20 μm.).
C. Serum osteocalcin levels in WT and tr/tr mice at three, six and nine months of age.
D. Increased numbers of CFU-ALP and CFU-OB from trNbr1 bone marrow stromal cells compared with WT. Staining ALP (left), ALP, von Kossa (right). ***p<0.001. (taken from Whitehouse et al. 2010).

1.7.5. The role of Nbr1 in muscle

The PB1 domain of NBR1 interacts with the serine-threonine kinase domain (TK) of the giant sarcomeric protein titin, suggesting a role for NBR1 in muscle (Lange et al., 2005). The smallest contractile unit of skeletal muscle is the sarcomere, which is composed of many different, highly ordered proteins. Titin is the third most abundant protein in striated muscle after myosin and actin and in developing muscle is thought to act as a template for the assembly of the sarcomere (Lange et al., 2006; Tskhovrebova and Trinick, 2003) (Figure 1.13).

Under basal conditions, NBR1 interacts with titin and subsequently forms a complex with p62 and the E3 ligase MuRF2 at the M-band of the sarcomere. This allows the serum response factor (SRF) transcription factor to activate gene transcription (Figure 1.14). Upon mechanical inactivity, this complex dissociates and MuRF2 translocates from the cytosol to the nucleus where it interacts with SRF and prevents gene transcription (Lange et al., 2005). This suggests that NBR1 acts as a scaffold to target p62 and MuRF2 to the TK region of titin and therefore modulate muscle gene expression. A point mutation in the TK region of titin was found in patients suffering from hereditary myopathy with early respiratory failure (HMERF). This mutation dramatically reduces NBR1 binding and results in the mislocalisation of NBR1 causing the loss of sarcomere structure. p62 and MuRF2 are no longer recruited to the signalling complex and NBR1 and p62 are found to accumulate in vesicular structures (Lange et al., 2005). This strongly suggests a role for NBR1 in regulating muscle gene expression via the correct targeting of signalling complexes. The expression of Nbr1, p62 and LC3 in early cardiac differentiation parallels that of MuRF2 suggesting an important role for ubiquitin-mediated protein turnover at this early stage of development (Perera et al., 2011).

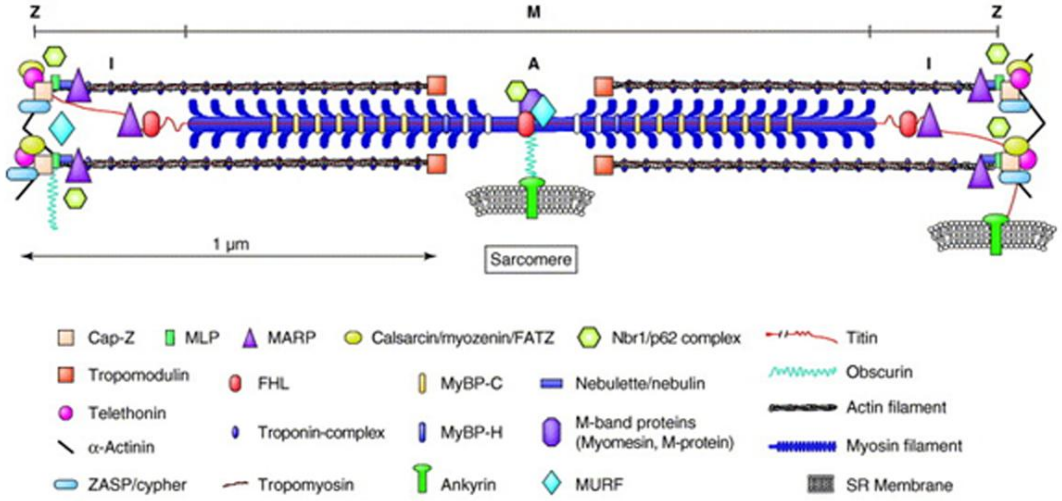

Figure 1.13. Schematic representation of the sarcomere. The smallest contractile unit of skeletal muscle is the sarcomere which is composed of a large number of highly ordered proteins. The organisation of these proteins is likely to be mediated by titin which spans from the Z-line to the M-band (taken from Lange et al. 2006).

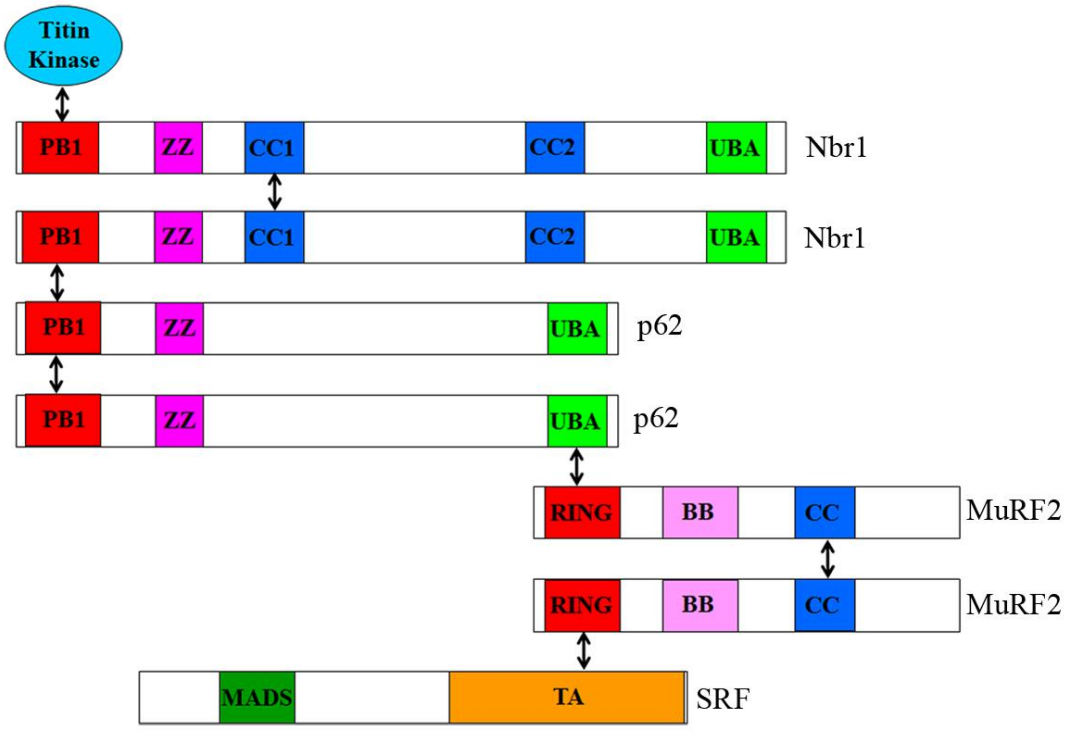

Figure 1.14. Nbr1 signalling in muscle. Nbr1 acts as a scaffold in the titin kinase signalling pathway. Nbr1 homodimerizes via its coiled-coil (CC) domain and interacts with both the kinase domain of titin and p62 via its PB1 domain. MuRF2 is recruited to this signalling complex via the interaction between its RING and B-box (BB) domain and the ubiquitin associated domain (UBA) of p62. Upon mechanical inactivity MuRF2 translocates to the nucleus where it interacts with the transactivation (TA) domain of serum response factor (SRF) and inhibits gene transcription (modified from Lange et al., 2005).

1.7.6. Additional roles for Nbr1

Since the outset of this project, further roles for Nbr1 have been identified, some of which will be discussed here and others will be discussed in subsequent chapters.

1.7.6.1. Nbr1 and receptor trafficking

NBR1 (aa835-966) has been identified as an interacting partner of the Sprouty related with Ena/VASP homology 1 domain 2 (SPRED2) protein (Mardakheh et al., 2009). This interaction is dependent on the EVH1 domain of SPRED2 and SPRED2 colocalises with NBR1-positive late endosomal vesicles. Sprouty related proteins are known to inhibit ERK1/2 signalling downstream of FGF (Minowada et al., 1999) and when overexpressed with SPRED2, NBR1 further enhances SPRED2-mediated ERK1/2 inhibition. Furthermore, there was a reduction in endogenous FGF receptor 2 (FGFR2) in SPRED2 expressing cells, however, knock-down of NBR1 significantly reduced this effect. In the absence of SPRED2 there was also a reduction of FGFR2 that localised to LAMP2 positive endosomes. This data suggests that through its interaction with NBR1, SPRED2 directs activated FGF receptors to the lysosomal degradation pathway therefore inhibiting ERK1/2 signalling (Mardakheh et al., 2009). SPRED2 has also been implicated in bone formation as mice lacking functional SPRED2 display a dwarfism phenotype. This is due to increased ERK phosphorylation in FGF stimulated chondrocytes suggesting that SPRED2 negatively regulates signalling downstream of FGF to ensure correct bone formation (Bundschu et al., 2005).

Further evidence now shows that Nbr1 has a direct effect on receptor tyrosine kinase (RTK) trafficking (Mardakheh et al., 2010). Live cell imaging demonstrated that ectopic expression of Nbr1 inhibited ligand-mediated degradation of epidermal growth factor receptor (EGFR) by trapping it at the cell surface, resulting in enhanced ERK1/2 signalling. This effect was minimal when cells were pretreated with Bafilomycin A_1 suggesting the effect is due to inhibition of lysosomal degradation. Furthermore, the UBA domain is essential for inhibition of receptor degradation but not sufficient whilst both the UBA and a region 10 amino acids N-terminal of the UBA named JUBA (juxta-UBA) are important for the late endosomal

localization of Nbr1. Together with the work by Mardakheh et al 2009, this provides evidence that the normal function of Nbr1 is to inhibit receptor degradation. The interaction of NBR1 with SPRED2 alters this inhibitory function, causing enhanced receptor degradation (Mardakheh et al., 2010).

1.7.6.2. Nbr1 and T helper cell differentiation

Evidence has also come to light for the role of Nbr1 in T helper 2 (Th2) cell differentiation (Yang et al., 2010). Yang et al. generated an activated T-cell specific Nbr1-deficient mouse model that exhibited impaired lung inflammation and defective Th2 cell differentiation. They showed that in Nbr1 deficient T cells, GATA3 and NFATc1 nuclear levels are reduced but NFκB and p38 signalling was unaffected. This suggests that Nbr1 plays a role in modulating signalling pathways important for Th2 differentiation and the immune response. Cell polarity, a mechanism whereby essential regulators are located to the immunological synapse (IS) is also important for T-cell activation. Yan et al. showed that NBR1 and p62 are recruited to the IS upon T cell activation and that NBR1 recruitment is dependent on p62 whilst p62 recruitment is dependent on NBR1. Additionally, lack of NBR1 or p62 leads to a reduction in the recruitment of the cell polarity markers talin and scribble to the IS (Yang et al., 2010).

1.8. Project Aims

Nbr1 is a ubiquitously expressed scaffold protein known to be involved in the maintenance of muscle and bone. The truncated Nbr1 mouse model has identified Nbr1 as a regulator of bone mass and bone mineral density however, the molecular mechanisms by which it exerts its function are still unclear. Through its interaction with polyubiquitin and SPRED2, Nbr1 has been implicated in protein degradation and modulation of signalling pathways by regulation of receptor internalisation.

The aims of this thesis were to gain further insight into the function of Nbr1 with particular interest in the regulation of bone. This was addressed using a number of different strategies:

- Nbr1 is a scaffold protein, involved in a number of protein-protein interactions, therefore yeast-2-hybrid screens were performed using previously uncharacterised regions of Nbr1 as bait with the goal of identifying new interacting partners. Putative interactions were further validated to gain information on Nbr1 function.
- A knock-in mouse model containing the D50R mutation in Nbr1 that abolishes its interaction with p62 was analysed to investigate the role of this interaction in the regulation and maintenance of bone.
- Due to the known roles of Nbr1 in bone remodelling, genomic DNA from a cohort of individuals with idiopathic high bone mass (HBM) was sequenced to identify any sequence variation in the coding exons of *NBR1* which may be contributing to the skeletal phenotype.

Chapter 2. Materials and Methods

2.1. Molecular biology

All chemicals were obtained from Sigma and enzymes from New England Biolabs (NEB) unless otherwise stated. All buffer constituents are shown in Table 2.23 (page 112).

2.1.1. Polymerase chain reaction (PCR)

PCR was performed for cloning, screening of bacterial colonies, genotyping and patient sequencing. Pfu (Stratagene) DNA polymerase was used for cloning as it possesses 3' to 5' exonuclease proof reading activity and therefore reduces the possibility of mutations being introduced. Taq DNA polymerase (Bioline) was used for all other PCR reactions. The standard PCR reaction mix was set up as shown in Table 2.1. DNA amplification was carried out in a PTC-100 thermal cycler (MJ Research, Inc) using the standard conditions shown in Table 2.2. Primer annealing temperatures were specific for each amplicon whilst a one minute extension time was used per Kb of template.

Reagent	Volume
10x buffer (Bioline)	5 µl
Primer (100ng/µl)	2.5 µl
Primer (100ng/µl)	2.5 µl
dNTPs (10mM, Amersham)	1 µl
taq (Bioline,5U/µl)	0.5 µl
DNA (100ng plasmid or, 1µg genomic DNA)	1 µl
H_2O	37.5 µl

Table 2.1. Standard PCR reaction mix.

Step	Condition
1	95°C for 2 minutes
2	95°C for 30 seconds
3	Tm (-5°C) for 1 minute
4	72°C for 1 minute/Kb of template
5	Go to step 1 x30
6	72°C for 10 minutes

Table 2.2. Standard PCR conditions

2.1.2. Colony PCR

Bacterial colonies were picked using a pipette tip and transferred into 100 µl LB broth supplemented with appropriate antibiotic. The tip was then transferred into 40 µl of H_2O, mixed and the LB culture incubated at 37°C for 4 hours with shaking. The H_2O containing bacterial cells was boiled at 95ºC for 2 minutes, centrifuged for 5 minutes at 1500 xg and 10 µl of the resulting supernatant was used in a subsequent PCR reaction. Overnight cultures were prepared from positive clones determined from the PCR reaction and DNA extracted using a QIAprepMiniprep Kit according to manufacturer's instructions.

2.1.3. Agarose gel electrophoresis

Typically, agarose (Invitrogen) was dissolved at 1% in 1x TAE buffer (Table 2.23), 0.1 µg/ml ethidium bromide added and the gel set at room temperature in a gel former. The appropriate volume of 5x DNA sample buffer was added to each sample and loaded into the wells. An appropriate molecular marker (NEB) was loaded alongside the samples (100 bp or 1 Kb ladder). Electrophoresis was carried out at 100 V until DNA fragments had separated adequately. DNA was then visualised using a Kodak UV gel documentation system. Molecular markers of known molecular weight enabled the size of the DNA fragments to be determined. Where appropriate, DNA bands were excised from the gel using a UV light box and purified

using a QIAquick Gel Extraction Kit (250, Cat no. 28706) according to manufacturer's instructions.

2.1.4. Restriction enzyme digest

PCR product or plasmid DNA was digested using the appropriate NEB restriction enzyme and buffer. The standard reaction mixture used is shown in Table 2.3. Reactions were incubated at 37°C for between 1 and 3 hours to ensure complete digestion.

Reagent	Volume
10x appropriate buffer	3µl
DNA	1µg
10x BSA (if necessary)	3µl
restriction enzyme	5 units
H_2O	Up to 30µl

Table 2.3. Standard restriction enzyme digest

2.1.5. DNA ligation reactions

Following digestion with appropriate restriction enzymes, separation by gel electrophoresis (section 2.1.3) and gel purification using the QIAquick gel extraction kit, vector and DNA insert were ligated using the reaction mixture outlined in Table 2.4.

Reagent	Volume
T4 ligase buffer (NEB)	1µl
T4 ligase (NEB)	1µl
vector DNA (50ng/µl)	1µl
DNA insert at a molar ratios of 1:1, 1:3, 1:5 with vector	variable
H_2O	Up to 10 µl

Table 2.4. Standard ligation reaction

Reactions were incubated at 16°C for 12 hours and transformed into chemically competent bacteria as described in section 2.1.8.

2.1.6. Purification of PCR products using ExoSAP-IT

PCR product was purified using ExoSAP-IT (USB). ExoSAP-IT contains Exonuclease I which removes residual single-stranded primers and any extraneous single-stranded DNA produced during the PCR reaction and Shrimp Alkaline Phosphatase (SAP) which removes the remaining, unincorporated dNTPs from the PCR mixture. A standard reaction was set up (Table 2.5) and incubated at 37°C for 15 minutes and at 80°C for 15 minutes. 3.5 µl of reaction mix was then used in a standard sequencing reaction (Table 2.6).

Reagent	Volume
ExoSAP-IT	0.25 µl
PCR product	1 µl
H_2O	5.75 µl

Table 2.5. Standard ExoSAP-IT reaction

2.1.7. DNA sequencing

A standard sequencing reaction was set up (Table 2.6) using the Dye Terminator V3.1 cycle sequencing kit (ABI) and carried out on a PTC-100 thermal cycler (MJ Research) using the cycling conditions in Table 2.7.

Reagent	Volume
Big dye mastermix	0.25 µl
5x sequencing buffer	1.25 µl
Primer (100ng/µl)	0.25 µl
DNA (0.5µg/µl)	1 µl
H_2O	3.25 µl

Table 2.6. Standard sequencing reaction

The following programme was used for the sequencing reaction (Table 2.6):

Step	Condition
1	96°C for 30 seconds
2	48°C for 30 seconds
3	60°C for 4 minutes
4	Go to step 1 x20

Table 2.7. Standard sequencing programme

DNA was precipitated in 25 µl 95% ethanol and 1 µl 3M NaOAc per sequencing reaction. Samples were then centrifuged at 1500 xg for 30 minutes at 4°C and the supernatant removed. 100 µl of 70% ethanol was added to each sample to wash the DNA and the sample was again centrifuged at 1500 xg for 15 minutes at 4°C and the supernatant removed. The pellet was air dried and resuspended in 10 µl of HiDi (ABI). Sequencing was performed on an ABI 3730xl, 96 capillary sequencer according to manufacturer's instructions.

2.1.8. Preparation and transformation of chemically competent bacteria

DH5α bacterial cells were streaked onto LB agar (Table 2.23) and incubated at 37°C overnight. The following day, one colony was used to inoculate 30 ml of LB broth (Table 2.23) and incubated overnight at 37°C with shaking at 180 rpm. 100 ml of LB broth (Table 2.23) was inoculated with 1 ml of overnight culture and incubated at 37°C, shaking at 180 rpm for 2-4 hours until the OD_{550} reached 0.48. The OD_{550} was measured in a 6300 Spectrophotometer (Jenway). The bacteria were then incubated on ice for 15 minutes and centrifuged at 1500 xg for 10 minutes at 4°C. The supernatant was discarded and cells resuspended in 40ml of ice cold TfbI buffer (Table 2.23). The bacteria were again incubated on ice for 15 minutes and centrifuged at 2500 xg for 10 minutes at 4°C. The supernatant was discarded and 4ml of TfbII buffer (Table 2.23) was used to resuspend the bacteria. The bacteria were then incubated on ice for a further 15 minutes, separated into 50 µl aliquots and frozen on dry ice before being stored at –80°C.

One aliquot of chemically competent bacteria was thawed on ice for each sample of DNA transformed. 5 ng of DNA was added to each vial and mixed gently by

tapping. Cells were then incubated on ice for 30 minutes, heat shocked at 42°C for 30 seconds then placed on ice for a further 2 minutes. 250 µl of pre-warmed LB broth (Table 2.23) was added to the bacteria and the bacteria were incubated at 37°C for 1 hour, shaking at 180 rpm. Between 20 µl and 200 µl of each transformation was plated onto LB agar containing appropriate antibiotic (50 µg/ml). The plates were inverted and incubated at 37°C overnight. Plasmids were then extracted from cells using the TENS method (section 2.1.10) or a QIAprep Miniprep Kit (Cat no. 27106) or High Speed Maxi Kit (Cat no. 12662) according to manufacturer's instructions. The nucleic acid concentration was determined using a Nanodrop 1000 spectrophotometer (Thermo Fisher Scientific).

2.1.9. Preparation and transformation of electrocompetent bacteria

DH5α bacterial cells were cultured on LB agar (Table 2.23) as in section 2.1.8. 10 ml of LB broth was then inoculated with one colony and incubated overnight at 37°C, shaking at 180 rpm. The overnight culture was used to inoculate 1 L of LB broth and incubated at 37°C, shaking at 180 rpm for 2-4 hours until the OD_{600} reached 0.5. The OD_{600} was measured in a 6300 Spectrophotometer (Jenway). Bacteria were chilled on ice and centrifuged at 1500 xg for 15 minutes at 4^{o}C. The supernatant was discarded and cells resuspended in original volume of ice cold 10% glycerol, 1mM Hepes (pH7). Bacteria were then centrifuged at 1500 xg for 15 minutes at 4°C. This was repeated twice more. The bacteria were then resuspended in 1/50 original volume of ice cold 10% glycerol and centrifuged at 1500 xg for 15 minutes at 4°C. The bacteria were then resuspended in 1/500 original volume of 10% glycerol. Cells were then divided into 50 µl aliquots, frozen on dry ice and stored at –80°C.

One aliquot of bacteria was thawed on ice per DNA sample to be transformed. 5 ng of DNA was transferred to a pre-chilled 0.2 cm electroporation cuvette (Biorad) and the thawed bacteria added to the DNA and gently mixed by tapping. The cuvette was then placed into the Biorad gene pulser II electroporator and bacteria electroporated at 2.5 kV; 25 capacitance; 200 low range; 500 high range. 200 µl of LB broth (Table 2.23) was then added and bacteria were incubated at 37°C, shaking

at 180 rpm for 1 hour and subsequently plated onto LB agar (Table 2.23) containing appropriate antibiotic (50 µg/ml). Plates were inverted and incubated at 37°C overnight. Plasmids were then extracted from cells using the TENS method (section 2.1.10) or a QIAprep Miniprep Kit according to manufacturers instructions. The nucleic acid concentration was determined using a Nanodrop 1000 spectrophotometer (Thermo Fisher Scientific).

2.1.10. TENS preps

LB broth (5 ml) containing the appropriate antibiotic was inoculated with one successfully transformed bacterial colony and incubated overnight at 37°C, shaking at 180 rpm. 1.5 ml of the overnight culture was centrifuged at 16000 xg for 30 seconds. The majority of the supernatant was removed, leaving 50-100 µl in the tube. The tube was briefly vortexed to resuspend the cell pellet and then 300 µl of TENS buffer (Table 2.23) and 150 µl 3M NaAc (pH 5.2) was added to each sample and vortexed briefly to precipitate the protein. The sample was then centrifuged at 16000xg for 5 minutes to pellet the cell debris. The supernatant was transferred to a new tube and 0.9 ml 100% ice cold ethanol added to precipitate out the nucleic acid. The samples were centrifuged for 10 minutes at 16000 xg, the supernatant discarded and the pellet washed in 0.5 ml 70% ethanol and centrifuged at 16000 xg for 10 minutes. The supernatant was again removed and the pellet air dried and then dissolved in 100 µl H_2O and stored at –20^{o}C.

2.1.11. DNA extraction from mouse ear clippings

Tail buffer (500 µl) (Table 2.23) was added to each ear clipping and incubated overnight at 50°C. Resulting digested tissue was centrifuged at 16000 xg for 10 minutes and the supernatant transferred to a new tube. 500 µl of phenol:chlorophorm:isoamylalcohol (25:24:1) was added to the supernatant, vortexed and centrifuged for 20 minutes at 13,000 rpm. The resulting aqueous layer was transferred to a new tube and DNA was precipitated with 500 µl isopropanol. DNA was then centrifuged at 16000 xg for 30 minutes and washed with 500 µl 70% ethanol. The DNA pellet was air dried and resuspended in 20 µl H_2O. The genotype of the mutant mice (generation of the mice is detailed in section 2.4) was then

determined using PCR (section 2.1.1) to amplify exons 3 and 4a and intron 3 of Nbr1 and a StuI restriction digest (section 2.1.4) to distinguish between WT and the D50R mutant. Mutant DNA had been engineered to contain a StuI restriction site, therefore upon restriction digest with StuI, two bands of 1134bp and 334bp could be visualised by gel electrophoresis (section 2.1.3) whereas the WT DNA could not be digested by the StuI enzyme and was visualised as a single band of 1470bp (see section 5.2). Primers utilized for genotyping are shown in Table 2.8.

Primer Name	Primer Sequence
Intron2F7CW	GCATTGAATCCCCAGCATCA
Intron4aR1	ACTATGAAGTCCAGAGTGCC

Table 2.8. Genotyping primer sequences. Exons 3 and 4a and intron 3 of Nbr1 was amplified using these primers.

2.1.12. Primers used for high bone mass patient sequencing of NBR1

Primers were designed to have a melting temperature (T_m) of between 60 and 64°C. A at T were predicted to have a T_m 2°C and G and C were predicted to have a T_m of 4°C. Where possible, primers started and ended in C or G.

Exon	PCR Primers & sequencing primer	PCR primer annealing temp (°C)	PCR $MgCl_2$ conc. (mM)	PCR Product size (bp)
1	**1F1:**GGGACAAGTGGTGAGAGCC **1R2:**GATTAGCTGTCCCGAAACACG **1F1:**GGGACAAGTGGTGAGAGCC (sequencing)	55.4	1.5	294
2	**2F1b:**CCCATATTGGGTCCTCACAAG **2R1b:**GTTGGTTCCCTTTATTGGGGC **2F1b:**CCCATATTGGGTCCTCACAAG (sequencing)	54	1	409
3	**3F1:**CTGGGTTGTTAATTGTATCATTAG **3R1:**CAGTGTTGCTTCTCCATTTCTC **3R2seq:**CTCAGATGCTGCAAGTC (sequencing)	63.2	1	433
4	**4F1:**CTAGCAAGTGATATGGAAAAGC **4R1:**GGACTGGCATCTTAAATATGAG **4F1:**CTAGCAAGTGATATGGAAAAGC (sequencing)	55	1.5	488

5	**5F1:**CAGTCCATCTTTAGGATTGGC **5R1:**GTGAAGACTGCAGCAACCCC **5F1:**CAGTCCATCTTTAGGATTGGC (sequencing)	55.4	2	320
6	**6F1:**CATAACTTACCACACTCTTCTG **6R1:**GCACATTCTGCACATGTATCTC1 **63F1:**CATAACTTACCACACTCTTCTG (sequencing)	55	1.5	420
7	**7F21:**GTACGCCTTCATACTGTGAC **7R21.5:**CTCTTCACCGGTACTAGAGG **74R1seq:**CAGCAGCCACCTGGGTTC (sequencing)	55	2	329
8	**8F11c:**GGGACAACTCTCTGCTTGAG **8R1c:**CTATCACTAGCTAGCTACTCC **8F1:**CTGTCTATTCAGTAGCAGTTG **8R1c:**CTATCACTAGCTAGCTACTCC (sequencing)	62.2	4	500
9	**9F1c:**GGCCCCATGTACTTTCACATC **9R1c:**GCAGAACTAAGGAGACTATCTG **9F1:**CATAGAAGTATGGTCTTATATC (sequencing)	55.4	1	509
10	**10F1c:**TGGAAGGGAGCCATGATTAG **10R1c:**TTCAGAGAGCTGGGCCTAAA **10F1c:**TGGAAGGGAGCCATGATTAG (sequencing)	61.7	4	442
11/12	**1112F1:**CAGACTCTCAAGCTAGTGTG **1112R1:**GCCAAATATCAGCATAGAGATG **1112F1:**CAGACTCTCAAGCTAGTGTG **12F1seq:**GATGAGGTGATTTGAAGTGGC (sequencing)	57.4	3	784
13	**13F1:**GTCAGCCTGCCTCTTCAGTT **13R1:**CTTGCTTCCATGGGTGATCTC **13F1:**GTCAGCCTGCCTCTTCAGTT (sequencing)	59.7	2	369
14	**14F1:**GAAATGGTCTACAGGTCCCAT **14R1:**CTCAAGTGATCCTCCTGCCT **14R2seq:**TTATAGACACGAGCCACCATA (sequencing)	57	1.5	402
15/16	**1516F1:**CTTCTGGACACTGACTGTTG **1516R1:**GTCTCAGTGAAGAAGAGCAC **1516F1:**CTTCTGGACACTGACTGTTG **1516R1:**GTCTCAGTGAAGAAGAGCAC (sequencing)	54	2	791
17	**17F1:**GATCCACAAGGCTTTACCAAG **17R1:**CCATAGCAAAGTCTGAATTTAG **17F1:**GATCCACAAGGCTTTACCAAG	57	1.5	658

	(sequencing)			
18	**18F1b:**GTAGCCCTTATGATGGAACCC **18R1b:**CAGGTTCATGTGATTCTCCTGC **18F1b:**GTAGCCCTTATGATGGAACCC (sequencing)	64	1	580
19	**19F1:**GCCTCAATAATAGCCTTGCTG **19R1:**CAGAACACTCTTAAACATCAGC **19F1:**GCCTCAATAATAGCCTTGCTG (sequencing)	58.1	4	320
20	**20F1:**GCTTGCACCAGTAGAGCTG **20R1:**CACAATGCCATGTTACTCTTC **20F2seq:**CATGATCTGTAGCTATAAAGC (sequencing)	61.1	2	401
21	**21F1:**GAGTGCCATAGCCTTGAATCT **21R1:**AGTTCTGGTCTTTAGTTTGCTC **21R2seq:**CGATGGGCTCTATACAGATTC (sequencing)	58.1	1.5	503

Table 2.9. Primers used for HBM patient DNA amplification and sequencing. Exon 1 corresponds to exon 1b of NBR1 which is out of the coding region of the protein but is included in the predominant NBR1 transcript.

2.2. Protein methods

2.2.1. SDS-Polyacrylamide gel electrophoresis (SDS-PAGE)

A Biorad Mini-PROTEAN Tetra System was used to prepare appropriate resolving and stacking gels (Table 2.10) for the separation of proteins according to their size. Where appropriate, a gradient gel was prepared ranging from 5% to 20% acrylamide using gradient forming apparatus (Table 2.11). SDS sample buffer (Table 2.23) was added to the protein samples, heated for 5 minutes at 95°C and loaded onto the gel along with 10 µl of known molecular weight protein markers (Amersham rainbow markers). Electrophoresis was performed at 100 V for 2 hours at room temperature in 1 x SDS PAGE running buffer (Table 2.23).

Constituent	Resolving Gel			Stacking Gel
	6%	10%	15%	5%
1.5M Tris (pH 8.8)	7.6 ml	7.6 ml	7.6 ml	-
1M Tris (pH 6.8)	-	-	-	1.25 ml
20% SDS	150 µl	150 µl	150 µl	50 µl
H2O	17.4 ml	14.5 ml	11.25 ml	7.3 ml
40% Acrylamide	4.5 ml	7.5 ml	10.69 ml	1.3 ml
10% APS	300 µl	300 µl	300 µl	100 µl
Temed	12 µl	12 µl	12 µl	10 µl

Table 2.10. SDS PAGE gel constituents. This makes up to three small (8.3cmx7.3cm) gels, 1.5mm thick.

Constituent	5% Resolving Gel	20% Resolving Gel
40% Acrylamide	2 ml	8 ml
1M Tris (pH8.8)	5.6 ml	5.6 ml
20% SDS	75 µl	75 µl
Glycerol	0.45 g	3 g
H_2O	7.95 ml	-

Table 2.11. Gradient SDS PAGE gel constituents. This makes one small (8.3cmx7.3cm) gel, 1.5mm thick.

2.2.2. Western blot analysis and enhanced chemiluminescence (ECL)

A Biorad mini trans blot system was used to transfer the proteins from the SDS polyacrylamide gel onto a PVDF membrane (Millipore) which was prepared according to manufactures instructions. Protein transfer was performed in 1 x transfer buffer (Table 2.23) at 100 V for 2 hours at room temperature or at 25 volts overnight at 4°C.

The membrane was blocked in 5% milk, 0.1% Tween 20/PBS for 1 hour with gentle shaking followed by a brief wash with 1% milk/PBS. The membrane was then incubated with the appropriate primary antibody (Table 2.16) diluted in 1% milk/PBS for 1 hour at room temperature with gentle shaking then subsequently washed three times for 5 minutes and once for 15 minutes in 1% milk/0.1%

Tween/PBS. The appropriate secondary antibody (Table 2.17) was applied to the membrane, diluted in 1% milk/0.1% Tween/PBS and incubated at room temperature for 1 hour. The membrane was again washed three times for 10 minutes and once for 15 minutes in 1% milk/0.1% Tween/PBS. Amersham Western Blotting Detection Reagent Kit (RPN2209) was used to detect proteins using ECL. The proteins were then visualised using Fuji X-ray film on a Laser 4S developer (IGP Ltd). Where appropriate, protein levels were estimated by quantifying the protein band intensity using ImageJ and normalising to the β-actin control.

2.2.3. Coomassie staining of polyacrylamide gels

Polyacrylamide gels were prepared and run as in section 2.2.1. The gel was then incubated in coomassie stain (National Diagnostics) (Table 2.23) for 1 hour with shaking at room temperature before being de-stained for 4 hours and visualised on a light box.

2.2.4. Recombinant protein induction

Chemically competent BL21 bacteria (Stratagene) were transformed with appropriate cDNA constructs (Table 2.12) and plated onto LB agar (Table 2.23) containing ampicillin or kanamycin (50 µg/ml). Single colonies were cultured overnight in 20 ml of LB broth at 37°C with shaking and then subcultured 1:10 into 100 ml LB broth (Table 2.23) containing appropriate antibiotic (50 µg/ml) and incubated for 1 hour at 37°C with shaking. Protein expression was then induced using IPTG at a final concentration of 1 mM and cultures incubated for a further 3-4 hours with shaking at 37°C. Cells were then centrifuged at 1500 xg for 15 minutes the supernatant removed and cell pellet stored at -20°C.

Name	Species	Residues and template origin	Restriction enzymes	Vector and antibiotic resistance	Source
GST-Osteocalcin	Mouse	1-95 (Yeast clone)	BamHI & EcoRI	pGEX2T (ampicillin)	K. Marchbank
GST-Pro-	Mouse	24-95	BamHI &	pGEX2T	K. Marchbank

osteocalcin		(Yeast clone)	EcoRI	(ampicillin)	
GST-Mature osteocalcin	Mouse	46-95 (Yeast clone)	BamHI & EcoRI	pGEX2T (ampicillin)	K. Marchbank
GST-Cystatin C	Mouse	26-140 (Mouse liver cDNA)	BamHI & EcoRI	pGEX2T (ampicillin)	K. Marchbank
GST-Nbr1-novel	Mouse	346-498 (HA-Nbr1 construct)	EcoRI	pGEX2T (ampicillin)	K. Marchbank
GST-Nbr1-UBA	Mouse	919-988 (Nbr1 cDNA in bluecript vector)	Bam	pGEX2T (ampicillin)	C. Whitehouse
GST-Nbr1aa1-135	Mouse	1-135 (Nbr1 cDNA in bluecript vector)	BamHI & EcoRI	pGEX2T (ampicillin)	C. Whitehouse
GST-NBR1-A	Human	486-903 (HA-NBR1)	XhoI & BamHI	GST2C (ampicillin)	S. Waters
GST-NBR1-B	Human	681-903 (HA-NBR1)	XhoI & BamHI	GST2C (ampicillin)	S. Waters
GST-NBR1-C	Human	737-903 (HA-NBR1)	XhoI & BamHI	GST2C (ampicillin)	S. Waters
GST-NBR1-D	Human	729-775 (HA-NBR1)	XhoI & BamHI	GST2C (ampicillin)	S. Waters
His-LC3	Human	Full length, cleaved (LC3-YFP construct)	XhoI & BamHI	PET6H (ampicillin)	S. Waters
His-MAP1B-LC1	Mouse	2227-2464 (Mouse brain cDNA)	XhoI & BamHI	PET6H (ampicillin)	K. Marchbank

Table 2.12. Constructs made for binding assays. The cloning strategy for each construct is shown detailing the template used for insert amplification, restriction sites, vector and antibiotic resistance. Vector maps are shown in Appendix A.3. PET6H and GST2C vectors were modified and kindly provided by M. Gautel.

2.2.5. Purification of recombinant GST tagged proteins

Bacterial cell pellets were thawed on ice and resuspended in 10 ml TEDG buffer (Table 2.23) per 200 ml original culture volume and incubated with 500 µl of lysozyme (10 mg/ml) for 30 minutes at room temperature with rocking. Samples were then sonicated three times at 4°C for 30 seconds with 30 second intervals and 1 ml 10% Triton x100 added. Following incubation for 30 minutes on ice, the resulting cell lysate was centrifuged for 30 minutes at 1500 xg at 4°C. The supernatant (soluble fraction) was removed and incubated with 5 ml NETN buffer (Table 2.23) and 500 µl of a 50% glutathione sepharose (GST) bead slurry (Sigma) for 2 hours at 4°C with end-over-end rotation. Beads were then washed three times with 5 ml H buffer (Table 2.23) and stored at 4°C in PBS containing 2mM azide and protease inhibitors. An aliquot was run on an SDS PAGE gel (section 2.2.1) and proteins visualised using coomassie stain (section 2.2.3) and where appropriate, protein concentrations were estimated.

2.2.6. Purification of histidine tagged MAP1B-LC1

Bacterial cell pellet (from 500 ml culture) was resuspended in 20 ml of lysis buffer (Table 2.23). 5 ml of lysozyme (5mg/ml) was added to the sample and incubated for 30 minutes at room temperature with rocking then sonicated three times for 30 seconds with 30 second intervals. The resulting cell lysate was centrifuged for 30 minutes at 1500 xg at 4°C and the supernatant transferred to a new tube. 1 ml of a 50% Ni Sepharose 6 Fast Flow bead slurry (Amersham Biosciences 17-5318-02) was added to the supernatant and incubated for 2 hours at 4°C with end-over-end rotation. Beads were then washed three times with 2 ml of low elution buffer (Table 2.23) and five times with 2 ml high elution buffer (Table 2.23). Fractions from the high elution buffer were combined and dialysed overnight at 4°C into dialysation buffer (Table 2.23). The dialysed proteins were then stored at -80°C in 2mM azide until further use.

2.2.7. Purification of histidine tagged LC3

Bacterial cell pellets (from 100 ml culture) were resuspended in 5 ml of Buffer A (Table 2.23) then sonicated twice for 10 seconds at 4°C. 5 ml of lysozyme (5mg/ml) was added and the lysate was made up to 35 ml with Buffer A (Table 2.23). The contents of one 20 ml Talon single step column purification (Clontech) were added and the sample rotated at 4°C overnight. The sample was then centrifuged for 5 minutes at 700 xg, 4°C and the unbound supernatant was retained for later analysis. The pink resin was washed six times in 20ml of Buffer B (Table 2.23) for 5 minutes. The protein was eluted from the column in 2 x 3ml of Buffer C (Table 2.23) (rotating in Buffer C at 4°C for 10 minutes, for each elution). Washes and elutions were dialysed in PBS with 10% glycerol overnight at 4°C and the frozen at -70°C. This method was carried out by Dr Sarah Waters (KCL).

2.2.8. Pulldown of YFP-LC3 by GST-NBR1

NBR1-A 486-903aa, NBR1-B 681-903aa, NBR1-C 737-903aa and NBR1-D 729-775) were cloned into pGST2C vector (Table 2.12). YFP-LC3 (a kind gift from Marco Sandri, Padova, Italy) was transfected into COS-7 cells that had previously been seeded into 6-well culture dishes (section 2.5.2). Cells were lysed after 24 hours in 400µl IP lysis buffer 1 (Table 2.23) per well for 20 minutes on ice. Lysate was centrifuged at 16000 xg for 10 minutes at 4°C and then incubated with 3 µg GST only, GST-NBR1–A, GST-NBR1-B, GST-NBR1-C or GST-NBR1-D for 2 hours at 4°C. Beads were then washed three times with 1 ml IP wash buffer 1 (Table 2.23) and bound proteins resolved by SDS PAGE and proteins visualised using a mouse monoclonal antibody that recognises GFP and YFP (Table 2.16). This method was carried out by Dr Sarah Waters (KCL).

2.2.9. Pulldown of MAP1B-LC1-myc by GST-Nbr1

The novel region of Nbr1 (aa346-498) was cloned into the pGEX2T vector (Table 2.12) and MAP1B-LC1 (aa2216-2464) was cloned in to the pcDNA3.1 vector (Table 2.15). GST-tagged recombinant proteins were expressed and purified as described in sections 2.2.4 & 2.2.5. MAP1B-LC1-myc was transfected (section 2.5.2) into COS-

7 cells that had previously been plated into 6-well culture dishes (using Fugene 6, Roche). Cells were lysed after 24 hours in 200 µl (per well of cells) IP lysis buffer 2 (Table 2.23). Lysate was centrifuged at 13,000 xg for 10 minutes at 4°C and incubated with GST only, GST-Nbr1-novel, GST-Nbr1-UBA or GST-Nbr1-aa1-135 (Table 2.12) at 4°C for 2 hours with end-over-end rotation. Beads were washed three times with IP wash buffer 2 (Table 2.23) and bound proteins resolved by SDS PAGE then visualised using a mouse monoclonal antibody (9E10) that recognises the myc tag (Table 2.16).

2.2.10. Pulldown of HA-Nbr1 by GST-osteocalcin and GST-cystatin C

Fragments of osteocalcin and cystatin C were cloned in to the pGEX2T vector (see Table 2.12) and GST-tagged recombinant proteins were expressed and purified as described in section 2.2.5 HA-Nbr1 was transfected into COS-7 cells that had previously been plated into 6-well culture dishes (using Fugene 6, Roche). Cells were lysed after 24 hours in 200 µl (per well of cells) lysis buffer 1 (Table 2.23). Lysate was centrifuged at 16000 xg for 10 minutes at 4°C and subsequently incubated with the GST-tagged purified proteins at 4°C overnight with end-over-end rotation. Beads were washed three times with 1ml IP wash buffer 1 (Table 2.23) and bound proteins resolved by SDS PAGE, Western blotted and probed with a rat polyclonal antibody that recognises the HA tag (Table 2.16).

2.2.11. Recombinant His-tagged LC3 binding assay

GST binding assays were performed as in section 2.2.8 but incubated with His-tagged LC3 (cleaved form) in IP buffer 1 (Table 2.23) for 2 hours at 4°C. Beads were washed three times with 1ml of wash buffer (Table 2.23) and bound proteins resolved by SDS PAGE, Western blotted and probed with an antibody that recognises LC3 (Table 2.16). This method was carried out by Dr Sarah Waters (KCL).

2.2.12. Recombinant His-tagged MAP1B-LC1 binding assay

GST binding assays were performed as in section 2.2.10 but incubated with His-tagged MAP1B-LC1 in IP buffer 2 (Table 2.23) for 2 hours at 4°C. Beads were washed three times in 1 ml of IP lysis buffer 2 (Table 2.23) and bound proteins resolved by SDS PAGE, Western blotted and probed with a mouse monoclonal antibody that recognises the His tag (Table 2.16).

2.2.13. Coimmunoprecipitation

For MAP1B-Nbr1 coimmunoprecipitation, COS-7 cells were seeded and transfected with HA-Nbr1 and MAP1B-LC1-myc as in section 2.4.2 and for Nbr1-p62 coimmunoprecipitation, mouse embryonic fibroblasts (MEFs) were prepared as in section 2.4.4 and seeded into 6-well tissue culture dishes. Both cell types were grown to 90% confluency and lysed in 200 µl IP lysis buffer 2 (Table 2.23) and the lysate centrifuged at 16000g for 10 minutes at 4°C. Lysate was then precleared with appropriate species of IgG and 40 µl of protein A beads (50% slurry-Millipore). Supernatant was removed and incubated with the appropriate antibody (Table 2.16) overnight at 4°C with end-over-end rotation (Table 2.13)

Tube	Components
1	MEFs cell lysate + anti-p62 antibody (mouse monoclonal)
2	MEFs cell lysate only
3	MEFs cell lysate + non specific antibody (anti-myc mouse monoclonal)
4	COS-7 cell lysate + anti-myc (A-14) antibody
5	COS-7 cell lysate only
6	COS-7 cell lysate + rabbit IgG

Table 2.13. Conditions for coimmunoprecipitation.

The following day, 40 µl of protein A beads (50% slurry) was added to each sample and incubated for a further 2 hours at 4°C with end-over-end rotation. Beads were then washed three times with 1 ml IP lysis buffer 2 (Table 2.23) and bound proteins

resolved by SDS PAGE, Western blotted and membranes probed with appropriate antibodies (Table 2.16).

2.3. Yeast-two-hybrid methods

The GAL4 Two-Hybrid System 3 was used for the yeast-2-hybrid screens. This technique can identify any proteins that interact with a protein of interest. A pretransformed 7 day old mouse calvaria cDNA library (cloned into the pGADT7 vector) was kindly supplied by Prof. Ikramuddin Aukhil (College of Dentistry, University of Florida) in the AH109 yeast strain. The bait constructs; murine Nbr1 aa355-694, and Nbr1 aa495-924 were cloned by Dr Caroline Whitehouse (Department of Medical and Molecular Genetics). Nbr1 aa346-498 was cloned into the pGBKT7 (kanamycin) vector using the EcoRI and SalI restriction sites and the HA-Nbr1 construct as a template for insert amplification. Y187 and AH109 yeast strains were streaked onto YPDA agar and incubated at 30°C for 3-4 days.

2.3.1. Phenotyping yeast strains

The yeast strains used for the yeast-2-hybrid assay (Y187 & AH109) are auxotrophic for leucine, tryptophan, histidine and adenine. In order to verify this phenotype, YPDA medium (50 µl) was inoculated with one yeast colony from each strain and vortexed to disperse cells. 100µl was then plated onto SD/-leucine, SD/-tryprophan, SD/-histidine, SD/-adenine and SD/-uracil agar and incubated at 30°C for 4 days.

2.3.2. Production and transformation of chemically competent yeast

Several 2-3mm colonies from Y187 and AH109 were used to separately inoculate 1ml of YPDA medium (Table 2.23) and vortexed to disperse cells. Cells were transferred to a sterile flask containing 50ml of YPDA medium (Table 2.23) and incubated for 16-18 hours at 30°C, shaking at 250 rpm until the OD_{600} reached >1.5. YPDA (300 ml) was then inoculated with the overnight culture to an OD_{600} of 0.2-0.3. Cells were incubated at 30°C, 250 rpm until the OD_{600} reached 0.5 ± 0.1 (2-4 hours). The OD_{600} was measured in a 6300 Spectrophotometer (Jenway). Cells were subsequently centrifuged at 1000 xg for 5 minutes at room temperature. The

supernatant was discarded and cells resuspended in 30 ml sterile H_2O. Cells were again centrifuged at 1000 xg for 5 minutes at room temperature, supernatant discarded and cells resuspended in 1.5 ml 1x TE/LiAC.

To transform, 1 µg of each DNA construct was mixed with 0.1 mg of herrings testes carrier DNA. The appropriate chemically competent yeast strain (0.1 ml) was added and vortexed, followed by the addition of 0.6 ml of PEG/LiAc solution. Cells were incubated at 30°C for 30 minutes shaking at 200 rpm. DMSO (70 µl) was added and gently mixed. Cells were heat shocked at 42°C for 15 minutes, chilled on ice for 2 minutes and centrifuged at room temperature for 5 seconds at 16000 xg. The supernatant was removed and cells resuspended in 0.5 ml 1x TE. Cells were plated on either SD/-leucine or SD/-tryptophan depending on the construct being transformed. The pGBKT7 vector contains the tryptophan gene and the pGADT7 vector contains the leucine gene, therefore, successfully transformed yeast will grow in the absence of these amino acids. Successfully mated yeast will grow in the absence of both these amino acids.

2.3.3. Preparation of yeast for protein extraction

One large colony from each of the transformed yeast plates and untransformed Y187 was used to inoculate 5ml of appropriate SD or YPDA medium respectively (Table 2.23). The inoculated medium was vortexed and incubated for 16-18 hours at 30°C with shaking (250 rpm). For each clone to be assayed, 50 ml of YPDA medium (Table 2.23) was separately inoculated with the entire overnight culture. Cells were incubated at 30°C, with shaking at 250 rpm until the OD_{600} reached between 0.4 and 0.6 (4-8 hours). The OD_{600} units were then calculated (OD_{600} x total culture volume). The culture was immediately poured into a centrifuge tube half filled with ice to chill the cells. The cells were then centrifuged at 1000 xg for 5 minutes at 4°C. The supernatant was discarded and the cell pellet resuspended in 50ml ice cold H_2O. The cells were again centrifuged at 1000 xg for 5 minutes at 4°C, the supernatant discarded and the pellet frozen on dry ice and stored at –80°C until required for protein extraction.

2.3.4. Yeast protein extraction (urea/SDS method)

Cracking buffer (Table 2.23) was prewarmed to 60°C. The cell pellets were immediately thawed by adding 100 µl of cracking buffer (Table 2.23) per 7.5 OD_{600} units and the cell suspension transferred to a 1.5ml microcentrifuge tube containing 80 µl of glass beads per 7.5 OD_{600} units of cells. Each sample was heated at 70°C for 10 minutes and vortexed vigorously for 1 minute. Cell debris and unbroken cells were pelleted by centrifugation at 16000 xg for 5 minutes at room temperature. The resulting supernatant was transferred to a new microcentrifuge tube and placed on ice (first supernatant). The tubes containing the cell debris were then heated at 100°C for 5 minutes, vortexed vigorously and centrifuged at 16000 xg for 5 minutes at room temperature. The resulting supernatant was combined with the corresponding first supernatant. Samples were briefly heated at 95°C for 1 minute and stored at –80^{o}C, ready to be analysed by SDS PAGE and Western blot using an antibody that recognises the GAL4 binding domain (BD) (Table 2.16).

2.3.5. Small scale yeast matings

Yeast matings were prepared between yeast strains expressing constructs in Table 2.14. One large colony (~3mm) from each transformed yeast plate were mated together by inoculating 0.5 ml of 2 x YPDA medium (Table 2.23) and incubating for 20-24 hours with shaking (200 rpm). Each mating culture was then diluted 1:10 with 0. 5ml YPDA medium (Table 2.23) and 30 µl spread onto SD minimal agar: SD/-leucine-tryptophan; triple drop-out media (TDO) - SD/-leucine-tryptophan-histidine supplemented with 1 mM, 3 mM, 5 mM, 8 mM and 15 mM 3-amino-1,2,4-triazole (3-AT) and quadruple drop-out media (QDO) - SD/-leucine-tryptophan-histidine-adenine. Plates were then incubated at 30°C for 3-4 days.

AH109 Strain	Y187 Strain	
pGADT7	pGBKT7	Negative control
pGADT7	pGBKT7-Nbr1 aa355-694	Check for autoactivation
pGADT7	pGBKT7-Nbr1 aa495-924	Check for autoactivation
pGADT7	pGBKT7-Nbr1 aa346-498	Check for autoactivation
pGADT7-T-antigen	pGBKT7-p53	Positive control

Table 2.14. Constructs used in small scale yeast matings

2.3.6. Large scale pretransformed yeast-2-hybrid library screen

SD/-tryptophan medium (50 ml) (Table 2.23) was inoculated with one large colony of Y187 expressing the appropriate Nbr1 bait construct. This was incubated at 30°C for 16-18 hours, shaking at 250 rpm until an OD_{600} of >0.8 was reached. The culture was centrifuged at 1000 xg for 5 minutes, the supernatant removed and the cell pellet resuspended in the residual liquid by vortexing.

The pretransformed library culture (1 ml) was thawed at room temperature in a water bath and gently vortexed. A 10 µl aliquot was transferred into a microcentrifuge tube and kept on ice for later library titration. 2 x YPDA medium (45 ml) (Table 2.23) containing kanamycin was inoculated with both the pretransformed library and the bait culture in a 2L flask. The culture was incubated at 30°C for 24 hours with shaking at 30 rpm and then centrifuged at 1000 xg for 10 minutes at room temperature. The supernatant was removed and the cells resuspended in 100ml of 2 x YPDA medium (Table 2.23). Cells were centrifuged again for 10 minutes at 1000 xg at room temperature. The supernatant was discarded and the cells resuspended in 10ml of 0.5x YPDA medium (Table 2.23) containing kanamycin. The total volume of cells and medium was noted.

100µl of a 1:10000, 1:1000, 1:100 and 1:10 dilution of the mating mixture was spread onto SD minimal agar SD/-leucine; SD/-tryptophan; SD/-leucine-tryptophan to calculate mating efficiency (section 2.3.7). The remaining mating mixture was spread in 200 µl aliquots onto 50 150 mm petri dishes containing TDO media and 3 mM 3-AT. Plates were incubated at 30°C for 3-8 days until colonies were visible.

Colonies were picked and re-plated onto TDO containing 3 mM and 6 mM 3-AT and incubated at 30°C for 3-11 days. Colonies were then re-plated a further three times to remove multiple AD/library plasmids.

2.3.7. Library titration and calculating mating efficiency

The 10µl aliquot of the library that was retained in section 2.3.6 was transferred to 1ml of YPDA medium (Table 2.23) containing kanamycin and vortexed gently (Dilution A). 10µl of this dilution was removed and added to 1 ml YPDA medium (Table 2.23) containing kanamycin and gently vortexed (Dilution B). 10 µl of Dilution A was added to 50µl of YPDA medium (Table 2.23) containing kanamycin (Dilution C) and the entire mixture was spread onto SD/-leucine (Table 2.23). 50 µl and 100 µl of dilution B were spread separately onto SD/-leucine (Table 2.23) plates. Plates were incubated at 30°C for 3-5 days. The number of colonies on each plate was then counted and the titration value calculated:

No. viable colonies (cfu)/ml) = (cfu x 1000µl/ml)/ (volume plated (µl) x dilution factor)

No. clones screened = No. cfu/ml of diploids x resuspension volume

2.3.8. Extraction of plasmids from yeast cells

A 1cm^2 patch of each yeast colony was scraped from the plates and vortexed in 200µl of H_2O. 200 µl of lysis solution (Table 2.23) was added, vortexed vigorously and 400 µl of phenol:chloroform: isoamyl (25:24:1) and a spoonful of glass beads were added and vortexed vigorously for 1 minute. Each sample was centrifuged at 13000rpm for 20 minutes at room temperature. The resulting aqueous layer was transferred to a new microcentrifuge tube and 800 µl of absolute ethanol and 1.5 µl 3M NaAc added to precipitate the DNA. Samples were then incubated at –20°C for 1 hour and centrifuged at 16000 xg for 20 minutes at room temperature. The supernatant was removed and 0.5ml 70% ethanol added to the DNA pellet, mixed and spun at 16000 xg for 10 minutes at room temperature. The supernatant was again removed and the pellet left to air dry. 20 µl of H_2O was added and the samples

stored at –20°C. 1 µl was used to transform the plasmid into electrocompetent cells (section 2.1.9). Bacteria were plated onto LB agar (Table 2.23) supplemented with ampicillin to select for those containing the pGADT7 vector and thus the ampicillin resistance gene. Plasmids were then extracted from transformed cells using the TENS method (section 2.1.10) and sequenced (section 2.1.7) using the T7 primer (TAATACGACTCACTATAGGGC). The NCBI BLAST tool (www.ncbi.nlm.gov/BLAST/Blast.cgi) was used to search the *Mus musculus* genome for any genes with homology to the plasmid insert.

2.4. Animal Methods

2.4.1. Generation of the D50R knock-in mouse model

The Nbr1^{D50R} knock-in mouse was generated by introducing the D50R mutation into exon 3 of Nbr1 (targeting vector construction and ES clone analysis was performed by Dr. C. Whitehouse, KCL). The targeting vector was inserted into the genome of mouse embryonic stem (ES) cells via homologous recombination and correctly targeted embryonic stem (ES) cells were selected for using thymidine kinase (TK) and neomycin. Two different ES cell clones were chosen, injected into mouse blastocysts and transferred into pseudo-pregnant females. Resulting chimeras were bred to produce heterozygote founder (F1) mice. The F1 generation were subsequently bred with Flp recombinase expressing mice to remove the neomycin cassette (generation of targeted mice was performed by GenoWay, Lyon, France) (Figure 2.1). Heterozygote mice were then crossed and offspring were born in expected Mendelian ratios (1:2:1; wild type:heterozygous:homozygous) demonstrating that the mutation had no effect on viability during development (data not shown). All animal procedures were carried out under the Animal (Scientific Procedures) Act 1986 under project license number PPL70/6766. The genotype of each mouse was verified as described in section 2.1.11. Cells were extracted from mice and differentiated into osteoblasts or osteoclasts as described in section 2.5.5 and 2.5.6.

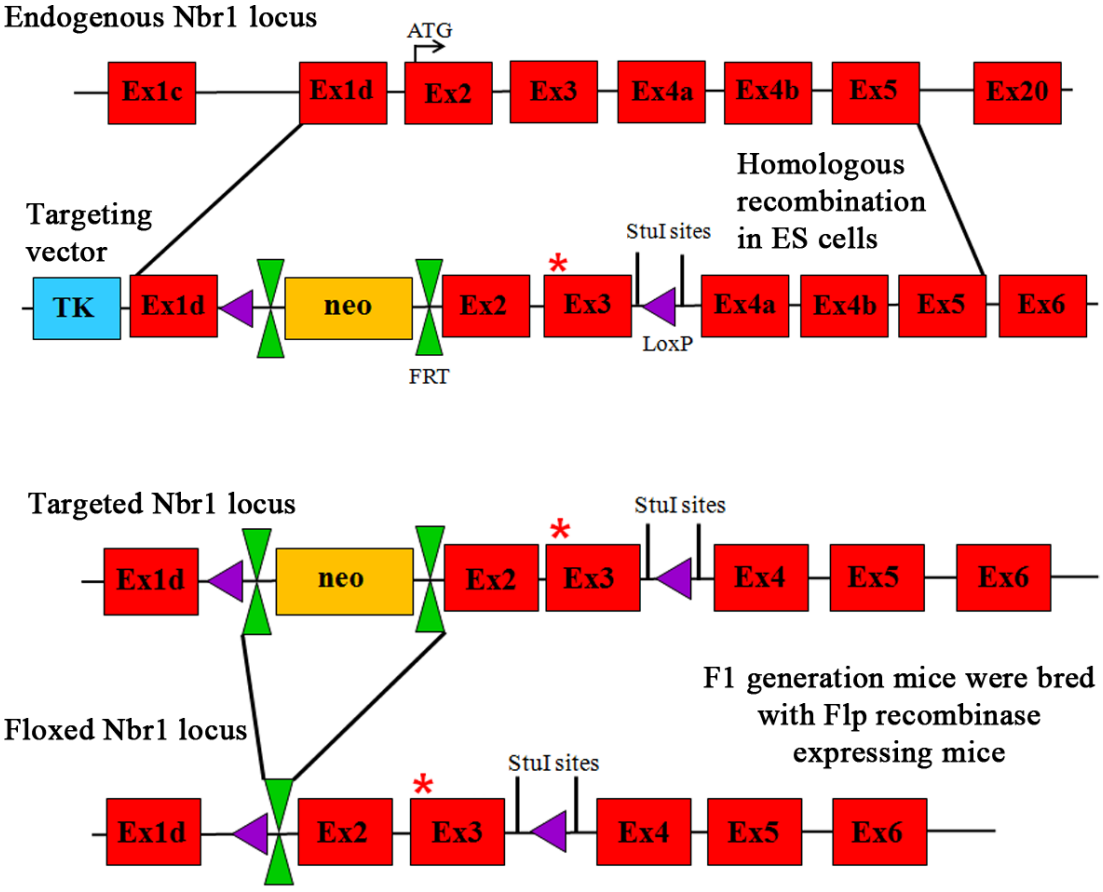

Figure 2.1. Schematic diagram showing the strategy for generating the Nbr1^{D50R} knock-in mouse model. Using homologous recombination, the targeting vector containing the desired mutation was inserted into the genomic DNA of mouse embryonic stem (ES) cells. The targeting vector also contained two StuI restriction enzyme sites for later genotyping to allow identification of mice carring the mutation. Correctly targeted ES cells were selected for using the selection markers thymidine kinase (TK) and neomycin (neo) and confirmed by PCR and Southern blotting before being injected into mouse blastocysts and transferred into pseudo-pregnant females. Resulting chimeras were bred against wild type mice to generate heterozygote founder mice (F1) as confirmed by genotyping and sequencing. Heterozygote mice were subsequently bred with Flp recombinase mice to remove the neomycin cassette. * indicates the location of the D50R mutation. FRT: Flp recombinase target sequence.

2.5. Cell biology methods

2.5.1. Cell line culture

COS-7 cells (African green monkey fibroblasts) and PC12 cells (a rat neuronal cell line derived from a pheochromocytoma) were maintained in sterile plastic tissue culture flasks in Dulbecco's Modified Eagle Medium (DMEM) supplemented with 10% Fetal Calf Serum (FCS), penicillin/streptomycin and L-glutamine at 37ºC in a humidified atmosphere of 5% CO_2. Cells grew as a monolayer and were regularly passaged up to 25 times.

For long term storage, cells were detached with trypsin, washed in DMEM media and centrifuged at 1000 xg for 5 minutes. Cells were then resuspended and stored in liquid nitrogen at a concentration of 2-4x10^6 cells/ml in 90% FCS, 10% DMSO.

2.5.2. Cell transfections

COS-7 cells were plated at 2x10^5 in 6-well tissue culture dishes and left to adhere overnight. Transfections were performed using FuGENE 6 (Roche) typically at a FuGENE (µl):DNA (µg) ratio of 3:1 as per manufacturer's instructions. Table 2.15 defines the constructs used for transfection. Vector maps are shown in appendix A.3.

Name	Species	Residues & template origin	Restriction enzymes	Vector & antibiotic resistance	Tag	Source
HA-Nbr1	Mouse	Full length (Nbr1 cDNA in bluescript vector)	KpnI & EcoRI	pHM6 (ampicillin)	HA	C. Whitehouse
YFP-LC3	Human	Full length, cleaved	unknown	modified pEGFP-Cl	YFP	M. Sandri
MAP1B-LC1-myc	Mouse	2216-2464 (Mouse brain cDNA)	XhoI & EcoRI	pcDNA3.1 (ampicillin)	Myc	K. Marchbank

Table 2.15. Constructs used for transfections in COS-7 cells. The cloning strategy for each construct is shown including the template used for insert amplification, restriction sites and vector. Vector maps are shown in Appendix A.3.

2.5.3. Cell treatments

PC12 cells or MEFs were treated with either Bafilomycin A_1 (0.2 µM) for 8 hours or serum starved in Hanks Balanced Salt Solution for 4 hours. For Western blot analysis of protein levels, PC12 cells were lysed directly into SDS sample buffer (Table 2.23).

2.5.4. Isolation and culture of mouse embryonic fibroblasts (MEFs)

All animal procedures conformed to the Animal (Scientific Procedures) Act 1986 under project license number PPL70/6766. 13.5 day old embryos of each genotype (WT and $Nbr1^{D50R}$) were isolated from pregnant females and head and guts were removed. Remaining tissue was homogenised and incubated at 37°C in 10x trypsin (PAA) for 30 minutes (3ml per 5-10 embryos). Cell culture media (DMEM, supplemented with 10% Fetal Calf Serum (FCS), penicillin/streptomycin and L-glutamine) was added and cells transferred into a T75 tissue culture flask and cultured overnight at 37°C in a humidified atmosphere (5% CO_2). Media was replaced the following day and cells passaged as required.

2.5.5. Isolation and culture of primary osteoclasts

Generation of enriched populations of osteoclasts *in vitro* was achieved by culturing bone marrow macrophages in the presence of M-CSF and RANKL to promote differentiation (Teitelbaum, 2007). Male mice of each genotype (WT and $Nbr1^{D50R}$) were culled by dislocation of the neck and the femur and tibia isolated. Bone marrow was subsequently flushed into culture media (α-MEM, 10% FCS, 1x P/S, 1x L-glut, 50 ng/ml M-CSF) using a 25 gauge needle and syringe. Cells were cultured overnight at 37°C in a humidified atmosphere (5% CO_2). The following day, all non-adherent cells were harvested, counted and plated into 96-well culture dishes lined with or without dentine slices at $5x10^4$. Cells were then cultured for a further 4 days in α-MEM, supplemented with 10% Fetal Calf Serum (FCS), penicillin/streptomycin, L-glutamine and 50 ng/ml M-CSF (R&D) before 5ng/ml of RANKL (R&D) was added to the media and the concentration of M-CSF reduced to 25 ng/ml. After a further 4 days, cells plated on plastic were fixed in 4% PFA whilst

those on dentine were cultured for a further three days in media containing concentrated HCl (8.2 µl/10ml). Cells were then fixed and TRAP stained (section 2.4.7.1). Using an Olympus CK40-F200 inverted phase contrast microscope with a Nikon D5-L2 digital camera, cells were counted and those on plastic scored for the number of nuclei. Dentine slices were then sonicated and resorption pits stained with 1% toluidine blue/0.1% sodium borate and imaged using a BX60 system microscope, Olympus Optical CO.(UK), SpectaMaster-1 wavelength dialled white-light source (Perkin Elmer, Cambridge, UK), Nikon 990 digital camera (Nikon UK, Kingston, UK) and Sony Trintron monitor. The total magnification before pit quantification was x72. Resorption pits were quantified using the point counting method. A grid (composed of 0.5cmx0.5cm squares) was superimposed onto the image, the number of occasions a pit crossed the middle of a square was quantified and the percentage resorbed area was calculated ((number of squares crossed by a pit/total number of squares) x 100).

2.5.6. Isolation and culture of primary osteoblasts

Mesenchymal stem cells in the bone marrow have the ability to differentiate into osteoblasts *in vitro* when cultured in media containing ascorbic acid and β-glycerophosphate (Pittenger et al., 1999). Male mice from each genotype (WT & $Nbr1^{D50R}$) were culled and bones flushed as in section 2.4.5. Cells were plated at $2x10^6$ per well into a 6-well tissue culture plate in α-MEM supplemented with 10% Fetal Calf Serum (FCS), penicillin/streptomycin, L-glutamine, 50 µg/ml ascorbic acid and 10 mM β-glycerophosphate. Media was replaced every four days and cells were cultured at 37°C in a humidified atmosphere (5% CO_2). After nine or 15 days in culture, cells were fixed in 4% PFA and stained for alkaline phosphatase or von Kossa (section 2.5.7).

2.5.7. Cell staining

2.5.7.1. TRAP staining of osteoclasts *in vitro*

TRAP is synthesized and secreted by mature osteoclasts and acts to degrade bone matrix, therefore is a good marker for osteoclast differentiation. Cells isolated and

cultured as in section 2.5.5 were fixed and stained using the Acid Phosphatase Kit (Sigma, Cat no. 387A) with 50 mM tartrate solution.

2.5.7.2. Alkaline phosphatase (ALP) staining

Cells fixed as per section 2.4.6 were washed with H_2O for 15 minutes. The H_2O was then removed and alkaline phosphatase (ALP) stain (Table 2.23) was added and incubated for 15 minutes at room temperature. The stain was removed and cells were washed three times with H_2O before being stored dry at 4°C. Cells were imaged using a HP Scanjet G4050 and staining quantified using Image J; the image was converted to grey scale and a threshold most representative of the staining was used to calculate the percentage area covered by the ALP stain (for the 9 day ALP staining the threshold was 116, for 15 day ALP staining the threshold was 95 and for the von Kossa staining, the threshold was 35).

2.5.7.3. Von Kossa staining

Following staining for alkaline phosphatase, cells were covered with 2.5% silver nitrate and incubated for 30 minutes in the absence of light. Silver nitrate was subsequently removed and cells were washed three times with distilled H_2O. Cells were then covered with sodium carbonate formaldehyde solution (25 ml formaldehyde, 5g Na_2CO_3, 75 ml H_2O) for 2-5 minutes until the mineralised colour had deepened sufficiently. Cells were washed three times in H_2O and stored at 4°C before the percentage area mineralised was quantified using ImageJ as described in section 2.5.7.2.

2.5.8. Immunostaining

Cells were seeded onto glass coverslips, incubates overnight to adhere and subsequently treated (section 2.5.3). Cells were fixed in 4% PFA/PBS for 10 minutes, washed with PBS and permeabilised in 0.1% Triton X 100/PBS for 5 minutes at room temperature. Cells were subsequently washed with PBS and blocked for 1 hour at room temperature in a blocking solution of 10% FCS/PBS. Block was removed and cells incubated with appropriate antibody diluted in 10%

FCS/PBS for 1 hour at room temperature. Cells were then washed three times in PBS, incubated with appropriate secondary antibody diluted in 10% FCS/PBS for 1 hour in the absence of light, then washed with PBS and DNA was stained with 1 mM Hoechst/PBS for 5 minutes. Cells were then washed in PBS and coverslips mounted on microscope slides using Fluorescent Mounting Medium (Dako S3023). Cells were imaged using a Zeiss LSM 510 confocal microscope in sequential scanning mode using a 63x oil immersion objective.

2.5.9. Antibodies

Primary and secondary antibodies used throughout this thesis are listed in Tables 2.16 and 2.17.

Protein	Species raised in	WB	ICC	Origin
GAL4 (DBD)	Mouse monoclonal	1 in 500	-	Santa Cruz
GFP	Mouse polyclonal	1:1000	-	Roche
HA	Rat monoclonal	1 in 1000	-	Roche
His	Mouse monoclonal	1:1000	-	Novagen
LC3	Rabbit polyclonal	1:400		Cell Signalling
MAP1B-HC	Rabbit polyclonal	1 in 10,000	-	P. Gordon-Weekes
MAP1B-HC	Goat polyclonal	-	1 in 50	Santa Cruz
MAP1B-LC	Rabbit polyclonal (H-130)	-	1 in 200	Santa Cruz
MAP1B-LC	Goat polyclonal (C-20)	1 in 500	-	Santa Cruz
Myc	Rabbit polyclonal (A-14)	1 in 1000	-	Santa Cruz
Myc	Mouse monoclonal (9E-10)	1 in 1000	-	Santa Cruz
Nbr1	Mouse monoclonal	1 in 1000	1 in 100	Abcam
Nbr1	Rabbit polyclonal (3517)	1 in 500	-	C. Whitehouse
P62	Mouse monoclonal	1 in 1000	-	Abnova
P62	Rabbit polyclonal	-	1 in 200	M. Gautel
β-actin	Rabbit polyclonal	1 in 2000	-	Abcam

Table 2.16. Primary antibodies utilized. Antibody dilutions for Western blot (WB) and immunocytochemistry (ICC).

Conjugate	Species	Dilution	Origin
Alexa Fluor 488	Donkey anti mouse polyclonal	1 in 1000	Invitrogen
Alexa Fluor 488	Donkey anti goat polyclonal	1 in 1000	Invitrogen
Alexa Fluor 555	Donkey anti rabbit polyclonal	1 in 1000	Invitrogen
Alexa Fluor 555	Donkey anti goat polyclonal	1 in 1000	Invitrogen
Horse radish peroxidase	Swine anti rabbit polyclonal	1 in 2000	Dako
Horse radish peroxidase	Rabbit anti mouse polyclonal	1 in 2000	Dako
Horse radish peroxidase	Rabbit anti rat polyclonal	1 in 2000	Dako
Horse radish peroxidase	Rabbit anti goat polyclonal	1 in 2000	Dako

Table 2.17. Secondary antibodies utilised.

2.6. Bone methods

2.6.1. Specimen preparation

Male mice from D50R knock-in mice (Mut) and wild type (WT) controls were culled using carbon dioxide (death was confirmed by cessation of circulation) at three, six or nine months of age (Table 2.18). They were then weighed before all skin and internal organs were removed and the remaining skeleton fixed in 70% EtOH for at least 1 month and stored at 4°C. Right femurs and tibias were then removed and stripped of all soft tissue in preparation for analysis.

Mouse Genotype	3 Months old	6 Months old	9 Months old
WT	9	6	6
Mutant	8	8	7

Table 2.18. Numbers of mice used of each age and genotype for *ex vivo* bone analysis.

2.6.2. Physical measurements

All femurs and tibiae were measured using GuoGen MC 01120028 digital calipers with a resolution of 0.01 mm and a reproducibility of 0.2 mm. Distance measured for the femur and tibia is shown in Figure 2.2.

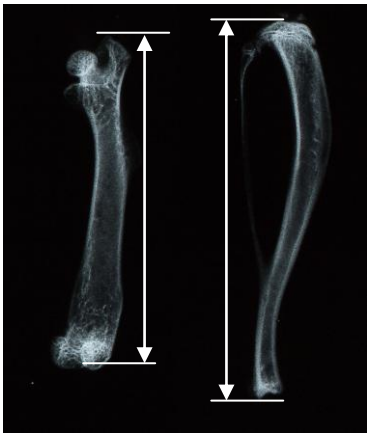

Figure 2.2. Regions measured for femur and tibia length

2.6.3. Radiographs

Radiographs were taken in a cabinet X-ray system (Hewlett Packard Faxitron X-ray Cabinet model 43855A). Specimens were exposed to 30kv for 45 seconds and films processed in a Curex 60 processor (AGFA).

2.6.4. Micro computer tomography (MicroCT)

3D MicroCT images of femurs and tibiae were captured using a SkyScan 1172 Desktop X-ray system (SkyScan). All specimens were scanned in plastic containers using a medium camera, 360^{o} rotation and a 0.5 mm filter with a resolution of 4.4µm for high resolution scans and 17.2µm for low resolution scans. The scans were then reconstructed using NRecon Version1.4.1.0 and analysed using CT Analyser version 1.10.1.0. Thresholds for whole bones, cortical and trabecular parameters are summarised in Table 2.19.

Bone	Resolution (µm)	Reconstruction Threshold (Arbitrary value)	3D Analysis Threshold (Arbitrary value)
Whole Femur and Tibia	17.2	0.16	92-255
Femur Trabecular	4.4	0.16	92-255
Femur Cortical	4.4	0.16	110-255
Tibia Trabecular	4.4	0.16	92-255
Tibia Cortical	4.4	0.16	110-255

Table 2.19. Threshold values for reconstruction and analysis.

Analysis of the reconstructions was carried out by initially drawing the region of interest (ROI). For whole bones, all cross sections were considered, however, for cortical and trabecular analysis a distinct region of the bone was taken into account, measured from a reference point. Reference points and regions analysed are summarised in Table 2.20.

Bone	Reference point	Offset	Height
Femur Trabecular	Fusion plate (distal end)	-268 (1.2mm)	223 (1mm)
Femur Cortical	Fusion plate (distal end)	-490 (2.2mm)	223 (1mm)
Tibia Trabecular	Fusion plate (proximal end)	-268 (1.2mm)	223 (1mm)
Tibia Cortical	Fusion plate (proximal end)	-490 (2.2mm)	223 (1mm)

Table 2.20. Cortical and trabecular ROI settings.

The ROIs were then analysed on CT Analyser using Batch Manager (BATMAN). For all parameters except endosteal and periosteal diameters, analysis settings were as follows; Thresholding (see Table 2.19 for specific thresholds), Despeckle (remove white speckles with volume less that 10 voxels within the 3D space) and 3D analysis. The parameters calculated were cortical bone volume (Ct.BV), cortical thickness (Ct.Th), trabecular bone volume/tissue volume (Tb.BV/TV) trabecular thickness (Tb.Th), trabecular number (Tb.N) and trabecular separation (Tb.Sp). Settings used to calculate endosteal and periosteal diameters are shown in Tables 2.21 and 2.22 respectively.

Task	Description
Thresholding	85-255
Despeckle	Sweep within 3D space all except larges object
Despeckle	Remove white speckles within 2D with space less than 1000 pixels
Morphological Operations	Type: close in 2D space; Kernel:round with a radius of 20; Apply to image.
Morphological Operations	Type: open in 3D space; Kernel:round with a radius of 4; Apply to image.
Bitwise Operations	Image=NOT image
Despeckle	Remove outer objects from 2D space
Individual Object Analysis	2D space

Table 2.21. Endosteal analysis settings

Task	Description
Thresholding	85-255
Despeckle	Sweep within 3D space all except largest object
Despeckle	Remove white speckles within 2D with space less than 1000 pixels
Morphological Operations	Type: close in 2D space; Kernel:round with a radius of 20; Apply to image.
Morphological Operations	Type: open in 3D space; Kernel:round with a radius of 4; Apply to image.
Despeckle	Remove pores from 2D space
Individual Object Analysis	2D space

Table 2.22. Periosteal analysis settings

Bone mineral density for all bone regions analysed was calculated from a hydroxyapatite standard. Two samples of known density were scanned using the same parameters used for all specimens and hydroxyapatite estimated using CTAnalyser version 1.10.1.0 and the thresholds in Table 2.19.

2.6.5. Statistical analysis

All statistical analysis was carried out using GraphPad Prism. Where data were normally distributed and variance homogenous, an unpaired student's t-test was used, otherwise, a Mann-Whitney U test was employed. All error bars are shown as standard deviation (SD).

2.7. Bioinformatics

2.7.1. Generation of a linkage disequilibrium map

A linkage disequilibrium (LD) map of the *NBR1* gene was generated using Haploview version 4.2 from the CEU (Caucasian European) HapMap population data (www.HapMap.org) of version 27 of the HapMap project. The chromosomal region used was Chr17: 41321910-41371844 bp.

2.7.2. Power calculations

The following calculation was used to estimate the power of identifying known SNPs in the high bone mass cases sequenced in Chapter 6:

Power = $1 - (1-p)^{2N}$ where p = minor allele frequency and N = no. of individuals.

2.7.3. Predicting the effect of amino acid substitutions

Polyphen (http://genetics.bwh.harvard.edu/pph2/index.htm) and SIFT (http://sift.jcvi.org/www/SIFT_enst_submit.html) were used to predict the effect of the amino acid substitution identified in a high bone mass patient.

2.8. Buffers and solutions

All buffers and solutions (Table 2.23) were made with deionised water unless otherwise stated and either filter sterilised through a 0.22 µm filter or autoclaved where necessary.

Name	Composition
Buffer A	50 mM sodium phosphate (pH7), 300 mM NaCl, 5% glycerol, 10 mM β-mercaptoethanol, EDTA free protease inhibitors (Roche)
Buffer B	50 mM sodium phosphate (pH7), 300 mM NaCl, 5% glycerol, 35 mM Imidazole, 10 mM β-mercaptoethanol, EDTA free protease inhibitors (Roche)
Buffer C	50 mM sodium phosphate (pH7), 300 mM NaCl, 5% glycerol, 250 mM Imidazole, 10 mM β-

	mercaptoethanol, EDTA free protease inhibitors (Roche)
Coomassie Stain	50% Methanol, 10% Acetic Acid, 0.05% Brilliant Blue
Cracking Buffer	Stock solution: 8 M urea, 5% SDS, 40 mM Tris-HCl (pH6.8), 0.1 mM EDTA, 0.4mg/ml bromophenol blue. 1 ml stock solution, 10 µl β-mercaptoethanol, protease inhibitors (Roche)
De-stain	45% Methanol, 10% Acetic Acid
Dialysation Buffer	50 mM Tris-HCl (pH7.5), 150 mM NaCl
High Elution Buffer	100 mM NaH_2PO_4, 10 mM Tris-HCl (pH8), 250 mM Imidazole (pH8), 6 M Urea, EDTA protease inhibitors (Roche)
H Buffer	20 mM Hepes (pH7.7), 50 mM KCl, 20% Glycerol, 0.1% NP-40, 0.007% B-mercaptoethanol (7 µl in 100ml), protease inhibitors
IP lysis buffer 1	10 mM Tris pH 7.5, 150 mM NaCl, 2 mM MgCl, 1% Triton, 1 mM sodium orthovanodate and protease inhibitors
IP lysis buffer 2	50 mM Tris (pH7.5), 150 mM NaCl, 0.5% NP-40, protease and phosphatase inhibitors (Roche)
IP wash buffer 1	10 mM Tris pH 7.5, 150 mM NaCl, 1% Triton
IP wash buffer 2	50 mM Tris (pH7.5), 200 mM NaCl, 0.5% NP-40
Lysis Buffer	100 mM NaH_2PO_4, 10 mM Tris-HCl (pH8), 6M Urea, 5 mM Imidazole (pH8), EDTA free protease inhibitors (Roche)
Lysis Solution (yeast):	2% triton (BDH Laboratory Supplies), 4% SDS, 100 mM NaCl (BDH), 10 mM Tris (pH8.0), 1 mM EDTA
NETN Buffer	0.5% NP-40, 20 mM Tris-HCL (pH8), 100 mM NaCl, 1 mM EDTA, protease inhibitors
PBS	1 tablet of phosphate buffer saline (Sigma P4417) per 200 ml H_20
PEG/Lithium Acetate	8 ml of 50% Polyetheleneglycol, 1 ml of 10x TAE, 1 ml 10x LiAc
SDS Sample Buffer	62.5 mM Tris-HCl (pH6.8), 6 M Urea, 2% SDS, 2% NP-40, 5% β-mercaptoethanol, bromophenol blue.
Tail Buffer	100 mM Tris-HCl pH8, 5 mM EDTA, 0.2% SDS, 200 mM NaCl, proteinase K (100 µg/ml)
TEDG Buffer	50 mM Tris-HCl (pH7.4), 1.5 mM EDTA, 10% Glycerol, 0.4 mM NaCl, 1 mM DTT, protease inhibitors
TENS Buffer	10 mM tris (pH8), 1 mM EDTA, 0.1 M NaOH (BDH), 0.5% SDS
Transfer Buffer	50 mM Tris, 380 mM Glycine, 0.1% SDS, 20% methanol
Low Elution Buffer	100 mM NaH_2PO_4, 10mM Tris-HCl (pH8), 6M Urea, 20 mM Imidazole (pH8), EDTA free protease inhibitors (Roche)
5x DNA Sample Buffer	33% glycerol, 3.75x TAE, 125 mM EDTA (pH 8), 0.008% bromophenol blue (BDH)
Minimal SD agar (pH	46.7 g/l minimal SD agar (Clonetech cat. 630412), 2%

5.8)	glucose , appropriate dropout supplement
Minimal SD medium (pH 5.8)	26.7 g/l minimal SD base (Clonetech cat. 630411), 2% glucose (Sigma), Appropriate dropout supplement
TfbI Buffer (pH 5.8)	30 mM potassium acetate (BDH), 100 mM rubidium chloride (Sigma), 10 mM calcium chloride (BDH), 50 mM magnesium chloride (BDH), 15% glycerol (BDH)
TfbII Buffer (pH 6.5)	10 mM MOPS (Sigma), 75 mM calcium chloride, 10 mM rubidium chloride, 15% glycerol
YPDA Agar (pH 6.5)	20 g/l Difco peptone (BD), 10 g/l yeast extract (BD), 20 g/l bacto agar (BD), 2% glucose, 0.003% adenine hemisulfate (Sigma)
YPDA Medium (pH 6.5)	20 g/l Difco peptone (BD), 10 g/l yeast extract (BD), 2% glucose, 0.003% adenine hemisulfate (Sigma)
LB Agar (pH 7)	15 g/l bacto agar in LB broth
LB Broth (pH 7)	10g bacto tryptone (BD), 5 g bacto yeast extract, 10 g NaCl
10x Running Buffer	0.25 M Tris, 2 M Glycine, 1% SDS
10x Lithium Acetate (pH 7.5)	1 M lithium acetate adjust to pH7.5 with dilute acetic acid.
50x TAE	242 g/l Tris base, 57.1 ml/l acetic acid, 100 ml/l 0.5M EDTA
50% PEG	Prepare in deionised water and heat to 50^{o}C to go into solution
PEG/lithium acetate	8 ml 50% PEG, 1 ml 10x TE, 1 ml 10x LiAc
10x TE	0.1 M Tris HCl pH7.5, 10 mM EDTA
Alkaline phosphatase stain	5 mg Naphtol AS MX-PO_4, 200 µl N, N-Dimethylformamide, 25 ml 0.2 M Tris-HCl (pH8.3), 30 mg Red Violet LB salt. Make up to 50 ml with H_2O and filter using Whatman's No1 filter paper.

Table 2.23. Buffers and solutions.

Chapter 3. Identification of Interacting Partners of the Central Region of Nbr1

3.1. Introduction

Protein-protein interactions are central to virtually every cellular process and alterations or inhibition of these can contribute to a diverse range of diseases. The yeast-2-hybrid method is widely used to screen protein libraries against a bait protein of interest in order to identify new interacting partners and gain further insight into protein function. This system has previously been employed to identify proteins that interact with Nbr1 (Figure 3.1). Full length human NBR1 was used to screen a human placental library and identified fasciculation and elongation protein zeta-1 (FEZ1) and calcium and integrin binding protein (CIB) as interacting partners (Whitehouse et al., 2002). A region of NBR1 that excluded the UBA and PB1 domains (aa93-903) was used to screen a human cardiac muscle library and identified interactions between Nbr1, a ubiquitin specific peptidase (USP8), and a ubiquitin conjugating enzyme (E2B) (Waters, 2009). Furthermore, a mouse calvarial library was screened using the UBA domain of Nbr1 and identified ubiquitin as an interacting partner. Collectively, these suggest a role for Nbr1 in ubiquitin mediated protein degradation (Waters et al., 2009). Finally, the N-terminal 135 amino acids of Nbr1 were used to screen a mouse calvarial library and identified the sumoylation enzyme UBC9 as an interacting partner (L. Bentley, Kings College London, unpublished data).

Nbr1 contains a number of conserved protein domains however the central region (aa355-924) is largely uncharacterised. This fragment was therefore used in a yeast-2-hybrid assay to probe a bone enriched cDNA library for novel interacting partners. The truncated Nbr1 (trNbr1) mouse model has a high bone mass phenotype (Whitehouse et al., 2010) however the molecular mechanisms involved are still unclear therefore bone specific protein interactors were of specific interest.

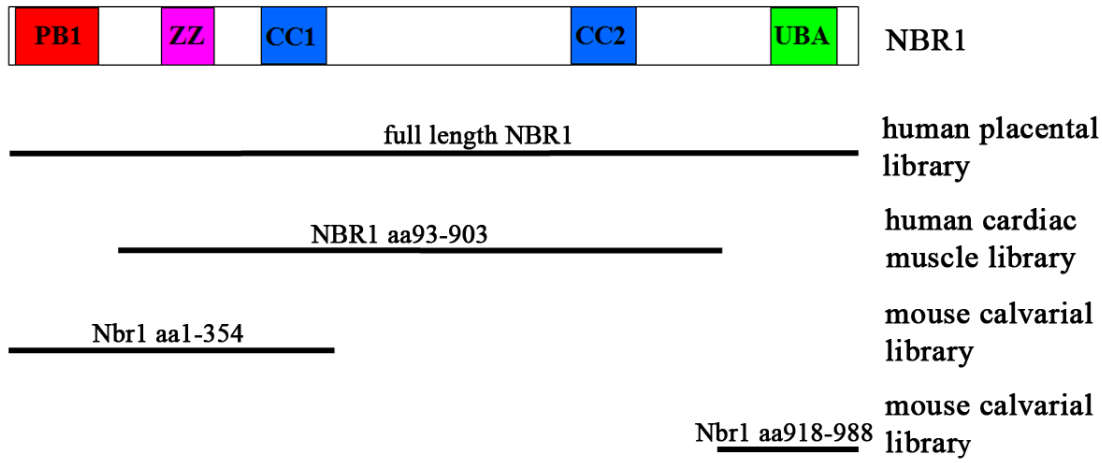

Figure 3.1. Regions of Nbr1/NBR1 previously utilised as bait proteins in the yeast-2- hybrid system. Full length human NBR1 was tested against a human placental library (Whitehouse et al. 2002), amino acids 93-903 of NBR1 were tested against a human cardiac muscle library (Waters et al. 2009) and amino acids 1-354 (unpublished data) and aa918-988 (Waters et al. 2009) of Nbr1 were tested against a mouse calvarial library.

3.2. Yeast-2-Hybrid

The yeast-2-hybrid technique was first pioneered by Fields and Song in 1989 (Fields and Song, 1989) and is used to identify novel protein-protein interactions. This system utilizes the GAL4 protein from *Saccharomyces cerevisiae* which is a potent activator of transcription. The N-terminal region of the GAL4 protein binds to DNA in a sequence specific manner but fails to activate transcription, while the C-terminal domain contains the activating region but is unable to activate transcription alone. These two domains can be expressed independently in yeast and will only activate transcription when they are brought into close proximity. A protein of interest can therefore be fused to the GAL4 DNA binding domain (BD) and screened against a library of proteins fused to the GAL4 activation domain (AD). When two fusion proteins interact, transcription of up to four reporter genes; *HIS3*, *ADE2*, *MEL1* and *LACZ* can occur resulting in the expression of proteins involved in the biogenesis of histidine, adenine, β-galactosidase (LacZ product) and α-galactosidase (MEL1 product). This enables yeast strains auxotrophic for histidine and adenine to grow on selection media deficient in these amino acids. α-galatosidase is a secreted enzyme and can be detected by the addition of X-α-gal to the media which is subsequently hydrolysed by α-galactosidase and manifests as blue coloured yeast colonies. This system enables the selection of yeast clones expressing two interacting proteins.

3.2.1. Yeast Phenotyping

Initially, it was important to determine the phenotype of the yeast strains and confirm that they were unable to grow on specific selection media. The yeast strains Y187 (MATα) and AH109 (MATa) were utilized in this screen to enable single transformations and subsequent matings, resulting in diploid cells. The phenotype of the yeast was confirmed by plating on minimal dropout media (SD) deficient in amino acids required for growth (Table 3.1). Both yeast strains failed to grow in the absence of leucine, tryptophan or adenine, showed minimal growth in the absence of histidine and grew in the absence of uracil. These results were expected as AH109 and Y187 are auxotrophic for leucine, tryptophan, histidine and adenine but not for uracil. Minimal growth was observed in the absence of histidine as the yeast display 'leaky' histidine production which will be addressed in section 3.2.2.

Yeast strain	SD/-Leu	SD/-Trp	SD/-His	SD/-Ade	SD/-Ura
AH109	no growth	no growth	a few small colonies	no growth	growth
Y187	no growth	no growth	a few small colonies	no growth	growth

Table 3.1. Analysis of yeast phenotype. Yeast strains were streaked onto minimal dropout media (SD) lacking each of the essential amino acids. Yeast were not able to grow in the absence of leucine, tryptophan or adenine, could grow in the absence of uracil and showed limited growth in the absence of histidine.

3.2.2. Autoactivation and 3-AT Titration

The large central region of Nbr1 (aa355-924) was previously shown to autonomously activate the reporter genes (C. Whitehouse, unpublished data), therefore this region was split into two overlapping segments encoding aa355-694 and aa495-924 and cloned into the pGBKT7 vector (containing the GAL4 BD and the *TRP1* nutritional marker). To establish if the new bait constructs autoactivated, they were transformed into yeast strain Y187. Resulting transformants were used in small scale matings with yeast strain AH109 transformed with the pGADT7 empty vector (containing the GAL4 AD and the *LEU2* nutritional marker). The SV40 Large T-antigen fused to the GAL4 AD (Clontech) and p53 protein (aa72-390) fused to the GAL4 BD (Clontech) were used as a positive control as they are known to interact. Empty vectors pGADT7 and pGBKT7 were used as a negative control (Table 3.2).

Small scale matings were plated onto double drop out (DDO) media deficient in leucine and tryptophan to confirm that matings had been successful. They were also plated onto triple drop out media (TDO) deficient in leucine, tryptophan and histidine supplemented with a range of 3-Amino-1,2,4-triazole (3-AT) concentrations. 3-AT is a competitive inhibitor of imidazoleglycerol-phosphate dehydratase, a catalytic enzyme required for the sixth step of histidine production. Supplementing the media with 3-AT ensures that yeast have to produce a higher than background level of histidine (i.e. one reminiscent of a protein-protein interaction) in order to grow.

Table 3.2 shows the extent of colony growth on SD/-Leu/-Trp/-His media containing increasing concentrations of 3-AT. The bait construct, Nbr1-aa355-694 (also containing a highly conserved region of Nbr1, discussed in chapter 4) was shown to

autoactivate as growth was observed on all 3-AT concentrations and in the absence of adenine. Nbr1-aa355-694 was therefore not used in the final library screen. The bait construct containing aa495-924 of Nbr1 did not autoactivate as growth was reduced with increasing 3-AT concentrations. A concentration of 3mM 3-AT was used for the final library screen as minimal colony growth was observed and this reduced the risk of ablating weak interactions. As expected, the positive control (p53+SV40 large T-antigen) showed growth on all concentrations of 3-AT and in the absence of adenine, while the negative control (pGADT7+pGBKT7) failed to grow in the absence of histidine or adenine (Table 3.2).

Mating	-Leu/-Trp	-Leu/-Trp/-His						-Leu/-Trp/-His/-Ade
		0mM 3-AT	1mM 3-AT	3mM 3-AT	5mM 3-AT	8mM 3-AT	15mM 3-AT	
p53 + T-antigen	√	√	√	√	√	√	√	√
pGBKT7 + pGADT7	√	X	X	X	X	X	X	X
Nbr1 aa355-694 + pGADT7	√	√	√	√	√	√	√	√
Nbr1 aa495-924 + pGADT7	√	Growth drops off with increasing 3-AT concentration						X

Table 3.2. 3-AT titration and test for bait autoactivation. Yeast were singly transformed with constructs shown, mated and plated on SD media lacking different combinations of amino acids. Yeast containing the bait construct, Nbr1 aa 355-694 and pGADT7 grew on all concentrations of 3-AT and without adenine suggesting autoactivation. Yeast containing the bait construct Nbr1 aa495-924 and pGADT7 showed growth dropping off with increased 3-AT concentration. The positive control grew on all concentrations of 3-AT and in the absence of adenine and the negative control did not grow in the absence of histidine or adenine, as expected.

3.2.3. Confirmation of bait protein expression

To verify that yeast were expressing the bait protein of interest (Nbr1 aa495-924 fused to GAL4 BD), protein was extracted (section 2.3.3/4), resolved by SDS PAGE and visualised by Western blot using an antibody that recognises the GAL4 BD. A protein band of ~58kDa was identified which is the same size as predicted for the bait protein (Nbr1 aa495-924) fused to the GAL4 BD thus confirming successful expression in Y187 yeast cells (Figure 3.2).

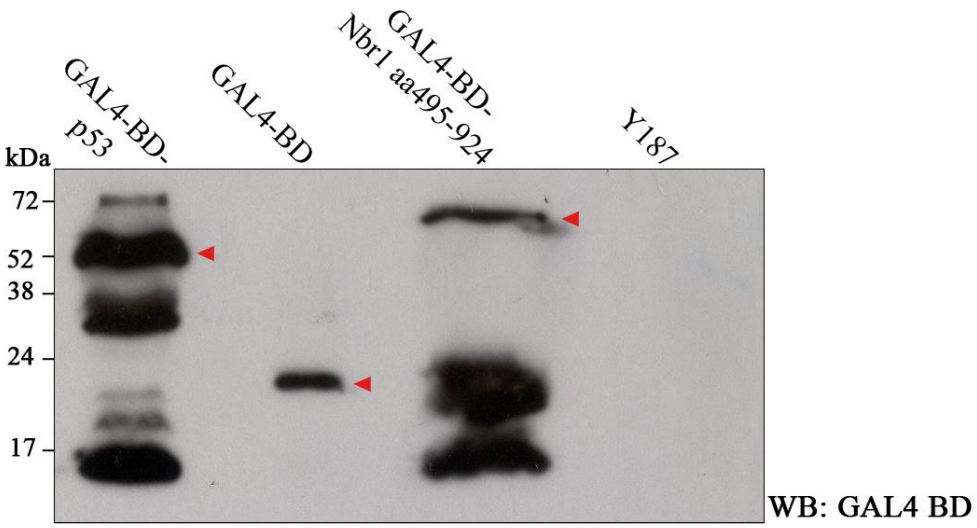

Figure 3.2. Western blot analysis of bait protein expression in yeast. Transformed yeast expressed the positive controls (p53 fused to the GAL4 binding domain (BD) and the GAL4 BD alone (empty vector)) and the bait construct of interest Nbr1 aa495-924 fused to the GAL4 BD (expected product size indicated by red arrows). Y187 cell extract alone was used as a negative control. Non-specific bands are likely to be degradation products.

3.2.4. Yeast-2-Hybrid Library Screen

The bait construct (Nbr1 aa495-924 fused to GAL4 BD) was transformed into yeast strain Y187 and the resulting transformants were mated with a pretransformed 7 day old mouse calvaria cDNA library (cloned into the pGADT7 vector) in the AH109 yeast strain (kindly supplied by Prof. Ikramuddin Aukhil, College of Dentistry, University of Florida). The resulting diploid yeast were subjected to nutritional selection by plating onto SD–Leu/-Trp/-His media supplemented with 3mM 3-AT. An estimated 5 x 10^6 yeast clones were screened which is considered to be the minimum required to screen the cDNA library to saturation (Van Criekinge and Beyaert, 1999).

Initially, 334 positive clones grew within 1-2 weeks of plating on nutritional selection media. These clones were restreaked onto SD–Leu/-Trp/-His containing 3mM 3-AT three times to selectively eliminate any multiple library plasmids and a total of 158 regrew on the TDO media. DNA was extracted from the yeast clones, transformed into *E.coli* and the DNA extraction repeated. All positive clones were analysed by sequencing. Clones where the DNA insert was out of frame with the GAL4 AD were discarded as false positives (27).

This yeast-2-hybrid screen identified many candidate genes as putative interactors of Nbr1. The most biologically relevant proteins are shown in Table 3.3 and discussed in more detail below. All other proteins identified but not discussed are shown in Table A.1 (Appendix).

Accession No.	Gene ID	No. of Clones
NM_173755.3	Ubiquitin conjugating enzyme E20 (UBE20)	2
NM_025735.1	Microtubule associated protein 1 light chain 3 (LC3)	3
NM_153762.3	Ring finger protein 26 (Rnf26)	1
NM_007541.2	bone gamma-carboxyglutamate protein 1/2 (Osteocalcin)	2
NM_009976.3	Cystatin C	1

Table 3.3. Positive clones identified from the yeast-2-hybrid library screen.

3.3 Putative interacting partners of Nbr1

3.3.1. Proteins involved in protein degradation

The yeast-2-hybrid screen performed in this study, has identified a number of proteins involved in both the autophagy pathway and the UPS as putative interactors of Nbr1.

Microtubule-associated protein light chain 3 (LC3) was identified in three of the yeast clones (aa18-end - deduced from the isolated yeast-2-hybrid clone). LC3 localizes to autophagosomal membranes (Kabeya, 2000), and its conjugation to the phospholipid PE is essential for autophagosomal formation (Sou et al., 2008). p62 has previously been shown to directly interact with LC3 (Pankiv et al., 2007b) and through this interaction is thought to tether ubiquitinated proteins to the forming autophagosome.

UBE20 (also known as UBE2-230K) is an E2 ubiquitin conjugating enzyme that is part of the enzyme cascade that transfers ubiquitin residues to proteins that are subsequently targeted for degradation. The human UBE20 homologue contains a conserved cysteine residue which represents the putative active site for thio-esterification of ubiquitin (Yokota et al., 2001). The functions of E2 enzymes have mainly been studied in yeast and E2-deficient yeast mutants exhibit defects in DNA repair, organelle biosynthesis and the stress response (Jentsch, 1992). UBE20 is

ubiquitously expressed (Yokota et al., 2001) and along with one other E2 enzyme; E2-20K, UBE20 expression is specifically upregulated in differentiating reticulocytes (immature red blood cells), a stage when enhanced protein degradation has been observed (Wefes et al., 1995).

The ring finger protein 26 (Rnf26) was first cloned in 2001 by Katoh and is upregulated in a number of cancer cell lines (Katoh, 2001) however very little is known about its function. The ring finger is a zinc-binding domain that can interact with E2 ubiquitin conjugating enzymes and is found in many proteins that act as E3 ubiquitin ligases (reviewed in (Freemont, 2000). E3 ubiquitin ligases are responsible for substrate recognition and promoting polyubiquitin ligation to a substrate. They are also known to regulate diverse cellular processes including DNA repair, signalling and the cell cycle (Joazeiro and Weissman, 2000).

3.3.2. Putative interactors involved in bone biology

The yeast-2-hybrid screen carried out in this study identified full length bone gamma-carboxyglutamate protein (also known as osteocalcin) and cystatin C (aa78-140) as putative interactors of Nbr1. Both proteins are known to be involved in bone formation and remodelling and therefore represent plausible candidates for a true Nbr1 interaction. They were of specific interest due to the high bone mass phenotype of the truncated Nbr1 (trNbr1) mouse model (Whitehouse et al., 2010).

Osteocalcin is the most abundant non-collagenous protein present in the extracellular bone matrix and is secreted by osteoblast cells in the later stages of maturation (Liu et al., 1994). It is synthesized as a prepromolecule which consists of an N-terminal signal peptide that is cleaved following translation. The resulting propeptide is further processed which results in a mature protein that is secreted from the cell (Gundberg and Clough, 1992a). The majority of the secreted protein is incorporated into the extracellular bone matrix, however a small proportion leaks into the blood circulation where it can be detected and used as a marker of bone formation (Seibel, 2005). Osteocalcin expression is regulated by the Runx2 and ATF4 transcription factors (Xiao et al., 2005) and promotes cell adhesion and differentiation of the

preosteoblastic cell line MC3T3-E1 (Kim et al., 2007b). The exact function of osteocalcin is still unclear, however the use of knock-out mice have shed further light on possible functions. Osteocalcin deficient mice exhibit a high bone mass phenotype characterised by increased cortical thickness and an increase in mineralized bone matrix. This suggests that osteocalcin is a negative regulator of bone formation and may act by a negative feedback mechanism (Ducy et al., 1996). There is also a growing body of evidence suggesting that osteocalcin has an endocrine function. It was demonstrated that osteocalcin deficient mice display glucose intolerance, insulin resistance and increased fat mass. This indicates that along with playing a functional role in bone formation, osteocalcin can also regulate energy metabolism (Lee et al., 2007b).

Cystatin C is a type 2 cystatin (Yamaza 2001) that has a variety of tissue specific functions and altered expression can lead to a number of human pathologies including aberrant kidney function (Laterza et al., 2002), and cancer (Strojan et al., 2004). Most interestingly for this study, cystatin C is expressed (mRNA) by osteoblasts early in differentiation (Candeliere et al., 1999) and is secreted by osteoclasts into the bone resorption lacunae under the ruffled border where it acts to inhibit bone resorption (Yamaza et al., 2001). It has been postulated that this is through the inhibition of cathepsin K, a cysteine protease that functions to degrade bone matrix (Brand et al., 2004). Cystatin C can also stimulate osteoblast differentiation and mineralisation activity *in vitro* (Danjo et al., 2007). Cystatin C localizes to the ER, Golgi apparatus, secretory and endocytic vesicles, granules and vacuoles throughout the cytoplasm of osteoclasts (Yamaza et al., 2001).

3.4 Nbr1 interacts with LC3

Due to the identification of LC3 as an interacting partner of p62 (Pankiv et al., 2007a), it was hypothesised by other members of the laboratory that Nbr1 may also interact with LC3. The interaction of Nbr1 with LC3 was therefore confirmed by Dr Sarah Waters (Ellen Solomon laboratory, KCL) using *in-vitro* binding assays. Purified GST tagged regions of NBR1 bound to glutathione beads were incubated with lysate from COS-7 cells expressing YFP-LC3. Beads were subsequently

washed and bound proteins were resolved by SDS-PAGE and visualized by Western blot using an antibody against GFP (which also recognizes YFP). The three GST constructs containing an eight amino acid region of NBR1 (SEDYIIIL) were all able to bind to LC3 however deletion of this acidic-hydrophobic stretch (NBR1-C) abrogated binding (Figure 3.3). This eight amino acid sequence was later termed the LC3 interacting region 1 (LIR1) by Kirkin et al. (Kirkin et al., 2009). This interaction was also confirmed in a cell free environment showing that it is a direct protein-protein interaction (Figure 3.3C). Subsequently, it was also demonstrated that NBR1 can bind six human ATG8 homologues; GABARAP, GABARAPL1, GABARAPL2, LC3A, LC3B and LC3C and that NBR1 has a second LC3 binding site (aa542-636) termed LIR2 (Kirkin et al., 2009).

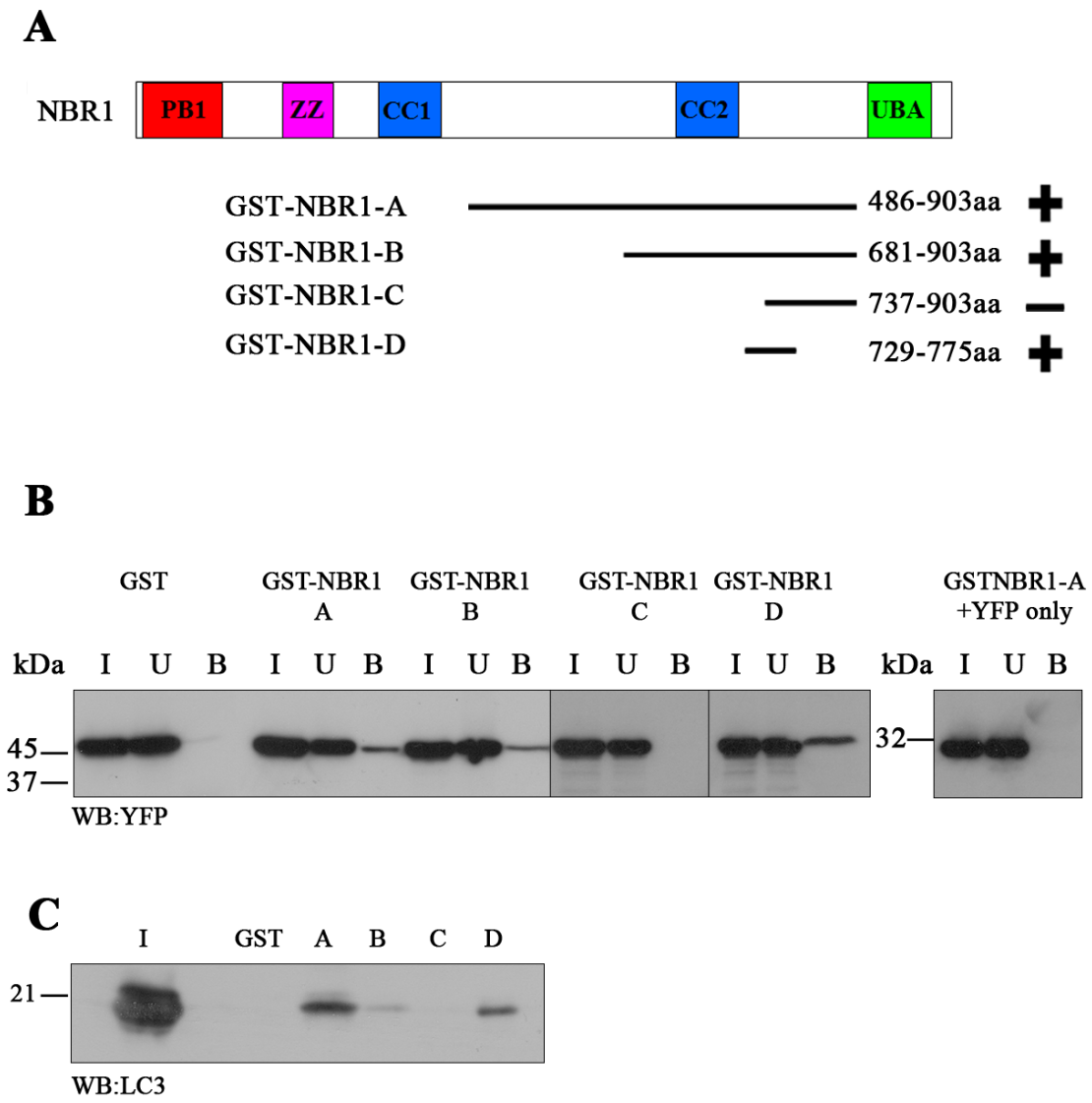

Figure 3.3. Nbr1 interacts with LC3

A. Schematic diagram of the domain structure of human NBR1 showing phasing of GST constructs. LC3 interactions are shown by + for positive, - for negative.

B. GST-tagged human NBR1 proteins (phased as in A) were bound to glutathione beads and incubated with cell lysates from YFP-LC3 transfected COS-7 cells. GST-tagged or YFP-tagged only proteins were used as negative controls. Samples were analysed by SDS PAGE and Western blot and probed against YFP. I, input; U, unbound; B, bound fractions. GST-NBR1-C which lacks the PB1, ZZ, CC1 and CC2 does not bind LC3 whereas GST-NBR1-D was able to bind LC3, suggesting that the 8 residues difference between the two constructs is critical for LC3 binding.

C.The same GST-tagged NBR1 proteins (abbreviated to A-D) were incubated with recombinant His-LC3. Samples were analysed by SDS PAGE, Western blot and probed with anti-LC3 antibody. Similar results were obtained which confirmed the results from the GST pull down. (modified from Waters et al. 2009).

3.5. Biochemical analysis of the potential interaction of Nbr1 with osteocalcin and cystatin C

Due to the known roles for Nbr1 in bone remodelling (Whitehouse et al., 2010) and the lack of previously identified bone specific interactors of Nbr1, osteocalcin provided an interesting candidate for further investigation. Additionally, the possible role of cystatin C in osteoblast differentiation and bone mineralisation suggests it is a key regulator of bone remodelling and therefore warranted further investigation.

Biochemical analysis was used to validate these interactions further. Full length mouse osteocalcin (aa1-95) the propeptide (aa24-95), the mature protein (aa46-95), and mature cystatin C (aa26-140) were cloned into a GST-tagged vector. Purified GST-tagged proteins bound to glutathione beads were incubated with cell lysate from COS-7 cells overexpressing HA-Nbr1. Beads were subsequently washed and bound proteins resolved by SDS PAGE, and visualized by Western blot using an antibody raised against the HA tag. Under these conditions, full length osteocalcin bound weakly to Nbr1, however deletion of the signal peptide abolished this interaction (Figure 3.4). An interaction between cystatin C and Nbr1 could not be confirmed using this method.

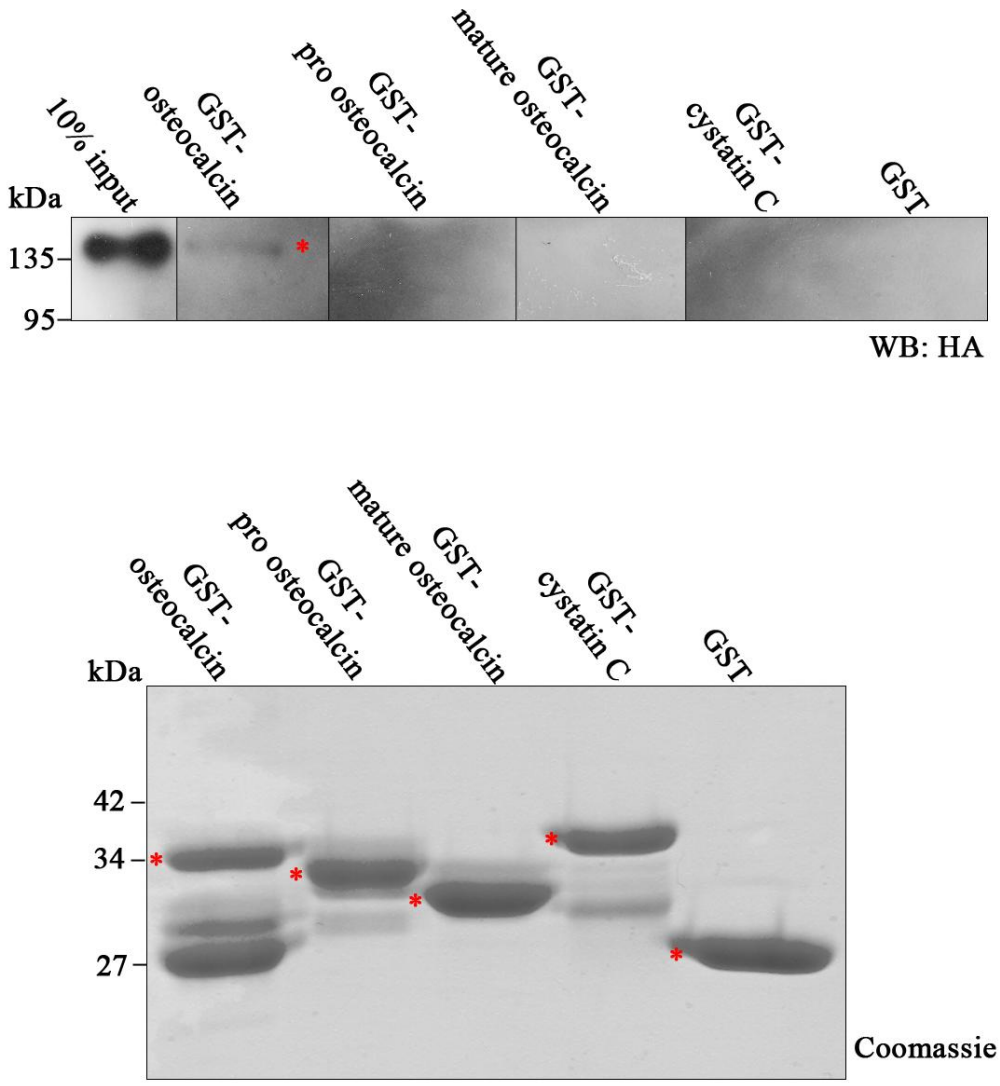

Figure 3.4. Osteocalcin interacts weakly with Nbr1.
GST-tagged osteocalcin fragments and cystatin C were bound to glutathione beads and incubated with cell lysates from HA-Nbr1 expressing COS-7 cells. GST was used as a negative control. Samples were analysed by SDS PAGE and Western blot and probed with an antibody against HA. Upper panel: Western blot to show that full length osteocalcin interacts weakly with Nbr1 (as shown by *) whilst the processed forms and cystatin C did not interact. Lower panel: Coomassie stained SDS PAGE showing 50% of the GST tagged protein used in the pulldown experiment. GST-fusion proteins are labelled with *.

3.6. Discussion

The Nbr1 protein is comprised of numerous conserved protein domains including a C-terminal UBA domain, an N-terminal PB1 domain and two coiled-coil domains. However, the region in the centre of Nbr1 is largely uncharacterised. A yeast-2-hybrid screen was performed using this central region of Nbr1 to identify novel interacting partners.

3.6.1. Interaction of Nbr1 with LC3 links it to autophagic protein degradation

LC3 was identified as an interacting partner of Nbr1 in the yeast-2-hybrid screen described in this chapter. p62 has previously been shown to interact with LC3 and other Atg8 homologues (Pankiv et al., 2007a). An 11 amino acid conserved sequence containing three acidic residues (DDD) followed by two conserved hydrophobic residues (WXXL) were shown to be essential and sufficient for LC3 binding to p62. This region was referred to as the LC3 interaction region (LIR) (Ichimura et al., 2008). Due to the structural homology of Nbr1 and p62, this data suggested that the putative interaction between LC3 and Nbr1 warranted further investigation. Other members of my laboratory had previously shown that Nbr1 and LC3 colocalise to discreet punctate vesicles in COS-7 cells (Waters et al., 2009), therefore biochemical studies were already underway to determine if Nbr1 and LC3 interact (Dr Sarah Waters, KCL). Using GST binding assays, the LC3 interaction region in NBR1 was mapped to an eight amino acid stretch (729-736 in human NBR1), C-terminal to the second coiled-coil domain (Figure 3.3). This region consists of two acidic residues at positions 730 and 731 and an aromatic residue at position 732 (SEDYIIIL). During this study, Kirkin et al. also reported a direct interaction between NBR1 and six Atg8 homologues including LC3 (Kirkin et al., 2009). Mutation of the aromatic tyrosine residue in NBR1 (aa732), corresponding to the acidic tryptophan residue in the LIR of p62 abolished LC3 binding (Kirkin et al., 2009). In addition to the primary LC3 binding region in NBR1, Kirkin et al. identified a secondary LC3 binding site corresponding to amino acids 542-636 of human NBR1 (LIR2). Interaction of LC3 with this region was much weaker,

therefore aa729-736 corresponding to LIR1 was considered as the major LC3 interaction surface (Kirkin et al., 2009). Subsequently, the structure of the GABARAPL-1/NBR1 complex has been determined and mutational analysis demonstrated that the presence of a tryptophan residue at position 732 of NBR1 increased GABARAP-1 binding affinity (Rozenknop et al., 2011). LIR motifs have been identified in a growing number of other autophagy receptors (discussed below) and therefore, the LIR motif is generally thought to consist of eight amino acids including at least one acidic residue and an aromatic residue at position four which is absolutely required for LC3 binding. The amino acid conservation of the LIR can be illustrated by the sequence logo (Figure 3.5) compiled by Johansen et al. using 25 LIR motifs from 21 different proteins (Johansen and Lamark, 2011).

Our laboratory and others have observed that inhibition of autophagy by treatment of cells with Bafilomycin A_1 stabilises Nbr1 protein levels suggesting that like p62, it is itself degraded by autophagy (Kirkin et al., 2009; Waters et al., 2009). In conjunction with the yeast-2-hybrid carried out in this thesis, these data show that Nbr1 is targeted to the autophagosome for degradation via its interaction with LC3. Recent research has also identified homologues of Nbr1 throughout the eukaryotic kingdom, whilst p62 is largely confined to metazoans. Furthermore, plant Nbr1 has hybrid properties of mammalian Nbr1 and p62 as it contains a conserved LIR which can bind Atg8 family members but can also homo-oligomerize via its PB1 domain (Svenning et al., 2011). This highlights the importance of Nbr1 as an autophagic receptor. Additionally, it has been shown that both Nbr1 and p62 can be targeted to the autophagosome formation site independently of Atg factors downstream of the PI3-kinase complex, but the LC3 interaction region is required for their degradation via the autophagosome (Itakura and Mizushima, 2011).

At its C-terminus Nbr1 contains a UBA domain that facilitates the binding of monoubiquitin, K48- and K63-linked polyubiquitinated chains (Kirkin et al., 2009; Waters et al., 2009). The UBA domain of Nbr1 is also essential for the formation of LC3 positive vesicles (Waters et al., 2009). Together, these data suggest that like p62, Nbr1 acts via its interaction with LC3 as an autophagic receptor selectively targeting ubiquitinated proteins for autophagic degradation (Figure 3.6). p62 is also

involved in other forms of selective autophagy and facilitates the degradation of peroxisomes (Kim et al., 2008b), mitochondria (Huang et al., 2011) and invading bacteria (Zheng et al., 2009). Other LC3 interacting proteins have also been identified that link the target-receptor complex to the autophagic machinery. Atg32 and NIX, both tether mitochondria to the autophagic machinery (Novak et al., 2010; Okamoto et al., 2009) whilst NPD52 and optineurin target pathogens for autophagic degradation (Mostowy et al., 2011; Wild et al., 2011). The selective targets of Nbr1 are yet to be identified however it is known that Nbr1 does not play a major role in the selective autophagic degradation of the bacteria *S. typhimurium* (Zheng et al., 2009). Recent data has demonstrated that p62 is also able to target specific proteins for degradation via its PB1 domain independent of ubiquitination (Watanabe and Tanaka, 2011). Interestingly, in some fungi, the UBA domain of Nbr1 has been lost suggesting that in these organisms Nbr1 may be able to bind cargo directly without requiring ubiquitination (Svenning et al., 2011). Through a mechanism similar to p62, it is likely that Nbr1 is able to interact directly with and target proteins for autophagic degradation independent of a polyubiquitin signal.

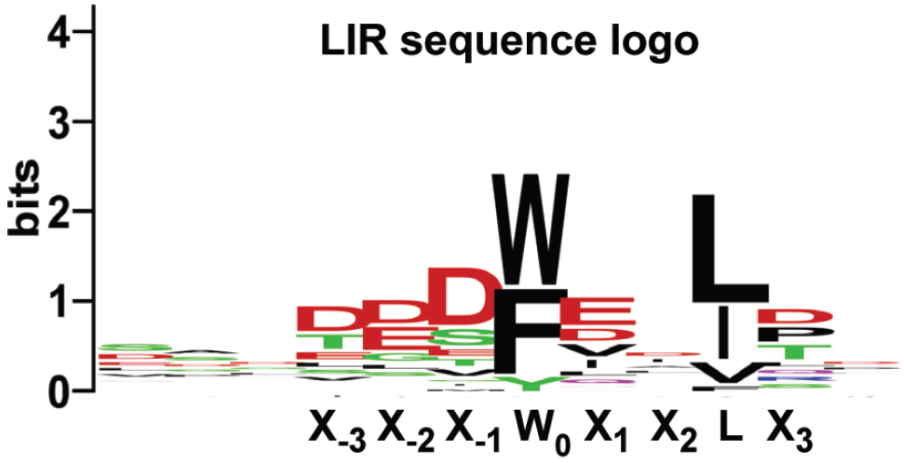

Figure 3.5. LIR sequence logo. 25 different LIR (LC3 interacting region) motifs from 21 different proteins were used to comprise this sequence logo; the more proteins that express a particular amino acid, the larger the letter appears. The LIR region consists of eight amino acid residues including at least one acidic residue at positions one, two or three (X_{-1}, X_{-2} or X_{-3}) and an aromatic residue at position 4 (W_0) (taken from Johansen et al 2011).

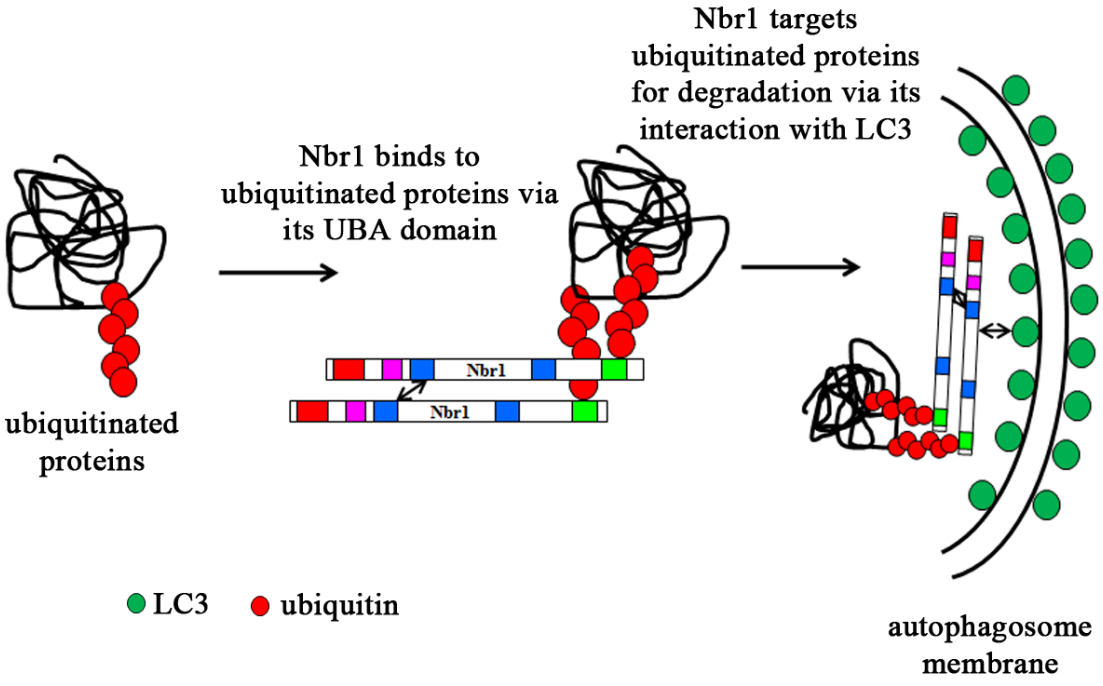

Figure 3.6. Nbr1 targets ubiquitinated proteins for degradation. Via its interaction with LC3, Nbr1 acts to target polyubiquitinated protein aggregates to sites of autophagosomal formation where they can be engulfed and degraded.

3.6.2. Potential interaction of Nbr1 with components of the ubiquitination machinery

Ubiquitination is an important post-translational modification that requires the coordinated action of three enzymes that facilitate the transfer of ubiquitin to a target protein. Polyubiquitination acts as a signal for protein degradation via the autophagosome or the proteasome (Tan et al., 2008; Thrower et al., 2000). The yeast-2-hybrid performed in this study has identified proteins of the ubiquitination machinery as putative interactors of Nbr1.

Members of the ubiquitination machinery are known to interact with adaptor proteins and this can regulate polyubiquitination. p62 binding to the E3 ligase TRAF6 is required for TRAF6 polyubiquitination (Sanz et al., 2000; Wooten et al., 2005). Additionally, the interaction of MdmX with the E3 ligase Mdm2 functions to enhance the ubiquitination potential of Mdm2 (Badciong and Haas, 2002) and p62 interacts with the E3 ligase MuRF2 and targets it to a signalling complex in muscle (Lange et al., 2005). The E2 ubiquitin conjugating enzyme (UBE2O) and the ring finger protein Rnf26 (that displays characteristics of an E3 ligase) were identified in this study as interacting partners of the central region of Nbr1 (Table 3.3). This suggests that Nbr1 could be acting as a scaffold to recruit ubiquitination machinery and regulate polyubiquitination. UBE20 is ubiquitously expressed however its expression is also upregulated during reticulocyte differentiation (immature red blood cells) (Wefes et al., 1995), a stage when an upregulation of protein degradation and organelle clearance has been observed (Schweers et al., 2007). Enhanced autophagic turnover of mitochondria, mediated by the autophagic receptor NIX has also been observed during reticulocyte differentiation (Schweers et al., 2007). There are currently no known roles for Nbr1 in reticulocyte differentiation however, Nbr1 is ubiquitously expressed and could function to target UBE20 to sites of action and therefore influence the polyubiquitination and subsequent degradation of proteins.

The deubiquitination of target proteins can also regulate cellular signalling pathways and endosomal trafficking of membrane receptors. This has been illustrated by the actions of the deubiquitinating enzyme USP10 which promotes endocytic recycling

of the CFTR chloride channel (Bomberger et al., 2009). In addition, TRAF6 ubiquitination is regulated by the deubiquitinating enzyme CYLD which acts to inhibit NFκB signalling (Sundaram, 2011). USP8 has recently been identified as an interacting partner of Nbr1 (Waters et al., 2009). This deubiquitinating enzyme has been implicated in the endocytic degradation of the EGFR receptor (Alwan and van Leeuwen, 2007). Nbr1 is also involved in the modulation of EGFR receptor internalisation, functioning to inhibit receptor endocytosis and therefore enhancing ERK 1/2 signalling (Mardakheh et al., 2010). It has not been identified whether this is regulated by ubiquitination however the interaction between Nbr1 and USP8 suggests a functional relationship may exist in order to regulate the endocytosis and degradation of EGFR.

The identification of E2 and E3 enzymes as putative interactors of Nbr1 in this thesis provides further evidence for the role of Nbr1 in regulating the ubiquitination status of proteins and has identified potential cell specific roles in reticulocyte differentiation. I addition, Nbr1 has been found in protein aggregates induced by proteasomal inhibition suggesting that Nbr1 is degraded by the UPS (Wilde et al., 2011).

3.6.3. Interaction of Nbr1 with proteins involved in bone formation and remodelling

Two proteins involved in the maintenance of bone have also been identified as putative interactors of Nbr1. Biochemical binding assays could not confirm the interaction between the cysteine protease inhibitor cystatin C, but did identify a weak interaction between osteocalcin and Nbr1 (Figure 3.4). Osteocalcin is synthesized as a prepromolecule, cleaved to form a promolecule which is subsequently γ-carboxylated. The propeptide is then removed and the mature protein secreted (Gundberg and Clough, 1992b). Osteocalcin can affect bone formation rate, probably via a negative feedback loop (Ducy et al., 1996) and can also influence glucose tolerance, fat mass and energy expenditure in mice (Lee et al., 2007b). Secreted proteins are usually co-translationally delivered to the endoplasmic reticulum (ER). This is mediated by the highly conserved signal-recognition particle (SRP) which recognizes the signal peptide sequence, halts translation and targets the

ribosomal complex to the ER membrane. This results in the translocation of the target protein across the membrane and into the lumen of the ER (Saraogi and Shan, 2011). A large proportion of proteins can however be cotranslationally degraded (Turner and Varshavsky, 2000) and this can be facilitated by the eukaryotic elongation factor, eEF1A (Chuang et al., 2005). Polyubiquitinated chains are well recognized as signals for cotranslational protein degradation, however direct binding of adapter proteins to their targets can also result in protein degradation (Watanabe and Tanaka, 2011). This suggests that Nbr1, through its interaction with osteocalcin could be involved in the cotranslational degradation of this protein. In addition, this could be facilitated by the putative interaction between Nbr1 and eEF1A (discussed in Chapter 4). Further work is required in order to establish whether osteocalcin is degraded by either autophagy or the proteasome and whether this is dependent on Nbr1. The truncated Nbr1 mouse model (lacking the osteocalcin binding site) displays increased levels of serum osteocalcin (Whitehouse et al., 2010), further suggesting that Nbr1 could be negatively regulating osteocalcin secretion and therefore osteoblast activity by targeting it for degradation.

Cell specific expression of the osteoblast transcription factor ATF4 can be regulated post-translationally. *ATF4* mRNA is expressed in a variety of mouse tissues and cell lines however ATF4 is only detectable in osteoblastic cell lines (Yang and Karsenty, 2004). Inhibition of the proteasome or the specific E3 ligase β-TrCP1 resulted in detectable ATF4 protein levels in non-osteoblastic cell lines suggesting that the osteoblast specific levels of ATF4 are controlled by ubiquitin-dependent proteasomal degradation (Yang and Karsenty, 2004). Nbr1 may act via a similar mechanism to specifically target yet to be identified proteins for degradation via either autophagy or the UPS in osteoblasts and therefore modulate osteoblast differentiation and function.

3.7. Future Work

Nbr1 and p62 have previously been identified as interacting with members of the ubiquitination machinery (Sanz et al., 2000; Waters et al., 2009). This yeast-2-hybrid has identified a number of novel putative interactors of Nbr1 that are involved in ubiquitination of target proteins (UBE20 and Rnf26). Validation of these interactors using GST binding assays and coimmunoprecipitation would shed further light on the specific roles of Nbr1 as a scaffold protein to facilitate ubiquitination. Colocalisation studies could also be used to establish if Nbr1 is localised to the same subcellular compartments as UBE20 and Rnf26 and thus determine if these interactions are plausible. Additionally, it would be interesting to validate the putative interaction between Nbr1 and Tmp21 (Table A1, Appendix) as Tmp21 is involved in vesicular trafficking (Schimmoller et al., 1995).

Data in this thesis identified osteocalcin as interacting weakly with Nbr1. Further colocalisation studies in osteoblast specific cells would determine if these proteins are present in the same cellular compartments and therefore gain further evidence as to the likely interaction of these proteins *in vivo*. Due to the putative link between Nbr1 and cotranslational degradation (see Chapter 4), siRNA knock-down of Nbr1, could be used to investigate if the degradation of osteocalcin is regulated by Nbr1. Additionally, proteasome inhibitors or bafilomycin could be used to block the degradation of proteins via the UPS and autophagy respectively to assess which degradation pathway is required for osteocalcin degradation.

It could not be proven that Nbr1 interacts with cystatin C *in vitro*, however this could be due to the conditions of the GST binding assay used or the possible transiency of the interaction. In addition, GST binding assays do not take into account possible posttranslational modifications, therefore, other assays such as FRET could be used to further validate this interaction.

The bone specific ubiquitinated targets of Nbr1 are still unknown. GST binding assays could be performed with the UBA domain of Nbr1 in primary osteoblasts. All bound proteins could then be resolved by SDS PAGE and identified by mass

spectrometry. This would identify possible ubiquitinated or non-ubiquitinated targets of Nbr1 which could be further investigated with regards to its role in autophagic and proteasomal protein turnover.

Chapter 4. Identification of Interacting Partners of a Highly Conserved Region of Nbr1

4.1. Introduction

During the course of this project, evolutionary analysis was carried out on the NBR1 protein by Dr R. Roberts (Kings College London). This revealed that NBR1 is highly conserved throughout the eukaryotic kingdom, and NBR1-like architecture is present in animals, plants and fungi (Figure 4.1). The plant Nbr1 contains an additional C-terminal UBA domain and fungi possess three extra ZZ domains. Along with the known protein domains, a conserved region (referred to from now on as the novel region) of approximately 110 amino acids consisting of an internal repeat of ~55 amino acids is present in NBR1 in the eukaryotic kingdom and also in a number of bacteria (Figure 4.2A). It spans from amino acids 372-479 of human NBR1 and resides in the largely uncharacterised central region (Figure 4.1). The novel region consists of a robustly predicted secondary structure of six β-strands. These six strands are predicted to form a compact "sandwich" comprising of two three β-stranded sheets. The only other known protein that contains the novel region is c6ORF106 however, the function of this protein is unknown (R. Roberts, unpublished data). Figure 4.2B shows a schematic diagram of the bovine Niemann-Pick C2 (NPC2) cholesterol-binding protein which contains a similar structure to that predicted for the novel region. During this study, the novel region was also identified by others and given the name NBR1 box by Kraft et al. (Kraft et al., 2010) and subsequently the FW (Four W (tryptophan)) domain by Johansen et al. due to the four highly conserved tryptophan residues found in this domain (Johansen and Lamark, 2011). This region is also absent in p62, suggesting it may mediate a functionally distinct role for Nbr1 (Svenning et al., 2011). As it was not included in the yeast-2-hybrid screen described in Chapter 3, the novel region will be used as bait and a further screen performed using a bone calvarial library to identify any potential interacting proteins.

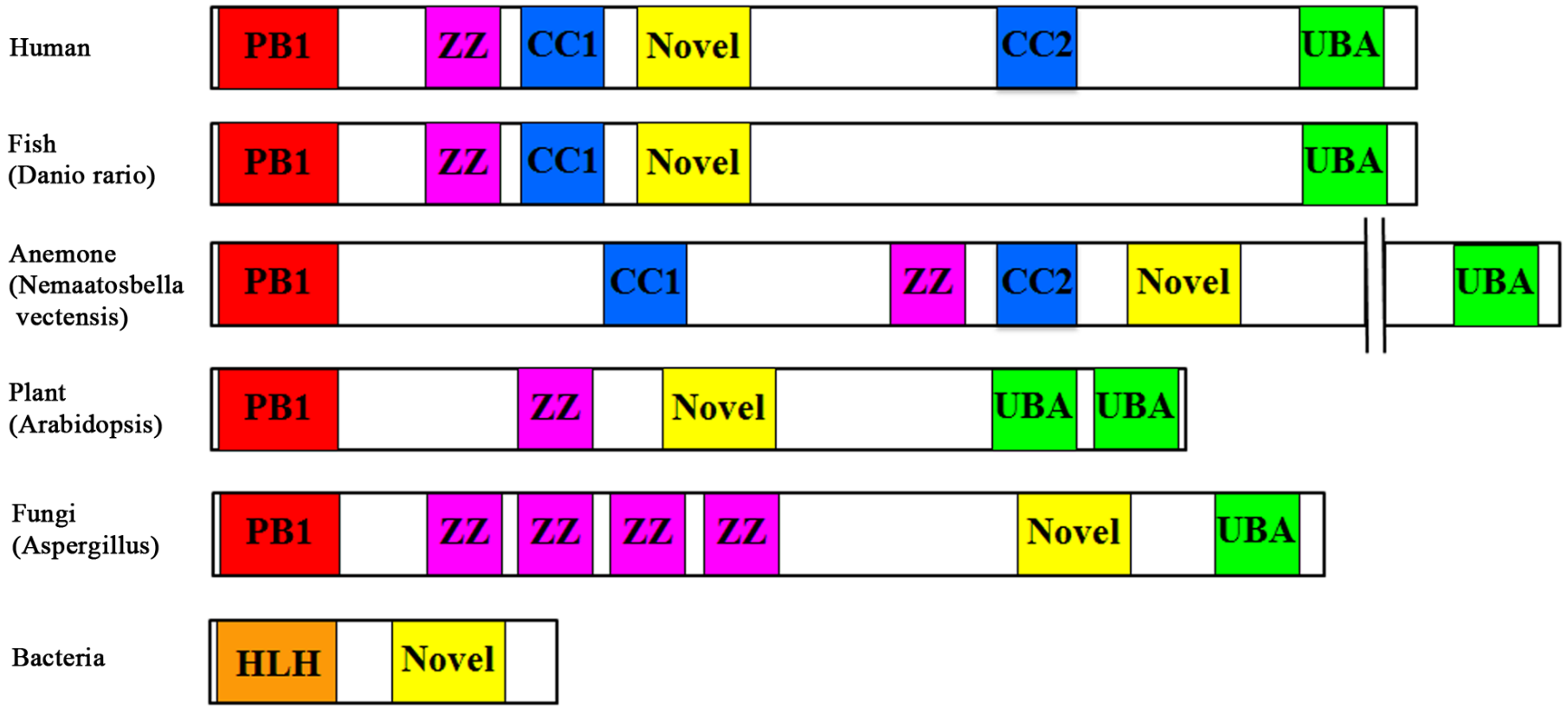

Figure 4.1. Domain structure of NBR1-like proteins in different organisms. NBR1 is highly conserved throughout the eukaryotic kingdom with proteins containing NBR1-like domains in fish, plants, and fungi. Each of these proteins also contains a conserved region (novel) of approximately 110 amino acids consisting of an internal repeat of ~55 amino acids, present in the eukaryotic kingdom and also in some bacteria. PB1, Phox and Bem1p domain; CC, coiled-coil domain; UBA, ubiquitin associated domain; HLH, helix-loop-helix (modified from unpublished data by R. Roberts, Kings College London).

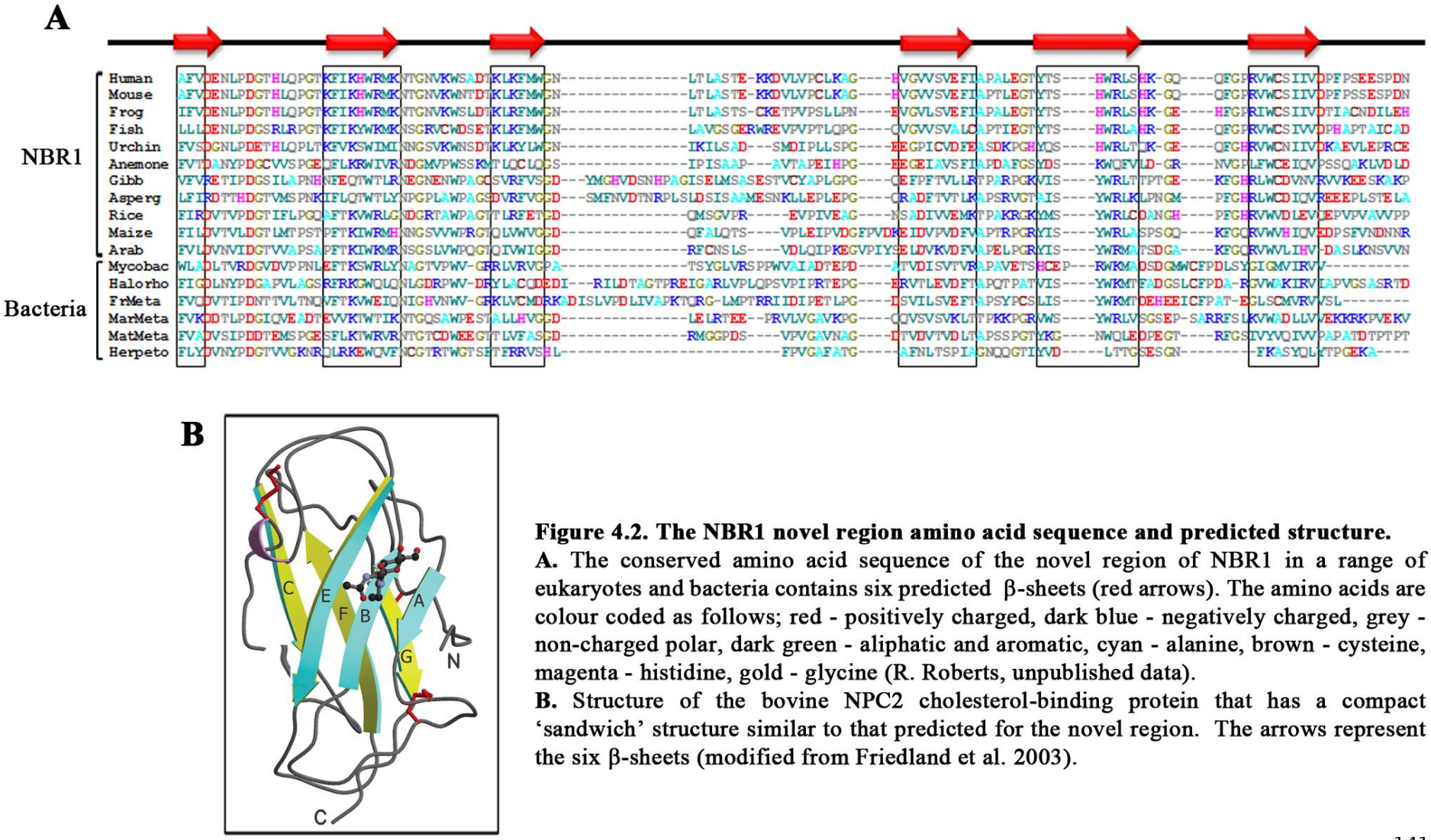

Figure 4.2. The NBR1 novel region amino acid sequence and predicted structure.
A. The conserved amino acid sequence of the novel region of NBR1 in a range of eukaryotes and bacteria contains six predicted β-sheets (red arrows). The amino acids are colour coded as follows; red - positively charged, dark blue - negatively charged, grey - non-charged polar, dark green - aliphatic and aromatic, cyan - alanine, brown - cysteine, magenta - histidine, gold - glycine (R. Roberts, unpublished data).
B. Structure of the bovine NPC2 cholesterol-binding protein that has a compact 'sandwich' structure similar to that predicted for the novel region. The arrows represent the six β-sheets (modified from Friedland et al. 2003).

4.2 Yeast-2-Hybrid

The phenotype of the yeast strains utilised (Y187 and AH109) were confirmed to be the same as described in section 3.2.1.

4.2.1. 3-AT Titration and Autoactivation.

The novel region of Nbr1 (aa346-498) was cloned into the pGBKT7 vector and transformed into yeast strain Y187. To test for autoactivation and 'leaky' histidine expression, successful transformants were mated with yeast strain AH109 transformed with the pGADT7 empty vector (containing the GAL4 activation domain). The SV40 Large T-antigen and p53 protein were used as a positive control as they are known to interact. Empty vectors pGADT7 and pGBKT7 were used as a negative control. Table 4.1 shows the extent of colony growth with increasing concentrations of 3-AT. No autoactivation was observed with the bait construct (Nbr1 aa346-498-GAL4 BD) and a 3-AT concentration of 3mM was chosen for the library screen.

Mating	**-Leu/-Trp**	**-Leu/-Trp/-His**				**-Leu/-Trp/-His/-Ade**
		0mM 3-AT	**1mM 3-AT**	**3mM 3-AT**	**5mM 3-AT**	
p53 + T-antigen	√	√	√	√	√	√
pGBKT7 + pGADT7	√	X	X	X	X	X
Nbr1 aa346-498+ pGADT7	√	X	X	X	X	X

Table 4.1. 3-AT Titration and test for bait autoactivation. Yeast were transformed with constructs indicated, mated and plated on SD media lacking different combinations of amino acids as shown. The positive and negative controls grew as expected. The bait construct (Nbr1aa346-498) exhibited no autoactivation and did not grow in the absence of histidine or adenine.

4.2.2. Confirmation of bait protein expression.

To verify that the transformed yeast (Y187) were expressing the bait protein of interest (GAL4BD-Nbr1 aa346-498), protein was extracted from transformed yeast, resolved by SDS PAGE and visualised by Western blot using an antibody that

recognises the GAL4 BD. A protein band of ~38kDa was identified which is the same size as predicted for the bait protein, thus confirming successful expression in Y187 yeast cells (Figure 4.3).

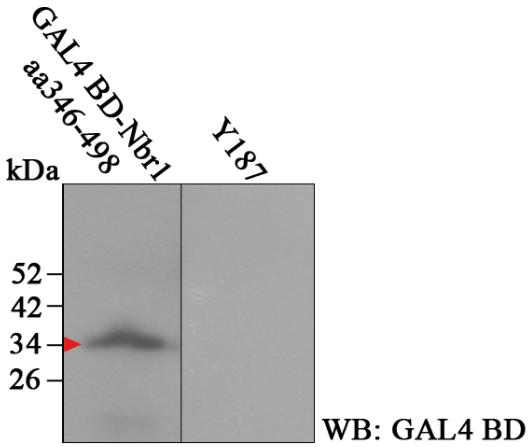

Figure 4.3. Western blot analysis of bait protein expression in yeast. Yeast (Y187) are expressing Nbr1 aa346-498 fused to the GAL4 BD (red arrow). Y187 alone was the negative control and did not show any GAL4 BD protein expression.

4.2.3. Yeast -2-Hybrid Library Screen

Y187 yeast expressing the bait protein (GAL4 BD-Nbr1 aa346-498) were mated with a pretransformed 7 day old mouse calvaria cDNA library (cloned into the pGADT7 vector) transformed into the AH109 yeast strain, kindly supplied by Prof. Ikramuddin Aukhil (College of Dentistry, University of Florida). The yeast from this mating were plated onto SD–Leu/-Trp/-His media supplemented with 3mM 3-AT. The number of colonies screened was calculated to be $9.5x10^5$.

A total of 83 positive clones grew on SD–Leu/-Trp/-His media supplemented with 3mM 3-AT and were restreaked onto SD–Leu/-Trp/-His media supplemented with 3mM 3-AT a further three times to eliminate any multiple library plasmids. This resulted in the regrowth of 59 clones. Plasmid DNA was extracted from these 59 yeast clones, transformed into chemically competent *E.coli*, the DNA extracted and sequenced. Clones that were out of frame with the GAL4 AD were discarded.

Twenty two proteins were identified as putative interactors of the novel region of Nbr1. The most biologically relevant candidates were microtubule associated protein 1B (MAP1B) and eukaryotic translation elongation factor 1A (eEF1A) (Table 4.2). Other candidates included a number of muscle specific proteins (Table 4.2), suggesting that the calvarial library was contaminated with muscle. Known false positives that often arise from yeast-2-hybrid assays independent of bait sequence (such as actin and procollagen) were also identified and not investigated any further (Hengen, 1997). All other proteins that will not be discussed are listed in Table A.2 (Appendix).

Accession No.	Gene ID	No. of Colonies
NM_008634	Microtubule-associated protein 1B	2
NM_010106.2	Eukaryotic translation elongation factor 1A	1
NM_023374.3	Succinate dehydrogenase complex subunit B	1
NM_001085509	Myomesin family member 3	2
NM_001033621.2	Myotilin (Myot)	1
NM_011890.4	Sarcoglycan B (dystrophin-associated glycoprotein	1
NM_009606.2¥	Actin α 1 (skeletal muscle)	5
NM_007742.3¥	Procollagen type 1 α 1	1

Table 4.2. Positive clones identified from the yeast-2-hybrid screen.
¥ indicates likely false positives.

4.3. Putative Interacting Partners of Nbr1

4.3.1. Eukaryotic translation elongation factor 1A (eEF1A)

The novel region of Nbr1 interacts with the C domain (aa283-400 - this was deduced from the isolated yeast-2-hybrid clone) of the eukaryotic translation elongation factor 1A (eEF1A). eEF1A is ubiquitously expressed (Lee et al., 1992) and traditionally known for its involvement in protein synthesis where it catalyses the first step of the elongation cycle (Lamberti et al., 2004). It is composed of three domains; the catalytic domain (G-domain), the middle domain (M-domain) and the C-terminal domain (C-domain). These domains are important for the binding of eEF1A to aminoacyl-tRNA during the elongation cycle (Berchtold et al., 1993). eEF1A is also involved in a number of other cellular functions including embryogenesis, cell proliferation and tumorigenesis (Lamberti et al., 2004). Most interestingly for this project, eEF1A has been linked to ubiquitin mediated protein degradation and this will be discussed further in section 4.8.

4.3.2. Microtubule associated protein 1B (MAP1B)

Microtubule associated protein (MAP1B) was first described over 20 years ago (Bloom et al., 1985) and is one of three high molecular weight MAP1 isoforms. It is

transcribed as a single mRNA, translated into a polypeptide of 2464 amino acids (mouse) which is subsequently cleaved at approximately aa2215. This produces a heavy chain - MAP1B-HC (2214aa) and a light chain - MAP1B-LC1 (250aa) (Tögel et al., 1999). Both the MAP1B-HC and –LC1 can bind to microtubules (Hammarback et al., 1991; Noiges et al., 2002) and to each other (Tögel et al., 1998). The light chain stabilises microtubules and this function is inhibited by the heavy chain (Tögel et al., 1998).

Much of the literature to date has focused on the function of MAP1B in the central nervous system due to its high expression during neuronal development (Schoenfeld et al., 1989) and in areas of high regenerative activities in adult brain (Viereck et al., 1989). Complete knock-out of the MAP1B gene in mice established that it is essential for the development and function of the nervous system as animals displayed impaired brain development (Meixner et al., 2000). An inhibition of axon formation and decreased microtubule synthesis and dynamics have also been observed in neurons deficient in MAP1B (Gonzalez-Billault et al., 2001). Additionally, MAP1B is present in Lewy bodies which contain increased levels of ubiquitin conjugates and are pathological hallmarks of Parkinsons disease and dementia (Jensen et al., 2000).

MAP1B has also been implicated in the regulation of autophagy. MAP1B-HC and its phosphorylated form (MAP1B-P) were identified as interacting partners of LC3 (Wang et al., 2006). In mice with degenerating axonal swellings of the nervous system, there was an accumulation of MAP1B-P that colocalised with LC3, therefore suggesting that the MAP1B-P-LC3 interaction provides a mechanism for targeting autophagosomes to axon terminals during neurodegeneration (Wang et al., 2006).

Nbr1 interacts with residues 2238-2465 of MAP1B (this was deduced from the isolated yeast-2-hybrid clone) which correspond to the light chain. The role of MAP1B-LC1 in autophagy has not been previously investigated however the known involvement of Nbr1 and microtubules in autophagy suggests this interaction warrants further investigation.

4.4. Nbr1 is found in a complex with MAP1B-LC1

A coimmunoprecipitation experiment was performed to establish if MAP1B-LC1 could be found in a complex with Nbr1. Lysate from COS-7 cells expressing HA-Nbr1 and MAP1B-LC1-myc was incubated with an antibody that recognises the myc tag. MAP1B-LC1 was immunoprecipitated and the immunocomplex bound to protein A beads. Bound proteins were resolved by SDS PAGE and subsequently visualised by Western blot using antibodies against the myc and HA tags. This demonstrated that MAP1B-LC1-myc was successfully immunoprecipitated (Figure 4.4, lanes 3&6) and that HA-Nbr1 was coimmunoprecipitated along with MAP1B-LC1-myc (Figure 4.4, lane 6). This result was specific to Nbr1 as an unrelated HA-tagged protein (HA-LacZ) could not be coimmunoprecipitated along with MAP1B-LC1-myc (Figure 4.4, lane 3).

4.5. Nbr1 interacts with the light chain of MAP1B

Biochemical analysis was used to further validate the interaction between MAP1B-LC1 and Nbr1. Lysate from COS-7 cells expressing MAP1B-LC1-myc was incubated with purified GST-Nbr1 aa346-498, GST alone or other regions of Nbr1 (aa1-135 and the UBA domain). GST beads were washed and bound proteins were resolved by SDS PAGE and visualised by Western blot using an antibody against the myc-tag. Under these conditions, the novel region of Nbr1 interacted with the MAP1B-LC1 (Figure 4.5A). Unexpectedly, the Nbr1 UBA domain also bound MAP1B-LC1.

To verify the interaction between the novel region of Nbr1 and MAP1B-LC1 in a cell free environment, MAP1B-LC1 was cloned into a His-tagged vector, expressed in bacteria and purified (sections 2.2.4 & 2.2.6). The purified protein was then incubated with GST-Nbr1 aa346-498 or GST alone. GST beads were washed and samples were analysed by SDS PAGE and visualised by Western blot using an antibody that recognises the His-tag. Under these conditions, the novel region of Nbr1 interacts with MAP1B-LC1 confirming that this was a direct protein-protein interaction (Figure 4.5B).

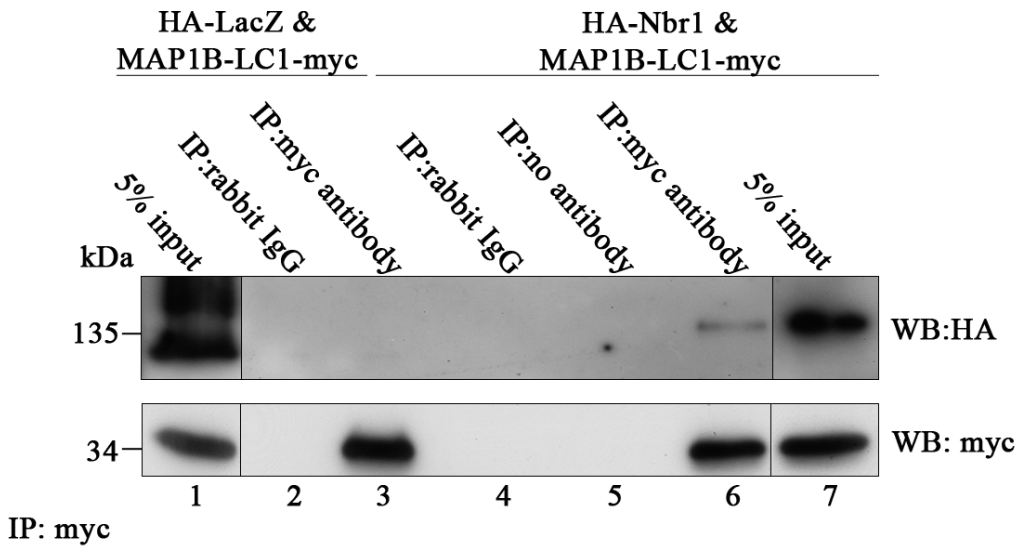

Figure 4.4. Nbr1 is found in a complex with MAP1B-LC1. Western blot showing that using an antibody that recognises the myc tag, HA-Nbr1 can be coimmunoprecipitated with MAP1B-LC1-myc from lysate of COS-7 cells expressing HA-Nbr1 and MAP1B-LC1-myc. HA-LacZ could not be coimmunoprecipitated with MAP1B-LC1-myc and all other controls were negative.

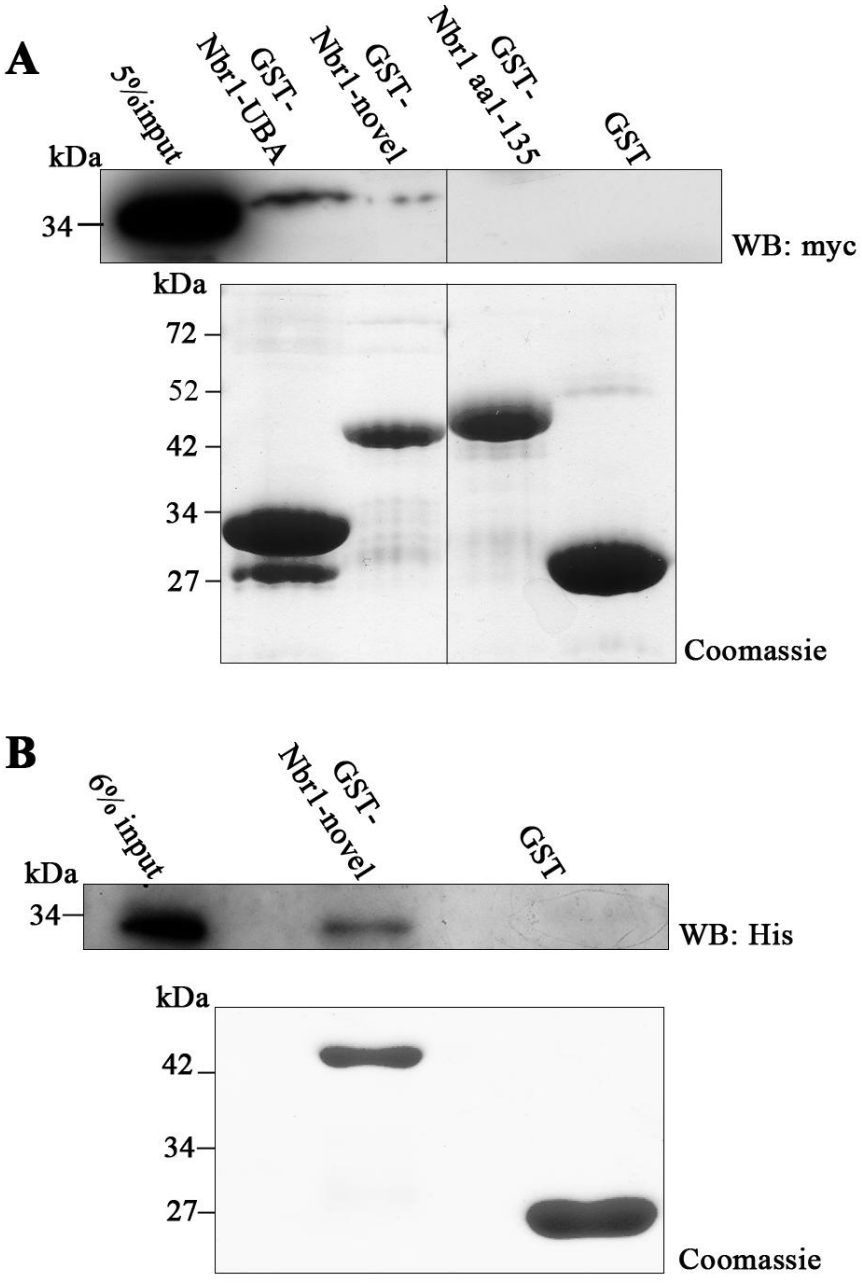

Figure 4.5. Nbr1 interacts with MAP1B-LC1.
A. Purified GST-tagged proteins were bound to glutathione beads and incubated with cell lysates from MAP1B-LC1-myc transfected COS-7 cells. Upper panel: Western blot showing that the novel region and the UBA domain of Nbr1 interact with MAP1B-LC1-myc. Lower panel: Coomassie stained SDS PAGE gel showing 100% of GST-tagged protein input.
B. Purified GST-tagged proteins were bound to glutathione beads and incubated with recombinant his-tagged MAP1B-LC1. Upper panel: Western blot showing that the novel region of Nbr1 interacts with His-MAP1B-LC1. Lower panel: Coomassie stained SDS PAGE gel showing 50% of GST-tagged protein input.

4.6. MAP1B-LC1 protein levels during inhibition of autophagic protein degradation

It has previously been observed that MAP1B-HC is not degraded by autophagy (Wang et al., 2006) however, it has not been reported whether the same is true for MAP1B-LC1. To determine if the function of the interaction between MAP1B-LC1 and Nbr1 is to facilitate the degradation of MAP1B-LC1 via autophagy, MAP1B-LC1 protein levels were analysed under conditions where autophagic protein degradation was blocked. PC12 cells (a rat neuronal cell line derived from a pheochromocytoma, known to express high levels of MAP1B) were treated with either Bafilomycin A_1 or DMSO as a control. Bafilomycin A_1 causes the accumulation of autophagosomes by inhibiting the vacuolar ATPase that drives the acidification of lysosomes, causing a reduction in lysosomal pH and the inhibition of protein degradation (Bowman et al., 1988). Cell lysates were resolved by SDS PAGE and proteins visualised by Western blot using antibodies that recognise p62, Nbr1, MAP1B-HC, MAP1B-LC1 or β-actin (Figure 4.6). Protein band intensity was quantified to estimate protein levels. Upon Bafilomycin A_1 treatment, the levels of both Nbr1 and p62 increased by 130% and 60% respectively (relative to a β-actin control). Nbr1 and p62 are both degraded by autophagy, therefore this demonstrated that protein degradation via autophagy was inhibited by Bafilomycin A_1 treatment. MAP1B-HC and MAP1B-LC1 protein levels showed a small but discernable increase upon the blockage of autophagic degradation relative to the β-actin control (10% and 20% respectively).

Analysis of MAP1B in primary osteoblasts was also attempted however protein levels could not be reproducibly detected by either Western blot or immunoflourescence.

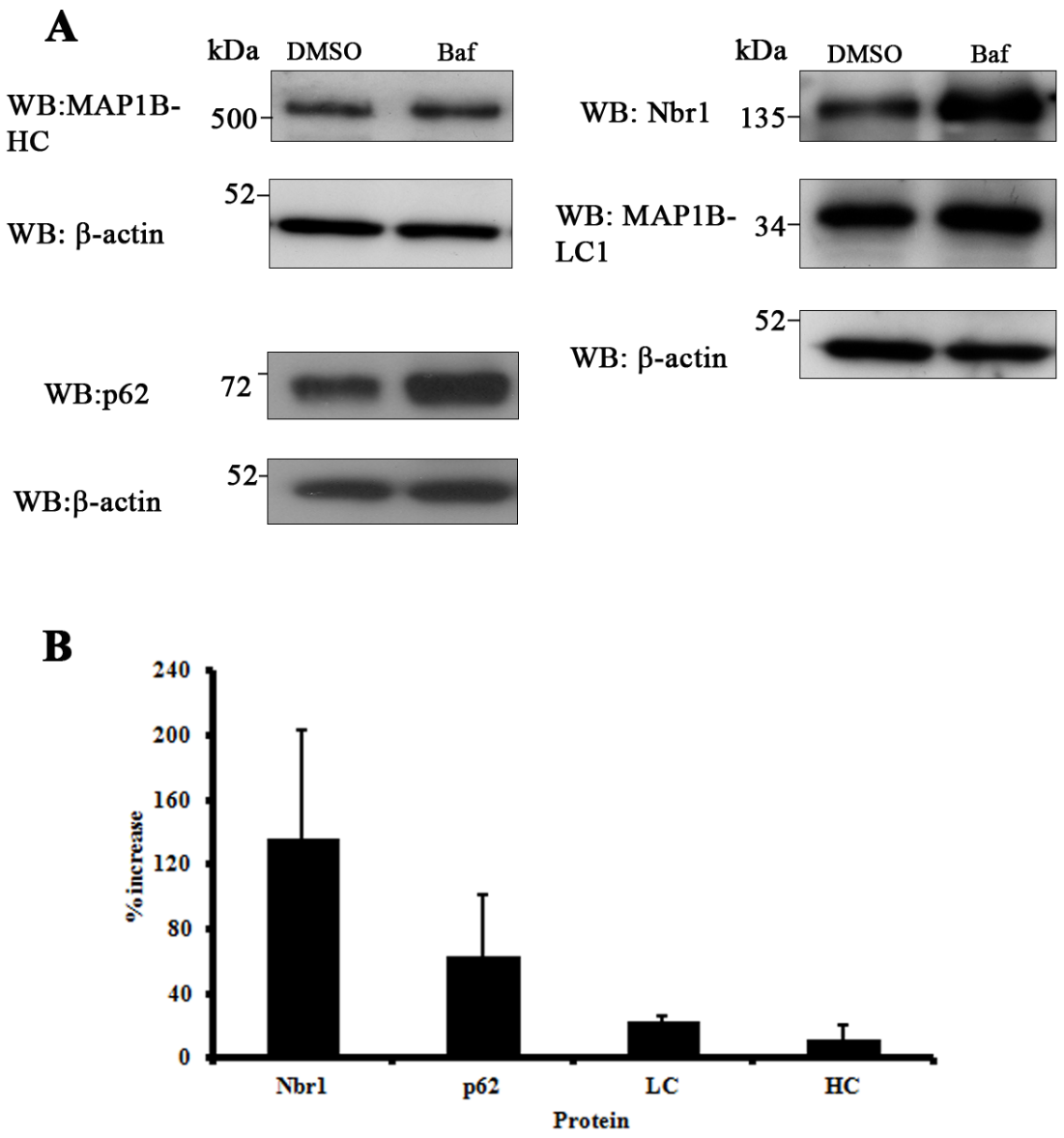

Figure 4.6. Western blot analysis of p62, Nbr1, MAP1B-HC and MAP1B-LC1 protein levels following blockage of autophagic protein degradation.
A. Western blots showing protein levels in cells treated with DMSO (control) or Bafilomycin A_1 (Baf) for 8 hours.
B. Protein band intensity of cell lysate treated with and without bafilomycin was quantified using ImageJ, normalised to β-actin and the % increase in protein levels after bafilomycin treatment was calculated. Nbr1 and p62 proteins levels increase dramatically and MAP1B-LC1 and MAP1B-HC protein levels increase by a small but discernable amount in cells treated with Bafilomycin A_1. Data represents the mean and SD of triplicate experiments.

4.7. Localisation of Nbr1 and MAP1B in mammalian cells.

Due to the direct interaction of Nbr1 and MAP1B-LC1, it was important to determine whether they colocalised *in vivo* and under what conditions. MAP1B has been widely studied in neuronal cells and is highly expressed in PC12 cells. This cell line was therefore utilised for endogenous protein colocalisation studies. Nbr1 and MAP1B-HC are both involved in the autophagy pathway. As MAP1B-LC1 interacts with MAP1B-HC, the cellular colocalisation of these two proteins was initially investigated under conditions where autophagy was blocked or induced. Cells were treated with DMSO (vehicle control), Bafilomycin A_1 or starved (to induce autophagy) then fixed and immunostained for endogenous proteins (Figure 4.7). MAP1B-HC and MAP1B-LC1 colocalise under all treatment conditions suggesting that the two MAP1B chains predominantly function as one unit. However, there were distinct areas where there was a lack of colocalisation.

MAP1B-HC and MAP1B-LC1 colocalise under conditions of autophagic inhibition and induction, which lead to the hypothesis that the interaction between Nbr1 and MAP1B-LC1 could be important for autophagic protein degradation. PC12 cells were treated as above and immunostained with antibodies against MAP1B-LC1 and Nbr1. Under starvation conditions, Nbr1 punctae often appeared adjacent to MAP1B-LC1 positive structures rather than directly colocalising (Figure 4.8). During conditions where protein degradation was blocked, MAP1B-LC1 was often excluded from Nbr1 positive vesicles. Under basal conditions (DMSO), Nbr1 showed a staining pattern more reminiscent of MAP1B-LC1 compared with the treatments to block or induce autophagy.

As MAP1B-HC and Nbr1 both interact with LC3 (Wang et al., 2006), the localisation of MAP1B-HC and Nbr1 was also studied. PC12 cells were prepared as above and stained with antibodies against MAP1B-HC and Nbr1. Cells treated with DMSO and Bafilomycin A_1 did not display any colocalisation however when cells were starved, Nbr1 and MAP1B-HC colocalised in distinct perinuclear vesicular structures (Figure 4.9).

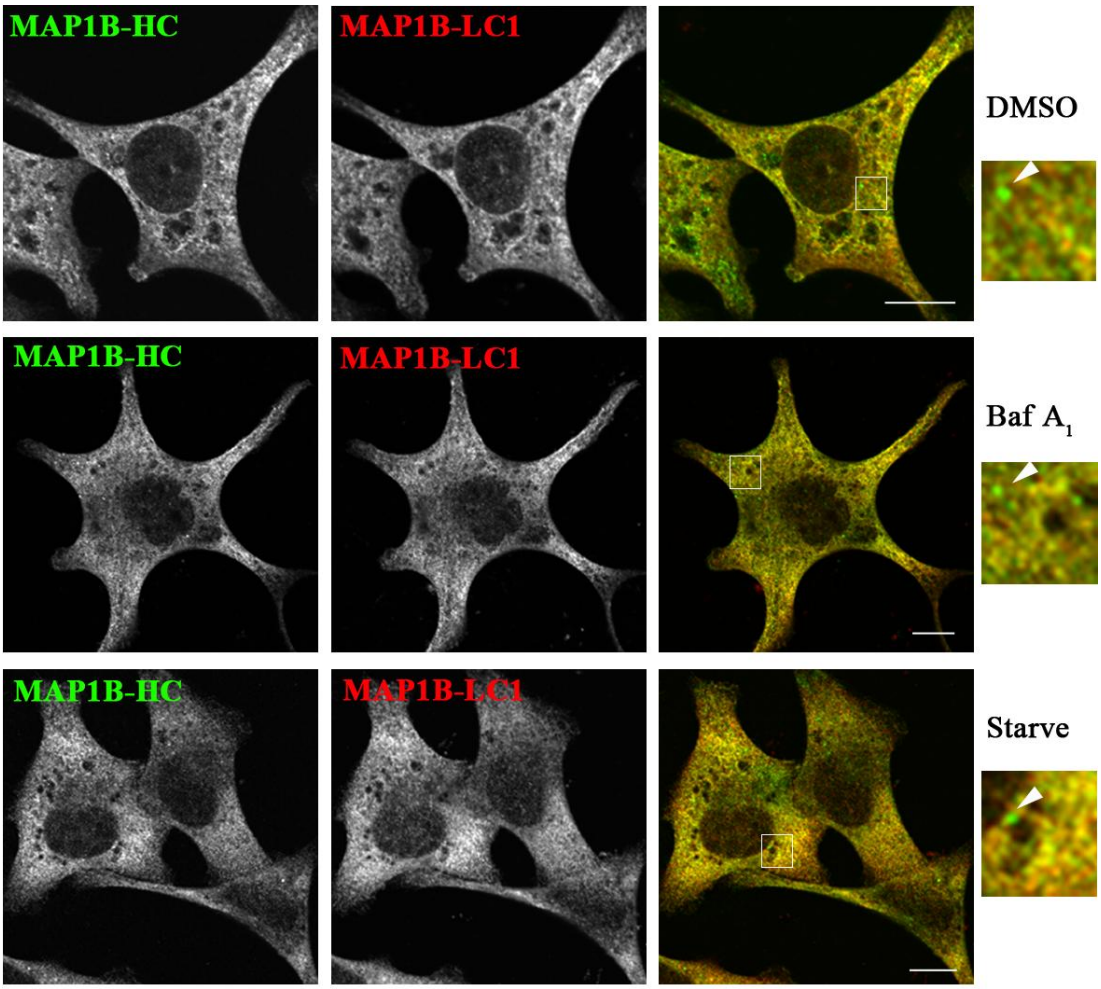

Figure 4.7. Intracellular localisation of MAP1B-HC and MAP1B-LC1 in PC12 cells. Cells were treated with DMSO, Bafilomycin A_1 or starved then fixed and immunostained with antibodies against the light and heavy chains of MAP1B. Under these conditions, both heavy (green) and light chain (red) colocalise however, there are distinct areas where no colocalisation was observed (arrows). Baf A_1=Bafilomycin A_1. Scale bars = 10µm. Images are represeantative of three experiments.

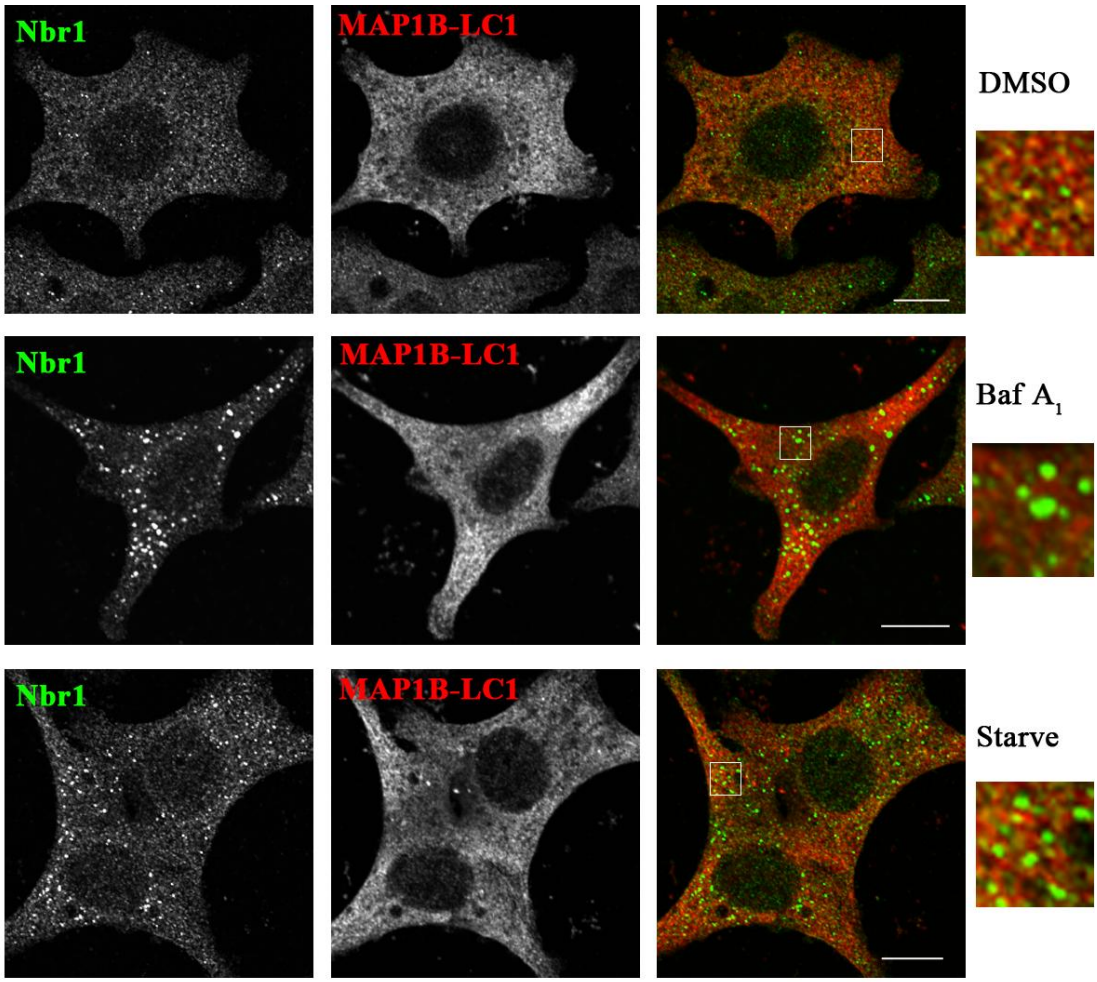

Figure 4.8. Intracellular localisation of MAP1B-LC1 and Nbr1 in PC12 cells. Cells were treated with DMSO, Bafilomycin A_1 or starved then fixed and immunostained with antibodies against MAP1B-LC1 (red) and Nbr1 (green). Under all conditions, MAP1B-LC1 shows diffuse staining across the cytoplasm of the cell with some punctate vesicular structures. Under conditions of autophagic inhibition, Nbr1 shows limited colocalisation with MAP1B-LC1 and when autophagy is induced by starvation, MAP1B-LC1 positive vesicles are often next to Nbr1 positive vesicles. Baf A_1=Bafilomycin A_1. Scale bars = 10µm. Images are representative of three experiments.

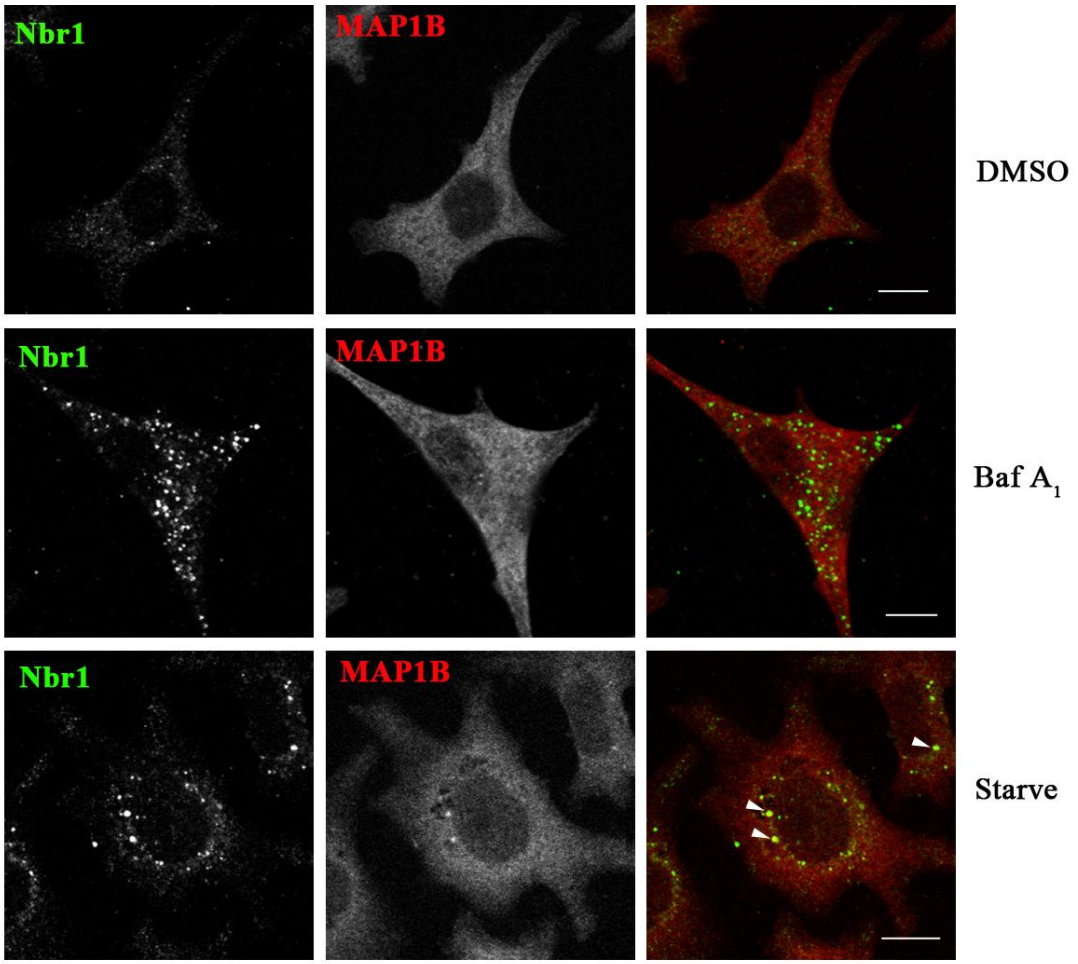

Figure 4.9. Nbr1 and MAP1B colocalise to discrete perinuclear vesicles upon induction of autophagy. PC12 cells were treated with DMSO, Bafilomycin A_1 or starved then fixed and stained with antibodies against Nbr1 (green) and MAP1B (red). Under basal conditions or when autophagic protein degradation was blocked, no colocalisation was observed. When cells were starved to induce autophagy, MAP1B and Nbr1 colocalised in distinct perinuclear vesicles. Baf A_1 = Bafilomycin A_1. Scale bars = 10µm. Images are representative of three experiments.

4.8. Discussion

Recent evolutionary studies performed in collaboration with Dr R. Roberts, KCL have identified a highly conserved region, located in the previously uncharacterised central region of Nbr1 (unpublished data). This domain, termed the novel region, is also present in a range of bacteria and contains two internal repeats of ~55 amino acids. It also has a predicted secondary structure consisting of two, three β-stranded sheets. Due to its high conservation and unknown function, a yeast-2-hybrid screen was carried out using a mouse calvarial library to identify interacting proteins of the novel region. This yeast-2-hybrid did not screen the cDNA library to saturation (Van Criekinge and Beyaert, 1999) therefore, some interacting partners may not have been identified.

4.8.1. Nbr1 interacts with the light chain of MAP1B

The light chain of MAP1B was identified as a putative interacting partner of the novel region of Nbr1 (Table 4.2). Subsequent coimmunoprecipitation and GST binding assays confirmed this direct interaction (Figures 4.4 and 4.5). MAP1B is a scaffold protein, transcribed as a single mRNA and subsequently cleaved to produce a heavy chain and a light chain. Both the heavy and light chains can bind to microtubules (Hammarback et al., 1991; Noiges et al., 2002) and to each other (Tögel et al., 1998). The microtubule network is known to facilitate autophagosomal formation (Fass et al., 2006; Köchl et al., 2006), the movement of mature autophagosomes towards lysosomes (Geeraert et al., 2010) and the recruitment of protein aggregates (Kawaguchi et al., 2003). The binding of adaptor proteins such as FYCO1 to both LC3 and microtubule motor proteins has also been suggested as a mechanism by which preautophagosomal membranes are targeted to sites of autophagosomal formation (Pankiv et al., 2010). This led to the hypothesis that the interaction between Nbr1 and MAP1B-LC1 could facilitate the targeting of ubiquitinated protein aggregates to the microtubule network, where they can be transported to sites of autophagosomal formation. In further support of this hypothesis, a similar mechanism has been proposed whereby MAP1B-HC is able to target autophagosomes to axon terminals during neurodegeneration through its interaction with LC3 (Wang et al., 2006). MAP1B has also been predicted to interact

with Atg12 and Atg3 suggesting that in addition to LC3, it is important for the targeting of other components of the autophagosome machinery to sites of autophagosomal formation (Behrends et al., 2010).

MAP1B-HC and MAP1B-LC1 are known to interact (Tögel et al., 1998) therefore, their localisation was assessed in PC12 cells. Under basal conditions and when autophagy was induced or blocked, MAP1B-HC and –LC1 colocalise (Figure 4.7). This suggests that indeed, MAP1B-LC1 could be acting together with MAP1B-HC in the recruitment of the autophagosomal machinery or autophagic receptors and their cargo to the microtubule network. However, distinct areas were observed where there was no colocalisation suggesting that they are also performing functions independent of each other. Analysis of Nbr1 and MAP1B-LC1 intracellular localisation demonstrated that under conditions where autophagy is blocked, Nbr1 and MAP1B-LC1 rarely colocalised and MAP1B-LC1 was often excluded from Nbr1 positive vesicles. Under conditions of autophagic induction, Nbr1 vesicles were largely observed adjacent to MAP1B-LC1 positive structures (Figure 4.8). This could suggest that the interaction between MAP1B-LC1 and Nbr1 is transient and occurs at the very early stages of autophagosome formation. Furthermore, under basal conditions, protein levels of Nbr1 were lower and staining was more reminiscent of MAP1B-LC1 localisation suggesting that the interaction between Nbr1 and MAP1B-LC1 could be prior to the recruitment of Nbr1 into autophagic vesicles.

Analysis of MAP1B-LC1 protein levels demonstrated that when autophagic protein degradation was blocked, there was a small but discernable increase in MAP1B-LC1 levels (Figure 4.6). This was not however comparable to the large increase observed in the protein levels of Nbr1 and p62 which are known to be degraded by autophagy. The small increase in MAP1B-LC1 after Bafilomycin A_1 treatment suggests that the primary role of the Nbr1-MAP1B-LC1 interaction is not to target MAP1B-LC1 for degradation via autophagy. Blockage of autophagosomal degradation also results in a reduction of protein turnover via the UPS (Qiao and Zhang, 2009), therefore as MAP1B-LC1 is degraded by the UPS (Allen et al., 2005), this could suggest that

Bafilomycin A_1 treatment results in the inhibition of MAP1B-LC1 degradation by the proteasome rather than by autophagy.

The UBA domain of Nbr1 also interacted with MAP1B-LC1 in the GST binding assay (Figure 4.5). The ubiquitin scaffolding protein gigaxonin interacts with both the E1 ubiquitin-activating enzyme and MAP1B-LC1. This facilitates the degradation of MAP1B-LC1 in neuronal cells via the UPS. Proteasome inhibition results in an increase in MAP1B protein levels which leads to neuronal cell death, a hallmark of mental retardation (Allen et al., 2005). This suggests that via a similar mechanism to gigaxonin, Nbr1 could also be acting as a scaffold protein, interacting with both E2 and E3 enzymes and MAP1B-LC1 to facilitate the ubiquitin-mediated degradation of MAP1B-LC1. As MAP1B-LC1 interacts with two different regions of Nbr1 (Figure 4.5) either directly or indirectly, this could also indicate a regulatory mechanism similar to that of p62 and TRAF6. The UBA domain and TRAF6 binding domain of p62 are required for TRAF6 polyubiquitination whilst the binding of TRAF6 to p62 is also required for the correct assembly of the receptor signalling complex that is responsible for the activation of the NF-κB pathway (Wooten et al., 2005; Wooten et al., 2001).

Under conditions of autophagic induction, Nbr1 colocalises in discreet perinuclear vesicular structures with MAP1B-HC (Figure 4.9). To confirm if these structures represent the autophagosome, localisation with autophagosomal markers would be required. However, MAP1B-HC interacts *in vivo* with LC3, and as Nbr1 also interacts with LC3, these proteins could be part of one protein complex. Although it is not known whether Nbr1 forms a direct interaction with MAP1B-HC, the colocalisation studies carried out in this thesis could suggest that MAP1B-HC and Nbr1 are together involved in autophagosomal vesicle formation and the targeting of protein for degradation. In support of this hypothesis, a recent study has demonstrated a similar mechanism whereby the ubiquitously expressed MAP1B homologue MAP1S facilitates autophagic degradation of mitochondria. This is thought to be through the interaction of MAP1S-HC with LC3 which functions to target LC3 to the microtubule network (Xie et al., 2011).

4.8.2. Potential interaction of Nbr1 with protein synthesis machinery

The yeast-2-hybrid screen described in this chapter also identified eukaryotic translation elongation factor 1A as a putative interacting partner of Nbr1 (Table 4.2). Although no further validation was performed, this interaction provides an interesting point for discussion. The primary and perhaps most well known function of eukaryotic elongation factor 1A (eEFlA) is to catalyze the first step of the elongation cycle during protein synthesis (Lamberti et al., 2004). In addition to this, eEF1A has also been implicated in ubiquitin-mediated protein degradation. Since up to 50% of all newly synthesised polypeptides can be cotranslationally degraded (Turner and Varshavsky, 2000), eEF1A is a likely candidate for the facilitation of this process as it interacts with both the proteasome and ubiquitinated proteins in the presence of protein synthesis inhibitors (Chuang et al., 2005). It can also function as an isopeptidase to enable proteins to be degraded by the proteasome (Gonen et al., 1996). As Nbr1 is a scaffold protein known to bind ubiquitinated proteins and potentially members of the ubiquitination machinery, it is interesting to speculate that Nbr1 may act as a scaffold to target the ubiquitination machinery to sites of cotranslational degradation via its interaction with eEF1A. Alternatively, Nbr1 could aid in the shuttling of ubiquitinated proteins from sites of protein translation to sites of protein degradation. p62 is known to bind to parts of the proteasome (Seibenhener et al., 2004), and although often classed as false positives (Hengen, 1997), a proteasomal subunit was identified as an interacting partner of Nbr1 in the yeast-2-hybrid screen described in Chapter 3 of this thesis (Table A.1). Together, these data suggest that like p62, Nbr1 could shuttle proteins for proteasomal degradation, facilitated by putative interactions with the proteasome and eEF1A.

4.8.3. Mitochondrial proteins

Mitochondrial proteins are identified in many yeast-2-hybrid screens and are generally considered to be false positives (Hengen, 1997). The screen carried out in this study was no exception, identifying a COX11 homolog (cytochrome c oxidase assembly protein) and succinate dehydrogenase complex subunit B as potential Nbr1 interaction partners. However, these proteins may be of relevance due to recent unpublished data presented at the 42nd Hardan Conference by Ivan Dikic (2010). It

was shown that the novel region of Nbr1 specifically binds the phospholipid, cardiolipin. Cardiolipin is located on the inner membrane of mitochondria and is required for the optimal activity of a number of mitochondrial proteins including cytochrome c oxidase (Paradies et al., 2010). Dikic et al. demonstrated that Nbr1 colocalises with damaged mitochondria in cells treated with the mitochondrial disruptor CCCP. This suggests that via its interaction with cardiolipin, Nbr1 is able to target damaged mitochondria for degradation via autophagy. The Niemann-Pick C2 (NPC2) protein has a similar structure to that predicted for the novel region of Nbr1 (Figure 4.2) and interacts with cholesterol; this provides further evidence for the likely role of the novel region of Nbr1 in lipid binding (Ko et al., 2003). Additionally, a number of highly conserved aromatic residues were important for NPC2 cholesterol binding (Ko et al., 2003). It may be that the highly conserved tryptophan residues in the novel region of Nbr1 are important for lipid binding or indeed other interactions such as that with MAP1B-LC1.

4.9. Future Work

Nbr1 was demonstrated to interact with MAP1B-LC1 however colocalisation was not observed under conditions of autophagic induction. To further investigate whether the Nbr1-MAP1B interaction is involved in targeting ubiquitinated proteins for autophagic degradation, live cell imaging could be used. This would enable the live visualisation of MAP1B-LC1 and Nbr1 and other members of the early forming autophagosome. Knock-down of MAP1B using siRNA would also establish if MAP1B is required for the correct localisation of Nbr1. Nbr1 protein levels could also be analysed in the absence of MAP1B to determine if MAP1B is required for the autophagosomal degradation of Nbr1. The novel region of Nbr1 is highly conserved therefore it is likely that specific residues within this region could be important for MAP1B binding. This could be addressed by mutating residues such as the four tryptophans and subsequently assessing the effects of MAP1B-LC1 binding. As MAP1B-HC was demonstrated to colocalise with Nbr1, it would be interesting to investigate whether it also interacts with Nbr1. To investigate if either MAP1B-LC1 or MAP1B-HC is required to target Nbr1 to the microtubule network, fractionation experiments could be performed with purified microtubules in the presence and

absence of MAP1B. Finally, Nbr1 may regulate the degradation of MAP1B-LC1 via the UPS. To investigate this, overexpression or siRNA knockdown of Nbr1 could be used to analyse the effects on MAP1B protein levels in the presence or absence of proteasomal inhibitors.

To further validate the interaction between Nbr1 and eEF1A, *in-vitro* GST binding assays and coimmunoprecipitation could be implemented. Additionally, cellular colocalisation experiments under conditions where protein synthesis is inhibited would assess whether Nbr1 specifically localises with eEF1A under these conditions. Binding assays could also be performed with Nbr1 and the proteasomal subunit identified in the yeast-2-hybrid screen in Chapter 3 (Table A.1). This would further establish if Nbr1 is involved in the degradation of proteins by the proteasome.

Chapter 5. Phenotypic Analysis of the Nbr1^{D50R} Knock-in Mouse Model

5.1. Introduction

Nbr1 and the structurally similar protein p62 have been identified as key factors in the regulation of bone formation. Mice deficient in p62 have a defect in osteoclastogenesis (Duran et al., 2004), whilst a truncated Nbr1 (trNbr1) mouse model exhibits an increase in bone mass and bone mineral density due to an increase in osteoblast differentiation and activity (Whitehouse et al., 2010). Despite this, the molecular mechanisms by which Nbr1 acts are largely unclear.

Nbr1 and p62 both contain a PB1 domain at their N-terminus. This domain is a protein-protein interaction module found in a range of proteins (Moscat et al., 2006). It is highly conserved and adopts a ubiquitin-like β-grasp fold and either contains an acidic OPCA motif (type I), an invariant lysine residue on the first β strand (type II) or both of these motifs (type I/II) (Sumimoto et al., 2007). Nbr1 has a type I PB1 domain (Figure 5.1) and through this forms a polar heterodimeric interaction with the type I/II PB1 domain of p62. The aspartic acid residue at position 50 of human NBR1 is essential for the NBR1-p62 interaction as when this is mutated to an arginine (D50R), the interaction is completely abolished (Lamark et al., 2003). This residue is also conserved in murine Nbr1 and the same mutation was confirmed by yeast-2-hybrid to inhibit the Nbr1 and p62 interaction (Louise Bentley, Ellen Solomon Laboratory, KCL).

The PB1 domain of p62 is important for a number of signalling pathways including the activation of NF-κB through its interaction with the MAP kinase kinase MEKK3 (Nakamura et al., 2010). Additionally, the interaction between Nbr1 and p62 is involved in muscle signalling (Lange et al., 2005) however its role in bone is unknown. The trNbr1 mouse model still contains a functional p62 interacting domain, therefore to investigate the significance of the p62-Nbr1 interaction, a knock-in mouse model was generated that contains a mutation in amino acid 50 of Nbr1 (Nbr1^{D50R}) (Figure 5.2). The strategy used to generate the Nbr1^{D50R} mouse is

outlined in section 2.4.1. Due to the known importance of Nbr1 and p62 in bone formation, the bone phenotype of these mice will be analysed. Micro Computer Tomography (MicroCT) will be used to determine cortical and trabecular bone parameters whilst *in vitro* assays will be used to gain an insight into the osteoblast and osteoclast cellular phenotype.

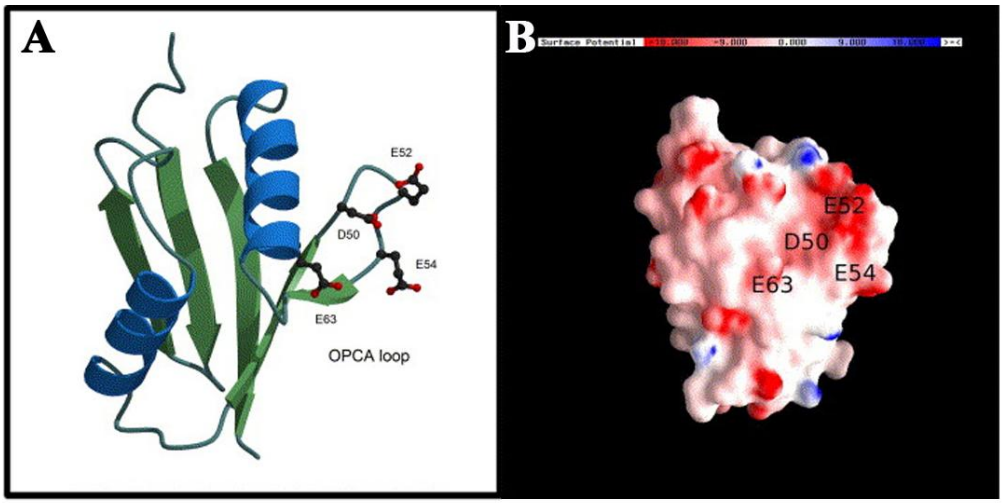

Figure 5.1. Structure of the PB1 domain of NBR1.
A. Ribbon representation - The type I PB1 domain residues are represented as balls and sticks (Asp-50, Glu-52, Glu-54, and Glu-63).
B. Electrostatic potential surface - Red indicates negatively charged surface area and blue indicates positively charged surface area. Asp-50 is part of the acidic cluster (taken from Müller et al., 2006).

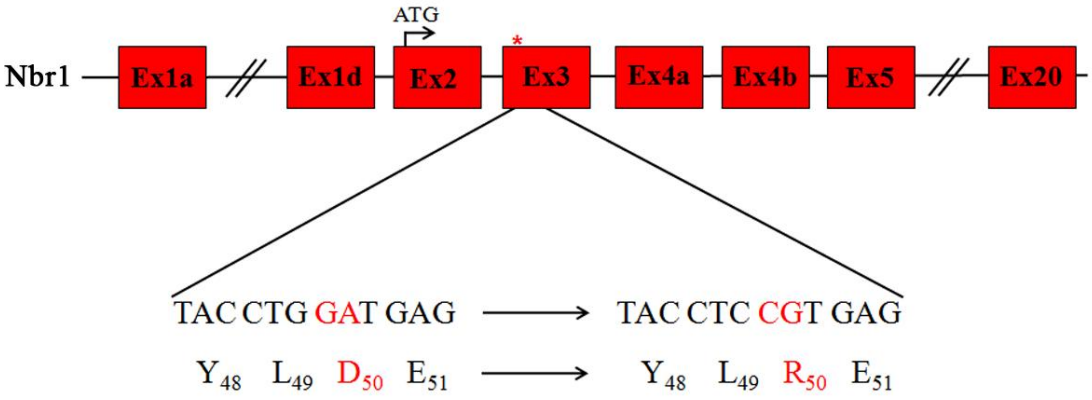

Figure 5.2. Position of the D50R mutation in the *Nbr1* gene. In the Nbr1^{D50R} knock-in mouse, amino acid 50 of Nbr1 is mutated from aspartic acid to arginine. This inhibits the interaction between Nbr1 and p62 via their PB1 domains. Red boxes represent Nbr1 exons. ATG represents the protein translational start site.
* indicates position of mutation.

5.2. Confirmation of mouse genotype

Mouse tissue was obtained by ear punch biopsy and genomic DNA extracted. PCR and subsequent restriction digest was performed to confirm mouse genotypes. Primers used for PCR amplification were located in intron 2 and intron 4a of *Nbr1* (Figure 5.3A), and were used to amplify the genomic region encoding the $Nbr1^{D50R}$ mutation (exon 3 and 4a). The resulting PCR product was digested with the StuI restriction enzyme and visualised by agarose gel electrophoresis. The absence of StuI restriction sites in the WT allele enabled it to be distinguished from the mutant allele which contained two engineered StuI sites either side of a LoxP site. The expected wild type (WT) allele PCR product size was 1470 bp whilst the mutant PCR product sizes were 1133 bp and 334 bp after StuI digestion (Figure 5.3B). Sequencing analysis confirmed the presence of the mutation (Figure 5.3C).

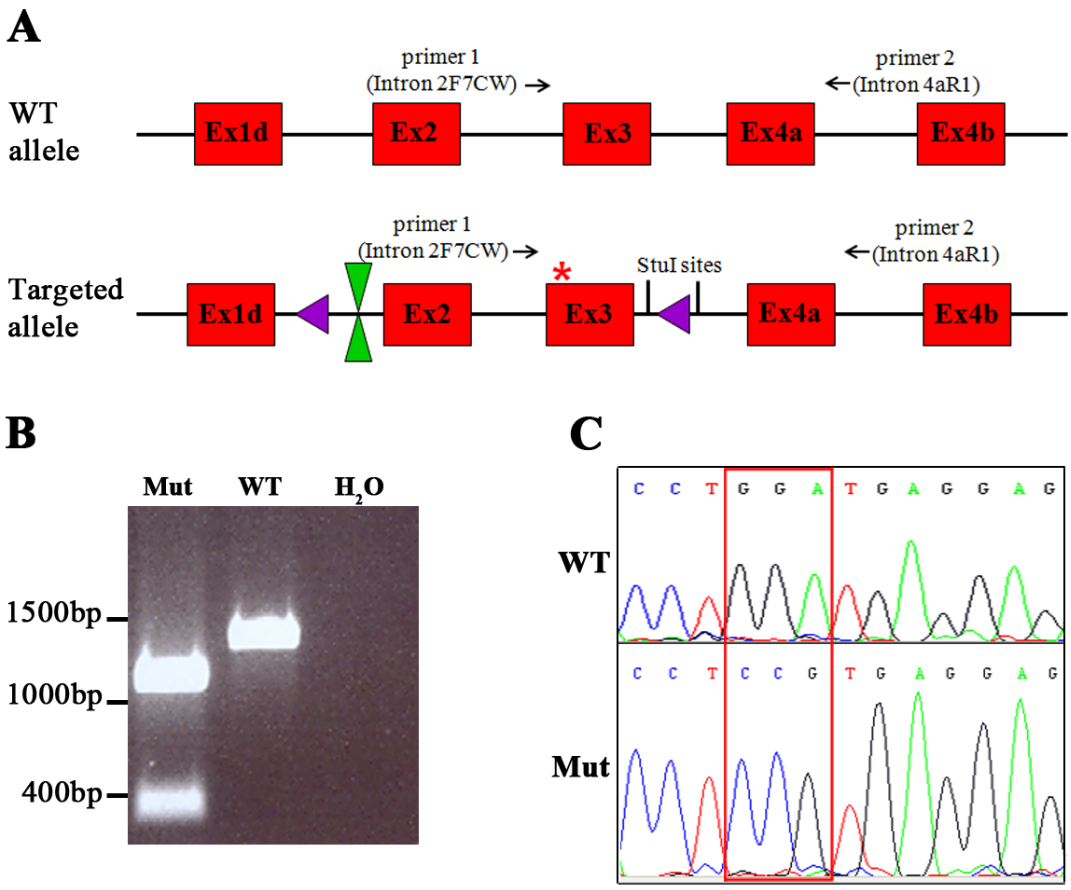

Figure 5.3. Confirmation of the Nbr1^{D50R} knock-in mouse genotype by genomic PCR and sequencing.
A. Schematic diagram showing the location of the PCR primers and StuI restriction enzyme sites used for genotyping.
B. Agarose gel electrophoresis separation of PCR product. The PCR product spans from intron 2 to intron 4a and the expected WT PCR product size is 1470bp. The mutant allele contains two introduced StuI restriction sites either side of the second LoxP site, therefore, on restriction enzyme digest, the mutant PCR product is cut into two sized bands of 1133bp and 334bp. The LoxP site is 40bp so cannot be visualised on this gel.
C. Electropherogram showing the correct mutation is present in the D50R knock-in mouse compared with WT (red box).
WT: Wild type; Mut: Nbr1^{D50R} mutant.

5.3. Confirmation that the Nbr1^{D50R} mutation inhibits the interaction between Nbr1 with p62

To confirm that the Nbr1-p62 interaction was inhibited in our mouse model, a co-immunoprecipitation between Nbr1 and p62 was performed. Prior to this, it was important to establish whether the Nbr1 antibody detected the mutant protein effectively. To test this, mouse embryonic fibroblasts (MEFs) were isolated from both WT and Nbr1^{D50R} homozygous mutant mice, lysed and proteins resolved by SDS PAGE, then visualised by Western blot using the rabbit polyclonal antibody, 3517 that recognises Nbr1. This antibody was raised against a recombinant protein encoding aa 57-266 of Nbr1 which is outside the mutated region (made in-house by Dr Caroline Whitehouse). Protein band intensities were quantified and established that the mutant protein could be detected with 90% efficiency compared with WT (Figure 5.4A). This could suggest that the mutant protein levels are 10% less than WT. Alternatively, the antibody may not be detecting the mutant protein as effectively as the WT protein. Due to the lack of other efficient antibodies raised to domains outside of the mutated region, and to the small differences in detection efficiency between the WT and mutant protein, the 3517 antibody was used for the detection of Nbr1 in the subsequent coimmunoprecipitation experiment.

The ability of Nbr1^{D50R} to form a complex with p62 was examined by coimmunoprecipitation. Wild type and Nbr1^{D50R} MEFs were treated with either DMSO or Bafilomycin A_1 (to increase Nbr1 and p62 protein levels) then lysed. p62 was immunoprecipitated and the immunocomplex bound to protein A beads. Beads were washed and bound proteins resolved by SDS PAGE then visualised using Western blot and the 3517 antibody raised against Nbr1 (Figure 5.4B). The amount of Nbr1 protein bound to p62 was calculated relative to the amount of p62 immunoprecipitated. In WT cells, Nbr1 coimmunoprecipitated with p62 as expected (Figure 5.4B, lane 3). In mutant cells, Nbr1^{D50R} was also coimmunoprecipitated with p62 (Figure 5.4B, lane 4) however this was at a significantly lower level (~20%) compared with WT (Figure 5.4B). Cells treated with DMSO gave similar results to those treated with Bafilomycin A_1 (data not shown). The very weak binding

observed in mutant cells could be attributable to the newly identified interaction between the UBA domains of Nbr1 and p62 (Whitehouse et al., 2010). Additionally, Nbr1 and p62 could be in a complex together due to common interacting partners such as LC3. Overall, it is clear that the $Nbr1^{D50R}$ mutation is having a strong negative effect on the interaction between Nbr1 and p62.

MEFs from WT and $Nbr1^{D50R}$ homozygous mutant mice were treated with DMSO or Bafilomycin A_1 then fixed and immunostained with antibodies against p62 and Nbr1. WT cells display a high degree of colocalisation between the two proteins. In mutant cells however, although Nbr1 can still form punctate vesicles, its colocalisation with p62 is almost completely abolished (Figure 5.5). This finding is in agreement with Lamark et al. (Lamark et al., 2003) and again confirms the abrogation of the interaction between the PB1 domains of Nbr1 and p62 in the $Nbr1^{D50R}$ knock-in mouse model.

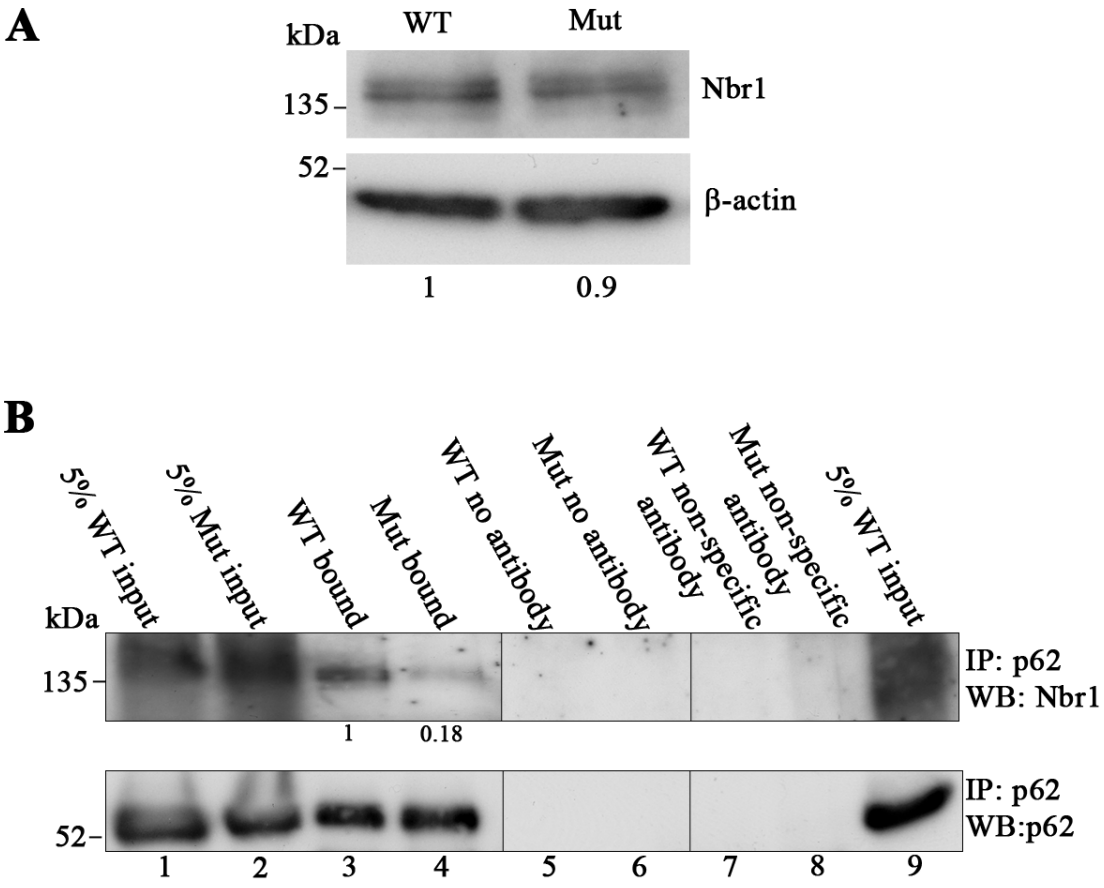

Figure 5.4. The effect of the Nbr1^{D50R} mutation on the Nbr1-p62 interaction.
A. Wild type (WT) and Nbr1^{D50R} homozygous mutant (Mut) MEFs were lysed and proteins resolved by SDS PAGE, Western blotted and probed with an antibody that recognises Nbr1. Protein band intensity was quantified relative to β-actin. Detection levels between genotypes were comparable.
B. WT and Mut MEFs were treated with Bafilomycin A_1, lysed then p62 immunoprecipitated and attached to Protein A beads. Beads were washed and bound proteins resolved by SDS PAGE then Western blotted for Nbr1 and p62. Protein band intensity was quantified. Lower panel: p62 was effectively immunoprecipitated. Upper panel: In WT cells, Nbr1 was coimmunoprecipitated with p62 and in Mut cells this coimmunoprecipitation was reduced by 80% (as compared with amount of p62 immunoprecipitated).

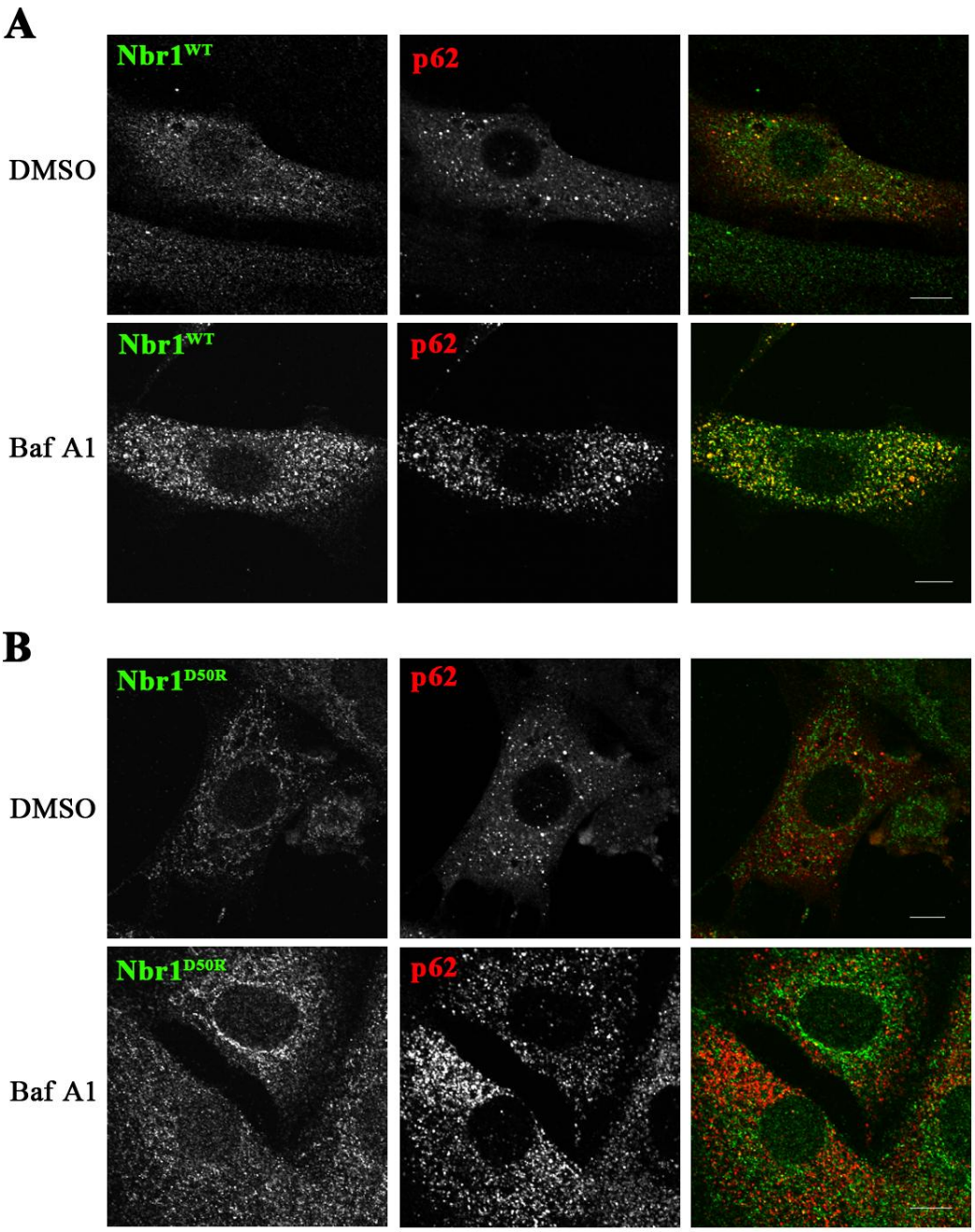

Figure 5.5. Nbr1 and p62 localisation in WT (A) and Nbr1^{D50R} mutant (B) MEFs. MEFs were isolated from WT (Nbr1^{WT}) and D50R (Nbr1^{D50R}) mutant embryos. After treatment with Bafilomycin A_1 or DMSO, cells were fixed and stained with antibodies against Nbr1 and p62. In WT cells there was a high degree of colocalisation between Nbr1 (green) and p62 (red) **(A)** however, in Nbr1^{D50R} mutant cells, this colocalisation is almost completely abolished **(B)**.
Scale bar = 10µm. Images are representative of two independent experiments.

5.4. *Ex vivo* bone phenotypic analysis

To establish if the p62-Nbr1 interaction is important for the formation and maintenance of bone tissue, it was necessary to perform detailed *ex vivo* analysis on femurs and tibiae from WT and $Nbr1^{D50R}$ mutant (Mut) mice. These bones were selected as they are routinely used to establish whether bone formation is altered in mouse models (Whitehouse et al., 2010; Williams et al., 2011). A cohort of three, six and nine month old animals from each genotype were used for *ex vivo* bone analysis (numbers of animals per group analysed is described in section 2.6.1). These age groups were chosen because the previous Nbr1 mouse model (trNbr1) displayed an age-dependent increase in bone mass and bone mineral density that became evident at three months of age (Whitehouse et al., 2010). All mice used in this study were male and either WT or homozygous for the $Nbr1^{D50R}$ mutation. No significant differences were seen in total body weight between WT and mutant mice of all ages (Figure 5.6).

5.4.1. Physical measurements and radiography

Femur and tibia length was measured using digital calipers following dissection. There were no significant differences in femur lengths of three ($p=0.227$), or six ($p=0.282$) month old WT compared to mutant mice however, at nine months of age, mutant mice had a slight but significant increase in femur length compared to WT ($p=0.008$, 2.9%). There was a slight significant decrease in tibia lengths of three month old mutant mice compared to WT ($p=0.039$, 1.7%), but no significant difference at six ($p=0.265$) or nine ($p=0.068$) months of age between the genotypes (Figure 5.7). Overall, there was a general trend for reduced long bone length at three months of age and a general increase in long bone length at six and nine months of age in mutant mice compared to WT however these differences were small.

Radiographs were taken of femurs (Figure 5.8) and tibiae (Figure 5.9) of three, six and nine month old mice. Whilst some variation was observed between bones, as viewed by eye, there were no consistent differences between WT and mutant mice at all ages.

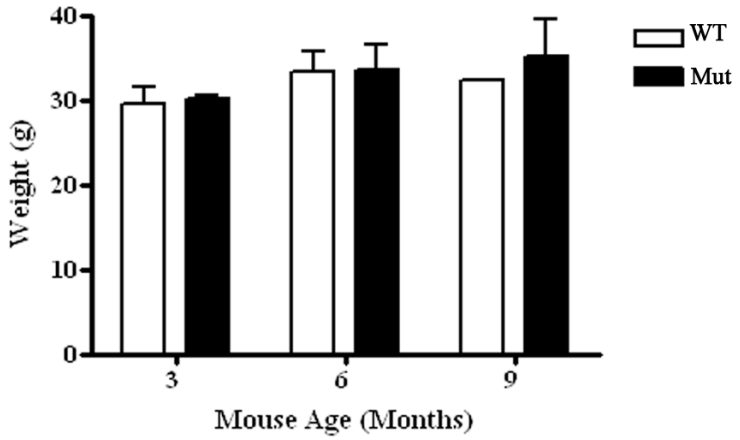

Figure 5.6. Body mass of three, six and nine month old WT and Nbr1^{D50R} mutant (Mut) mice. There were no differences in body mass observed between genotypes at all ages studies. Columns represent the mean and error bars represent SD. At least six mice were analysed in each group.

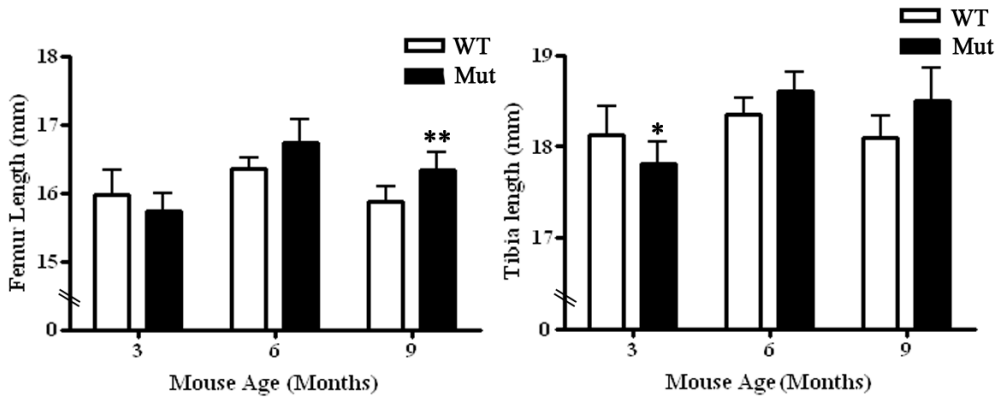

Figure 5.7. Femur and tibia lengths of three, six and nine month old WT and Nbr1^{D50R} mutant (Mut) mice. There was a significant decrease in tibiae length of three month old mutant mice compared with WT and a significant increase in femur length of nine month old mutant mice compared with WT. Columns represent the mean and error bars represent SD. At least six mice were analysed in each group. *$p<0.05$, **$p<0.01$.

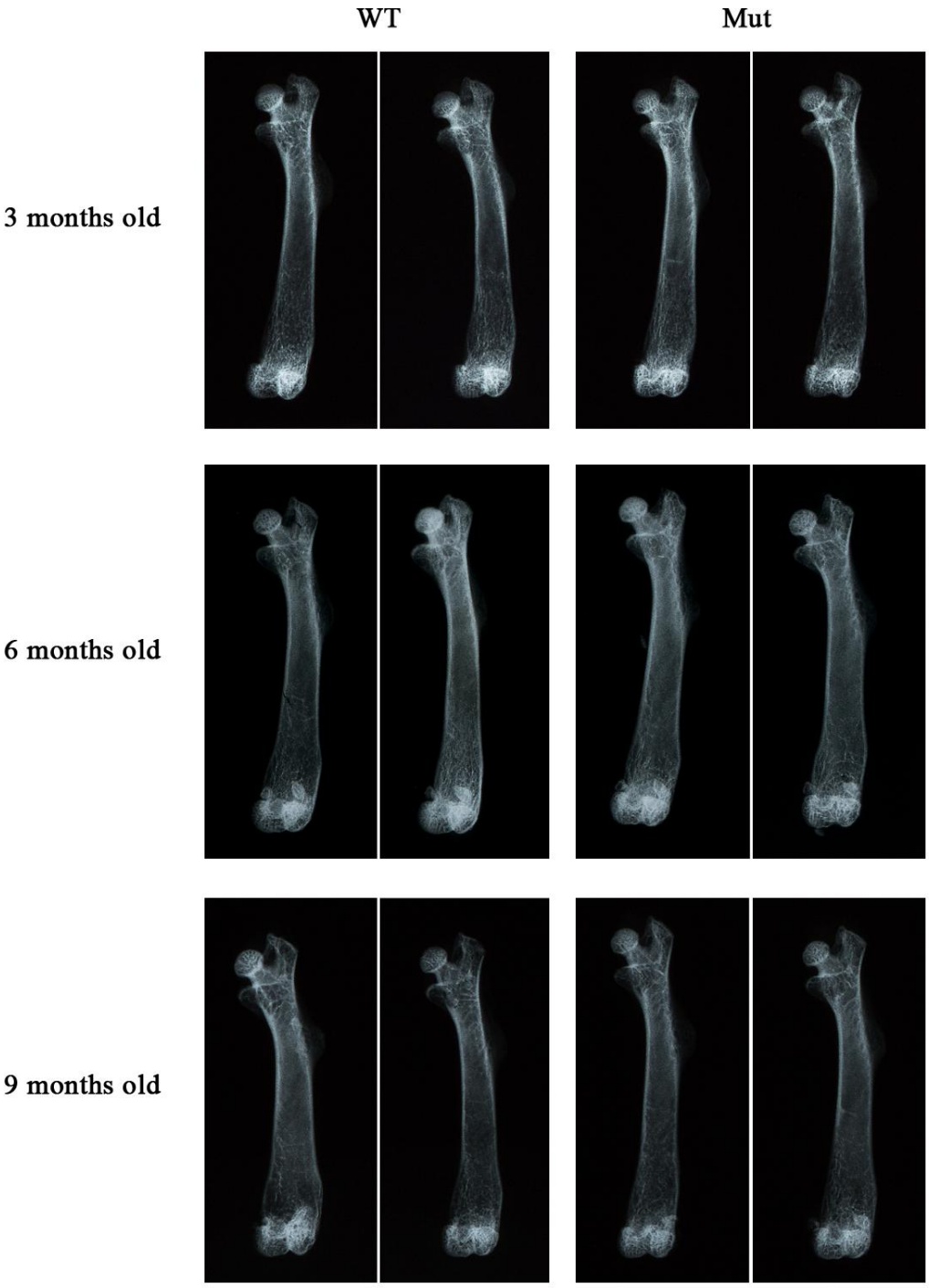

Figure 5.8. Representative X-rays of femurs from three, six and nine month old WT and Nbr1^{D50R} mutant (Mut) mice. No consistent structural differences were observed between genotypes at any age studied.

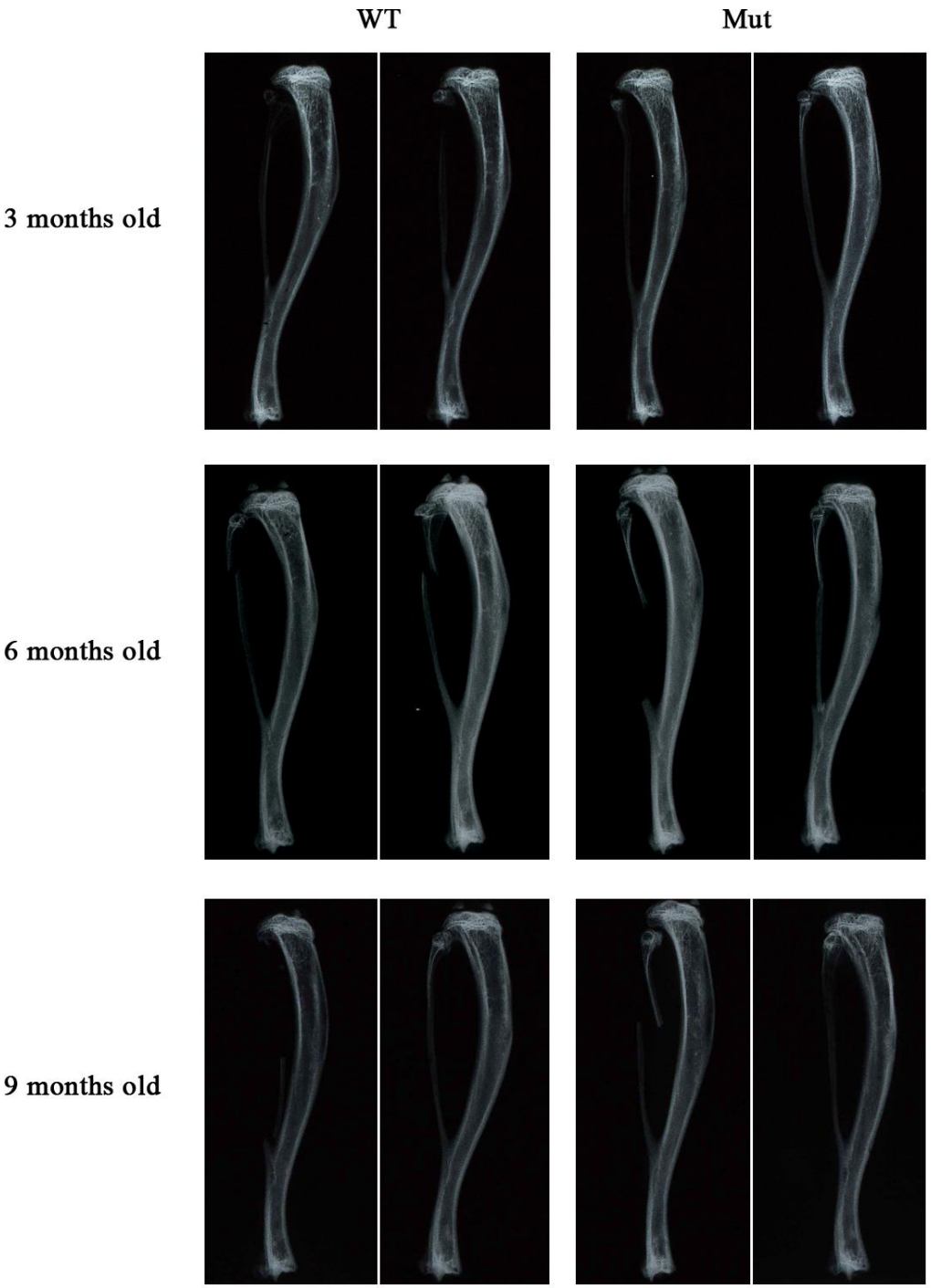

Figure 5.9. Representative X-rays of tibiae from three, six and nine month old WT and Nbr1^{D50R} mutant (Mut) mice. No consistent structural differences were observed between genotypes at any age studied.

5.4.2. Micro Computer Tomography (MicroCT)

In this study, low resolution (17µm) Micro Computer Tomography (microCT) images were acquired of whole femur and tibiae to gain information on whole bone volume and bone mineral density (BMD). High resolution (4.4µm) imaging was subsequently performed to allow analysis of cortical and trabecular bone parameters.

5.4.2a. Whole bone analysis

Whole bone volumes and BMD were obtained from the low resolution scans. Whilst there was variation within groups, no significant differences were observed in whole bone volume in femurs of six month ($p=0.751$) or nine month old ($p=0.492$) mutant mice compared with WT. There were also no significant differences in whole bone volume of tibiae from six month ($p=0.650$) or nine month old ($p=0.692$) mutant mice compared with WT (Figure 5.10). At three months of age there was a significant decrease in whole bone volume in the tibiae of mutant mice compared with WT ($p=0.036$, 12%) and although the same trend was observed, there was no significant difference in whole bone volume in femurs from three month old mutant mice compared with WT ($p=0.139$) (Figure 5.10). Overall, whole bone volumes exhibited significant differences at three months of age but not at six and nine months of age between genotypes.

Whole BMD (as compared with that of a hydroxyapatite standard-section 2.6.4) established no significant difference between genotypes in femurs of six month ($p=0.727$) or nine month old animals ($p=0.606$) or in the tibiae of six month ($p=0.589$) or nine month old animals ($p=0.457$). At three months of age, both femurs and tibiae showed a significant decrease in whole BMD in mutant mice compared with WT ($p=0.009$ and 0.005 respectively) (Figure 5.11). However, these differences were small (2% and 2.5% respectively).

Overall, the whole bone analysis revealed there is a significant decrease in bone volume and bone mineral density in three month old mutant mice compared with WT and this difference is resolved by six months of age. The trend in whole bone volume and BMD with age between the genotypes was comparable, with an increase

between three and six months and a decrease between six and nine months of age. This suggests that, unlike the truncated mouse model, there appears to be an early reduced bone volume and BMD. Further analysis of younger mice is required to confirm the age of onset. There was also some variation within groups and although group size was within the range used by others (Hoff et al., 2002; Rauch et al., 2010), it would be useful to analyse more mice.

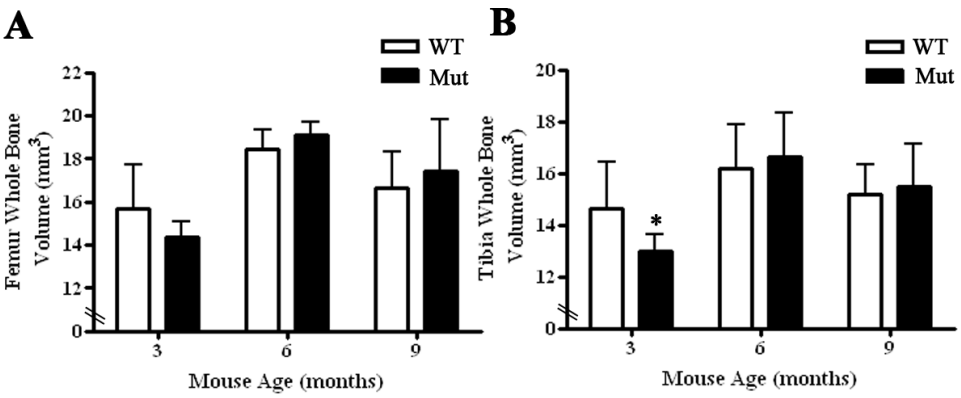

Figure 5.10. Femur (A) and tibiae (B) whole bone volumes from wild type (WT) and Nbr1^{D50R} mutant (Mut) mice of three, six and nine months of age. There was a significant decrease in tibiae whole bone volume in mutant mice compared with WT at three months of age. Columns represent the mean and error bars represent SD. At least six mice were analysed in each group. *p<0.05.

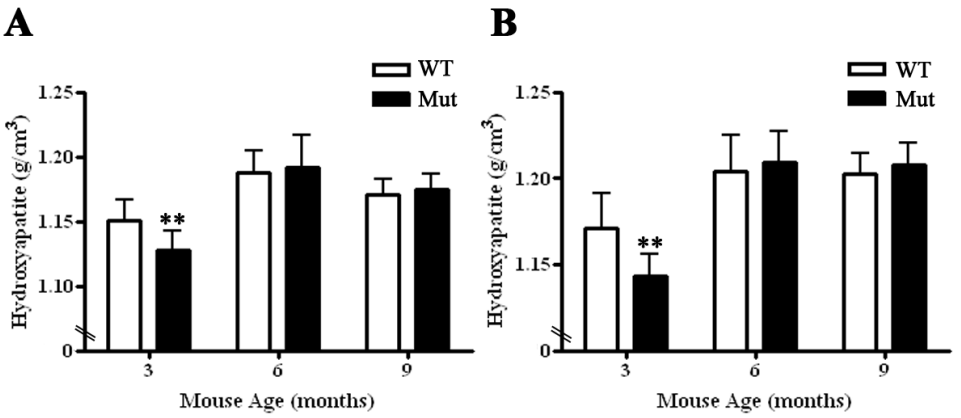

Figure 5.11. Femur (A) and tibia (B) whole bone mineral density (BMD) from wild type (WT) and Nbr1^{D50R} mutant (Mut) mice at three, six and nine months of age. There was a significant decrease in femur and tibia BMD of mutant (Mut) mice compared with WT at three months of age. Columns represent the mean and error bars represent SD. At least six mice were analysed in each group. **p<0.01.

5.4.2b. Cortical and trabecular bone analysis

Low resolution scans are useful to determine differences in whole bone parameters however the resolution is not high enough to accurately analyse the cortical and trabecular bone parameters. Any differences in trabecular bone may be masked by the cortical bone. Therefore, high resolution scans (4.4μm) were performed on all bones to establish whether the inhibition of the p62-Nbr1 interaction has any effect on cortical or trabecular bone. The distal and proximal ends of femurs and tibiae respectively were scanned, reconstructed and parameters were calculated using a region of interest (ROI) selected as described in section 2.6.4.

5.5.2b.i Cortical analysis

There were no significant differences observed in cortical bone volume (Ct.BV) between femurs from WT and mutant three month old mice ($p=0.640$). A significant decrease in femur cortical thickness (Ct.Th) ($p<0.001$, 14%) in three month old mutant mice compared with WT was however observed (Figure 5.12A and B). Tibiae from three month old mutant mice displayed a significant decrease in both Ct.BV ($p=0.028$, 13%) and Ct.Th ($p=0.014$, 8%) compared with WT (Figure 5.12A and B). There were no significant differences in femur or tibia Ct.BV from six month ($p=0.163$ and $p=0.148$ respectively) or nine month old mutant mice compared with WT ($p=0.230$ and $p=0.476$ respectively) (Figure 5.12A). There were also no significant differences in femur or tibia Ct.Th in six ($p=0.862$ and $p=0.081$ respectively) or nine month old mutant mice compared with WT ($p=0.064$ and $p=0.365$ respectively) (Figure 5.12B). These data support the whole bone analysis where there were significant differences at three months of age and no significant differences at six and nine months of age between WT and mutant mice.

To explain the apparent decrease in Ct.Th observed in femurs from three month old mutant mice but no accompanying difference in Ct.BV, endosteal and periosteal diameters were calculated from three regions spanning the cortical ROI. These were the distal most cross section, the proximal most cross section and a cross section in the middle. No significant differences were observed in endosteal diameters at any of the regions studied but a significant increase was observed in the periosteal

diameter at only the proximal most section studied in mutant mice compared with WT (Figure 5.12C). This slight increase could be contributing to the lack of differences in bone volume observed in the Ct.Th from three month old femurs between genotypes. It is important to note that the endosteal and periosteal analysis highlights the heterogeneity within the bones and although there was largely no differences in these parameters between genotypes, only a very small section of the bone was analysed compared with a much larger area studied for the other cortical parameters.

There was a significant decrease in Ct.BMD in femurs ($p=0.0004$, 2.6%) and tibiae ($p=0.009$, 2%) of three month old mutant mice compared to WT (Figure 5.12D). This is in agreement with the small decrease in whole BMD observed in the whole bone scans (Figure 5.12D). At six months of age there was no significant difference in cortical BMD in femurs ($p=0.751$) and a small increase in tibiae ($p=0.029$, 3%) in mutant mice compared with WT. At nine months of age, there was a small but significant decrease in femur Ct.BMD ($p=0.013$, 3%) but no difference in tibiae Ct.BMD ($p=0.713$) in mutant mice compared with WT.

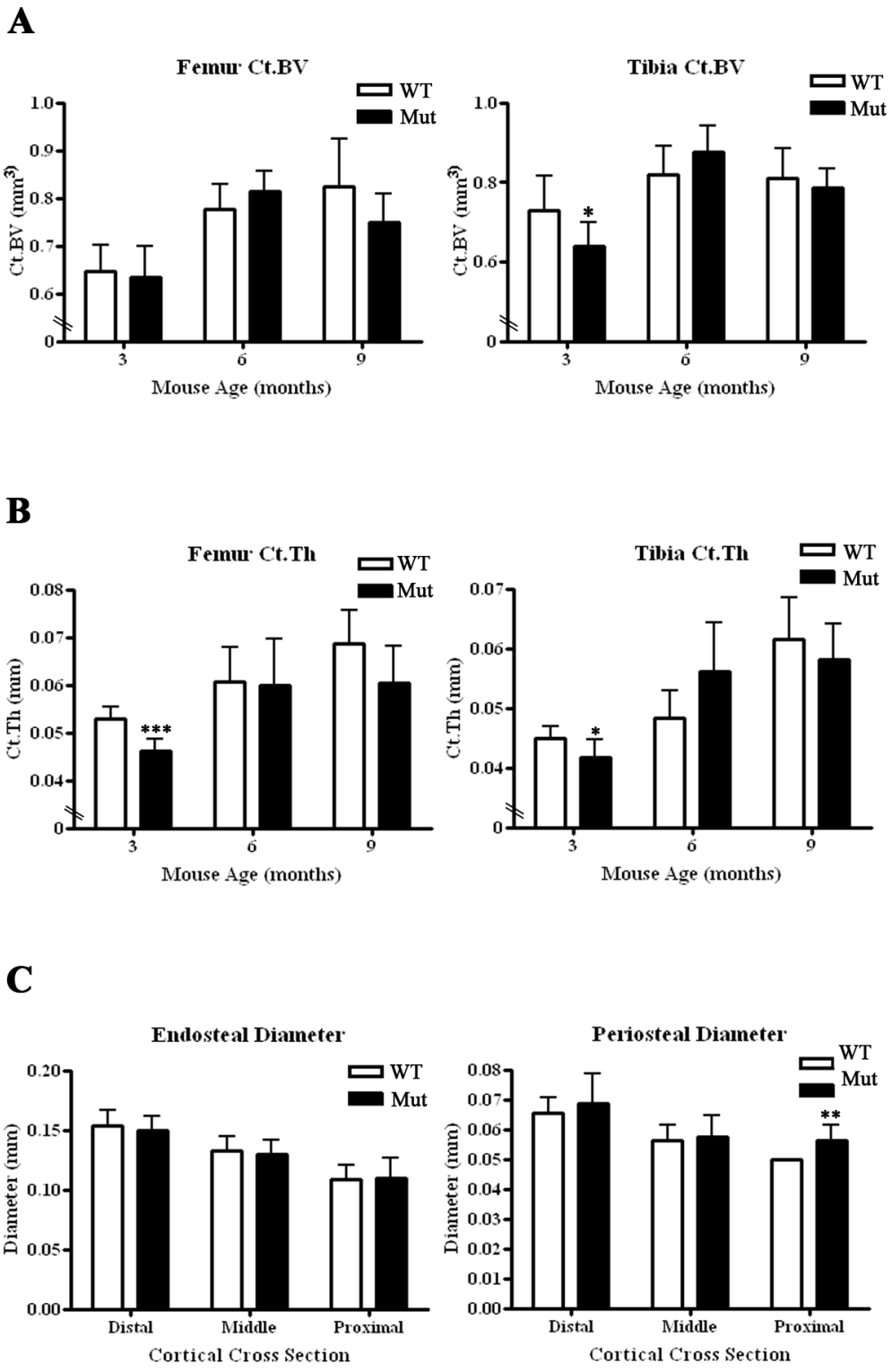
A
Femur Ct.BV
WT
Mut
Ct.BV (mm3)
1.0
0.9
0.8
0.7
0.6
0
3
6
9
Mouse Age (months)
Tibia Ct.BV
WT
Mut
Ct.BV (mm3)
1.0
0.8
0.6
0
*
3
6
9
Mouse Age (months)
B
Femur Ct.Th
WT
Mut
Ct.Th (mm)
0.08
0.07
0.06
0.05
0.04
0
***
3
6
9
Mouse Age (months)
Tibia Ct.Th
WT
Mut
Ct.Th (mm)
0.07
0.06
0.05
0.04
0
*
3
6
9
Mouse Age (months)
C
Endosteal Diameter
WT
Mut
Diameter (mm)
0.20
0.15
0.10
0.05
0.00
Distal
Middle
Proximal
Cortical Cross Section
Periosteal Diameter
WT
Mut
Diameter (mm)
0.08
0.07
0.06
0.05
0.04
0.03
0.02
0.01
0.00
**
Distal
Middle
Proximal
Cortical Cross Section

D

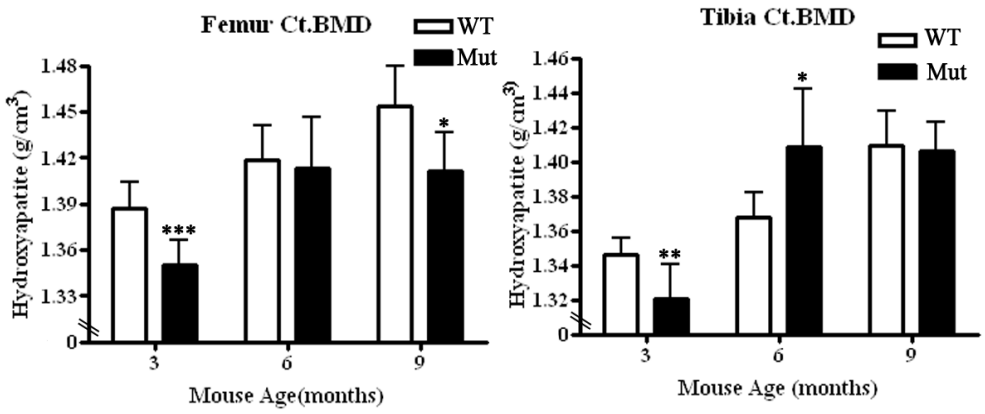

Figure 5.12. MicroCT analysis of cortical bone parameters in femurs and tibiae from three, six and nine month old wild type (WT) and Nbr1^{D50R} mutant (Mut) mice.

A. Cortical bone volume (Ct.BV). There was a significant decrease in Ct.BV in tibiae from three month old mutant mice compared to WT.

B. Cortical thickness (Ct.Th). There was a significant decrease in Ct.Th in femurs and tibiae from three month old mutant mice compared to WT.

C. Endosteal and periosteal diameters of femurs from three month old mice. There was a significant increase in periosteal diameter in the proximal most slice of femurs from mutant mice compared to WT.

D. Cortical bone mineral density (Ct.BMD). There was a significant decrease in femurs and tibiae from three month old mutant mice compared with WT. There was also a significant increase in tibiae Ct.BMD from six month old mutant mice compared to WT and a significant decrease in Ct.BMD of femurs from nine month old mutant mice compared with WT.

Columns represent the mean and error bars represent SD. At least six mice were analysed in each group.

*p<0.05, **p<0.01, ***p<0.001.

5.4.2b.ii. Trabecular analysis

At three, six and nine months of age in both femur and tibiae, no significant differences were observed in Trabecular Bone Volume/Tissue Volume (BV/TV) (Figure 5.13A), Trabecular Separation (Tb.Sp) (Figure 5.13B), or Trabecular Number (Tb.N) (Figure 5.13C) in mutant mice compared with WT. No differences were observed in trabecular thickness (Tb.Th) in six and nine month old mutant mice compared with WT or in the tibiae of three month old mutant mice compared to WT. There was a significant decrease in Tb.Th (6%) and Tb.BMD (2.5%) in femurs from three month old mutant mice compared with WT (Figure 5.13D&E). There was also a significant decrease (4%) in the Tb.BMD of femurs from nine month old mutant mice compared to WT (Figure 5.13E). All statistical p values for trabecular parameters are shown below in Table 5.1.

Mouse age and bone type	**Trabecular BV/TV**	**Trabecular Separation**	**Trabecular Number**	**Trabecular Thickness**	**Trabecular BMD**
3 Month Femurs	0.271	0.224	0.068	**0.015**	**0.002**
3 Month Tibiae	0.207	0.078	0.091	0.147	0.558
6 Month Femurs	0.227	0.755	0.345	0.652	0.313
6 Month Tibiae	0.476	0.965	0.706	0.140	0.282
9 Month Femurs	0.422	0.753	0.295	0.300	**0.007**
9 Month Tibiae	0.145	0.612	0.247	0.981	0.803

Table 5.1. Statistical analysis results for trabecular bone parameters of three, six and nine month old WT and Nbr1^{D50R} mutant mice. Values in bold are statistically significant ($p<0.05$).

A

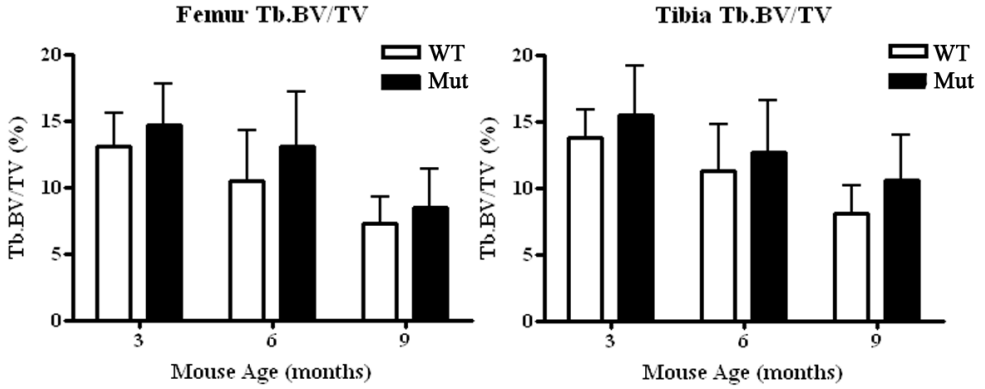
Femur Tb.BV/TV
Tibia Tb.BV/TV
WT
Mut
Tb.BV/TV (%)
0
5
10
15
20
3
6
9
Mouse Age (months)

B

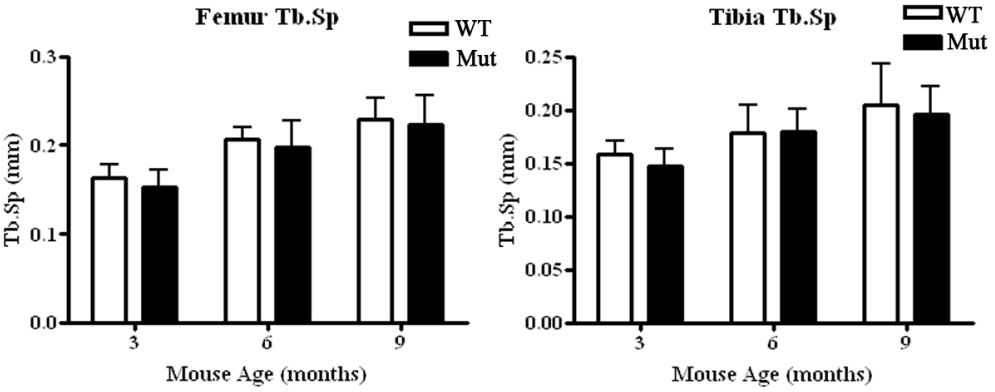
Femur Tb.Sp
Tibia Tb.Sp
WT
Mut
Tb.Sp (mm)
0.0
0.1
0.2
0.3
0.00
0.05
0.10
0.15
0.20
0.25
3
6
9
Mouse Age (months)

C

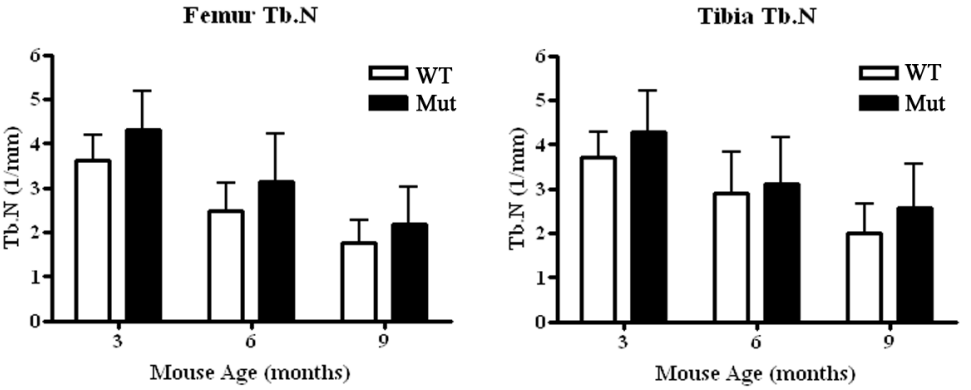
Femur Tb.N
Tibia Tb.N
WT
Mut
Tb.N (1/mm)
0
1
2
3
4
5
6
3
6
9
Mouse Age (months)

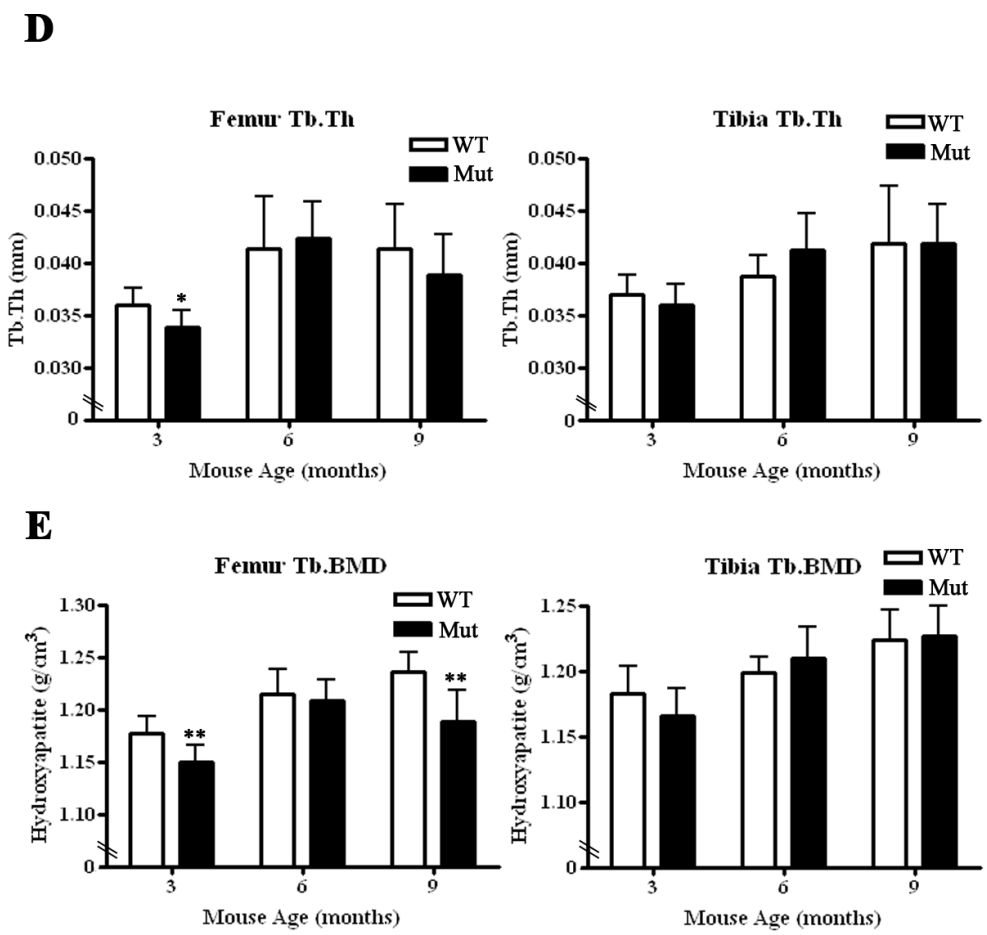

Figure 5.13. MicroCT analysis of trabecular bone parameters in femurs and tibiae from three, six and nine month old Nbr1^{D50R} mutant (Mut) and wild type (WT) mice.

A. Trabecular bone volume/tissue volume (Tb.BV/TV). No significant differences were observed at any age studied between the genotypes.

B. Trabecular separation (Tb.Sp). No significant differences were observed at any age studied between the genotypes.

C. Trabecular number (Tb.N). No significant differences were observed at any age studied between the genotypes.

D. Trabecular thickness (Tb.Th). A significant decrease was observed in mutant mice compared with WT in femurs from three month old mice.

E. Trabecular bone mineral density (Tb.BMD). A significant decrease was observed in femurs from three month and nine month old mutant mice compared with WT.

Columns represent the mean and error bars represent SD. At least six mice were analysed in each group. *$p<0.05$, **$p<0.01$.

5.5. *In vitro* bone analysis

MicroCT analysis has established that three month old Nbr1^{D50R} mutant mice have reduced Ct.Th, Tb.Th and BMD compared with WT controls and that this effect is resolved at six and nine months of age. To establish the cellular mechanisms involved, bone marrow stromal cells were isolated from WT and mutant mice, and osteoclast and osteoblast differentiation assays were performed. Due to the apparent early phenotype of the Nbr1^{D50R} knock-in mouse model, all *in vitro* analysis was carried out using one month old male animals.

5.5.1. Analysis of osteoclast differentiation from bone marrow stromal precursor cells derived from WT and Nbr1^{D50R} mutant mice

In vitro generation of osteoclasts from M-CSF- and RANKL-dependent bone marrow precursors was utilised to analyse osteoclast differentiation in Nbr1^{D50R} mutant cells compared to WT (section 2.5.5). TRAP staining revealed that mutant cells were much larger in size than WT (Figure 5.14A). Subsequent quantification demonstrated the number of cells with 10-19 nuclei and 20 or more nuclei were significantly increased in mutant cultures compared to WT ($p=0.008$ and 0.012 respectively) (Figure 5.14B).

To establish whether osteoclast resorption activity was significantly different in Nbr1^{D50R} mutant osteoclasts compared to WT, bone marrow precursor cells were plated onto dentine slices, TRAP +ve cells were counted and resorption activity quantified (section 2.5.5). There was a significantly greater number of TRAP +ve mutant cells per dentine slice compared with WT ($p=0.029$) (Figure 5.15B). No significant difference in total resorption area was observed between genotypes (Figure 5.15C). It is important to note that the number of osteoclasts on each dentine slice did not appear to correlate with the level of resorption. The giant osteoclast phenotype observed in mutant cells cultured on plastic was not observed when cultured on dentine.

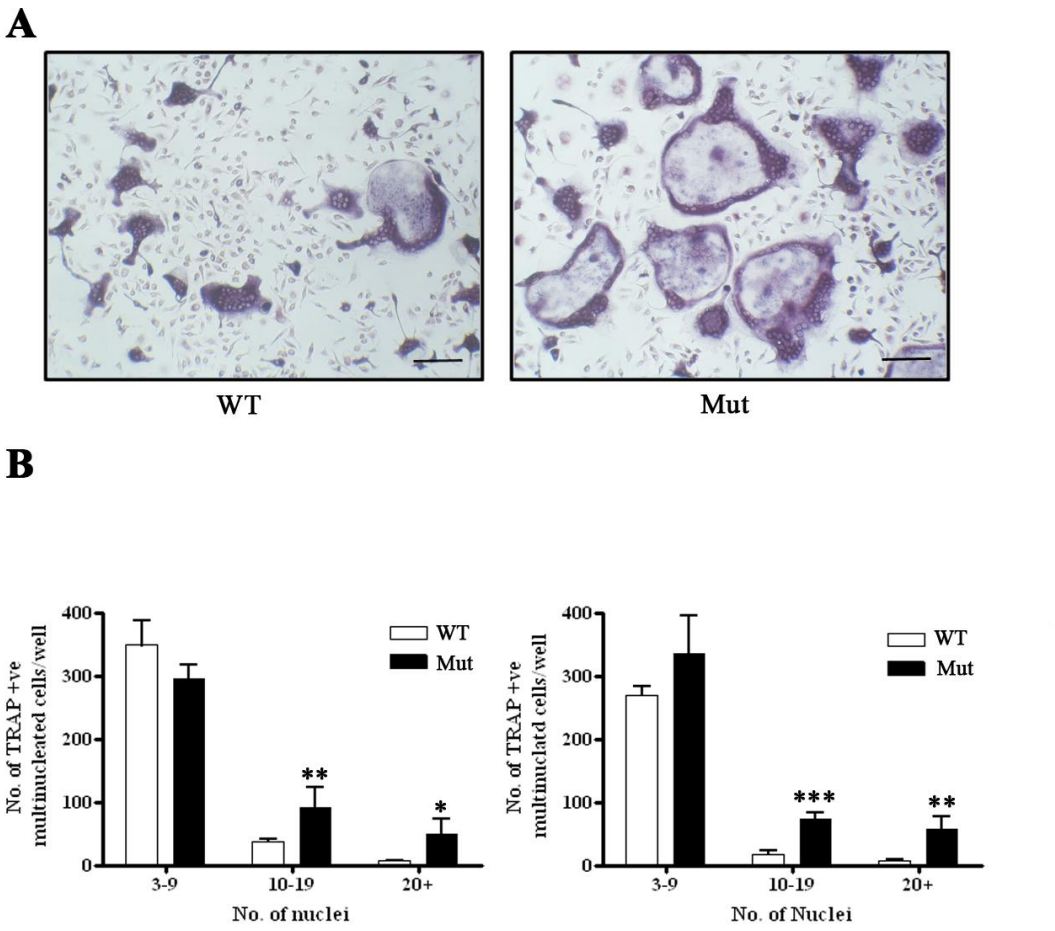

Figure 5.14. Increased size and nuclearity in TRAP +ve cells from Nbr1^{D50R} mutant mice (Mut) compared with wild type (WT). Bone marrow stromal cells were cultured in the presence of RANKL and M-CSF and subsequently stained for TRAP activity.

A. Represenatative images of TRAP staining of multinucleated cells cultured on plastic. Scale bar = 100µm.

B. Quantification of the number of multinucleated TRAP +ve cells/well. There was a significant increase in the number of cells containing 10 nuclei or more in mutant cultures compared to WT.

*p<0.05, **p<0.01 ***p<0.001. Columns represent the mean and error bars represent the SD of quadruplicate dentine slices. Graphs represent results from two independent experiments.

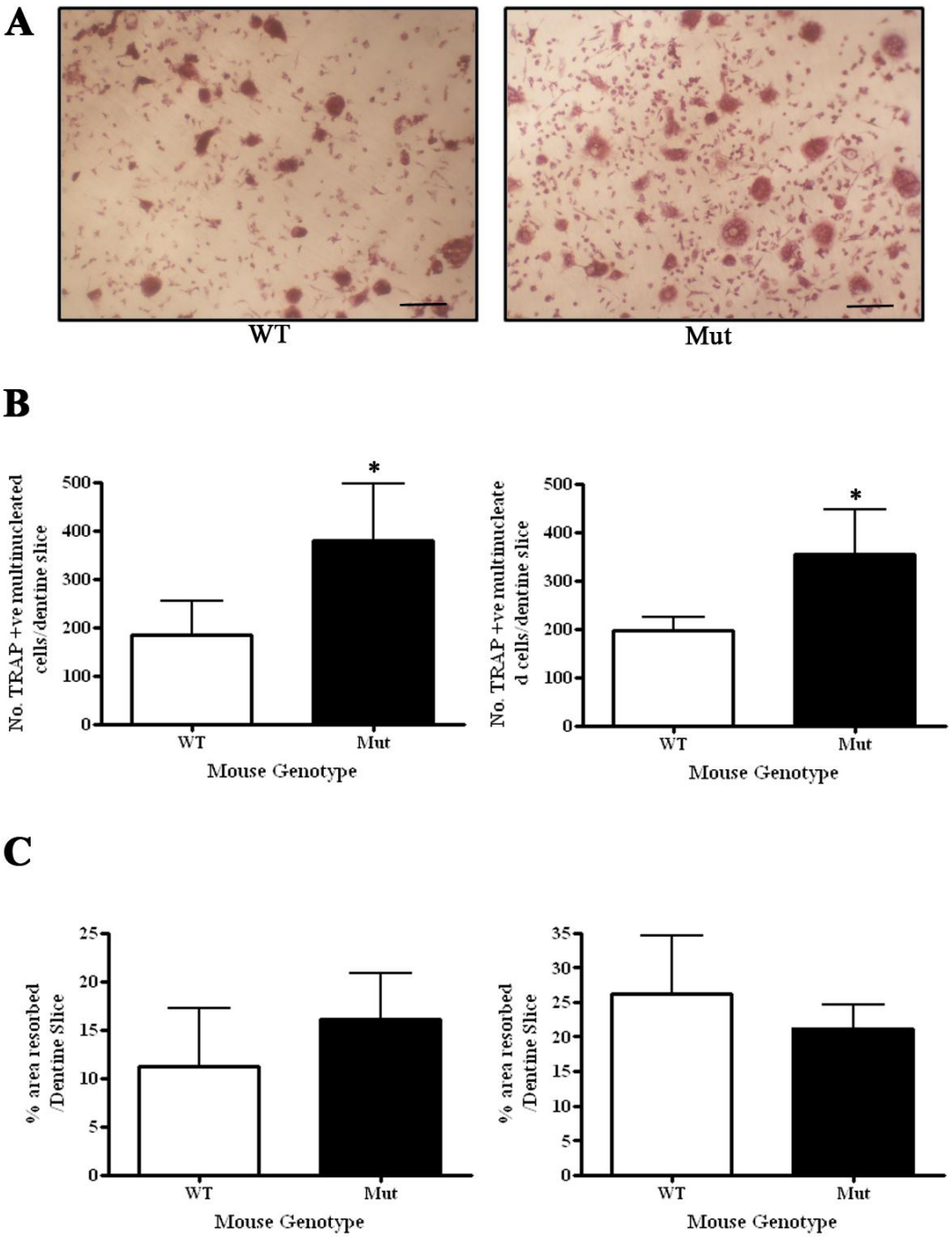

Figure 5.15. Increased number of TRAP +ve multinucleated cells in Nbr1^{D50R} mutant (Mut) cultures compared with wild type (WT). Bone marrow precursor cells were cultured on dentine in the presence of RANKL and M-CSF and subsequently stained for TRAP activity.

A. Representative images of TRAP staining on dentene.

B. Quantification of the number of multinucleated cells/slice. There was a significant increase in TRAP +ve cells in mutant cultures compared to WT.

C. Quantification of osteoclast resorption area on dentine. There was no significant difference in pit resortion area between genotypes.

*$p<0.05$, Scale bar = 100µm. Columns represent the mean and error bars represent the SD of quadruplicate dentine slices. Graphs represent results from two independent experiments.

5.5.2. Analysis of osteoblast differentiation from bone marrow stromal precursor cells derived from WT and Nbr1^{D50R} mutant mice

To establish if the reduced Tb.Th, Ct.Th and BMD observed in younger mutant animals compared with WT was due to reduced osteoblast differentiation and activity, an *in vitro* colony forming unit (CFU) assay was performed and cells were stained with ALP and von Kossa. After nine days in culture, fewer ALP positive colonies were observed in mutant cultures compared with WT ($p=0.0009$) however, this difference was resolved after 15 days, as a greater number of ALP positive colonies in the mutant cultures was observed compared with the WT ($p=0.03$). The mutant cells also displayed significantly fewer von Kossa positive colonies compared with WT at 15 days ($p=0.002$) (Figure 5.16). Overall this data suggests that there is an early osteoblast differentiation defect in the Nbr1^{D50R} mutant cells that is resolved later in differentiation.

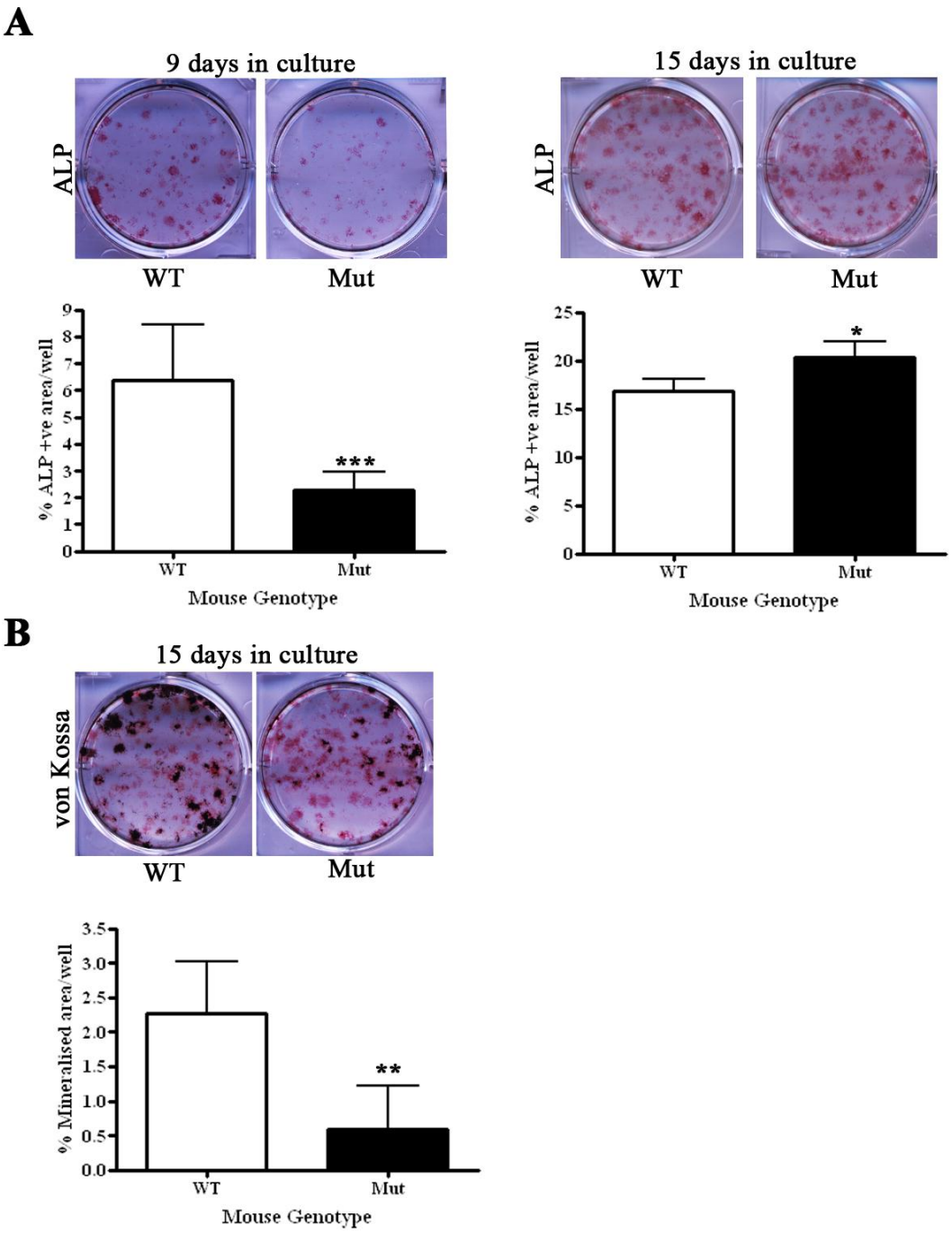

Figure 5.16. Bone marrow stromal cells derived from Nbr1^{D50R} mutant (Mut) mice show delayed osteoblast differentiation and reduced mineralisation activity compared to wild type (WT).
A. ALP staining of cells cultured for nine and 15 days.
B. Von Kossa staining of cells cultured for 15 days.
*p<0.05, **p<0.01, ***p<0.001. Data represent the mean and error bars represent the SD of six wells. This experiment was carried out once.

5.6. Discussion

The adult skeleton is continually undergoing self renewal and remodelling at a rate of 10%/year (Manolagas, 2000). The process of bone resorption and formation is tightly coupled and an imbalance can give rise to a broad spectrum of skeletal pathologies (Harada and Rodan, 2003; Janssens and Van Hul, 2002). The generation of mutant mouse models has proven invaluable for understanding the molecular mechanisms governing the regulation of bone and has therefore aided the identification of therapeutic targets to treat human skeletal diseases.

Nbr1 and p62 are both involved in different aspects of bone remodelling. Published data suggests that Nbr1 regulates osteoblast differentiation and activity whilst p62 is involved in regulating osteoclastogenesis. These proteins interact via their PB1 domains however, the importance of this interaction in the regulation of bone was previously unknown. To study this interaction further, a knock-in mouse model was generated. Affected mice have a mutation in amino acid 50 of Nbr1 (D50R) that inhibits its interaction with p62. The effectiveness of this mutation in disrupting this interaction between Nbr1 and p62 was confirmed by yeast-2-hybrid, co-immunoprecipitation (Figure 5.4) and immunofluorescence (Figure 5.5). MicroCT is widely used to study bone microarchitecture and was utilised in this investigation to analyse the effects of the $Nbr1^{D50R}$ mutation on bone structure. A cohort of three, six and nine month old mice from each genotype were studied due to the age dependent phenotype of the truncated Nbr1 mouse model (Whitehouse et al., 2010).

5.6.1. Abrogation of the p62-Nbr1 interaction causes an age dependent osteoporotic phenotype

MicroCT analysis of whole femurs and tibiae established that the $Nbr1^{D50R}$ mutation results in a decrease in whole bone volume (Figure 5.10) and BMD (Figure 5.11) at three months of age. Ct.Th and Tb.Th were also significantly reduced at three months of age (Figure 5.12 & 5.13). Interestingly, this phenotype appeared to resolve itself and by six months of age there were largely no differences between WT and mutant mice. An early bone phenotype that alters with age has previously been

documented in a number of other mouse models. The postnatal osteoblast specific disruption of the BMP type 1A receptor (BMPR1A) causes a decrease in bone volume and formation rate in younger (up to 6 months) mutant mice due to a decrease in the ability of osteoblasts to form bone. This difference resolved as mice aged and by 10 months there was an increase in bone volume in mutant mice compared with WT. This was due to a decrease in bone resorption by osteoclasts (Mishina et al., 2004). These data demonstrate that BMP signalling can regulate osteoblast function in an age-dependent manner, initially by supporting bone formation and then later by regulating the osteoblast control of osteoclast function (Mishina et al., 2004). Mice deficient in the $P2X_2$ receptor display a significant increase in BMD at 2 months of age however, these differences decreased in magnitude as the animals aged, suggesting a compensatory mechanism to overcome receptor deletion (Orriss, 2005). Finally, Apolipoprotein E deficient mice had decreased Ct.Th at 10 weeks of age but by 40 weeks, the Ct.Th was increased in mutant mice compared with WT. In addition, mutant femurs were shorter than controls at ten weeks of age but there was no difference observed at 40 weeks of age between genotypes. This was attributed to an increase in the adaptational response in ApoE deficient mice compared to WT controls (Robertson, 2004). The mouse models discussed above suggest that molecules and signalling pathways important for bone formation and remodelling can have differing effects depending on the age of mice. The early osteoporotic phenotype observed in the $Nbr1^{D50R}$ mutant mouse model in this study suggests that similar to the BMPR1A deficient mice, the p62-Nbr1 interaction could be involved in the regulation of bone mass by different mechanisms depending on mouse age. Alternatively, the resolution of the osteoporotic phenotype in the $Nbr1^{D50R}$ mutant mice could be due to a compensatory mechanism that is counteracting the effect of abrogating the Nbr1-p62 interaction in older mice.

5.6.2. Bone length

X-rays of femurs and tibiae from WT and $Nbr1^{D50R}$ mutant mice showed no consistent structural differences between genotypes (Figure 5.8 & 5.9). Initial physical measurements established a small but significant decrease in the tibia

lengths of three month old mutant mice and a small but significant increase in femur length of nine month old animals (Figure 5.7). These data suggest that the Nbr1^{D50R} mutation is having a small but negative effect on bone length in early development which is compensated for by six months of age. During endochondral ossification, the proliferation and differentiation of chondrocytes is carefully coordinated and regulates the rate of longitudinal bone growth which occurs at the epiphyseal plate, a thin layer of cartilage at the distal end of long bones (Emons et al., 2011). Given the slight differences in long bone length observed between WT and Nbr1^{D50R} mutant mice, the interaction between Nbr1 and p62 could be contributing to the regulation of this process. Mutations targeting fibroblast growth factors (FGFs) result in a variety of skeletal malformations (Ornitz and Marie, 2002). Mice lacking the FGF receptor three (FGFR3) display an increase in bone length (Deng et al., 1996) whilst mice overexpressing FGF2, showed a shortening of long bones (Coffin et al., 1995). Interestingly, Nbr1 has been implicated in the regulation of FGF2 signalling (Mardakheh et al., 2009), suggesting the interaction between Nbr1 and p62 may influence FGF signalling in chondrocytes of the growth plate.

Furthermore, a mouse model with the FGFR3^{Y367C} mutation, causing constitutive activation of the receptor, displayed a delay in ossification at one week of age resulting in shorter long bone length. However, an age-dependent acceleration in ossification in mutant mice was observed so that by six weeks of age, there was no difference in bone age between WT and mutant mice, although bone length was still significantly reduced (Pannier et al., 2010). In the Nbr1^{D50R} mutant mice, the small decrease in bone length observed at three months is resolved by nine months of age as bone length in mutant mice increased compared with WT. This suggests that similar to the FGFR3^{Y367C} mutant mice, there could be an age dependent misregulation of chondrocyte proliferation in Nbr1^{D50R} mutant mice, possibly due to changes in intracellular signalling that may affect the timing and regulation of gene expression. This could result in the initial decrease in bone length and the subsequent acceleration so that by six months, there was no difference between genotypes. There are a number of other growth factors and hormones that affect bone growth including VEGF, TGF-β, BMPs, Wnt, oestrogens and androgens

(Emons et al., 2011) and the actions of any of these could potentially be affected by the abrogation of the Nbr1-p62 interaction.

5.6.3. Cellular effects of the abrogation of the p62-Nbr1 interaction

Osteoclasts derived from bone marrow precursor cells of $Nbr1^{D50R}$ mutant mice appeared larger and contained more nuclei when cultured on plastic compared to WT (Figure 5.14). However when cultured on dentine, a more physiologically relevant environment, although there were a greater number of TRAP +ve cells suggesting a greater differentiation potential (Figure 5.15), the resorption area was comparable to WT cultures (Figure 5.15). This suggests that the resorption activity per osteoclast was reduced. There was however, variation between dentine slices which could have been masking a small affect. Confirmation of this result is therefore required before any firm conclusions can be made as to the effect of the $Nbr1^{D50R}$ mutation on osteoclast resorption activity.

The clear morphological differences observed in TRAP +ve cells cultured on plastic from $Nbr1^{D50R}$ mutant mice could suggest that the p62-Nbr1 interaction is involved in the regulation of osteoclast size and fusion. Increased osteoclast size and numbers are a hallmark of disorders such as PDB and multiple myeloma (Ehrlich and Roodman, 2005). Larger osteoclasts containing more nuclei have been observed in a mouse model harbouring a PDB mutation in p62 (Daroszewska et al., 2011) whilst p62 deficient mice display impaired osteoclastogenesis upon stimulation with PTHrP (Duran et al., 2004). Additionally, overexpression of $p62^{P392L}$ in osteoclasts causes an increase in osteoclast activity and survival as well as an increase in multinucleated cells that contain more nuclei (Chamoux et al., 2009). Together, these data suggest that p62 is involved in the regulation of osteoclastogenesis. The work described in this thesis suggests that the interaction between Nbr1 and p62 is of specific importance to osteoclast differentiation. The interaction between Nbr1 and p62 could be involved in the assembly of signalling complexes similar to that described in muscle (Lange et al., 2005) and its abolition could result in changes in osteoclastogenesis. Alteration of signalling pathways in osteoclasts has been demonstrated to influence osteoclast size as observed in Fra-2 deficient mice which

have larger osteoclasts and an increase in phosphorylated ERK1/2 (Bozec et al., 2008).

In vitro cellular assays also demonstrated that the early bone phenotype observed in the $Nbr1^{D50R}$ mutant mouse model could be due in part to a defect in osteoblast function. Bone marrow precursors from $Nbr1^{D50R}$ mutant mice, stimulated with ascorbic acid and β-glycerophosphate showed an early reduction in ALP positive colonies and reduced mineralised bone nodule formation (Figure 5.16). This suggests that there could be a defect in osteoblast differentiation and activity or a relative decrease in osteoblast precursor numbers in the bone marrow. The resolution of the observed decrease in ALP positive colonies at a later time point suggests that there could be a compensatory mechanism taking place. To establish if the mineralisation activity of the mutant osteoblasts also resolved with time, a later time point is required. The reduced BMD observed *in vivo* at three months of age (Figure 5.11) suggests that the secretion of bone matrix components by osteoblasts is impaired which supports the reduction in osteoblast activity observed *in vitro*.

Osteoblasts are responsible for bone formation and mineralisation and a reduction in their activity causes phenotypes observed in a number of mouse models. Osteoblast precursors from the BMPR1A deficient mice (described above) formed fewer ALP positive colonies and showed weaker von Kossa staining suggesting a reduction in bone formation and mineralisation, which could explain the observed *in vivo* phenotype (Mishina et al., 2004). In contrast, osteoblasts from mice deficient in the Wnt antagonist Frizzled-related protein 1 displayed an increase in osteoblast differentiation and mineralization, explaining the increase in BMD and trabecular bone volume observed *in vivo* (Bodine et al., 2004). These data show that *in vitro* culture of osteoblasts can be a predictor of *in vivo* osteoblast activity and therefore suggests that the reduction in cortical and trabecular thickness observed in the $Nbr1^{D50R}$ mutant mouse model could be the result of a decrease in osteoblast differentiation and activity.

Protein degradation has been highlighted as an important regulatory mechanism for the modulation of signalling pathways. Smurf1, an E3 ubiquitin ligase, interacts with

Runx2 and Smad1 and facilitates their degradation in an ubiquitin- and proteasome-dependent manner, thereby negatively regulating BMP signalling and osteoblast differentiation (Zhao et al., 2004; Zhao et al., 2003). In addition, the proteasome inhibitor bortezomib is able to stimulate bone formation (Giuliani et al., 2007). The cell specific accumulation of ATF4 is also important for osteoblast differentiation and this is controlled by the UPS (Yang and Karsenty, 2004). Together, these data suggest that degradation of specific proteins is an important mechanism for regulating osteoblast differentiation and activity. p62 is involved in the proteasomal degradation of polyubiquitinated proteins (Babu et al., 2005) and interacts with components of the proteasome (Seibenhener et al., 2004) whilst Nbr1 potentially interacts with components of the ubiquitination machinery (Chapter 3). The p62-Nbr1 interaction could be important for the facilitation of protein degradation and its abrogation may therefore result in protein accumulation and altered osteoblast activity.

This study has made substantial progress towards the characterisation of the bone phenotype in the $Nbr1^{D50R}$ mutant mouse model. Figure 5.17 represents a schematic diagram of the proposed effects of abrogating the Nbr1-p62 interaction on osteoblast and osteoclast differentiation and activity and subsequently bone architecture.

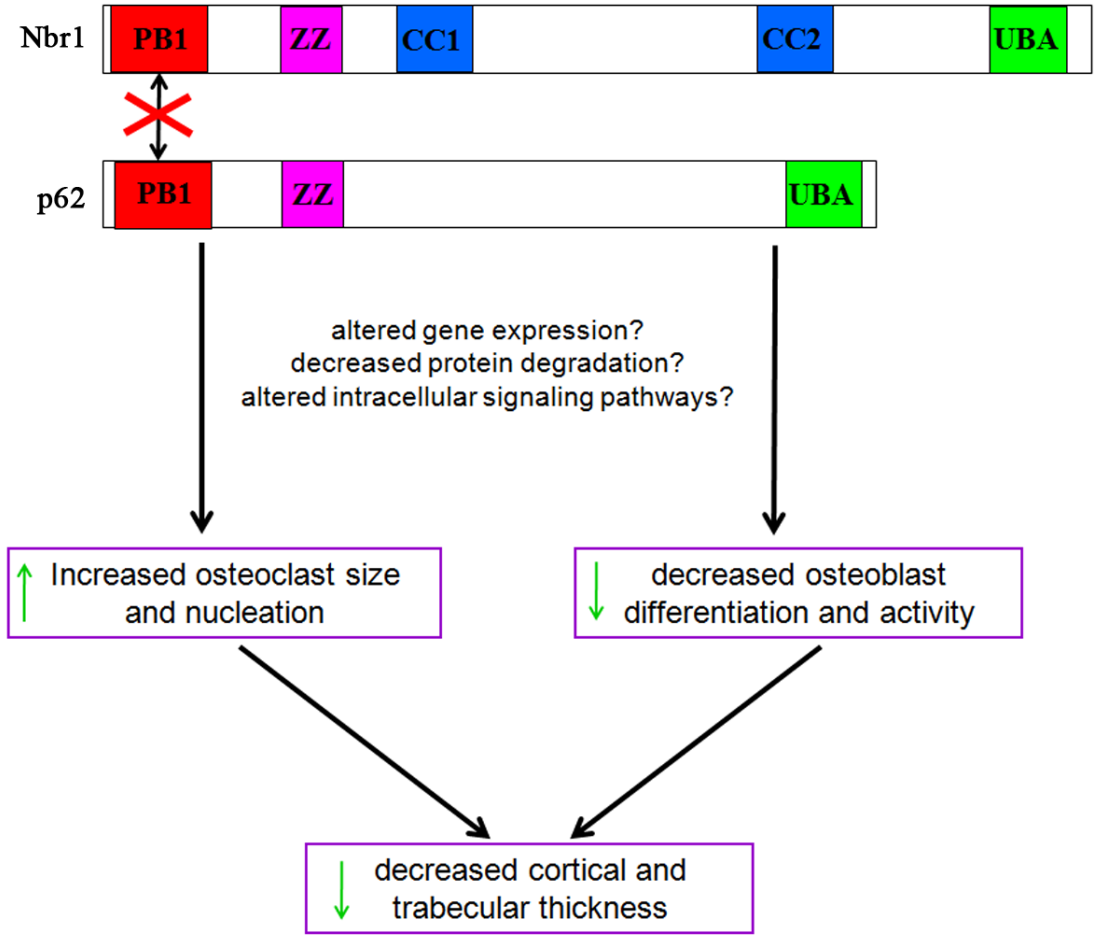

Figure 5.17. Schematic representation of the proposed effects of the Nbr1^{D50R} mutation on the regulation of bone. Upon inhibition of the Nbr1-p62 interaction, osteoblast differentiation and activity is decreased and osteoclast size and nucleation is increased. This could result in a decrease in cortical and trabecular thickness.

5.7. Future work

To fully confirm the observed phenotype of the Nbr1^{D50R} mouse model, additional experiments are required.

There were slight differences observed in a number of cortical and trabecular parameters in the Nbr1^{D50R} mutant mice therefore, to confirm that these are not due to random variation, a larger number of mice at each age will need to be analysed. Unlike the trNbr1 mouse model, the Nbr1^{D50R} mice have an early phenotype that is resolved with age therefore to establish if this phenotype is also present earlier that three months of age, microCT analysis of mice at younger ages is required. Additionally, H&E staining would enable the analysis of overall bone structure in the mutant mice at different ages.

Due to the differences observed between mutant and WT osteoclasts cultured on plastic, it is of paramount importance to assess the size, nucleation and morphology of mutant osteoclasts *in vivo*. Electron microscopy is currently being performed in collaboration with Miep Helfrich, University of Aberdeen to address this question. Additionally, to examine the effects of the Nbr1-p62 interaction on signalling pathways in osteoclasts, *in vitro* analysis of the activation of signalling pathways such as NF-κB and ERK 1/2 should be performed. As p62 is important in RANKL signalling, assessing the sensitivity of osteoclasts precursors to increasing levels of RANKL would be interesting to explore.

Due to the observed *in vitro* osteoblast phenotype, dynamic histomorphometry could be used to assess if the bone formation rate is altered *in vivo*. This could be analysed in mice of varying ages to establish if the number and activity of osteoblasts is influenced by the developmental stage. An in depth analysis of the signalling pathways that govern osteoblast differentiation and activity such as Wnt, BMP and FGF would also need to be performed to determine which pathway(s) require the functional p62-Nbr1 interaction. Additionally, differentiation and activity of osteoblasts derived from bone marrow stromal cells and calvaria should be analysed over a longer time course (21 days).

To establish if the development of the growth plate is altered by the abrogation of the p62-Nbr1 interaction, histomorphological measurements could be carried out in young mice (~10 days) as the size of the growth plate is known to positively correlate with bone growth rate (Sanger et al., 2011). Additionally, in situ hybridization experiments could be performed to establish if the expression of molecules such as osteocalcin, PTHrP, Indian hedgehog or collagen type I are affected.

Chapter 6. Sequence Analysis of Individuals with High Bone Mass

6.1. Introduction

The maintenance of normal bone mass and skeletal integrity is reliant on the dynamic balance between bone formation (by osteoblasts) and bone resorption (by osteoclasts). This is regulated by a complex network of signalling pathways, hormones and environmental factors. An imbalance in this process can lead to a wide range of skeletal pathologies including the sclerosing bone dysplasias, characterised by an increase in bone mass (Van Wesenbeeck et al., 2003).

Bone dysplasias are often caused by genetic mutations resulting in reduced bone resorption or increased bone formation (a selection of these are discussed here and in Chapter 1). Albers-Schonberg disease is characterised by sclerosing bone of varying degrees and is caused by mutations in *CLCN7*, encoding chloride channel 7, a transmembrane protein that permits the exchange of Cl^- ions across the osteoclast ruffled border (Kornak et al., 2001). Furthermore, inactivating mutations in the carbonic anhydrase II enzyme can lead to defective hydrogen ion transport by osteoclasts resulting in increased bone mass due to impaired bone resorption (Sly et al., 1985). Conversely, an increase in bone formation has been identified as a cause of some sclerosing bone disorders. Activating mutations in *LRP5* (low-density lipoprotein receptor-related protein 5) and de-activating mutations in the *SOST* gene (encoding sclerostin) lead to increased Wnt signalling resulting in high bone mass (Brunkow et al., 2001; Van Wesenbeeck et al., 2003). Other signalling pathways can also be affected; mutations in TGF-β1 cause Camurati-Engelmann disease which is characterised by cortical thickening in a number of bones (Janssens et al., 2000).

Genome wide association studies (GWAS) can be employed to identify genetic variants that may be contributing to common genetic traits or disease phenotypes. A study by Duncan et al. focused on post-menopausal women with extreme high or low hip bone mineral density (BMD) and identified association at six new genetic loci. One of these was in the *GALNT3* gene that encodes N-

acetylgalactosaminyltransferase 3, an enzyme involved in O-glycosylation of serine and threonine residues. A mouse model with a loss-of-function mutation in *GALNT3* displays a high bone mass phenotype, supporting the involvement of this gene in determining BMD (Duncan et al., 2011). Previous sequencing analysis of the PB1 and UBA domains of *NBR1* in individuals with idiopathic Paget's disease of bone (PDB) failed to identify any disease causing mutations (C. Whitehouse, unpublished data) whilst GWAS studies on PDB have not yet found any association with sequence variation in or near *NBR1* (Omar Albagha, personal communication).

Whilst a number of sclerosing bone phenotypes can be accounted for by mutations such as those described above, there are many cases where HBM cannot be explained (Gregson et al., 2011). As Nbr1 has been implicated in the regulation of bone mass and BMD in mice (Whitehouse et al., 2010), it could be hypothesised that genetic mutations in the *NBR1* gene may account for some of the unexplained HBM phenotypes. In order to investigate this, DNA was obtained from a total of 82 idiopathic HBM patients who participated in a larger study carried out at the University of Bristol, directed by Dr Celia Gregson (DNA kindly supplied by Prof. Jon Tobias). All the exons, including the 5' untranslated region (UTR) of *NBR1* were sequenced with the aim of identifying potentially pathogenic novel mutations or genetic variations that may be affecting gene function. Such findings could then lead to new and important insights into the molecular mechanisms that govern the regulation of bone mass and may identify new therapeutic targets.

6.2. Genomic Details of Nbr1

The human *NBR1* gene has 21 exons of varying sizes. The first exon encodes the 5' untranslated region (5'UTR) and the translational start methionine (ATG) resides in exon 2 (Figure 6.1). Exon 1 was included in the sequencing analysis as it is possible that mutations in this region could infer alternative translational start sites, affect gene structure or alter mRNA stability. *NBR1* contains relatively few known exonic single nucleotide polymorphisms (SNPs) (Table 6.1) and as yet, none of these have been implicated in bone disease. The frequency of all detectable *NBR1* coding SNPs will be determined in the HBM patients sequenced in this study.

SNP	Change	Type	CEU Frequency (HapMap)	Position (aa)	Position (exon)
rs11657883	C/T	-	T = 0.65 C = 0.35	c.165+9	Intron 4
rs112368175	C/T	synonymous	*	p.83	6
rs79648394	C/T (A/V)	non-synonymous	*	p.112	6
rs36054317	C/T	synonymous	*	p.167	8
rs117060970	G/C (V/L)	non-synonymous	G = 0.992 C = 0.008	p.182	8
rs113187111	T/C (L/S)	non-synonymous	*	p.204	8
rs35263078	-/C	frameshift	unknown	p.234	9
rs115552058	G/A (R/H)	non-synonymous	*	p.312	10
rs35043576	C/T	synonymous	*	p.330	10
rs111821306	T/C (I/T)	non-synonymous	unknown	p.534	13
rs111808644	G/A (D/N)	non-synonymous	unknown	p.559	14
rs34372250	A/G (M/V)	non-synonymous	A = 1 G = 0	p.623	16
rs61740594	G/C (E/D)	non-synonymous	*	p.716	17
rs34660735	C/-	frameshift	unknown	p.744	17
rs56320937	T/C (M/T)	non-synonymous	unknown	p.921	21
rs8482	A/G (H/R)	non-synonymous	G = 0.66 A = 0.34	p.923	21

Table 6.1. Known exonic SNPs in NBR1. Compiled from dbSNP132 (*frequency not reported in the Caucasian European (CEU) population.

A

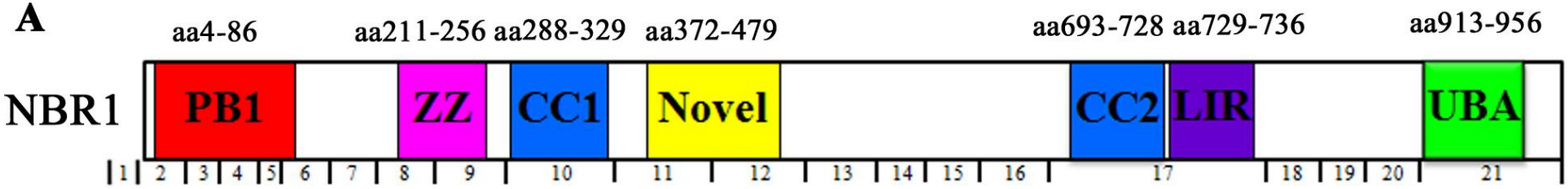

B

Exon	Amino Acids	Exon	Animo Acids
1	out of coding region	**12**	412 – 508
2	1 – 34	**13**	509 – 558
3	35 – 55	**14**	559 – 584
4	56 -62	**15**	585 – 621
5	62-69	**16**	622 – 676
6	70 – 134	**17**	677 – 823
7	135 – 160	**18**	824 – 855
8	161 – 232	**19**	856 – 874
9	233 – 288	**20**	875 – 909
10	289 – 358	**21**	910 - 966
11	358 - 411		

Figure 6.1. Positions of coding exons in NBR1.
A. Schematic diagram indicating the positions of each coding exon in relation to the domain structure of NBR1 (not to scale). Nbr1 contains a Phox and Bem1p (PB1) domain at its N-terminus (red), a zinc binding domain (pink), two coiled-coil domains (blue), an LC3 interacting region (LIR), a highly conserved novel region (yellow) and a C-terminal ubiquitin-associated (UBA) domain (green).
B. Table showing the amino acids encoded by each exon in NBR1.

To gain further information on the SNPs present in *NBR1*, a linkage disequilibrium (LD) map was generated from the CEU (Caucasian European) HapMap population data (www.HapMap.org) (Figure 6.2). LD occurs when particular alleles at two or more neighbouring loci occur together with frequencies significantly different from those predicted from the individual allele frequencies. Thus, LD maps establish the likelihood of alleles at two or more SNPs segregating together in the population. LD can be measured using the correlation coefficient R^2 of SNP genotypes from a large homogeneous population. Maximum LD (R^2 = 100%) is reached when two SNPs are completely correlated such that the presence of one allele at one SNP locus on the chromosome can predict the presence of the allele at the other locus in the same chromosome with 100% certainty. The LD map of *NBR1* reveals that it is largely within one LD block and there is limited recombination within the gene.

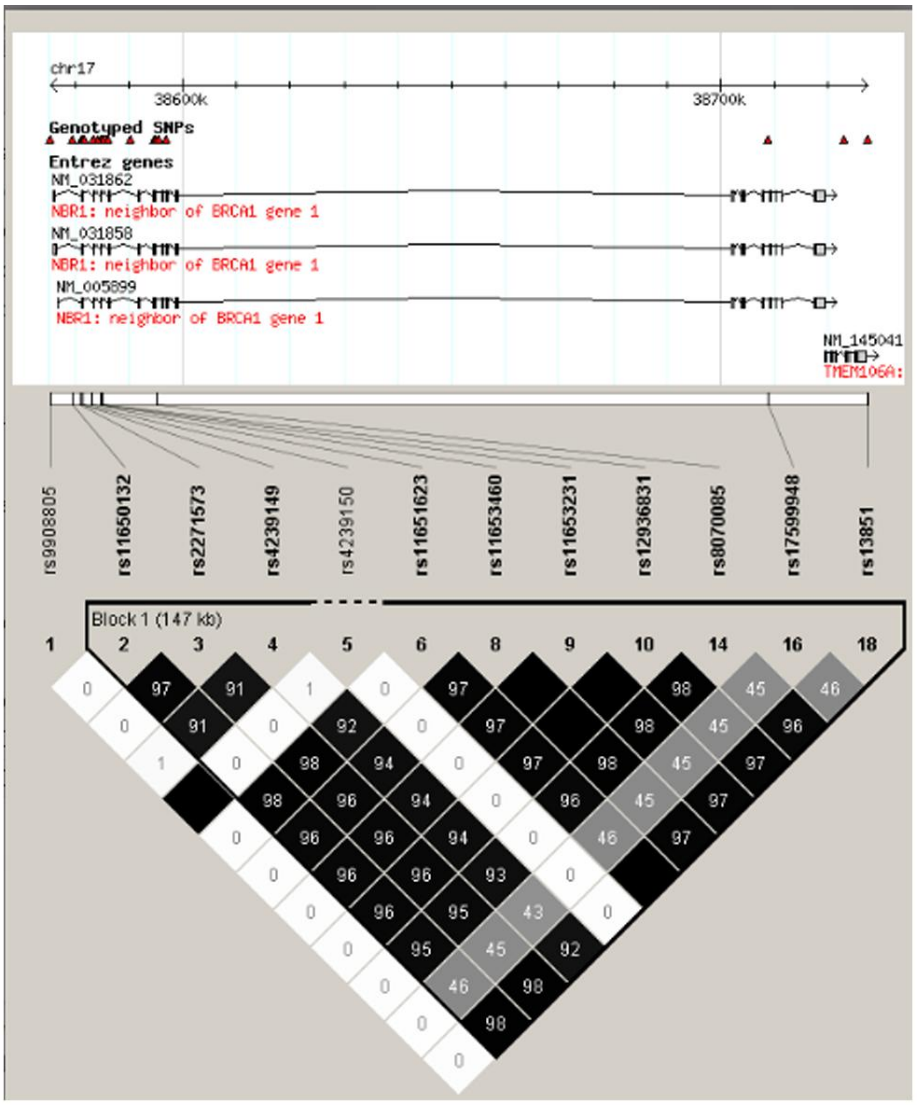

Figure 6.2. *NBR1* linkage disequilibrium (LD) map.
A. Using the CEU (Caucasian European) population from version 27 of the HapMap project, an LD map was generated using the HaploView software. This shows that *NBR1* is largely within one LD block. Output=R^2.

6.3. Patient Information

NBR1 genetic screening was performed on 82 patients with unexplained HBM[1] defined by dual energy X-ray absorptiometry (DXA) as having (a) vertebrae L1 Z-score of >+3.2 and total hip Z score of no lower than +1.2 or (b) a total hip Z score >+3.2 and an L1 Z score no lower than +1.2. A total of 55 out of the 82 individuals analysed also had relatives with HBM suggesting an underlying genetic cause. All individuals were white British and were recruited as part of a larger study directed by Dr Celia Gregson (University of Bristol) with the aim of identifying the clinical characteristics of HBM. Compared to unaffected controls, individuals had increased odds of multiple HBM associated phenotypes including enlarged mandible, broad frame, misshapen or extra bone at the site of tendon and/or ligament insertion and larger shoe size. They also reported increased odds of sinking when trying to swim, had an increased BMI and reduced odds of reporting a family history of fracture (Gregson et al., 2011).

6.4. PCR Optimisation

To sequence the exons of *NBR1*, the genomic DNA was amplified on an exon-by-exon basis. A standard PCR reaction was used (section 2.1.1) and the optimal primer annealing temperatures and $MgCl_2$ concentrations were established (Table 2.9).

To confirm successful DNA amplification, a proportion of the PCR product was analysed by agarose gel electrophoresis. PCR product was purified using ExoSAP-IT and sequenced using a standard sequencing reaction (section 2.1.6 and 2.1.7). Electropherograms were obtained for 95% of the amplicons and were analysed using the programme Sequencher version 4.10.1.

[1] Ethical approval was granted by COREC (Reference 05/Q2001/78 - Bath Research Ethics Committee).

6.5. Identification of Genetic Variation in High Bone Mass Patients

Initially, genomic DNA was obtained from blood samples of 32 of the total 82 individuals and all *NBR1* exons were sequenced. Subsequently, genomic DNA from a further 50 patients was obtained and due to time constraints the LC3 interacting region (LIR), PB1 and UBA domains of NBR1 were prioritised for sequencing. These regions were chosen due to their known importance to skeletal maintenance in the structurally similar protein p62. Mutations in both the UBA domain and LIR of p62 have been identified in patients with Paget's Disease of Bone (PDB) (Falchetti et al., 2009; Goode and Layfield, 2010), whilst the PB1 domain is known to be important for the regulation of the NF-κB signalling pathway and osteoclast differentiation (Lamark et al., 2003; Puls et al., 1997; Sanz et al., 2000).

6.5.1. Novel variations

Sequencing of *NBR1* in HBM individuals identified one novel non-synonymous variant (Figure 6.3) that had not previously been reported at the time of this study and was not present in any other DNA sample sequenced. This variant was confirmed by repeating the PCR and sequencing in both directions in order to rule out polymerase error. It is located in exon 8 at residue 182 in the NBR1 protein and results in a valine to leucine substitution. Two online programmes were used to predict if this amino acid change is likely to be deleterious to protein function. PolyPhen2 predicted that this change is 'benign' whilst SIFT predicted it to be 'tolerated'. To determine if this residue was conserved, a cross species comparison was performed (Figure 6.4). In all mammals analysed, this residue was conserved as a valine, however in chicken and zebrafish, the equivalent amino acid is an isoleucine and a cysteine respectively.

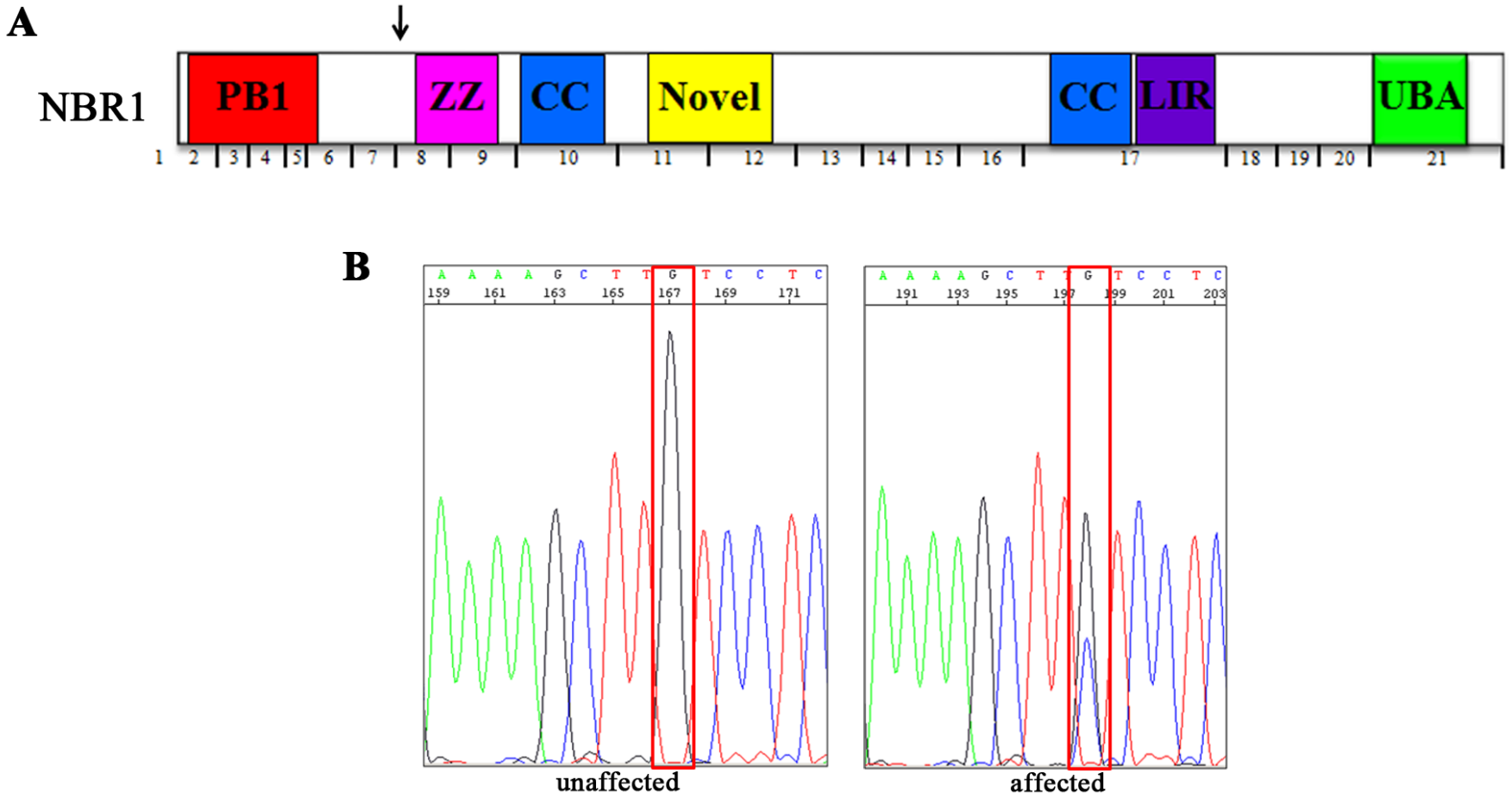

Figure 6.3. A novel *NBR1* variant found in a HBM patient.
A. Schematic diagram of NBR1 illustrating the position of the novel variant at amino acid 182 (arrow).
B. Electropherogram depicting the DNA sequence from the affected and an unaffected indivdual (red box).

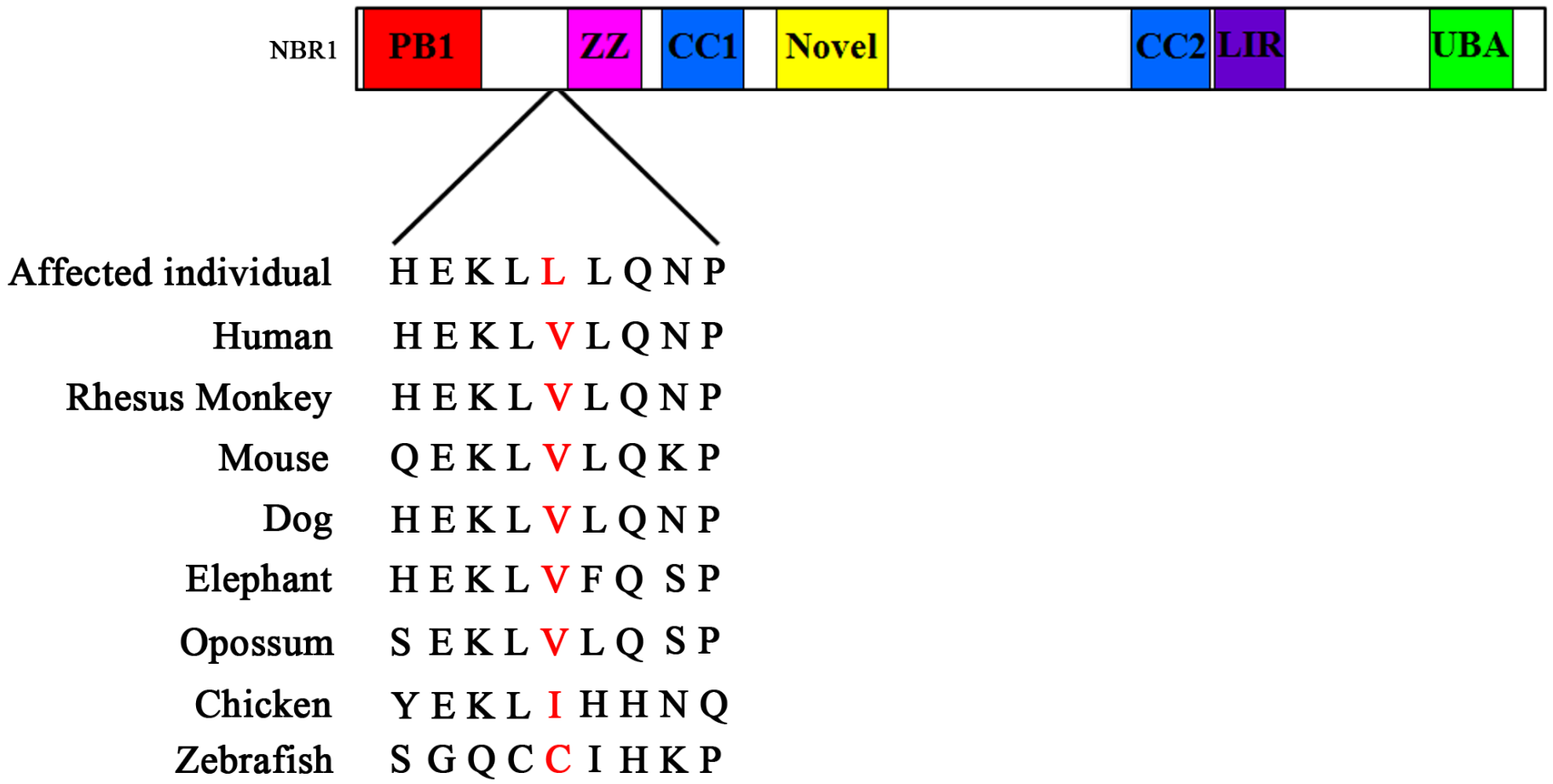

Figure 6.4. Cross species comparison of the NBR1 residue affected by the novel variant found in an individual with HBM. The novel variant was located at residue 182 in NBR1 (shown in red). This amino acid is conserved in mammals however in chicken the corresponding amino acid is isoleucine (I) and in zebrafish is a cysteine (C).

6.5.2. Frequency of known exonic SNPs

Using the reported allele frequencies (Table 6.1), and the formulae in section 2.6.2 it was predicted that there was sufficient power to detect rs8482 in the individuals sequenced in this study (80% is considered acceptable power). All other SNPs are either not reported in the Caucasian European (CEU) population or their minor allele frequency is too low to have sufficient power to detect it in the number of individuals sequenced. Analysis of the sequence variation in all individuals confirmed this prediction as rs8482 was the only SNP to be detected. The allele frequency gained for rs8482 in the HBM individuals was the opposite to that reported on NCBI (www.ncbi.nlm.nih.gov) therefore to gain further reliability, additional HBM individuals and controls[2] were genotyped and frequencies obtained are shown in Table 6.2. This revealed that there was no difference between cases and controls and it was likely that the SNP allele frequency reported on NCBI was incorrect. Supporting this, an additional SNP residing in intron 4 of *NBR1* (rs11657883) was found to be in complete LD with rs8482 in the first 32 individuals studied. The frequency of the C allele of this SNP is reported as 0.35 in dbSNP, which is in agreement with the calculated frequency of the G allele of rs8482 from the HBM cases and controls in this study.

	A/A	A/G	G/G	Frequency of G allele
Cases	54	55	14	0.34
Controls	77	71	23	0.34

Table 6.2. Allele frequencies from HBM cases and controls for rs8482.

[2] Controls were obtained from Dr Natalie Prescott and Prof. Christopher Matthew, KCL (personal communication) from a similar study on inflammatory bowel disease where controls were taken from the 1958 British Cohort DNA Collection, funded by the Medical Research Council and Wellcome Trust).

6.6. Discussion

An imbalance in the bone remodelling process any time throughout life can lead to a large number of skeletal pathologies including the sclerosing bone dysplasias which are generally characterised by an increase in bone mass (de Vernejoul and Kornak, 2010). Mutations in a number of genes have been identified as contributing to HBM, however there are a growing number of cases where the cause is still unknown (Gregson et al., 2011). Due to the previously identified roles of Nbr1 in bone remodelling (Whitehouse et al., 2010), this study aimed to identify mutations in the coding region of *NBR1* that may be contributing to the HBM phenotype seen in some of these individuals.

Sequencing of the *NBR1* gene in individuals with HBM identified one novel genetic variation (Figure 6.3). This resulted in a valine to leucine substitution at amino acid 182 (V182L) of the NBR1 protein. Valine and leucine have similar structures and properties as both are hydrophobic and neutral in charge. This suggests that substitution from one to the other is less likely to alter protein structure and therefore function suggesting that this mutation is unlikely to cause disease. Analysis of this mutation using two programs that predict the functional affect of coding mutations - PolyPhen and SIFT - predicted that this amino acid change is benign or tolerated respectively and therefore unlikely to have a large effect on protein structure and function. Additionally, comparison of the amino acid sequence of this gene from several species (Figure 6.4) showed that valine 182 is not highly conserved in evolution. The corresponding residue in chickens and zebrafish is an isoleucine or a cysteine respectively thus suggesting that valine 182 is not essential for protein function. Isoleucine has very similar properties to leucine and valine and therefore is unlikely to alter protein function, cysteine is slightly more polar, however SIFT predicted that an amino acid change from valine to cysteine at this position in NBR1 is also likely to be tolerated perhaps as expected due to its existence in zebrafish. Taken together, these data suggests that the novel variation identified in NBR1 is unlikely to be the primary cause of the high bone mass in this individual.

Following the completion of this sequencing analysis, in May 2011 the 1000 genomes project (www.1000genomes.org) made public its latest SNP genotyping calls based on the pilot release of whole genome sequencing data in 1000 individuals and all new SNPs were entered into dbSNP. This identified the V182L variant in two individuals (out of 120 CEU) and confirmed that it is indeed a SNP. It was allocated the reference SNP number rs117060970 and the frequency of the V182L allele based on the 1000 genomes data is 0.008. Using this reported SNP frequency, this study had 73% power to identify the variant in the 82 individuals sequenced. As sample size can affect reported SNP frequencies, to fully confirm that this SNP is not associated with HBM, a larger number of cases will need to be sequenced to reliably report the allele frequencies in the HBM population.

This study has shown that there is relatively little known genetic variation in NBR1 (Table 6.1), especially in the Caucasian population. The LD map based on common variation across NBR1 (Figure 6.2) shows that the gene is located in one LD block and recombination events within the gene are rare. The recent GWAS by Duncan et al. (Duncan et al., 2011) could not detect any genetic association between common variants at the *NBR1* locus and BMD in 1955 postmenopausal women with high or low BMD (1055 high, 900 low) suggesting that this gene is unlikely to be a major contributing factor to heritable differences in BMD in women of European origin. However, it is possible that rare mutations in *NBR1* that are not covered by the various GWAS SNP arrays could underlie less common HBM phenotypes.

There was sufficient power to detect only one of the known exonic SNPs in the 82 individuals sequenced in this study. This SNP was rs8482 and is of particular interest because it is non-synonymous and resides in the UBA domain of NBR1 which is known to bind mono- and polyubiquitinated chains (Waters et al., 2009). Although this SNP does not affect ubiquitin binding as tested in an *in vitro* binding assay (Waters, 2009), it alters the protein sequence and could therefore still affect protein function in a way that is not yet understood. Genotyping of this SNP in cases and controls showed that its frequency in HBM individuals did not differ significantly from normal (Table 6.2) suggesting that it is not important in determining bone mass.

Overall, this study has been important in revealing that the idiopathic HBM phenotype seen in 82 individuals is unlikely to be caused by genetic mutations in the coding region of *NBR1*. To fully confirm that any known genetic variation in *NBR1* is not associated with disease, a larger cohort of cases and controls will need to be analysed (see section 6.7).

6.7. Future Work

One novel variation was identified in the coding region of *NBR1* that has now been reported as a SNP. Due to the low amino acid conservation among species, this variation is unlikely to be the main cause of the HBM seen in the individuals in this study. However, it would be useful to further genotype this SNP and the rest of the *NBR1* gene in a larger number of cases and controls to establish if this or any other as yet undetected sequence variants are associated with HBM. The number of individuals required to detect a specific SNP will very much depend on the frequency of the SNP in the population.

Whole exome sequencing is now being used to identify genetic variation in individuals with unexplained disease phenotypes (Glazov et al., 2011). Work is now underway at the University of Bristol to sequence the complete exome of individuals with HBM to try to identify the cause of the phenotype. Many of the patients have affected relatives and therefore the cause is likely to be of genetic origin.

Genome-wide association studies (GWAS) have been successful in identifying genes involved in disease and this has been illustrated by the recent study in PDB patients where the *TNFRSF11A* gene encoding RANK was shown to be associated with disease (Albagha et al., 2010). GWAS studies in bone mineral density have yet to find any association with *NBR1*. This is probably due to the presence of very few SNP markers in or near *NBR1* in any of the GWAS SNP arrays and could suggest that a more detailed genotyping study is required in a larger cohort of HBM individuals. Due to the phenotype of the $Nbr1^{D50R}$ knock-in mouse model, it would also be interesting to analyse patients with low bone mass.

Chapter 7. General Discussion

Nbr1 is a ubiquitously expressed scaffold protein that contains numerous conserved protein domains. At its N-terminus, Nbr1 has a PB1 domain and a ZZ zinc-finger domain whilst at its C-terminus it contains a ubiquitin-associated (UBA) domain. Two CC domains are also present, the first of which facilitates homodimerisation. In bone, truncation of Nbr1 leads to an age dependent increase in bone mass and bone mineral density due to an increase in osteoblast activity and p38 MAPK activation (Whitehouse et al., 2010). In muscle, Nbr1 interacts with the giant sarcomeric protein titin and is part of a signalling complex that can modulate gene transcription (Lange et al., 2005). Nbr1 is also involved in receptor internalisation and degradation via endocytosis and can modulate signal transduction pathways (Mardakheh et al., 2010; Mardakheh et al., 2009).

The studies presented in this thesis aimed to further investigate the roles of Nbr1 by identifying novel interacting partners and subsequently characterising their significance with respect to Nbr1 function. Additionally, to advance the knowledge of Nbr1 with regard to bone, a knock-in mouse model that contained a mutation in the PB1 domain of Nbr1 resulting in the abrogation of the interaction between Nbr1 and p62 was created. This thesis describes the bone phenotypic analysis of this mouse. Due to the high bone mass (HBM) phenotype observed in the truncated Nbr1 mouse model, genomic DNA from individuals with idiopathic HBM was sequenced for genetic variation in the coding exons of *NBR1*.

7.1. The interaction potential of Nbr1

Nbr1 is a scaffold protein, likely to be involved in multiple protein-protein interactions. Therefore, in the first two chapters of this thesis, yeast-2-hybrid screens were performed with regions of Nbr1 as bait. A number of putative interacting partners were identified that provide further insight into the functions of Nbr1. First, the autophagosomal marker LC3 was revealed as an interacting partner of Nbr1. Further *in vitro* binding assays determined that an eight amino acid region of Nbr1 termed the LC3 interacting region (LIR) was required for the interaction with LC3

(Waters et al., 2009). This finding was in agreement with that of Kirkin et al. who also demonstrated that through its ability to bind polyubiquitinated chains, and its interaction with LC3, Nbr1 is an autophagic receptor that targets polyubiquitinated proteins for autophagosomal degradation (Kirkin et al., 2009; Waters et al., 2009). A number of other proteins including p62 (Pankiv et al., 2007a), Nix (Novak et al., 2010) and NDP52 (Thurston et al., 2009) contain LIR domains. There is now a major drive to identify additional proteins containing an LC3 interacting region as this mechanism is thought to be the major route by which proteins can be selectively targeted for autophagic degradation (Johansen and Lamark, 2011). The ubiquitinated protein targets that are specific to Nbr1 are still unknown, therefore identifying these has become of paramount importance to the further understanding of Nbr1 function. Evolutionary analysis has shown that the yeast homologue of Nbr1 is Atg19, a cargo receptor in the yeast Cvt selective autophagy pathway (Xie and Klionsky, 2007). The degradation of proteins via the Cvt pathway does not involve ubiquitin however, the similarity between Nbr1 and Atg19 suggests that the Cvt pathway is evolutionarily related to the Nbr1-mediated 'ubiquitinophagy' system (Kraft et al., 2010). It is also plausible that in higher organisms a non-UBA region of Nbr1 is required for recognising and targeting specific cargo for autophagic degradation (Kraft et al., 2010). In this respect, p62 has been identified as binding to and facilitating the autophagic degradation of STAT5A_ΔE18 through a ubiquitin independent mechanism (Watanabe and Tanaka, 2011).

The light chain of the microtubule associated protein MAP1B was identified as an interacting partner of the highly conserved novel region of Nbr1 and subsequent *in vitro* binding assays confirmed this interaction. Microtubules are known to facilitate autophagosome formation (Fass et al., 2006; Köchl et al., 2006). The binding of adaptor proteins such as FYCO1 to both LC3 and microtubule motor proteins has been suggested as a mechanism by which preautophagosomal membranes are targeted to sites of autophagosomal formation (Pankiv et al., 2010). The interaction between Nbr1 and MAP1B-LC1 provides evidence of a further mechanism by which proteins targeted for degradation via autophagic receptors are directed to sites of autophagosomal degradation via microtubule binding proteins.

In addition to the interaction between Nbr1 and MAP1B being involved in autophagy, it could be facilitating other processes. MAP1B-LC1 is also involved in the endocytosis of the AMPA receptor which regulates synaptic transmission (Davidkova and Carroll, 2007). It is proposed that through its interaction with the glutamate-receptor interacting protein (GRIP1), MAP1B-LC1 is able to mediate receptor endocytosis in neurons (Davidkova and Carroll, 2007; Seog, 2004). Nbr1 has also been implicated in the lysosomal degradation of cell surface receptors via its interaction with SPRED2 (Mardakheh et al., 2009). This suggests that the interaction between MAP1B-LC1 and Nbr1 could mediate receptor internalisation and therefore regulate intracellular signalling pathways. Additionally, Nbr1 interacts with monoubiquitin. Monoubiquitin is required for the process of receptor internalisation and degradation. Ligand binding to the epidermal growth factor receptor (EGFR) induces receptor activation and recruitment of ubiquitin ligases that mediate ubiquitination of the EGFR at the plasma membrane leading to receptor internalisation (Haglund et al., 2003). Proteins such as Eps15 bind to the monoubiquitin modifications on receptors and function as adaptors between ubiquitinated membrane cargo and the endocytic machinery (Polo et al., 2002). Therefore, similar to Esp15, through its interactions with MAP1B-LC1, SPRED2, monoubiquitin and the deubiquitinating enzyme USP8, all of which have been implicated in receptor degradation, Nbr1 could be acting as a scaffold to regulate receptor internalisation at the plasma membrane.

Abnormal accumulation of MAP1B-LC1 results in neuronal death in giant axonal neuropathy (GAN) due to the inhibition of its degradation via it interaction with gigaxonin (Allen et al., 2005). Additionally, the aggregation of MAP1B-LC1 is prevented by its interaction with DJ-1. This has been implicated in neurodegenerative disorders such as Parkinson's disease that are characterised by the presence of large protein aggregates (Wang et al., 2011). The leucine-rich acidic nuclear protein (LANP) interacts with MAP1B-LC1 and modulates the effects of MAP1B-LC1 on neurite extension (Opal et al., 2003). Therefore, it is clear that through specific interactions, MAP1B-LC1 function can be modulated and misregulation can contribute to the pathogenesis of aggregate prone neurological

diseases. Collectively, these data suggest that through specific protein-protein interactions, Nbr1 could also be modulating MAP1B-LC1 function.

Several components of the ubiquitination machinery were identified as putative interactors of Nbr1 in this thesis. This suggests that Nbr1 could be acting as a scaffold to target such proteins to their sites of action and affect ubiquitination and subsequently protein degradation via the UPS. Additionally, the identification of the eukaryotic elongation factor 1A (eEF1A) as a putative interacting partner of Nbr1 may also suggest an involvement for Nbr1 in the cotranslational degradation of proteins. Further work is required to confirm these putative interactions however, this study has been important in proposing new and exciting roles for Nbr1 in the control of protein degradation.

7.2. Nbr1 and the regulation of bone

This study has revealed that the interaction between Nbr1 and p62 is important in the early maintenance of normal bone volume, cortical thickness and bone mineral density. Mice that are homozygous for the $Nbr1^{D50R}$ mutation which inhibits the Nbr1-p62 interaction, display an early onset mild osteoporotic phenotype, probably due to a decrease in osteoblast differentiation and activity as well as an increase in osteoclast size and nucleation. This phenotype is very different to the trNbr1 mouse model which maintains a functional p62, PB1 domain mediated interaction and displays an age dependent increase in bone mass and mineral density (Whitehouse et al., 2010). Together, these mutant mouse models show that distinct regions of the Nbr1 protein are likely to be important for different functions within bone tissue. The C-terminus of Nbr1 may be more important for the regulation of bone mass as the trNbr1 mouse has a more severe phenotype than the $Nbr1^{D50R}$ mouse model. Mice deficient in p62 also develop an age dependent increase in bone density (Rodriguez et al., 2006). Recent data has demonstrated that additional deletion of Nbr1 reverted this phenotype (Sengupta et al., 2011). This could suggest that Nbr1 and p62 could have opposing functions in relation to controlling bone mass.

The Nbr1-p62 interaction is important for the formation of signalling complexes in muscle (Lange et al., 2005). Although not yet investigated, it is therefore likely that the abrogation of this interaction could affect signalling pathways in a range of other tissues including bone. The trNbr1 mouse model identified Nbr1 to be involved in the activation of downstream signalling molecules. TrNbr1 osteoblasts treated with the p38 MAPK activator anisomycin, displayed enhanced p38 MAPK activation whilst trNbr1 osteoclasts treated with RANKL displayed enhanced ERK and p38 MAPK activation (Whitehouse et al., 2010). This suggests that Nbr1 normally acts to inhibit these signalling pathways. p62 inhibits ERK signalling (Rodriguez et al., 2006) and is required for TNFα induced p38 MAPK activation but not for anisomycin induced p38 MAPK activation (Kawai et al., 2008). This again suggests that as well as acting in unison to affect intracellular signalling (Lange et al., 2005), Nbr1 and p62 also act separately in response to different stimuli to coordinate distinct downstream signalling pathways.

The trNbr1 protein is unable to bind a number of known Nbr1 interacting partners including FEZ1, CIB (Whitehouse et al., 2002) and SPRED2 (Mardakheh et al., 2009). The interaction between Nbr1 and SPRED2 inhibits FGF signalling, a pathway that activates ERK, JNK and p38 MAPK (Keren-Politansky et al., 2009; Makino et al., 2010). FGF signalling is important in the regulation of bone formation and osteoblast differentiation (Ornitz and Marie, 2002). Therefore, via its interaction with SPRED2, Nbr1 could be involved in the regulation of FGF signalling and subsequently bone formation. Additionally, the $Nbr1^{D50R}$ mouse model displayed slight changes in bone length. SPRED2 deficient mice have a dwarfism phenotype due to earlier and augmented ERK phosphorylation in response to FGF (Bundschu et al., 2005). It is therefore interesting to speculate that Nbr1, through its interactions with p62 and SPRED2 could be regulating FGF signalling in bone.

Nbr1 has been implicated in the control of receptor tyrosine kinase degradation. Ectopic expression of Nbr1 can inhibit the ligand-mediated degradation of EGFR by trapping it at the cell surface, resulting in enhanced ERK 1/2 signalling (Mardakheh et al., 2010). As the trNbr1 mouse model has lost the UBA domain (Whitehouse et al., 2010) which is vital for the inhibition of receptor degradation, this could be a

possible mechanism by which Nbr1 is regulating downstream signalling in osteoblasts and osteoclasts and therefore affecting bone remodelling.

Due to the known involvement of Nbr1 in the maintenance of bone, it was considered possible that genetic mutations in the *NBR1* gene that affect protein structure and function could be causing the idiopathic high bone mass phenotype identified in a number of individuals. Genetic screening of *NBR1* in these individuals did not identify any mutations suggesting that altered NBR1 function was not the cause of the high bone mass phenotype. As the trNbr1 protein may act in a dominant negative manner, it would be interesting to examine NBR1 genetic variation in osteoporotic individuals to assess if NBR1 is involved in this disease.

7.3. Vesicular trafficking, protein degradation, Nbr1 and bone

Osteoclasts rely on intricate vesicular trafficking pathways including endocytic/lysosomal transport of acidic vesicles containing proteases for bone resorption and transcytosis of the digested bone matrix. These pathways are mediated by a multitude of Rab GTPases (Coxon and Taylor, 2008). Mutations in the gene encoding the Plekhm1 protein which is involved in the Rab-7 dependent endosomal lysosomal transport of proteins to the osteoclast ruffled border causes osteopetrosis due to the absence of the osteoclast ruffled border (Van Wesenbeeck et al., 2007). As Nbr1 is now known to play a role in autophagy and vesicular transport, it is possible that Nbr1 may be playing a role in these processes in bone cells. FEZ1, an interacting partner of Nbr1 interacts with the Rab3 GTPase activating protein (Assmann et al., 2006) suggesting a link between Nbr1, Rab proteins and vesicular trafficking. Nbr1 also interacts weakly with osteocalcin suggesting that Nbr1 could mediate the cotranslational degradation of osteocalcin and therefore inhibit osteoblast matrix secretion. Indeed, the trNbr1 mouse model lacks the osteocalcin interacting region of Nbr1 and has elevated serum levels of osteocalcin (Whitehouse et al., 2010) which supports the possibility of Nbr1 acting to degrade osteocalcin prior to its secretion.

Recently, there has been increased research into the role of autophagy in bone. The upregulation of autophagy in response to stress stimuli such as hypoxia has been identified in osteocytes (Zahm et al., 2011). Additionally, the autophagy protein ALFY was shown to interact with p62 in the nucleus of osteoclasts and their precursors. Under autophagic induction p62 and ALFY translocate to the cytoplasm where they form large cytoplasmic aggregates. This relocalisation was more rapid in mature osteoclasts compared with their precursors suggesting a cell specific function for this interaction (Hocking et al., 2010). Along with p62, Nbr1 is also known to be involved in the autophagy pathway, therefore through similar cell specific protein-protein interactions Nbr1 could be regulating protein degradation and cellular activity in bone cells. Furthermore, several studies have shown that proteasomal degradation is important for the regulation of osteoblast differentiation (Yang and Karsenty, 2004; Zhao et al., 2003). This study has identified Nbr1 as a possible scaffold for the localisation of ubiquitination machinery therefore Nbr1 could be involved in the regulation of protein ubiquitination and degradation in osteoblasts and osteoclasts.

7.4. Implications for NBR1 in other diseases

NBR1 has been identified in ubiquitin- and p62-positive aggregates in the liver of patients with alcoholic steatohepatitis (Kirkin et al., 2009) suggesting the tissue specific accumulation of protein aggregates. p62 has also been identified in protein aggregation diseases such as Parkinson's and Alzheimer's disease (Wooten et al., 2006). Due to the known function of Nbr1 in the removal of protein aggregates, it would be interesting to investigate its role in the pathogenesis of these and other aggregation diseases such as inclusion body myopathy associated with Paget's disease of bone and frontotemporal dementia.

Nbr1 could also be linked to a number of chronic inflammatory diseases through its known protein interactors and downstream signalling effects. A recent GWAS study has identified genetic association between SPRED2 and rheumatoid arthritis (Stahl et al., 2010). As Nbr1 interacts with SPRED2, this could link Nbr1 with the pathogenesis of the disease. Nbr1 could be further implicated in arthritis due to its

involvement in p38 MAPK activation (Whitehouse et al., 2010). P38 MAPK is activated by proinflammatory cytokines such as IL-1 and TNFα which are elevated in rheumatoid arthritis and stimulate bone resorption by osteoclasts (Jean-Michel, 2002; Jimi et al., 1999b; Kumar et al., 2001). Nbr1 could therefore be involved in regulating p38 MAPK in rheumatoid arthritis individuals. Inhibition of p38 MAPK activation could therefore represent an effective therapeutic target for the treatment of rheumatoid arthritis (Kumar et al., 2001). Additionally, the generation of an activated T-cell specific Nbr1-deficient mouse model identified a role for Nbr1 in promoting lung inflammation and Th2 differentiation (Yang et al., 2010) again suggesting that through the control of intracellular signalling pathways, Nbr1 modulates tissue inflammation. (Kumar et al., 2001).

7.5. Concluding remarks

Nbr1 was first cloned over 15 years ago by expression screening with an antibody raised against the ovarian tumour antigen CA125 (Campbell et al., 1994). In the following years progress was slow in identifying the biological functions of this protein. Prior to the commencement of the work presented here, it was known that Nbr1 contained a number of conserved protein domains and interacting partners (Whitehouse et al., 2002), and was involved in muscle signalling (Lange et al., 2005) and bone remodelling (Whitehouse et al., 2010). The studies presented in this thesis have furthered current knowledge of Nbr1 function.

In chapters three and four, yeast-2-hybrid screens identified a number of novel Nbr1 protein-protein interactions. These were instrumental in contributing to the discovery of Nbr1 as an autophagic receptor, targeting ubiquitinated proteins to sites of autophagosomal degradation via the microtubule network. Additionally, putative interactors have alluded to a role for Nbr1 in targeting components of the ubiquitination machinery to their sites of action and in facilitating the cotranslational degradation of proteins by the proteasome.

In chapters five and six, the involvement of Nbr1 in bone formation and remodelling was further investigated and demonstrated the importance of the Nbr1-p62

interaction in the regulation of postnatal bone volume and bone mineral density. Analysis of genetic variation in *NBR1* in patients with idiopathic HBM also demonstrated that mutations in NBR1 are unlikely to be the cause of the observed phenotype.

Interest in Nbr1 biology has dramatically increased in the past few years and much work has focused on its role as an autophagic receptor. Further studies building on the data presented in this thesis will be instrumental in providing additional knowledge of Nbr1 function and may contribute to the identification of therapeutic targets for the treatment of bone and protein aggregation diseases.

Appendix

A.1. Positive clones from yeast-2-hybrid screen 1

Table A.1. illustrates additional positive clones identified in the yeast-2-hybrid screen carried out with amino acids 495-924 of Nbr1 as bait against a pretransformed 7 day old mouse calvaria cDNA library. These putative interactors include possible candidates that were not followed up in this study and likely false positives that are often identified in yeast-2-hybrid screens (Hengen, 1997). A number of muscle specific proteins were alos pulled out of this library screen suggesting that the calvarial library was contaminated with muscle.

Accession No.	Gene ID	No. of Colonies
NM_007507.2	ATPase, Ca++ transporting, cardiac muscle	1
NM_013593.2	Myoglobin	1
NM_00771.02	Creatine kinase, muscle	1
NM_009394.2	Troponin	3
NM_026775.4	Transmembrane enp24-like trafficking protein 10 (Tmp21)	1
NM_010227.2	Filamin α	1
NM_008509.2	Lipoprotein lipase	1
NM_181582	Eukaryotic translation initiation factor 5A	2
NM_007807.3	Cytochrome b-245, β-poltpeptide	1
NM_026644.2	1-acylglycerol-3-phosphate o-acyltransferase 4	1
NM_011305.3	Retinoid X receptor α	3
NM_025552.4	RNA polymerase II	1
NM_019704.2	Transmembrane protein 115	1
NM_001081654.1	Testis expression gene 264 variant 2	1
NM_012015.1	H2A histone family, member Y	3
NM_008218.1¥	Hemoglobin α, adult chain 1	8
NM_011184.3¥	Proteasome subunit, α type 3	3
NM_010240.2¥	Ferritin	2
NM_172946.2¥	Keratin 222	25
NM_025589.2¥ NM_022891.2¥ NM_009080.2¥ NM_029751.3¥	Ribosomal proteins	27

NM_013725.2¥		
NM_009606.2¥	Actin	8
NM_011756.4¥	Zinc finger protein 36	1
NM_009943.2¥	Cytochrome C oxidase	2
NM_008188.2	Procollagen C-endopeptidase enhancer protein	2
NM_007743.2¥	Procollagen, type 1, α2	6
NM_017476.2¥	Procollagen type 1, α1	8

Table A.1. Additional positive clones identified from the yeast-2-hybrid screen carried out in chapter 3. ¥ indicates likely false positives

A.2. Positive clones from yeast-2-hybrid screen 2

Table A.2. illustrates additional positive clones identified in the yeast-2-hybrid screen carried out with amino acids 346-498 of Nbr1(novel region) as bait against a pretransformed 7 day old mouse calvaria cDNA library. These putative interactors include possible candidates that were not followed up in this study and likely false positives that are often identified in yeast-2-hybrid screens (Hengen, 1997).

Accession No.	Gene ID	No. of Colonies
NM_182993.2	Solute carrier family 17	1
NT_039460	Solute carrier protein 25	1
NM_146259.3	Zinc Finger protein 668	3
NM_011747.2	Zinc finger protein 13	2
NM_007563.3	2, 3-bisphosphoglycerate mutase	1
NM_146169.2	Poly (A) binding protein interacting protein 2B	1
NM_011865.3	Poly (rC) binding protein 1	1
NM_010729.2	Lysyl oxidase-like 1	1
NM_010227.2	Filamin α	8
NM_009606.2¥	Actin α 1 (skeletal muscle)	5
NM_007742.3¥	Procollagen type 1 α 1	1
NM_007743.2¥	Procollagen type 1 α 2	3
NM_199008.2¥	Cox11 Homolog, cytochrome C oxidase assembly protein	11
NM_007743.2¥	Procollagen type 1 α 2	3

Table A.2. Additional positive clones identified from the yeast-2-hybrid screen carried out in Chapter 4. ¥ indicates likely false positives.

A.3. Vector Maps

A.3.1. pGEX2T

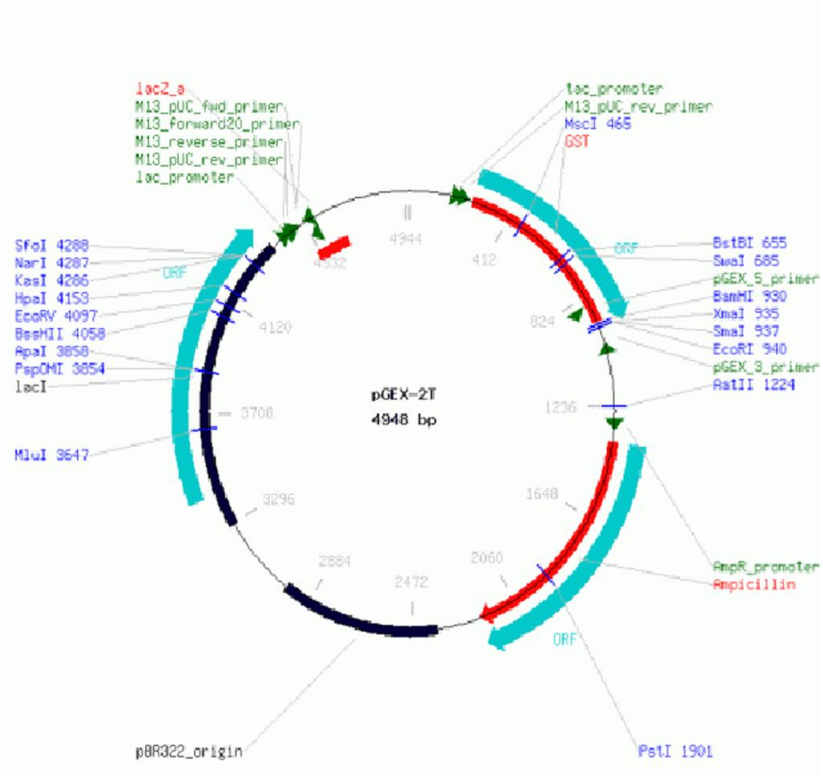

A.3.2. pGBKT7

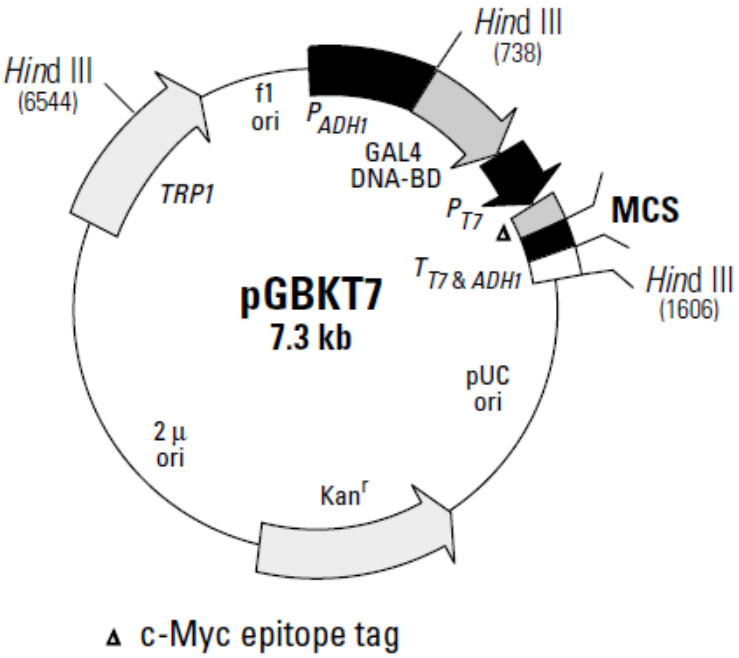

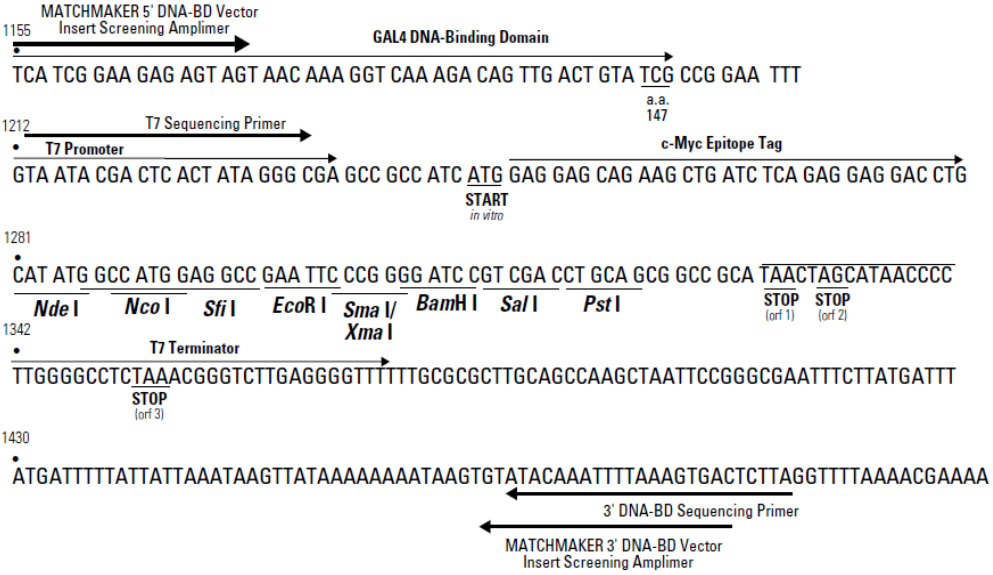
MATCHMAKER 5' DNA-BD Vector
Insert Screening Amplimer
1155
GAL4 DNA-Binding Domain
TCA TCG GAA GAG AGT AGT AAC AAA GGT CAA AGA CAG TTG ACT GTA TCG CCG GAA TTT
a.a.
147
1212
T7 Sequencing Primer
T7 Promoter
c-Myc Epitope Tag
GTA ATA CGA CTC ACT ATA GGG CGA GCC GCC ATC ATG GAG GAG CAG AAG CTG ATC TCA GAG GAG GAC CTG
START
in vitro
1281
CAT ATG GCC ATG GAG GCC GAA TTC CCG GGG ATC CGT CGA CCT GCA GCG GCC GCA TAACTAGCATAACCCC
Nde I
Nco I
Sfi I
EcoR I
Sma I/
Xma I
BamH I
Sal I
Pst I
STOP
(orf 1)
STOP
(orf 2)
1342
T7 Terminator
TTGGGGCCTCTAAACGGGTCTTGAGGGGTTTTTTGCGCGCTTGCAGCCAAGCTAATTCCGGGCGAATTTCTTATGATTT
STOP
(orf 3)
1430
ATGATTTTTATTATTAAATAAGTTATAAAAAAAATAAGTGTATACAAATTTTAAAGTGACTCTTAGGTTTTAAAACGAAAA
3' DNA-BD Sequencing Primer
MATCHMAKER 3' DNA-BD Vector
Insert Screening Amplimer

A.3.3. pHM6

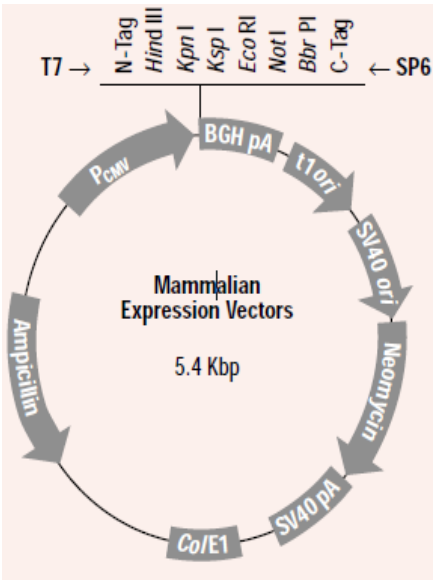
T7 →
N-Tag
Hind III
Kpn I
Ksp I
Eco RI
Not I
Bbr PI
C-Tag
← SP6
PCMV
BGH pA
f1 ori
SV40 ori
Neomycin
SV40 pA
ColE1
Ampicillin
Mammalian
Expression Vectors
5.4 Kbp

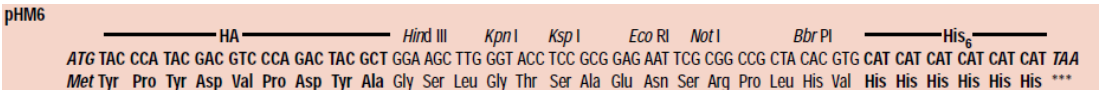
pHM6
HA
Hind III
Kpn I
Ksp I
Eco RI
Not I
Bbr PI
His6
ATG TAC CCA TAC GAC GTC CCA GAC TAC GCT GGA AGC TTG GGT ACC TCC GCG GAG AAT TCG CGG CCG CTA CAC GTG CAT CAT CAT CAT CAT CAT TAA
Met Tyr Pro Tyr Asp Val Pro Asp Tyr Ala Gly Ser Leu Gly Thr Ser Ala Glu Asn Ser Arg Pro Leu His Val His His His His His His ***

A.3.4. pcDNA3.1

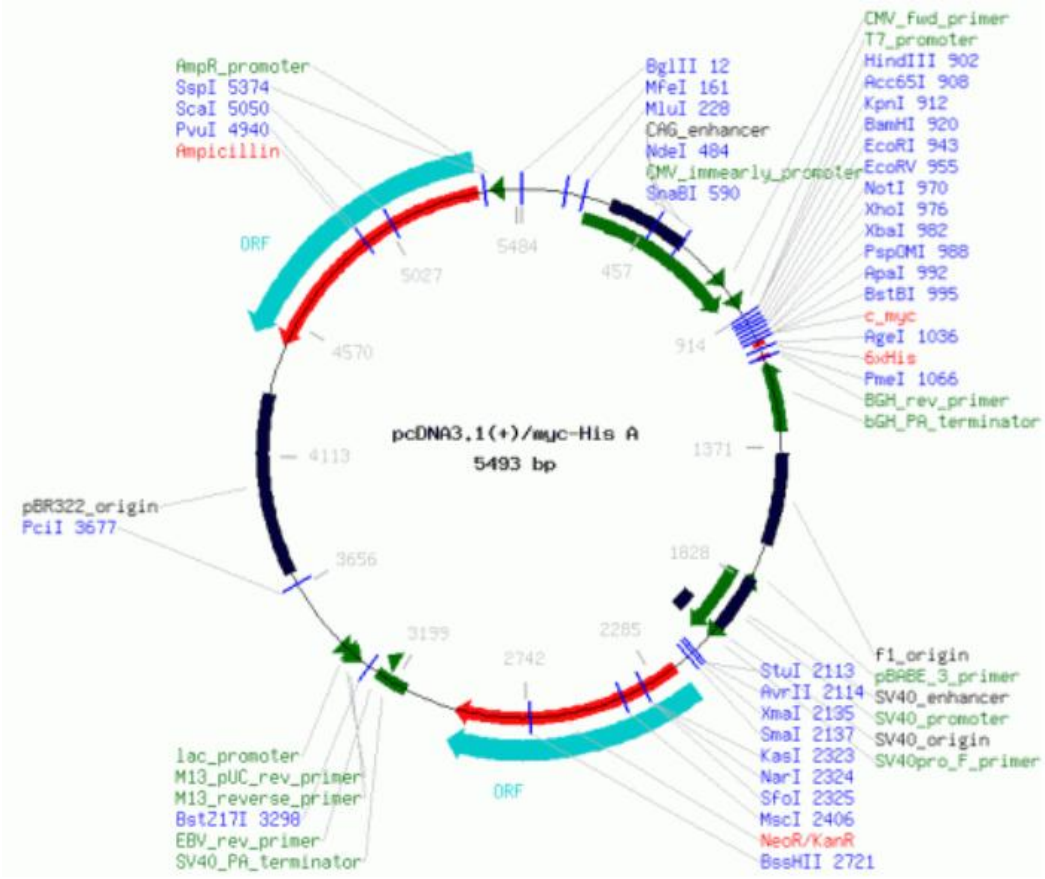
pcDNA3.1(+)/myc-His A
5493 bp
AmpR_promoter
SspI 5374
ScaI 5050
PvuI 4940
Ampicillin
ORF
BglII 12
MfeI 161
MluI 228
CAG_enhancer
NdeI 484
CMV_immearly_promoter
SnaBI 590
CMV_fwd_primer
T7_promoter
HindIII 902
Acc65I 908
KpnI 912
BamHI 920
EcoRI 943
EcoRV 955
NotI 970
XhoI 976
XbaI 982
PspOMI 988
ApaI 992
BstBI 995
c_myc
AgeI 1036
6xHis
PmeI 1066
BGH_rev_primer
bGH_PA_terminator
f1_origin
pBABE_3_primer
SV40_enhancer
SV40_promoter
SV40_origin
SV40pro_F_primer
StuI 2113
AvrII 2114
XmaI 2135
SmaI 2137
KasI 2323
NarI 2324
SfoI 2325
MscI 2406
NeoR/KanR
BssHII 2721
ORF
lac_promoter
M13_pUC_rev_primer
M13_reverse_primer
Bst217I 3298
EBV_rev_primer
SV40_PA_terminator
pBR322_origin
PciI 3677
5484
457
914
1371
1828
2285
2742
3199
3656
4113
4570
5027

Publications associated with this thesis

Waters S., **Marchbank K**., Solomon E., Whitehouse C., and Gautel M. (2009). Interactions with LC3 and polyubiquitin chains link Nbr1 to autophagic turnover. FEBS Lett. 583(12):1846-52.

Whitehouse CA, Waters S, **Marchbank K**, Horner A, McGowan NW, Jovanovic JV, Xavier GM, Kashima TG, Cobourne MT, Richards GO, Sharpe PT, Skerry TM, Grigoriadis AE, Solomon E. (2010). Neighbor of Brca1 gene (Nbr1) functions as a negative regulator of postnatal osteoblastic bone formation and p38 MAPK activity. PNAS. 107(29):12913-8.

Waters S., **Marchbank K**., Solomon E., Whitehouse CA. (2010) Autophagic receptors Nbr1 and p62 coregulate skeletal remodelling. Autophagy 6:7, 1-3.

References from figures:

(Fischer, 2011)

(Gilbert, 2000; Hartmann, 2009)

(Dijke, 2006)

(Suda et al., 1999)

(Carmona, 2004)

(Xie and Klionsky, 2007)

(Hill and Baehrecke, 2001)

(Wooten et al., 2006)

(Lange et al., 2006)

References

Albagha, O.M.E. (2011). Genome-wide association identifies three new susceptibility loci for Paget's disease of bone. Nat Genet *43*, 685-689.

Albagha, O.M.E., Visconti, M.R., Alonso, N., Langston, A.L., Cundy, T., Dargie, R., Dunlop, M.G., Fraser, W.D., Hooper, M.J., Isaia, G., *et al.* (2010). Genome-wide association study identifies variants at CSF1, OPTN and TNFRSF11A as genetic risk factors for Paget's disease of bone. Nat Genet *42*, 520-524.

Allen, E., Ding, J., Wang, W., Pramanik, S., Chou, J., Yau, V., and Yang, Y. (2005). Gigaxonin-controlled degradation of MAP1B light chain is critical to neuronal survival. Nature *438*, 224-228.

Alwan, H.A.J., and van Leeuwen, J.E.M. (2007). UBPY-mediated Epidermal Growth Factor Receptor (EGFR) De-ubiquitination Promotes EGFR Degradation. Journal of Biological Chemistry *282*, 1658-1669.

Ambrosetti, D., Holmes, G., Mansukhani, A., and Basilico, C. (2008). Fibroblast Growth Factor Signaling Uses Multiple Mechanisms To Inhibit Wnt-Induced Transcription in Osteoblasts. Mol Cell Biol *28*, 4759-4771.

Aplin, A., Jasionowski, T., Tuttle, D.L., Lenk, S.E., and Dunn, W.A. (1992). Cytoskeletal elements are required for the formation and maturation of autophagic vacuoles. Journal of Cellular Physiology *152*, 458-466.

Arnett, T.R., Gibbons, D.C., Utting, J.C., Orriss, I.R., Hoebertz, A., Rosendaal, M., and Meghji, S. (2003). Hypoxia is a major stimulator of osteoclast formation and bone resorption. Journal of Cellular Physiology *196*, 2-8.

Assmann, E.M., Alborghetti, M.R., Camargo, M.E.R., and Kobarg, J. (2006). FEZ1 Dimerization and Interaction with Transcription Regulatory Proteins Involves Its Coiled-coil Region. Journal of Biological Chemistry *281*, 9869-9881.

Axe, E.L., Walker, S.A., Manifava, M., Chandra, P., Roderick, H.L., Habermann, A., Griffiths, G., and Ktistakis, N.T. (2008). Autophagosome formation from membrane compartments enriched in phosphatidylinositol 3-phosphate and dynamically connected to the endoplasmic reticulum. The Journal of Cell Biology *182*, 685-701.

Azuma, Y., Kaji, K., Katogi, R., Takeshita, S., and Kudo, A. (2000). Tumor Necrosis Factor-α Induces Differentiation of and Bone Resorption by Osteoclasts. Journal of Biological Chemistry *275*, 4858-4864.

Babu, J.R., Geetha, T., and Wooten, M.W. (2005). Sequestosome 1/p62 shuttles polyubiquitinated tau for proteasomal degradation. Journal of Neurochemistry *94*, 192-203.

Badciong, J.C., and Haas, A.L. (2002). MdmX Is a RING Finger Ubiquitin Ligase Capable of Synergistically Enhancing Mdm2 Ubiquitination. Journal of Biological Chemistry *277*, 49668-49675.

Bain, G., Müller, T., Wang, X., and Papkoff, J. (2003). Activated [beta]-catenin induces osteoblast differentiation of C3H10T1/2 cells and participates in BMP2 mediated signal transduction. Biochemical and Biophysical Research Communications *301*, 84-91.

Balemans, W., Patel, N., Ebeling, M., Van Hul, E., Wuyts, W., Lacza, C., Dioszegi, M., Dikkers, F.G., Hildering, P., Willems, P.J., *et al.* (2002). Identification of a 52 kb deletion downstream of the SOST gene in patients with van Buchem disease. J Med Genet *39*, 91-97.

Beck, K., and Brodsky, B. (1998). Supercoiled Protein Motifs: The Collagen Triple-Helix and the [alpha]-Helical Coiled Coil. Journal of Structural Biology *122*, 17-29.

Behrends, C., Sowa, M.E., Gygi, S.P., and Harper, J.W. (2010). Network organization of the human autophagy system. Nature *466*, 68-76.

Bellot, G., Garcia-Medina, R., Gounon, P., Chiche, J., Roux, D., Pouyssegur, J., and Mazure, N.M. (2009). Hypoxia-Induced Autophagy Is Mediated through Hypoxia-Inducible Factor Induction of BNIP3 and BNIP3L via Their BH3 Domains. Mol Cell Biol *29*, 2570-2581.

Bennett, C.N., Ouyang, H., Ma, Y.L., Zeng, Q., Gerin, I., Sousa, K.M., Lane, T.F., Krishnan, V., Hankenson, K.D., and MacDougald, O.A. (2007). Wnt10b Increases Postnatal Bone Formation by Enhancing Osteoblast Differentiation. Journal of Bone and Mineral Research *22*, 1924-1932.

Berchtold, H., Reshetnikova, L., Reiser, C.O.A., Schirmer, N.K., Sprinzl, M., and Hilgenfeld, R. (1993). Crystal structure of active elongation factor Tu reveals major domain rearrangements. Nature *365*, 126-132.

Berke, S.J.S., and Paulson, H.L. (2003). Protein aggregation and the ubiquitin proteasome pathway: gaining the UPPer hand on neurodegeneration. Current Opinion in Genetics & Development *13*, 253-261.

Bilezikian, J.P., Raisz, L. G., Rodan, G. A. (2002). Principles of Bone Biology (Academic Press).

Bjørkøy, G., Lamark, T., and Johansen, T. (2006). p62/SQSTM1: A Missing Link between Protein Aggregates and the Autophagy Machinery. Autophagy *2*, 138-139.
Blair, H.C., Teitelbaum, S.L., Ghiselli, R., and Gluck, S. (1989). Osteoclastic bone resorption by a polarized vacuolar proton pump. Science *245*, 855-857.

Bloom, G.S., Luca, F.C., and Vallee, R.B. (1985). Microtubule-associated protein 1B: identification of a major component of the neuronal cytoskeleton. Proceedings of the National Academy of Sciences *82*, 5404-5408.

Bodine, P.V.N., Zhao, W., Kharode, Y.P., Bex, F.J., Lambert, A.-J., Goad, M.B., Gaur, T., Stein, G.S., Lian, J.B., and Komm, B.S. (2004). The Wnt Antagonist Secreted Frizzled-Related Protein-1 Is a Negative Regulator of Trabecular Bone Formation in Adult Mice. Molecular Endocrinology *18*, 1222-1237.

Bolland, M.J., Tong, P.C., Naot, D., Callon, K.E., Wattie, D.J., Gamble, G.D., and Cundy, T. (2007). Delayed Development of Paget's Disease in Offspring Inheriting SQSTM1 Mutations. Journal of Bone and Mineral Research *22*, 411-415.

Bomberger, J.M., Barnaby, R.L., and Stanton, B.A. (2009). The Deubiquitinating Enzyme USP10 Regulates the Post-endocytic Sorting of Cystic Fibrosis Transmembrane Conductance Regulator in Airway Epithelial Cells. Journal of Biological Chemistry *284*, 18778-18789.

Bonewald, L.F. (2011). The amazing osteocyte. Journal of Bone and Mineral Research *26*, 229-238.

Bouxsein, M.L., Boyd, S.K., Christiansen, B.A., Guldberg, R.E., Jepsen, K.J., and Müller, R. (2010). Guidelines for assessment of bone microstructure in rodents using micro–computed tomography. Journal of Bone and Mineral Research *25*, 1468-1486.

Bowman, E.J., Siebers, A., and Altendorf, K. (1988). Bafilomycins: a class of inhibitors of membrane ATPases from microorganisms, animal cells, and plant cells. Proceedings of the National Academy of Sciences *85*, 7972-7976.

Boyden, L.M., Mao, J., Belsky, J., Mitzner, L., Farhi, A., Mitnick, M.A., Wu, D., Insogna, K., and Lifton, R.P. (2002). High Bone Density Due to a Mutation in LDL-Receptor–Related Protein 5. New England Journal of Medicine *346*, 1513-1521.

Bozec, A., Bakiri, L., Hoebertz, A., Eferl, R., Schilling, A.F., Komnenovic, V., Scheuch, H., Priemel, M., Stewart, C.L., Amling, M., *et al.* (2008). Osteoclast size is controlled by Fra-2 through LIF/LIF-receptor signalling and hypoxia. Nature *454*, 221-225.

Brand, H.S., Lerner, U.H., Grubb, A., Beertsen, W., Nieuw Amerongen, A.V., and Everts, V. (2004). Family 2 cystatins inhibit osteoclast-mediated bone resorption in calvarial bone explants. Bone *35*, 689-696.

Brunkow, M.E., Gardner, J.C., Van Ness, J., Paeper, B.W., Kovacevich, B.R., Proll, S., Skonier, J.E., Zhao, L., Sabo, P.J., Fu, Y.-H., *et al.* (2001). Bone Dysplasia Sclerosteosis Results from Loss of the SOST Gene Product, a Novel Cystine Knot-Containing Protein. The American Journal of Human Genetics *68*, 577-589.

Buckwalter, J.A., Glimcher, M. J., Cooper, R. R., Recker R. (1995). Bone Biology Part I: Structure, Blood Supply, Cell Matrix and Mineralisation. The Journal of Bone and Joint Surgery *77*, 1256-1275.

Bundschu, K., Knobeloch, K.-P., Ullrich, M., Schinke, T., Amling, M., Engelhardt, C.M., Renné, T., Walter, U., and Schuh, K. (2005). Gene Disruption of Spred-2 Causes Dwarfism. Journal of Biological Chemistry *280*, 28572-28580.

Camozzi, V., Vescini, F., Luisetto, G., and Moro, L. (2010). Bone organic matrix components: their roles in skeletal physiology. J Endocrinol Invest *33*, 13-15.

Campbell, I.G., Nicolai, H.M., Foulkes, W.D., Senger, G., Stamp, G.W., Allan, G., Boyer, C., Jones, K., Bast, R.C., Jr., and Solomon, E. (1994). A novel gene encoding a B-box protein within the BRCA1 region at 17q21.1. Hum Mol Genet *3*, 589-594.

Canalis, E. (2009). Growth factor control of bone mass. Journal of Cellular Biochemistry *108*, 769-777.

Canalis, E., Economides, A.N., and Gazzerro, E. (2003). Bone Morphogenetic Proteins, Their Antagonists, and the Skeleton. Endocrine Reviews *24*, 218-235.

Candeliere, G.A., Rao, Y., Floh, A., Sandler, S.D., and Aubin, J.E. (1999). cDNA fingerprinting of osteoprogenitor cells to isolate differentiation stage-specific genes. Nucleic Acids Research *27*, 1079-1083.

Carmona, R.H. (2004). Chapter 2: The Basics of Bone in Health and Disease. In Bone Health and Osteoporosis: A Report of the Surgeon General.

Cavey, J., Ralston, S., Sheppard, P., Ciani, B., Gallagher, T., Long, J., Searle, M., and Layfield, R. (2006). Loss of Ubiquitin Binding Is a Unifying Mechanism by Which Mutations of <i>SQSTM1</i> Cause Paget's Disease of Bone. Calcified Tissue International *78*, 271-277.

Cavey, J.R., Ralston, S.H., Hocking, L.J., Sheppard, P.W., Ciani, B., Searle, M.S., and Layfield, R. (2005). Loss of Ubiquitin-Binding Associated With Paget's Disease of Bone p62 (SQSTM1) Mutations. Journal of Bone and Mineral Research *20*, 619-624.

Chambers, J.A., and Solomon, E. (1996). Isolation of the MurineNbr1Gene Adjacent to the MurineBrca1Gene. Genomics *38*, 305-313.

Chamoux, E., Couture, J., Bisson, M., Morissette, J., Brown, J.P., and Roux, S. (2009). The p62 P392L Mutation Linked to Paget's Disease Induces Activation of Human Osteoclasts. Molecular Endocrinology *23*, 1668-1680.

Chen, P., Evans, C.-L., Hirst, J.D., and Searle, M.S. (2010). Structural Insights into the Two Sequential Folding Transition States of the PB1 Domain of NBR1 from Φ Value Analysis and Biased Molecular Dynamics Simulations. Biochemistry *50*, 125-135.

Chen, Y., Whetstone, H.C., Youn, A., Nadesan, P., Chow, E.C.Y., Lin, A.C., and Alman, B.A. (2007). β-Catenin Signaling Pathway Is Crucial for Bone Morphogenetic Protein 2 to Induce New Bone Formation. Journal of Biological Chemistry *282*, 526-533.

Chuang, S.-M., Chen, L., Lambertson, D., Anand, M., Kinzy, T.G., and Madura, K. (2005). Proteasome-Mediated Degradation of Cotranslationally Damaged Proteins Involves Translation Elongation Factor 1A. Mol Cell Biol *25*, 403-413.

Chung, P., Beyens, G., Boonen, S., Papapoulos, S., Geusens, P., Karperien, M., Vanhoenacker, F., Verbruggen, L., Fransen, E., Van Offel, J., *et al.* (2010). The majority of the genetic risk for Paget's disease of bone is explained by genetic variants close to the <i>CSF1</i>, <i>OPTN</i>, <i>TM7SF4</i>, and <i>TNFRSF11A</i> genes. Human Genetics *128*, 615-626.

Clausen, T.H., Lamark, T., Isakson, P., Finley, K.D., Larsen, K.B., Brech, A., Øvervatn, A., Stenmark, H., Bjørkøy, G., Simonsen, A., *et al.* (2010). p62/SQSTM1 and ALFY interact to facilitate the formation of p62 bodies/ALIS and their degradation by autophagy. Autophagy *6*, 330-344.

Coffin, J.D., Florkiewicz, R.Z., Neumann, J., Mort-Hopkins, T., Dorn, G.W., Lightfoot, P., German, R., Howles, P.N., Kier, A., and O'Toole, B.A. (1995). Abnormal bone growth and selective translational regulation in basic fibroblast growth factor (FGF-2) transgenic mice. Molecular Biology of the Cell *6*, 1861-1873.

Coxon, F.P., and Taylor, A. (2008). Vesicular trafficking in osteoclasts. Seminars in Cell & Developmental Biology *19*, 424-433.

Cuervo, A.M., and Dice, J.F. (2000). Age-Related Decline in Chaperone-Mediated Autophagy. J Biol Chem, M002102200.

Danjo, A., Yamaza, T., Kido, M.A., Shimohira, D., Tsukuba, T., Kagiya, T., Yamashita, Y., Nishijima, K., Masuko, S., Goto, M., *et al.* (2007). Cystatin C stimulates the differentiation of mouse osteoblastic cells and bone formation. Biochemical and Biophysical Research Communications *360*, 199-204.

Darnay, B.G., Haridas, V., Ni, J., Moore, P.A., and Aggarwal, B.B. (1998). Characterization of the Intracellular Domain of Receptor Activator of NF-κB (RANK). Journal of Biological Chemistry *273*, 20551-20555.

Daroszewska, A., van 't Hof, R.J., Rojas, J.A., Layfield, R., Landao-Basonga, E., Rose, L., Rose, K., and Ralston, S.H. (2011). A point mutation in the ubiquitin-associated domain of SQSMT1 is sufficient to cause a Paget's disease-like disorder in mice. Human Molecular Genetics *20*, 2734-2744.

Davidkova, G., and Carroll, R.C. (2007). Characterization of the Role of Microtubule-Associated Protein 1B in Metabotropic Glutamate Receptor-Mediated Endocytosis of AMPA Receptors in Hippocampus. The Journal of Neuroscience *27*, 13273-13278.

de Crombrugghe, B., Lefebvre, V., and Nakashima, K. (2001). Regulatory mechanisms in the pathways of cartilage and bone formation. Current Opinion in Cell Biology *13*, 721-728.

de Vernejoul, M.-C., and Kornak, U. (2010). Heritable sclerosing bone disorders. Annals of the New York Academy of Sciences *1192*, 269-277.

Deng, C., Wynshaw-Boris, A., Zhou, F., Kuo, A., and Leder, P. (1996). Fibroblast Growth Factor Receptor 3 Is a Negative Regulator of Bone Growth. Cell *84*, 911-921.

Devlin, R.D., Du, Z., Pereira, R.C., Kimble, R.B., Economides, A.N., Jorgetti, V., and Canalis, E. (2003). Skeletal Overexpression of Noggin Results in Osteopenia and Reduced Bone Formation. Endocrinology *144*, 1972-1978.

Diamond, T., Smith, A., Schnier, R., and Manoharan, A. (2002). Syndrome of myelofibrosis and osteosclerosis: a series of case reports and review of the literature. Bone *30*, 498-501.

Dijke, P.t. (2006). Bone morphogenetic protein signal transduction in bone. Current Medical Research and Opinion *22*, S7-S11.

Dikic, I., Wakatsuki, S., and Walters, K.J. (2009). Ubiquitin-binding domains [mdash] from structures to functions. Nat Rev Mol Cell Biol *10*, 659-671.

Dimitrov, S., Brennerova, M., and Forejt, J. (2001). Expression profiles and intergenic structure of head-to-head oriented Brca1 and Nbr1 genes. Gene *262*, 89-98.

Ducy, P., Desbois, C., Boyce, B., Pinero, G., Story, B., Dunstan, C., Smith, E., Bonadio, J., Goldstein, S., Gundberg, C., *et al.* (1996). Increased bone formation in osteocalcin-deficient mice. Nature *382*, 448-452.

Ducy, P., Zhang, R., Geoffroy, V., Ridall, A.L., and Karsenty, G. (1997). Osf2/Cbfa1: a transcriptional activator of osteoblast differentiation. Cell *89*, 747-754.

Duncan, E.L., Danoy, P., Kemp, J.P., Leo, P.J., McCloskey, E., Nicholson, G.C., Eastell, R., Prince, R.L., Eisman, J.A., Jones, G., *et al.* (2011). Genome-Wide Association Study Using Extreme Truncate Selection Identifies Novel Genes Affecting Bone Mineral Density and Fracture Risk. PLoS Genet *7*, e1001372.

Duran, A., Serrano, M., Leitges, M., Flores, J.M., Picard, S., Brown, J.P., Moscat, J., and Diaz-Meco, M.T. (2004). The atypical PKC-interacting protein p62 is an important mediator of RANK-activated osteoclastogenesis. Dev Cell *6*, 303-309.
Edwards, J.R., and Mundy, G.R. (2011). Advances in osteoclast biology: old findings and new insights from mouse models. Nat Rev Rheumatol *7*, 235-243.

Ehrlich, L.A., and Roodman, G.D. (2005). The role of immune cells and inflammatory cytokines in Paget's disease and multiple myeloma. Immunological Reviews *208*, 252-266.

Eisenberg-Lerner, A., Bialik, S., Simon, H.U., and Kimchi, A. (2009). Life and death partners: apoptosis, autophagy and the cross-talk between them. Cell Death Differ *16*, 966-975.

Ejersted, C., Andreassen, T.T., Hauge, E.M., Melsen, F., and Oxlund, H. (1995). Parathyroid hormone (1-34) increases vertebral bone mass, compressive strength, and quality in old rats. Bone *17*, 507-511.

Emons, J., Chagin, A.S., Sävendahl, L., Karperien, M., and Wit, J.M. (2011). Mechanisms of Growth Plate Maturation and Epiphyseal Fusion. Hormone Research in Paediatrics *75*, 383-391.

Eriksen, E. (2010). Cellular mechanisms of bone remodeling. Reviews in Endocrine & Metabolic Disorders *11*, 219-227.

Everts, V., Delaissé, J.M., Korper, W., Jansen, D.C., Tigchelaar-Gutter, W., Saftig, P., and Beertsen, W. (2002). The Bone Lining Cell: Its Role in Cleaning Howship's Lacunae and Initiating Bone Formation. Journal of Bone and Mineral Research *17*, 77-90.

Faccio, R., Takeshita, S., Zallone, A., Ross, F.P., and Teitelbaum, S.L. (2003). c-Fms and the alphavbeta3 integrin collaborate during osteoclast differentiation. J Clin Invest *111*, 749-758.

Falchetti, A., Di Stefano, M., Marini, F., Ortolani, S., Ulivieri, M., Bergui, S., Masi, L., Cepollaro, C., Benucci, M., Di Munno, O., *et al.* (2009). Genetic Epidemiology of Paget's Disease of Bone in Italy: s<i>equestosome1/p62</i> Gene Mutational Test and Haplotype Analysis at 5q35 in a Large Representative Series of Sporadic and Familial Italian Cases of Paget's Disease of Bone. Calcified Tissue International *84*, 20-37.

Falchetti, A., Masi, L., and Brandi, M.L. (2010). Paget's disease of bone: there's more than the affected skeletal--a clinical review and suggestions for the clinical practice. Curr Opin Rheumatol *22*, 410-423.

Faller, E.M., Villeneuve, T.S., and Brown, D.L. (2009). MAP1a associated light chain 3 increases microtubule stability by suppressing microtubule dynamics. Molecular and Cellular Neuroscience *41*, 85-93.

Fass, E., Shvets, E., Degani, I., Hirschberg, K., and Elazar, Z. (2006). Microtubules Support Production of Starvation-induced Autophagosomes but Not Their Targeting and Fusion with Lysosomes. Journal of Biological Chemistry *281*, 36303-36316.

Feldkamp, L.A., Goldstein, S.A., Parfitt, M.A., Jesion, G., and Kleerekoper, M. (1989). The direct examination of three-dimensional bone architecture in vitro by computed tomography. Journal of Bone and Mineral Research *4*, 3-11.

Feng, J.Q., Ward, L.M., Liu, S., Lu, Y., Xie, Y., Yuan, B., Yu, X., Rauch, F., Davis, S.I., Zhang, S., *et al.* (2006). Loss of DMP1 causes rickets and osteomalacia and identifies a role for osteocytes in mineral metabolism. Nat Genet *38*, 1310-1315.

Feng, X., and McDonald, J.M. (2011). Disorders of Bone Remodeling. Annual Review of Pathology: Mechanisms of Disease *6*, 121-145.

Ferrell, K., Wilkinson, C.R.M., Dubiel, W., and Gordon, C. (2000). Regulatory subunit interactions of the 26S proteasome, a complex problem. Trends in Biochemical Sciences *25*, 83-88.

Fields, S., and Song, O.-k. (1989). A novel genetic system to detect protein–protein interactions. Nature *340*, 245-246.

Fischer, T.G. (2011). Anatomy and Physiology I.

Flinn, R.J., Yan, Y., Goswami, S., Parker, P.J., and Backer, J.M. (2010). The Late Endosome is Essential for mTORC1 Signaling. Mol Biol Cell *21*, 833-841.

Franz-Odendaal, T.A. (2011). Induction and patterning of intramembranous bone. Front Biosci *17*, 3734-3746.

Franz-Odendaal, T.A., Hall, B.K., and Witten, P.E. (2006). Buried alive: How osteoblasts become osteocytes. Developmental Dynamics *235*, 176-190.

Freemont, P.S. (2000). Ubiquitination: RING for destruction? Current Biology *10*, R84-R87.

Frost, H.M. (1969). Tetracycline-based histological analysis of bone remodeling. Calcified Tissue International *3*, 211-237.

Fujita, T., Maturana, A.D., Ikuta, J., Hamada, J., Walchli, S., Suzuki, T., Sawa, H., Wooten, M.W., Okajima, T., Tatematsu, K., *et al.* (2007). Axonal guidance protein FEZ1 associates with tubulin and kinesin motor protein to transport mitochondria in neurites of NGF-stimulated PC12 cells. Biochemical and Biophysical Research Communications *361*, 605-610.

Gareau, J.R., and Lima, C.D. (2010). The SUMO pathway: emerging mechanisms that shape specificity, conjugation and recognition. Nat Rev Mol Cell Biol *11*, 861-871.

Garner, T.P., Long, J., Layfield, R., and Searle, M.S. (2011). Impact of p62/SQSTM1 UBA Domain Mutations Linked to Paget's Disease of Bone on Ubiquitin Recognition. Biochemistry *50*, 4665-4674.

Gaur, T., Lengner, C.J., Hovhannisyan, H., Bhat, R.A., Bodine, P.V.N., Komm, B.S., Javed, A., van Wijnen, A.J., Stein, J.L., Stein, G.S., *et al.* (2005). Canonical WNT Signaling Promotes Osteogenesis by Directly Stimulating Runx2 Gene Expression. Journal of Biological Chemistry *280*, 33132-33140.

Geeraert, C., Ratier, A., Pfisterer, S.G., Perdiz, D., Cantaloube, I., Rouault, A., Pattingre, S., Proikas-Cezanne, T., Codogno, P., and Poüs, C. (2010). Starvation-induced Hyperacetylation of Tubulin Is Required for the Stimulation of Autophagy by Nutrient Deprivation. Journal of Biological Chemistry *285*, 24184-24194.

Geetha, T., Seibenhener, M.L., Chen, L., Madura, K., and Wooten, M.W. (2008). p62 serves as a shuttling factor for TrkA interaction with the proteasome. Biochemical and Biophysical Research Communications *374*, 33-37.

Gelb, B.D., Shi, G.-P., Chapman, H.A., and Desnick, R.J. (1996). Pycnodysostosis, a Lysosomal Disease Caused by Cathepsin K Deficiency. Science *273*, 1236-1238.

Genevieve, D., Proulle, V., Isidor, B., Bellais, S., Serre, V., Djouadi, F., Picard, C., Vignon-Savoye, C., Bader-Meunier, B., Blanche, S., *et al.* (2008). Thromboxane synthase mutations in an increased bone density disorder (Ghosal syndrome). Nat Genet *40*, 284-286.

Gilbert, S.F. (2000). Developmental Biology, 6 edn.

Giuliani, N., Morandi, F., Tagliaferri, S., Lazzaretti, M., Bonomini, S., Crugnola, M., Mancini, C., Martella, E., Ferrari, L., Tabilio, A., *et al.* (2007). The proteasome inhibitor bortezomib affects osteoblast differentiation in vitro and in vivo in multiple myeloma patients. Blood *110*, 334-338.

Glass Ii, D.A., and Karsenty, G. (2006). Molecular Bases of the Regulation of Bone Remodeling by the Canonical Wnt Signaling Pathway. In Current Topics in Developmental Biology, P.S. Gerald, ed. (Academic Press), pp. 43-84.

Glazov, E.A., Zankl, A., Donskoi, M., Kenna, T.J., Thomas, G.P., Clark, G.R., Duncan, E.L., and Brown, M.A. (2011). Whole-Exome Re-Sequencing in a Family Quartet Identifies <italic>POP1</italic> Mutations As the Cause of a Novel Skeletal Dysplasia. PLoS Genet *7*, e1002027.

Gonen, H., Dickman, D., Schwartz, A.L., and Ciechanover, A. (1996). Protein synthesis elongation factor EF-1 alpha is an isopeptidase essential for ubiquitin-dependent degradation of certain proteolytic substrates. Adv Exp Med Biol *389*, 209-219.

Gong, Y., Slee, R.B., Fukai, N., Rawadi, G., Roman-Roman, S., Reginato, A.M., Wang, H., Cundy, T., Glorieux, F.H., Lev, D., *et al.* (2001). LDL Receptor-Related Protein 5 (LRP5) Affects Bone Accrual and Eye Development. Cell *107*, 513-523.

Gonzalez-Billault, C., Avila, J., and Caceres, A. (2001). Evidence for the Role of MAP1B in Axon Formation. Mol Biol Cell *12*, 2087-2098.

Goode, A., and Layfield, R. (2010). Recent advances in understanding the molecular basis of Paget disease of bone. Journal of Clinical Pathology *63*, 199-203.

Gori, F., Hofbauer, L.C., Dunstan, C.R., Spelsberg, T.C., Khosla, S., and Riggs, B.L. (2000). The Expression of Osteoprotegerin and RANK Ligand and the Support of Osteoclast Formation by Stromal-Osteoblast Lineage Cells Is Developmentally Regulated. Endocrinology *141*, 4768-4776.

Gregson, C., Steel, S., O'Rourke, K., Allan, K., Ayuk, J., Bhalla, A., Clunie, G., Crabtree, N., Fogelman, I., Goodby, A., *et al.* (2011). 'Sink or swim': an evaluation

of the clinical characteristics of individuals with high bone mass. Osteoporosis International, 1-12.

Grigoriadis, A., Wang, Z., Cecchini, M., Hofstetter, W., Felix, R., Fleisch, H., and Wagner, E. (1994). c-Fos: a key regulator of osteoclast-macrophage lineage determination and bone remodeling. Science *266*, 443-448.

Guicheux, J., Lemonnier, J., Ghayor, C., Suzuki, A., Palmer, G., and Caverzasio, J. (2003). Activation of p38 Mitogen-Activated Protein Kinase and c-Jun-NH2-Terminal Kinase by BMP-2 and Their Implication in the Stimulation of Osteoblastic Cell Differentiation. Journal of Bone and Mineral Research *18*, 2060-2068.

Gundberg, C.M., and Clough, M.E. (1992a). The osteocalcin propeptide is not secreted in vivo or in vitro. J Bone Miner Res *7*, 73-80.

Gundberg, C.M., and Clough, M.E. (1992b). The osteocalcin propeptide is not secreted in vivo or in vitro. Journal of Bone and Mineral Research *7*, 73-80.

Günther, T., and Schinke, T. (2000). Mouse Genetics Have Uncovered New Paradigms in Bone Biology. Trends in Endocrinology and Metabolism *11*, 189-193.
Hadjidakis, D.J., and Androulakis, I.I. (2006). Bone Remodeling. Annals of the New York Academy of Sciences *1092*, 385-396.

Haglund, K., Di Fiore, P.P., and Dikic, I. (2003). Distinct monoubiquitin signals in receptor endocytosis. Trends in Biochemical Sciences *28*, 598-604.

Hammarback, J.A., Obar, R.A., Hughes, S.M., and Vallee, R.B. (1991). MAP1B is encoded as a polyprotein that is processed to form a complex N-terminal microtubule-binding domain. Neuron *7*, 129-139.

Harada, S.-i., and Rodan, G.A. (2003). Control of osteoblast function and regulation of bone mass. Nature *423*, 349-355.

Hargus, G., Kist, R., Kramer, J., Gerstel, D., Neitz, A., Scherer, G., and Rohwedel, J. (2008). Loss of Sox9 function results in defective chondrocyte differentiation of mouse embryonic stem cells in vitro. Int J Dev Biol *52*, 323-332.

Hartmann, C. (2009). Transcriptional networks controlling skeletal development. Current Opinion in Genetics & Development *19*, 437-443.

Hauge, E.M., Qvesel, D., Eriksen, E.F., Mosekilde, L., and Melsen, F. (2001). Cancellous Bone Remodeling Occurs in Specialized Compartments Lined by Cells Expressing Osteoblastic Markers. Journal of Bone and Mineral Research *16*, 1575-1582.

He, C., and Klionsky, D.J. (2009). Regulation Mechanisms and Signaling Pathways of Autophagy. Annual Review of Genetics *43*, 67-93.

He, H., Dang, Y., Dai, F., Guo, Z., Wu, J., She, X., Pei, Y., Chen, Y., Ling, W., Wu, C., *et al.* (2003). Post-translational Modifications of Three Members of the Human

MAP1LC3 Family and Detection of a Novel Type of Modification for MAP1LC3B. Journal of Biological Chemistry *278*, 29278-29287.

Hedgecock, N.L., Hadi, T., Chen, A.A., Curtiss, S.B., Martin, R.B., and Hazelwood, S.J. (2007). Quantitative regional associations between remodeling, modeling, and osteocyte apoptosis and density in rabbit tibial midshafts. Bone *40*, 627-637.

Heineke, J., Auger-Messier, M., Correll, R.N., Xu, J., Benard, M.J., Yuan, W., Drexler, H., Parise, L.V., and Molkentin, J.D. (2010). CIB1 is a regulator of pathological cardiac hypertrophy. Nat Med *16*, 872-879.

Helfrich, M.H., Hobson, R.P., Grabowski, P.S., Zurbriggen, A., Cosby, S.L., Dickson, G.R., Fraser, W.D., Ooi, C.G., Selby, P.L., Crisp, A.J., *et al.* (2000). A Negative Search for a Paramyxoviral Etiology of Paget's Disease of Bone: Molecular, Immunological, and Ultrastructural Studies in U.K. Patients. Journal of Bone and Mineral Research *15*, 2315-2329.

Helfrich, M.H., and Hocking, L.J. (2008). Genetics and aetiology of Pagetic disorders of bone. Archives of Biochemistry and Biophysics *473*, 172-182.

Hengen, P.H. (1997). Methods and reagents : False positives from the yeast two-hybrid system. Trends in Biochemical Sciences *22*, 33-34.

Hicke, L. (2001). Protein regulation by monoubiquitin. Nat Rev Mol Cell Biol *2*, 195-201.

Hill, J.H., and Baehrecke, E.H. (2001). Autophagy in Nonmammalian Systems. In eLS (John Wiley & Sons, Ltd).

Hiruma, Y., Kurihara, N., Subler, M.A., Zhou, H., Boykin, C.S., Zhang, H., Ishizuka, S., Dempster, D.W., Roodman, G.D., and Windle, J.J. (2008). A SQSTM1/p62 mutation linked to Paget’s disease increases the osteoclastogenic potential of the bone microenvironment. Human Molecular Genetics *17*, 3708-3719.

Hocking, L.J., Herbert, C.A., Nicholls, R.K., Williams, F., Bennett, S.T., Cundy, T., Nicholson, G.C., Wuyts, W., Van Hul, W., and Ralston, S.H. (2001). Genomewide Search in Familial Paget Disease of Bone Shows Evidence of Genetic Heterogeneity with Candidate Loci on Chromosomes 2q36, 10p13, and 5q35. The American Journal of Human Genetics *69*, 1055-1061.

Hocking, L.J., Lucas, G.J.A., Daroszewska, A., Mangion, J., Olavesen, M., Cundy, T., Nicholson, G.C., Ward, L., Bennett, S.T., Wuyts, W., *et al.* (2002). Domain-specific mutations in sequestosome 1 (SQSTM1) cause familial and sporadic Paget's disease. Human Molecular Genetics *11*, 2735-2739.

Hocking, L.J., Mellis, D.J., McCabe, P.S., Helfrich, M.H., and Rogers, M.J. (2010). Functional interaction between Sequestosome-1/p62 and Autophagy-Linked FYVE-containing protein WDFY3 in human osteoclasts. Biochemical and Biophysical Research Communications *402*, 543-548.

Hodgkinson, C.A., Moore, K.J., Nakayama, A., Steingrímsson, E., Copeland, N.G., Jenkins, N.A., and Arnheiter, H. (1993). Mutations at the mouse microphthalmia locus are associated with defects in a gene encoding a novel basic-helix-loop-helix-zipper protein. Cell *74*, 395-404.

Hoff, A.O., Catala-Lehnen, P., Thomas, P.M., Priemel, M., Rueger, J.M., Nasonkin, I., Bradley, A., Hughes, M.R., Ordonez, N., Cote, G.J., *et al.* (2002). Increased bone mass is an unexpected phenotype associated with deletion of the calcitonin gene. The Journal of Clinical Investigation *110*, 1849-1857.

Hofmann, K., and Bucher, P. (1996). The UBA domain: a sequence motif present in multiple enzyme classes of the ubiquitination pathway. Trends in Biochemical Sciences *21*, 172-173.

Hojo, H., Ohba, S., Yano, F., and Chung, U.-i. (2010). Coordination of chondrogenesis and osteogenesis by hypertrophic chondrocytes in endochondral bone development. Journal of Bone and Mineral Metabolism *28*, 489-502.

Hosokawa, N., Hara, T., Kaizuka, T., Kishi, C., Takamura, A., Miura, Y., Iemura, S.-i., Natsume, T., Takehana, K., Yamada, N., *et al.* (2009a). Nutrient-dependent mTORC1 Association with the ULK1-Atg13-FIP200 Complex Required for Autophagy. Mol Biol Cell *20*, 1981-1991.

Hosokawa, N., Sasaki, T., Iemura, S.-i., Natsume, T., Hara, T., and Mizushima, N. (2009b). Atg101, a novel mammalian autophagy protein interacting with Atg13. Autophagy *5*, 973-979.

Hu, H., Hilton, M.J., Tu, X., Yu, K., Ornitz, D.M., and Long, F. (2005). Sequential roles of Hedgehog and Wnt signaling in osteoblast development. Development *132*, 49-60.

Huang, C., Andres, A.M., Ratliff, E.P., Hernandez, G., Lee, P., and Gottlieb, R.A. (2011). Preconditioning Involves Selective Mitophagy Mediated by Parkin and p62/SQSTM1. PLoS ONE *6*, e20975.

Hughes, A.E., Ralston, S.H., Marken, J., Bell, C., MacPherson, H., Wallace, R.G., van Hul, W., Whyte, M.P., Nakatsuka, K., Hovy, L., *et al.* (2000). Mutations in TNFRSF11A, affecting the signal peptide of RANK, cause familial expansile osteolysis. Nat Genet *24*, 45-48.

Ichimura, Y., Kumanomidou, T., Sou, Y.-s., Mizushima, T., Ezaki, J., Ueno, T., Kominami, E., Yamane, T., Tanaka, K., and Komatsu, M. (2008). Structural Basis for Sorting Mechanism of p62 in Selective Autophagy. Journal of Biological Chemistry *283*, 22847-22857.

Iotsova, V., Caamano, J., Loy, J., Yang, Y., Lewin, A., and Bravo, R. (1997). Osteopetrosis in mice lacking NF-[kappa]B1 and NF-[kappa]B2. Nat Med *3*, 1285-1289.

Ishida, Y., Yamamoto, A., Kitamura, A., Lamande, S.R., Yoshimori, T., Bateman, J.F., Kubota, H., and Nagata, K. (2009). Autophagic Elimination of Misfolded Procollagen Aggregates in the Endoplasmic Reticulum as a Means of Cell Protection. Mol Biol Cell *20*, 2744-2754.

Itakura, E., and Mizushima, N. (2010). Characterization of autophagosome formation site by a hierarchical analysis of mammalian Atg proteins. Autophagy *6*, 764-776.
Itakura, E., and Mizushima, N. (2011). p62 targeting to the autophagosome formation site requires self-oligomerization but not LC3 binding. The Journal of Cell Biology *192*, 17-27.

Ito, T., Matsui, Y., Ago, T., Ota, K., and Sumimoto, H. (2001). Novel modular domain PB1 recognizes PC motif to mediate functional protein-protein interactions. EMBO J *20*, 3938-3946.

Iwata, A., Riley, B.E., Johnston, J.A., and Kopito, R.R. (2005). HDAC6 and Microtubules Are Required for Autophagic Degradation of Aggregated Huntingtin. Journal of Biological Chemistry *280*, 40282-40292.

Jahreiss, L., Menzies, F.M., and Rubinsztein, D.C. (2008). The Itinerary of Autophagosomes: From Peripheral Formation to Kiss-and-Run Fusion with Lysosomes. Traffic *9*, 574-587.

Janssens, K., Gershoni-Baruch, R., Guanabens, N., Migone, N., Ralston, S., Bonduelle, M., Lissens, W., Van Maldergem, L., Vanhoenacker, F., Verbruggen, L., *et al.* (2000). Mutations in the gene encoding the latency-associated peptide of TGF-[beta]1 cause Camurati-Engelmann disease. Nat Genet *26*, 273-275.

Janssens, K., and Van Hul, W. (2002). Molecular genetics of too much bone. Hum Mol Genet *11*, 2385-2393.

Jean-Michel, D. (2002). The saga of the discovery of IL-1 and TNF and their specific inhibitors in the pathogenesis and treatment of rheumatoid arthritis. Joint Bone Spine *69*, 123-132.

Jensen, P.H., Islam, K., Kenney, J., Nielsen, M.S., Power, J., and Gai, W.P. (2000). Microtubule-associated Protein 1B Is a Component of Cortical Lewy Bodies and Binds α-Synuclein Filaments. Journal of Biological Chemistry *275*, 21500-21507.
Jentsch, S. (1992). The Ubiquitin-Conjugation System. Annual Review of Genetics *26*, 179-207.

Jimi, E., Akiyama, S., Tsurukai, T., Okahashi, N., Kobayashi, K., Udagawa, N., Nishihara, T., Takahashi, N., and Suda, T. (1999a). Osteoclast Differentiation Factor Acts as a Multifunctional Regulator in Murine Osteoclast Differentiation and Function. The Journal of Immunology *163*, 434-442.

Jimi, E., Nakamura, I., Duong, L.T., Ikebe, T., Takahashi, N., Rodan, G.A., and Suda, T. (1999b). Interleukin 1 Induces Multinucleation and Bone-Resorbing Activity of Osteoclasts in the Absence of Osteoblasts/Stromal Cells. Experimental Cell Research *247*, 84-93.

Jin, W., Chang, M., Paul, E.M., Babu, G., Lee, A.J., Reiley, W., Wright, A., Zhang, M., You, J., and Sun, S.-C. (2008). Deubiquitinating enzyme CYLD negatively regulates RANK signaling and osteoclastogenesis in mice. The Journal of Clinical Investigation *118*, 1858-1866.

Joazeiro, C.A.P., and Weissman, A.M. (2000). RING Finger Proteins: Mediators of Ubiquitin Ligase Activity. Cell *102*, 549-552.

Jochum, W., David, J.-P., Elliott, C., Wutz, A., Plenk, H., Matsuo, K., and Wagner, E.F. (2000). Increased bone formation and osteosclerosis in mice overexpressing the transcription factor Fra-1. Nat Med *6*, 980-984.

Johansen, T., and Lamark, T. (2011). Selective autophagy mediated by autophagic adapter proteins. Autophagy *7*, 279-296.

Joung, I., Strominger, J.L., and Shin, J. (1996). Molecular cloning of a phosphotyrosine-independent ligand of the p56lck SH2 domain. Proceedings of the National Academy of Sciences *93*, 5991-5995.

Ju, J.-S., Fuentealba, R.A., Miller, S.E., Jackson, E., Piwnica-Worms, D., Baloh, R.H., and Weihl, C.C. (2009). Valosin-containing protein (VCP) is required for autophagy and is disrupted in VCP disease. The Journal of Cell Biology *187*, 875-888.

Ju, J.-S., Miller, S.E., Hanson, P.I., and Weihl, C.C. (2008). Impaired Protein Aggregate Handling and Clearance Underlie the Pathogenesis of p97/VCP-associated Disease. Journal of Biological Chemistry *283*, 30289-30299.

Ju, J.-S., and Weihl, C.C. (2010). Inclusion body myopathy, Paget's disease of the bone and fronto-temporal dementia: a disorder of autophagy. Human Molecular Genetics *19*, R38-R45.

Kabeya, T.M., N. Ueno, T. Yamamoto, A. Kirisako, T. Noda, T. Kominami, E. Ohsumi, Y. Yoshimoro, T. (2000). LC3, a mammalian homologue of yeast Apg8p, is localised in autophagosome membranes after processing. Embo J *19*, 5720-5728.

Kabeya, Y., Mizushima, N., Ueno, T., Yamamoto, A., Kirisako, T., Noda, T., Kominami, E., Ohsumi, Y., and Yoshimori, T. (2000). LC3, a mammalian homologue of yeast Apg8p, is localized in autophagosome membranes after processing. EMBO J *19*, 5720-5728.

Kabeya, Y., Mizushima, N., Yamamoto, A., Oshitani-Okamoto, S., Ohsumi, Y., and Yoshimori, T. (2004). LC3, GABARAP and GATE16 localize to autophagosomal membrane depending on form-II formation. Journal of Cell Science *117*, 2805-2812.
Kamioka, H., Sugawara, Y., Honjo, T., Yamashiro, T., and Takano-Yamamoto, T. (2004). Terminal differentiation of osteoblasts to osteocytes is accompanied by dramatic changes in the distribution of actin-binding proteins. J Bone Miner Res *19*, 471-478.

Karsenty, G. (1999). The genetic transformation of bone biology. Genes Dev *13*, 3037-3051.

Karsenty, G., and Wagner, E.F. (2002). Reaching a Genetic and Molecular Understanding of Skeletal Development. Developmental Cell *2*, 389-406.

Katagiri, T., and Takahashi, N. (2002). Regulatory mechanisms of osteoblast and osteoclast differentiation. Oral Diseases *8*, 147-159.

Katagiri, T., Yamaguchi, A., Komaki, M., Abe, E., Takahashi, N., Ikeda, T., Rosen, V., Wozney, J.M., Fujisawa-Sehara, A., and Suda, T. (1994). Bone morphogenetic protein-2 converts the differentiation pathway of C2C12 myoblasts into the osteoblast lineage. The Journal of Cell Biology *127*, 1755-1766.

Kato, M., Patel, M.S., Levasseur, R., Lobov, I., Chang, B.H.-J., Glass, D.A., Hartmann, C., Li, L., Hwang, T.-H., Brayton, C.F., *et al.* (2002). Cbfa1-independent decrease in osteoblast proliferation, osteopenia, and persistent embryonic eye vascularization in mice deficient in Lrp5, a Wnt coreceptor. The Journal of Cell Biology *157*, 303-314.

Katoh, M. (2001). Molecular Cloning and Characterization of RNF26 on Human Chromosome 11q23 Region, Encoding a Novel RING Finger Protein with Leucine Zipper. Biochemical and Biophysical Research Communications *282*, 1038-1044.

Kawaguchi, Y., Kovacs, J.J., McLaurin, A., Vance, J.M., Ito, A., and Yao, T.-P. (2003). The Deacetylase HDAC6 Regulates Aggresome Formation and Cell Viability in Response to Misfolded Protein Stress. Cell *115*, 727-738.

Kawai, K., Saito, A., Sudo, T., and Osada, H. (2008). Specific Regulation of Cytokine-Dependent p38 MAP Kinase Activation by p62/SQSTM1. Journal of Biochemistry *143*, 765-772.

Kawata, A., and Mikuni-Takagaki, Y. (1998). Mechanotransduction in Stretched Osteocytes—Temporal Expression of Immediate Early and Other Genes. Biochemical and Biophysical Research Communications *246*, 404-408.

Keren-Politansky, A., Keren, A., and Bengal, E. (2009). Neural ectoderm-secreted FGF initiates the expression of Nkx2.5 in cardiac progenitors via a p38 MAPK/CREB pathway. Developmental Biology *335*, 374-384.

Kim, E.-A., Kim, J.E., Sung, K.S., Choi, D.W., Lee, B.J., and Choi, C.Y. (2010). Homeodomain-interacting protein kinase 2 (HIPK2) targets [beta]-catenin for phosphorylation and proteasomal degradation. Biochemical and Biophysical Research Communications *394*, 966-971.

Kim, H.T., Kim, K.P., Lledias, F., Kisselev, A.F., Scaglione, K.M., Skowyra, D., Gygi, S.P., and Goldberg, A.L. (2007a). Certain Pairs of Ubiquitin-conjugating Enzymes (E2s) and Ubiquitin-Protein Ligases (E3s) Synthesize Nondegradable Forked Ubiquitin Chains Containing All Possible Isopeptide Linkages. Journal of Biological Chemistry *282*, 17375-17386.

Kim, J.-H., Park, S., Kim, H.-W., and Jang, J.-H. (2007b). Recombinant expression of mouse osteocalcin protein in <i>Escherichia coli</i&gt. Biotechnology Letters *29*, 1631-1635.

Kim, K., Lee, S.-H., Ha Kim, J., Choi, Y., and Kim, N. (2008a). NFATc1 Induces Osteoclast Fusion Via Up-Regulation of Atp6v0d2 and the Dendritic Cell-Specific Transmembrane Protein (DC-STAMP). Molecular Endocrinology *22*, 176-185.

Kim, P.K., Hailey, D.W., Mullen, R.T., and Lippincott-Schwartz, J. (2008b). Ubiquitin signals autophagic degradation of cytosolic proteins and peroxisomes. Proceedings of the National Academy of Sciences *105*, 20567-20574.

Kimura, S., Noda, T., and Yoshimori, T. (2008). Dynein-dependent Movement of Autophagosomes Mediates Efficient Encounters with Lysosomes. Cell Structure and Function *33*, 109-122.

Kirisako, T., Ichimura, Y., Okada, H., Kabeya, Y., Mizushima, N., Yoshimori, T., Ohsumi, M., Takao, T., Noda, T., and Ohsumi, Y. (2000). The Reversible Modification Regulates the Membrane-Binding State of Apg8/Aut7 Essential for Autophagy and the Cytoplasm to Vacuole Targeting Pathway. The Journal of Cell Biology *151*, 263-276.

Kirkin, V., Lamark, T., Sou, Y.-S., Bjørkøy, G., Nunn, J.L., Bruun, J.-A., Shvets, E., McEwan, D.G., Clausen, T.H., Wild, P., *et al.* (2009). A Role for NBR1 in Autophagosomal Degradation of Ubiquitinated Substrates. Molecular Cell *33*, 505-516.

Kitaura, H., Zhou, P., Kim, H.-J., Novack, D.V., Ross, F.P., and Teitelbaum, S.L. (2005). M-CSF mediates TNF-induced inflammatory osteolysis. The Journal of Clinical Investigation *115*, 3418-3427.

Ko, D.C., Binkley, J., Sidow, A., and Scott, M.P. (2003). The integrity of a cholesterol-binding pocket in Niemann–Pick C2 protein is necessary to control lysosome cholesterol levels. Proceedings of the National Academy of Sciences *100*, 2518-2525.

Köchl, R., Hu, X.W., Chan, E.Y.W., and Tooze, S.A. (2006). Microtubules Facilitate Autophagosome Formation and Fusion of Autophagosomes with Endosomes. Traffic *7*, 129-145.

Koegl, M., Hoppe, T., Schlenker, S., Ulrich, H.D., Mayer, T.U., and Jentsch, S. (1999). A Novel Ubiquitination Factor, E4, Is Involved in Multiubiquitin Chain Assembly. Cell *96*, 635-644.

Koga, T., Matsui, Y., Asagiri, M., Kodama, T., de Crombrugghe, B., Nakashima, K., and Takayanagi, H. (2005). NFAT and Osterix cooperatively regulate bone formation. Nat Med *11*, 880-885.

Komatsu, M., Kurokawa, H., Waguri, S., Taguchi, K., Kobayashi, A., Ichimura, Y., Sou, Y.-S., Ueno, I., Sakamoto, A., Tong, K.I., *et al.* (2010). The selective autophagy

substrate p62 activates the stress responsive transcription factor Nrf2 through inactivation of Keap1. Nat Cell Biol *12*, 213-223.

Komori, T., Yagi, H., Nomura, S., Yamaguchi, A., Sasaki, K., Deguchi, K., Shimizu, Y., Bronson, R.T., Gao, Y.H., Inada, M., *et al.* (1997). Targeted Disruption of Cbfa1 Results in a Complete Lack of Bone Formation owing to Maturational Arrest of Osteoblasts. Cell *89*, 755-764.

Kornak, U., Kasper, D., Bösl, M.R., Kaiser, E., Schweizer, M., Schulz, A., Friedrich, W., Delling, G., and Jentsch, T.J. (2001). Loss of the ClC-7 Chloride Channel Leads to Osteopetrosis in Mice and Man. Cell *104*, 205-215.

Korolchuk, V.I., Mansilla, A., Menzies, F.M., and Rubinsztein, D.C. (2009). Autophagy Inhibition Compromises Degradation of Ubiquitin-Proteasome Pathway Substrates. Molecular Cell *33*, 517-527.

Kraft, C., Peter, M., and Hofmann, K. (2010). Selective autophagy: ubiquitin-mediated recognition and beyond. Nat Cell Biol *12*, 836-841.

Kumar, S., Votta, B.J., Rieman, D.J., Badger, A.M., Gowen, M., and Lee, J.C. (2001). IL-1- and TNF-induced bone resorption is mediated by p38 mitogen activated protein kinase*. Journal of Cellular Physiology *187*, 294-303.

Kurihara, N., Hiruma, Y., Yamana, K., Michou, L., Rousseau, C., Morissette, J., Galson, D.L., Teramachi, J., Zhou, H., Dempster, D.W., *et al.* (2011). Contributions of the Measles Virus Nucleocapsid Gene and the SQSTM1/p62P392L Mutation to Paget's Disease. Cell Metabolism *13*, 23-34.

Kuroda, S.i., Nakagawa, N., Tokunaga, C., Tatematsu, K., and Tanizawa, K. (1999). Mammalian Homologue of the Caenorhabditis elegans UNC-76 Protein Involved in Axonal Outgrowth Is a Protein Kinase C ζ–interacting Protein. The Journal of Cell Biology *144*, 403-411.

Lam, Y.A., Xu, W., DeMartino, G.N., and Cohen, R.E. (1997). Editing of ubiquitin conjugates by an isopeptidase in the 26S proteasome. Nature *385*, 737-740.

Lamark, T., Perander, M., Outzen, H., Kristiansen, K., Øvervatn, A., Michaelsen, E., Bjørkøy, G., and Johansen, T. (2003). Interaction Codes within the Family of Mammalian Phox and Bem1p Domain-containing Proteins. Journal of Biological Chemistry *278*, 34568-34581.

Lamberti, A., Caraglia, M., Longo, O., Marra, M., Abbruzzese, A., and Arcari, P. (2004). The translation elongation factor 1A in tumorigenesis, signal transduction and apoptosis: Review article. Amino Acids *26*, 443-448.

Lamothe, B., Campos, A.D., Webster, W.K., Gopinathan, A., Hur, L., and Darnay, B.G. (2008). The RING Domain and First Zinc Finger of TRAF6 Coordinate Signaling by Interleukin-1, Lipopolysaccharide, and RANKL. Journal of Biological Chemistry *283*, 24871-24880.

Lange, S., Ehler, E., and Gautel, M. (2006). From A to Z and back? Multicompartment proteins in the sarcomere. Trends in Cell Biology *16*, 11-18.

Lange, S., Xiang, F., Yakovenko, A., Vihola, A., Hackman, P., Rostkova, E., Kristensen, J., Brandmeier, B., Franzen, G., Hedberg, B., *et al.* (2005). The Kinase Domain of Titin Controls Muscle Gene Expression and Protein Turnover. Science *308*, 1599-1603.

Laterza, O.F., Price, C.P., and Scott, M.G. (2002). Cystatin C: An Improved Estimator of Glomerular Filtration Rate? Clin Chem *48*, 699-707.

Laurin, N., Brown, J.P., Morissette, J., and Raymond, V. (2002). Recurrent Mutation of the Gene Encoding sequestosome 1 (SQSTM1/p62) in Paget Disease of Bone. The American Journal of Human Genetics *70*, 1582-1588.

Lawrence, B.P., and Brown, W.J. (1992). Autophagic vacuoles rapidly fuse with pre-existing lysosomes in cultured hepatocytes. Journal of Cell Science *102*, 515-526.

Lazner, F., Gowen, M., Pavasovic, D., and Kola, I. (1999). Osteopetrosis and Osteoporosis: Two Sides of the Same Coin. Human Molecular Genetics *8*, 1839-1846.

Lee, J.-A., Beigneux, A., Ahmad, S.T., Young, S.G., and Gao, F.-B. (2007a). ESCRT-III Dysfunction Causes Autophagosome Accumulation and Neurodegeneration. Current Biology *17*, 1561-1567.

Lee, N.K., Sowa, H., Hinoi, E., Ferron, M., Ahn, J.D., Confavreux, C., Dacquin, R., Mee, P.J., McKee, M.D., Jung, D.Y., *et al.* (2007b). Endocrine Regulation of Energy Metabolism by the Skeleton. Cell *130*, 456-469.

Lee, S.-H., Rho, J., Jeong, D., Sul, J.-Y., Kim, T., Kim, N., Kang, J.-S., Miyamoto, T., Suda, T., Lee, S.-K., *et al.* (2006). v-ATPase V0 subunit d2-deficient mice exhibit impaired osteoclast fusion and increased bone formation. Nat Med *12*, 1403-1409.

Lee, S., Francoeur, A.M., Liu, S., and Wang, E. (1992). Tissue-specific expression in mammalian brain, heart, and muscle of S1, a member of the elongation factor-1 alpha gene family. Journal of Biological Chemistry *267*, 24064-24068.

Leroy, E., Boyer, R., Auburger, G., Leube, B., Ulm, G., Mezey, E., Harta, G., Brownstein, M.J., Jonnalagada, S., Chernova, T., *et al.* (1998). The ubiquitin pathway in Parkinson's disease. Nature *395*, 451-452.

Levine, B., and Kroemer, G. (2008). Autophagy in the Pathogenesis of Disease. Cell *132*, 27-42.

Li, X., Qin, L., Bergenstock, M., Bevelock, L.M., Novack, D.V., and Partridge, N.C. (2007). Parathyroid Hormone Stimulates Osteoblastic Expression of MCP-1 to Recruit and Increase the Fusion of Pre/Osteoclasts. Journal of Biological Chemistry *282*, 33098-33106.

Li, X., Udagawa, N., Itoh, K., Suda, K., Murase, Y., Nishihara, T., Suda, T., and Takahashi, N. (2002). p38 MAPK-Mediated Signals Are Required for Inducing Osteoclast Differentiation But Not for Osteoclast Function. Endocrinology *143*, 3105-3113.

Lin, C., Jiang, X., Dai, Z., Guo, X., Weng, T., Wang, J., Li, Y., Feng, G., Gao, X., and He, L. (2009). Sclerostin Mediates Bone Response to Mechanical Unloading Through Antagonizing Wnt/β-Catenin Signaling. Journal of Bone and Mineral Research *24*, 1651-1661.

Lin, G.L., and Hankenson, K.D. (2011). Integration of BMP, Wnt, and Notch signaling pathways in osteoblast differentiation. Journal of Cellular Biochemistry, n/a-n/a.

Liou, W., Geuze, H.J., Geelen, M.J.H., and Slot, J.W. (1997). The Autophagic and Endocytic Pathways Converge at the Nascent Autophagic Vacuoles. The Journal of Cell Biology *136*, 61-70.

Liu, F., Malaval, L., Gupta, A.K., and Aubin, J.E. (1994). Simultaneous Detection of Multiple Bone-Related mRNAs and Protein Expression during Osteoblast Differentiation: Polymerase Chain Reaction and Immunocytochemical Studies at the Single Cell Level. Developmental Biology *166*, 220-234.

Long, F., Chung, U.-i., Ohba, S., McMahon, J., Kronenberg, H.M., and McMahon, A.P. (2004). Ihh signaling is directly required for the osteoblast lineage in the endochondral skeleton. Development *131*, 1309-1318.

Long, J., Garner, T.P., Pandya, M.J., Craven, C.J., Chen, P., Shaw, B., Williamson, M.P., Layfield, R., and Searle, M.S. (2010). Dimerisation of the UBA Domain of p62 Inhibits Ubiquitin Binding and Regulates NF-κB Signalling. Journal of Molecular Biology *396*, 178-194.

Longatti, A., and Tooze, S.A. (2009). Vesicular trafficking and autophagosome formation. Cell Death Differ *16*, 956-965.

Lorget, F., Kamel, S., Mentaverri, R., Wattel, A., Naassila, M., Maamer, M., and Brazier, M. (2000). High Extracellular Calcium Concentrations Directly Stimulate Osteoclast Apoptosis. Biochemical and Biophysical Research Communications *268*, 899-903.

Luchin, A., Suchting, S., Merson, T., Rosol, T.J., Hume, D.A., Cassady, A.I., and Ostrowski, M.C. (2001). Genetic and Physical Interactions betweenMicrophthalmia Transcription Factor and PU.1 Are Necessary for Osteoclast Gene Expression and Differentiation. Journal of Biological Chemistry *276*, 36703-36710.

Ma, Y.L., Cain, R.L., Halladay, D.L., Yang, X., Zeng, Q., Miles, R.R., Chandrasekhar, S., Martin, T.J., and Onyia, J.E. (2001). Catabolic Effects of Continuous Human PTH (1–38) in Vivo Is Associated with Sustained Stimulation of RANKL and Inhibition of Osteoprotegerin and Gene-Associated Bone Formation. Endocrinology *142*, 4047-4054.

Makino, T., Jinnin, M., Muchemwa, F.C., Fukushima, S., Kogushi-Nishi, H., Moriya, C., Igata, T., Fujisawa, A., Johno, T., and Ihn, H. (2010). Basic fibroblast growth factor stimulates the proliferation of human dermal fibroblasts via the ERK1/2 and JNK pathways. British Journal of Dermatology *162*, 717-723.

Manganelli, P., Giuliani, N., Fietta, P., Mancini, C., Lazzaretti, M., Pollini, A., Quaini, F., and Pedrazzoni, M. (2005). OPG/RANKL system imbalance in a case of hepatitis C-associated osteosclerosis: the pathogenetic key? Clinical Rheumatology *24*, 296-300.

Mann, S.S., and Hammarback, J.A. (1994). Molecular characterization of light chain 3. A microtubule binding subunit of MAP1A and MAP1B. Journal of Biological Chemistry *269*, 11492-11497.

Manolagas, S.C. (2000). Birth and Death of Bone Cells: Basic Regulatory Mechanisms and Implications for the Pathogenesis and Treatment of Osteoporosis. Endocrine Reviews *21*, 115-137.

Mardakheh, F.K., Auciello, G., Dafforn, T.R., Rappoport, J.Z., and Heath, J.K. (2010). Nbr1 Is a Novel Inhibitor of Ligand-Mediated Receptor Tyrosine Kinase Degradation. Mol Cell Biol *30*, 5672-5685.

Mardakheh, F.K., Yekezare, M., Machesky, L.M., and Heath, J.K. (2009). Spred2 interaction with the late endosomal protein NBR1 down-regulates fibroblast growth factor receptor signaling. The Journal of Cell Biology *187*, 265-277.

Mathew, R., Karp, C.M., Beaudoin, B., Vuong, N., Chen, G., Chen, H.-Y., Bray, K., Reddy, A., Bhanot, G., Gelinas, C., *et al.* (2009). Autophagy Suppresses Tumorigenesis through Elimination of p62. Cell *137*, 1062-1075.

Meixner, A., Haverkamp, S., Wässle, H., Führer, S., Thalhammer, J., Kropf, N., Bittner, R.E., Lassmann, H., Wiche, G., and Propst, F. (2000). Map1b Is Required for Axon Guidance and Is Involved in the Development of the Central and Peripheral Nervous System. The Journal of Cell Biology *151*, 1169-1178.

Menaa, C., Reddy, S.V., Kurihara, N., Maeda, H., Anderson, D., Cundy, T., Cornish, J., Singer, F.R., Bruder, J.M., and Roodman, G.D. (2000). Enhanced RANK ligand expression and responsivity of bone marrow cells in Paget's disease of bone. The Journal of Clinical Investigation *105*, 1833-1838.

Mikuni-Takagaki, Y., Suzuki, Y., Kawase, T., and Saito, S. (1996). Distinct responses of different populations of bone cells to mechanical stress. Endocrinology *137*, 2028-2035.

Minowada, G., Jarvis, L.A., Chi, C.L., Neubuser, A., Sun, X., Hacohen, N., Krasnow, M.A., and Martin, G.R. (1999). Vertebrate Sprouty genes are induced by FGF signaling and can cause chondrodysplasia when overexpressed. Development *126*, 4465-4475.

Miraoui, H., and Marie, P.J. (2010). Fibroblast Growth Factor Receptor Signaling Crosstalk in Skeletogenesis. Sci Signal *3*, re9-.

Mishina, Y., Starbuck, M.W., Gentile, M.A., Fukuda, T., Kasparcova, V., Seedor, J.G., Hanks, M.C., Amling, M., Pinero, G.J., Harada, S.-i., *et al.* (2004). Bone Morphogenetic Protein Type IA Receptor Signaling Regulates Postnatal Osteoblast Function and Bone Remodeling. Journal of Biological Chemistry *279*, 27560-27566.

Mizuno, A., Amizuka, N., Irie, K., Murakami, A., Fujise, N., Kanno, T., Sato, Y., Nakagawa, N., Yasuda, H., Mochizuki, S.-i., *et al.* (1998). Severe Osteoporosis in Mice Lacking Osteoclastogenesis Inhibitory Factor/Osteoprotegerin. Biochemical and Biophysical Research Communications *247*, 610-615.

Mizushima, N., Kuma, A., Kobayashi, Y., Yamamoto, A., Matsubae, M., Takao, T., Natsume, T., Ohsumi, Y., and Yoshimori, T. (2003). Mouse Apg16L, a novel WD-repeat protein, targets to the autophagic isolation membrane with the Apg12-Apg5 conjugate. Journal of Cell Science *116*, 1679-1688.

Mizushima, N., Yamamoto, A., Hatano, M., Kobayashi, Y., Kabeya, Y., Suzuki, K., Tokuhisa, T., Ohsumi, Y., and Yoshimori, T. (2001). Dissection of Autophagosome Formation Using Apg5-Deficient Mouse Embryonic Stem Cells. The Journal of Cell Biology *152*, 657-668.

Mizushima, N., Yoshimori, T., and Levine, B. (2010). Methods in Mammalian Autophagy Research. Cell *140*, 313-326.

Mizushima, N., Yoshimori, T., and Ohsumi, Y. (2011). The Role of Atg Proteins in Autophagosome Formation. Annual Review of Cell and Developmental Biology *27*, null.

Monastyrska, I., Rieter, E., Klionsky, D.J., and Reggiori, F. (2009). Multiple roles of the cytoskeleton in autophagy. Biol Rev Camb Philos Soc *84*, 431-448.

Montero, A., Okada, Y., Tomita, M., Ito, M., Tsurukami, H., Nakamura, T., Doetschman, T., Coffin, J.D., and Hurley, M.M. (2000). Disruption of the fibroblast growth factor-2 gene results in decreased bone mass and bone formation. J Clin Invest *105*, 1085-1093.

Mori, D., Yamada, M., Mimori-Kiyosue, Y., Shirai, Y., Suzuki, A., Ohno, S., Saya, H., Wynshaw-Boris, A., and Hirotsune, S. (2009). An essential role of the aPKC-Aurora A-NDEL1 pathway in neurite elongation by modulation of microtubule dynamics. Nat Cell Biol *11*, 1057-1068.

Moscat, J., Diaz-Meco, M.T., Albert, A., and Campuzano, S. (2006). Cell Signaling and Function Organized by PB1 Domain Interactions. Molecular Cell *23*, 631-640.
Mostowy, S., Sancho-Shimizu, V., Hamon, M.A., Simeone, R., Brosch, R., Johansen, T., and Cossart, P. (2011). p62 and NDP52 Proteins Target Intracytosolic Shigella and Listeria to Different Autophagy Pathways. Journal of Biological Chemistry *286*, 26987-26995.

Mueller, T.D., and Feigon, J. (2002). Solution Structures of UBA Domains Reveal a Conserved Hydrophobic Surface for Protein-Protein Interactions. Journal of Molecular Biology *319*, 1243-1255.

Müller, J.M.M., Deinhardt, K., Rosewell, I., Warren, G., and Shima, D.T. (2007). Targeted deletion of p97 (VCP/CDC48) in mouse results in early embryonic lethality. Biochemical and Biophysical Research Communications *354*, 459-465.
Müller, S., Kursula, I., Zou, P., and Wilmanns, M. (2006). Crystal structure of the PB1 domain of NBR1. FEBS Letters *580*, 341-344.

Naik, M.U., and Naik, U.P. (2011). Calcium- and integrin-binding protein 1 regulates microtubule organization and centrosome segregation through polo like kinase 3 during cell cycle progression. The International Journal of Biochemistry & Cell Biology *43*, 120-129.

Najat, D., Garner, T., Hagen, T., Shaw, B., Sheppard, P.W., Falchetti, A., Marini, F., Brandi, M.L., Long, J.E., Cavey, J.R., *et al.* (2009). Characterization of a Non-UBA Domain Missense Mutation of Sequestosome 1 (SQSTM1) in Paget's Disease of Bone. Journal of Bone and Mineral Research *24*, 632-642.

Nakagawa, N., Kinosaki, M., Yamaguchi, K., Shima, N., Yasuda, H., Yano, K., Morinaga, T., and Higashio, K. (1998). RANK Is the Essential Signaling Receptor for Osteoclast Differentiation Factor in Osteoclastogenesis. Biochemical and Biophysical Research Communications *253*, 395-400.

Nakamura, K., Kimple, A.J., Siderovski, D.P., and Johnson, G.L. (2010). PB1 Domain Interaction of p62/Sequestosome 1 and MEKK3 Regulates NF-κB Activation. Journal of Biological Chemistry *285*, 2077-2089.

Nakamura, T., Imai, Y., Matsumoto, T., Sato, S., Takeuchi, K., Igarashi, K., Harada, Y., Azuma, Y., Krust, A., Yamamoto, Y., *et al.* (2007). Estrogen Prevents Bone Loss via Estrogen Receptor [alpha] and Induction of Fas Ligand in Osteoclasts. Cell *130*, 811-823.

Nakashima, K., Zhou, X., Kunkel, G., Zhang, Z., Deng, J.M., Behringer, R.R., and de Crombrugghe, B. (2002). The Novel Zinc Finger-Containing Transcription Factor Osterix Is Required for Osteoblast Differentiation and Bone Formation. Cell *108*, 17-29.

Nakatsuka, K., Nishizawa, Y., and Ralston, S.H. (2003). Phenotypic Characterization of Early Onset Paget's Disease of Bone Caused by a 27-bp Duplication in the TNFRSF11A Gene. Journal of Bone and Mineral Research *18*, 1381-1385.

Nandi, D., Tahiliani, P., Kumar, A., and Chandu, D. (2006). The ubiquitin-proteasome system. J Biosci *31*, 137-155.

Ng, K.W., Romas, E., Donnan, L., and Findlay, D.M. (1997). Bone biology. Baillière's Clinical Endocrinology and Metabolism *11*, 1-22.

Noda, N.N., Ohsumi, Y., and Inagaki, F. (2010). Atg8-family interacting motif crucial for selective autophagy. FEBS Letters *584*, 1379-1385.

Noda, T., Kim, J., Huang, W.-P., Baba, M., Tokunaga, C., Ohsumi, Y., and Klionsky, D.J. (2000). Apg9p/Cvt7p Is an Integral Membrane Protein Required for Transport Vesicle Formation in the Cvt and Autophagy Pathways. The Journal of Cell Biology *148*, 465-480.

Noiges, R., Eichinger, R., Kutschera, W., Fischer, I., Németh, Z., Wiche, G., and Propst, F. (2002). Microtubule-Associated Protein 1A (MAP1A) and MAP1B: Light Chains Determine Distinct Functional Properties. The Journal of Neuroscience *22*, 2106-2114.

Novack, D.V., and Faccio, R. (2011). Osteoclast motility: Putting the brakes on bone resorption. Ageing Research Reviews *10*, 54-61.

Novak, I., Kirkin, V., McEwan, D.G., Zhang, J., Wild, P., Rozenknop, A., Rogov, V., Lohr, F., Popovic, D., Occhipinti, A., *et al.* (2010). Nix is a selective autophagy receptor for mitochondrial clearance. EMBO Rep *11*, 45-51.

Obara, K., Sekito, T., Niimi, K., and Ohsumi, Y. (2008). The Atg18-Atg2 Complex Is Recruited to Autophagic Membranes via Phosphatidylinositol 3-Phosphate and Exerts an Essential Function. Journal of Biological Chemistry *283*, 23972-23980.

Ohmori, H., Makita, Y., Funamizu, M., Hirooka, K., Hosoi, T., Orimo, H., Suzuki, T., Ikari, K., Nakajima, T., Inoue, I., *et al.* (2002). Linkage and association analyses of the osteoprotegerin gene locus with human osteoporosis. J Hum Genet *47*, 400-406.

Okamoto, K., Kondo-Okamoto, N., and Ohsumi, Y. (2009). Mitochondria-Anchored Receptor Atg32 Mediates Degradation of Mitochondria via Selective Autophagy. Developmental Cell *17*, 87-97.

Okumura, F., Hatakeyama, S., Matsumoto, M., Kamura, T., and Nakayama, K.I. (2004). Functional Regulation of FEZ1 by the U-box-type Ubiquitin Ligase E4B Contributes to Neuritogenesis. Journal of Biological Chemistry *279*, 53533-53543.

Opal, P., Garcia, J.J., Propst, F., Matilla, A., Orr, H.T., and Zoghbi, H.Y. (2003). Mapmodulin/Leucine-rich Acidic Nuclear Protein Binds the Light Chain of Microtubule-associated Protein 1B and Modulates Neuritogenesis. Journal of Biological Chemistry *278*, 34691-34699.

Ornitz, D.M., and Marie, P.J. (2002). FGF signaling pathways in endochondral and intramembranous bone development and human genetic disease. Genes & Development *16*, 1446-1465.

Orriss, I.R., Knight,G, Arnett,T, Burnstock,G. (2005). P2X2 but not P2X3 receptor knockout mice demonstrate increased bone mass and weight. In JBMR, pp. 1293.

Pankiv, S., Alemu, E.A., Brech, A., Bruun, J.-A., Lamark, T., Øvervatn, A., Bjørkøy, G., and Johansen, T. (2010). FYCO1 is a Rab7 effector that binds to LC3 and PI3P to mediate microtubule plus end–directed vesicle transport. The Journal of Cell Biology *188*, 253-269.

Pankiv, S., Clausen, T.H., Lamark, T., Brech, A., Bruun, J.-A., Outzen, H., Øvervatn, A., Bjørkøy, G., and Johansen, T. (2007a). p62/SQSTM1 Binds Directly to Atg8/LC3 to Facilitate Degradation of Ubiquitinated Protein Aggregates by Autophagy. Journal of Biological Chemistry *282*, 24131-24145.

Pankiv, S., Clausen, T.H., Lamark, T., Brech, A., Bruun, J.A., Outzen, H., Overvatn, A., Bjorkoy, G., and Johansen, T. (2007b). p62/SQSTM1 binds directly to Atg8/LC3 to facilitate degradation of ubiquitinated protein aggregates by autophagy. J Biol Chem *282*, 24131-24145.

Pannier, S., Mugniery, E., Jonquoy, A., Benoist-Lasselin, C., Odent, T., Jais, J.-P., Munnich, A., and Legeai-Mallet, L. (2010). Delayed bone age due to a dual effect of FGFR3 mutation in Achondroplasia. Bone *47*, 905-915.

Paradies, G., Petrosillo, G., Paradies, V., Reiter, R.J., and Ruggiero, F.M. (2010). Melatonin, cardiolipin and mitochondrial bioenergetics in health and disease. Journal of Pineal Research *48*, 297-310.

Passmore, L.A., and Barford, D. (2004). Getting into position: the catalytic mechanisms of protein ubiquitylation. Biochem J *379*, 513-525.

Perera, S., Holt, M.R., Mankoo, B.S., and Gautel, M. (2011). Developmental regulation of MURF ubiquitin ligases and autophagy proteins nbr1, p62/SQSTM1 and LC3 during cardiac myofibril assembly and turnover. Developmental Biology *351*, 46-61.

Pfaff, M., and Jurdic, P. (2001). Podosomes in osteoclast-like cells. Journal of Cell Science *114*, 2775-2786.

Pittenger, M.F., Mackay, A.M., Beck, S.C., Jaiswal, R.K., Douglas, R., Mosca, J.D., Moorman, M.A., Simonetti, D.W., Craig, S., and Marshak, D.R. (1999). Multilineage Potential of Adult Human Mesenchymal Stem Cells. Science *284*, 143-147.

Polo, S., Sigismund, S., Faretta, M., Guidi, M., Capua, M.R., Bossi, G., Chen, H., De Camilli, P., and Di Fiore, P.P. (2002). A single motif responsible for ubiquitin recognition and monoubiquitination in endocytic proteins. Nature *416*, 451-455.

Proikas-Cezanne, T., Waddell, S., Gaugel, A., Frickey, T., Lupas, A., and Nordheim, A. (2004). WIPI-1[alpha] (WIPI49), a member of the novel 7-bladed WIPI protein family, is aberrantly expressed in human cancer and is linked to starvation-induced autophagy. Oncogene *23*, 9314-9325.

Provot, S., and Schipani, E. (2005). Molecular mechanisms of endochondral bone development. Biochemical and Biophysical Research Communications *328*, 658-665.

Puls, A., Schmidt, S., Grawe, F., and Stabel, S. (1997). Interaction of protein kinase C ζ with ZIP, a novel protein kinase C-binding protein. Proceedings of the National Academy of Sciences *94*, 6191-6196.

Pursiheimo, J.P., Rantanen, K., Heikkinen, P.T., Johansen, T., and Jaakkola, P.M. (2008). Hypoxia-activated autophagy accelerates degradation of SQSTM1/p62. Oncogene *28*, 334-344.

Qiang, Y.-W., Kopantzev, E., and Rudikoff, S. (2002). Insulinlike growth factor–I signaling in multiple myeloma: downstream elements, functional correlates, and pathway cross-talk. Blood *99*, 4138-4146.

Qiao, L., and Zhang, J. (2009). Inhibition of lysosomal functions reduces proteasomal activity. Neuroscience Letters *456*, 15-19.

Raasi, S., and Pickart, C.M. (2003). Rad23 Ubiquitin-associated Domains (UBA) Inhibit 26 S Proteasome-catalyzed Proteolysis by Sequestering Lysine 48-linked Polyubiquitin Chains. Journal of Biological Chemistry *278*, 8951-8959.

Raasi, S., Varadan, R., Fushman, D., and Pickart, C.M. (2005). Diverse polyubiquitin interaction properties of ubiquitin-associated domains. Nat Struct Mol Biol *12*, 708-714.

Rabinovich, E., Kerem, A., Frohlich, K.-U., Diamant, N., and Bar-Nun, S. (2002). AAA-ATPase p97/Cdc48p, a Cytosolic Chaperone Required for Endoplasmic Reticulum-Associated Protein Degradation. Mol Cell Biol *22*, 626-634.

Ralston, S.H. (2008). Pathogenesis of Paget's disease of bone. Bone *43*, 819-825.
Rauch, D.A., Hurchla, M.A., Harding, J.C., Deng, H., Shea, L.K., Eagleton, M.C., Niewiesk, S., Lairmore, M.D., Piwnica-Worms, D., Rosol, T.J., *et al.* (2010). The ARF Tumor Suppressor Regulates Bone Remodeling and Osteosarcoma Development in Mice. PLoS ONE *5*, e15755.

Rauch, F., and Glorieux, F.H. (2004). Osteogenesis imperfecta. The Lancet *363*, 1377-1385.

Ravikumar, B., Moreau, K., Jahreiss, L., Puri, C., and Rubinsztein, D.C. (2010). Plasma membrane contributes to the formation of pre-autophagosomal structures. Nat Cell Biol *12*, 747-757.

Razi, M., Chan, E.Y.W., and Tooze, S.A. (2009). Early endosomes and endosomal coatomer are required for autophagy. The Journal of Cell Biology *185*, 305-321.

Rea, S.L., Walsh, J.P., Ward, L., Magno, A.L., Ward, B.K., Shaw, B., Layfield, R., Kent, G.N., Xu, J., and Ratajczak, T. (2009). Sequestosome 1 Mutations in Paget's Disease of Bone in Australia: Prevalence, Genotype/Phenotype Correlation, and a Novel Non-UBA Domain Mutation (P364S) Associated With Increased NF-κB Signaling Without Loss of Ubiquitin Binding. Journal of Bone and Mineral Research *24*, 1216-1223.

Rechsteiner, M., and Rogers, S.W. (1996). PEST sequences and regulation by proteolysis. Trends Biochem Sci *21*, 267-271.

Reunanen, H., Marttinen, M., and Hirsimäki, P. (1988). Effects of griseofulvin and nocodazole on the accumulation of autophagic vacuoles in ehrlich ascites tumor cells. Experimental and Molecular Pathology *48*, 97-102.

Robertson, G. (2004). QUANTIFICATION OF SKELETAL PHENOTYPE USING MICRO-CT AND
MECHANICAL TESTING (Georgia Institute of Technology), pp. 85.

Robling, A.G., Niziolek, P.J., Baldridge, L.A., Condon, K.W., Allen, M.R., Alam, I., Mantila, S.M., Gluhak-Heinrich, J., Bellido, T.M., Harris, S.E., *et al.* (2008). Mechanical Stimulation of Bone in Vivo Reduces Osteocyte Expression of Sost/Sclerostin. Journal of Biological Chemistry *283*, 5866-5875.

Rodriguez, A., Duran, A., Selloum, M., Champy, M.F., Diez-Guerra, F.J., Flores, J.M., Serrano, M., Auwerx, J., Diaz-Meco, M.T., and Moscat, J. (2006). Mature-onset obesity and insulin resistance in mice deficient in the signaling adapter p62. Cell Metab *3*, 211-222.

Rozenknop, A., Rogov, V.V., Rogova, N.Y., Löhr, F., Güntert, P., Dikic, I., and Dötsch, V. (2011). Characterization of the Interaction of GABARAPL-1 with the LIR Motif of NBR1. Journal of Molecular Biology *410*, 477-487.

Ryu, J., Kim, H.J., Chang, E.-J., Huang, H., Banno, Y., and Kim, H.-H. (2006). Sphingosine 1-phosphate as a regulator of osteoclast differentiation and osteoclast-osteoblast coupling. EMBO J *25*, 5840-5851.

Sabatakos, G., Sims, N.A., Chen, J., Aoki, K., Kelz, M.B., Amling, M., Bouali, Y., Mukhopadhyay, K., Ford, K., Nestler, E.J., *et al.* (2000). Overexpression of [Delta]FosB transcription factor(s) increases bone formation and inhibits adipogenesis. Nat Med *6*, 985-990.

Sakae, N., Yamasaki, N., Kitaichi, K., Fukuda, T., Yamada, M., Yoshikawa, H., Hiranita, T., Tatsumi, Y., Kira, J.-i., Yamamoto, T., *et al.* (2008). Mice lacking the schizophrenia-associated protein FEZ1 manifest hyperactivity and enhanced responsiveness to psychostimulants. Human Molecular Genetics *17*, 3191-3203.

Sakata, T., Wang, Y., Halloran, B.P., Elalieh, H.Z., Cao, J., and Bikle, D.D. (2004). Skeletal Unloading Induces Resistance to Insulin-Like Growth Factor-I (IGF-I) by Inhibiting Activation of the IGF-I Signaling Pathways. Journal of Bone and Mineral Research *19*, 436-446.

Salo, J., Lehenkari, P., Mulari, M., Metsikkö, K., and Väänänen, H.K. (1997). Removal of Osteoclast Bone Resorption Products by Transcytosis. Science *276*, 270-273.

Sanchez-Fernandez, M.A., Gallois, A., Riedl, T., Jurdic, P., and Hoflack, B. (2008). Osteoclasts Control Osteoblast Chemotaxis via PDGF-BB/PDGF Receptor Beta Signaling. PLoS ONE *3*, e3537.

Sanger, T.J., Norgard, E.A., Pletscher, L.S., Bevilacqua, M., Brooks, V.R., Sandell, L.J., and Cheverud, J.M. (2011). Developmental and genetic origins of murine long bone length variation. Journal of Experimental Zoology Part B: Molecular and Developmental Evolution *316B*, 146-161.

Sanz, L., Diaz-Meco, M.T., Nakano, H., and Moscat, J. (2000). The atypical PKC-interacting protein p62 channels NF-[kappa]B activation by the IL-1-TRAF6 pathway. EMBO J *19*, 1576-1586.

Sanz, L., Sanchez, P., Lallena, M.-J., Diaz-Meco, M.T., and Moscat, J. (1999). The interaction of p62 with RIP links the atypical PKCs to NF-[kappa]B activation. EMBO J *18*, 3044-3053.

Saraogi, I., and Shan, S.-o. (2011). Molecular Mechanism of Co-translational Protein Targeting by the Signal Recognition Particle. Traffic *12*, 535-542.

Schimmoller, F., Singer-Kruger, B., Schroder, S., Kruger, U., Barlowe, C., and Riezman, H. (1995). The absence of Emp24p, a component of ER-derived COPII-coated vesicles, causes a defect in transport of selected proteins to the Golgi. EMBO J *14*, 1329-1339.

Schoenfeld, T., McKerracher, L., Obar, R., and Vallee, R. (1989). MAP 1A and MAP 1B are structurally related microtubule associated proteins with distinct developmental patterns in the CNS. The Journal of Neuroscience *9*, 1712-1730.

Schweers, R.L., Zhang, J., Randall, M.S., Loyd, M.R., Li, W., Dorsey, F.C., Kundu, M., Opferman, J.T., Cleveland, J.L., Miller, J.L., *et al.* (2007). NIX is required for programmed mitochondrial clearance during reticulocyte maturation. Proceedings of the National Academy of Sciences *104*, 19500-19505.

Seibel, M.J. (2005). Biochemical markers of bone turnover: part I: biochemistry and variability. Clin Biochem Rev *26*, 97-122.

Seibenhener, M.L., Babu, J.R., Geetha, T., Wong, H.C., Krishna, N.R., and Wooten, M.W. (2004). Sequestosome 1/p62 Is a Polyubiquitin Chain Binding Protein Involved in Ubiquitin Proteasome Degradation. Mol Cell Biol *24*, 8055-8068.

Sengupta, A., Duran, Angeles, Pratt, Ronald, Dunn,, Susan, F., Ashley, Diaz-Meco, Maria, Moscat, Jorge,, and Cancelas, J. (2011). SQSTM1 (P62) EXTRINSICALLY REGULATES HEMATOPOIETIC STEM CELL AND PROGENITOR MOBILIZATION. International society for stem cell research - 9th annual meeting, Poster 2392.

Seog, D.H. (2004). Glutamate receptor-interacting protein 1 protein binds to the microtubule-associated protein. Biosci Biotechnol Biochem *68*, 1808-1810.

Shin, J. (1998). P62 and the sequestosome, a novel mechanism for protein metabolism. Arch Pharm Res *21*, 629-633.

Shintani, T., Mizushima, N., Ogawa, Y., Matsuura, A., Noda, T., and Ohsumi, Y. (1999). Apg10p, a novel protein-conjugating enzyme essential for autophagy in yeast. EMBO J *18*, 5234-5241.

Shpilka, T., Weidberg, H., Pietrokovski, S., and Elazar, Z. (2011). Atg8: an autophagy-related ubiquitin-like protein family. Genome Biology *12*, 1-11.

Shvets, E., Fass, E., Scherz-Shouval, R., and Elazar, Z. (2008). The N-terminus and Phe52 residue of LC3 recruit p62/SQSTM1 into autophagosomes. Journal of Cell Science *121*, 2685-2695.

Sims, N.A., and Gooi, J.H. (2008). Bone remodeling: Multiple cellular interactions required for coupling of bone formation and resorption. Seminars in Cell & Developmental Biology *19*, 444-451.

Sly, W.S., Whyte, M.P., Sundaram, V., Tashian, R.E., Hewett-Emmett, D., Guibaud, P., Vainsel, M., Baluarte, H.J., Gruskin, A., Al-Mosawi, M., *et al.* (1985). Carbonic Anhydrase II Deficiency in 12 Families with the Autosomal Recessive Syndrome of Osteopetrosis with Renal Tubular Acidosis and Cerebral Calcification. New England Journal of Medicine *313*, 139-145.

Sommerfeldt, and Rubin (2001). Biology of bone and how it orchestrates the form and function of the skeleton. European Spine Journal *10*, S86-S95.

Sou, Y.-s., Waguri, S., Iwata, J.-i., Ueno, T., Fujimura, T., Hara, T., Sawada, N., Yamada, A., Mizushima, N., Uchiyama, Y., *et al.* (2008). The Atg8 Conjugation System Is Indispensable for Proper Development of Autophagic Isolation Membranes in Mice. Molecular Biology of the Cell *19*, 4762-4775.

Spotila, L.D., Rodriguez, H., Koch, M., Adams, K., Caminis, J., Tenenhouse, H.S., and Tenenhouse, A. (2000). Association of a Polymorphism in the TNFR2 Gene with Low Bone Mineral Density. Journal of Bone and Mineral Research *15*, 1376-1383.

Stahl, E.A., Raychaudhuri, S., Remmers, E.F., Xie, G., Eyre, S., Thomson, B.P., Li, Y., Kurreeman, F.A.S., Zhernakova, A., Hinks, A., *et al.* (2010). Genome-wide association study meta-analysis identifies seven new rheumatoid arthritis risk loci. Nat Genet *42*, 508-514.

Strojan, P., Svetic, B., Smid, L., and Kos, J. (2004). Serum cystatin C in patients with head and neck carcinoma. Clinica Chimica Acta *344*, 155-161.

Suda, T., Takahashi, N., Udagawa, N., Jimi, E., Gillespie, M.T., and Martin, T.J. (1999). Modulation of Osteoclast Differentiation and Function by the New Members of the Tumor Necrosis Factor Receptor and Ligand Families. Endocrine Reviews *20*, 345-357.

Sumimoto, H., Kamakura, S., and Ito, T. (2007). Structure and Function of the PB1 Domain, a Protein Interaction Module Conserved in Animals, Fungi, Amoebas, and Plants. Sci STKE *2007*, re6-.

Sundaram, K., Shanmugarajan, S., Rao, S., Reddy, S. (2011). Mutant p62 p392L Stimulation of Osteoclast Differentiation in Paget's Disease of Bone. Endocrinology *152*.

Suzuki, K., Kirisako, T., Kamada, Y., Mizushima, N., Noda, T., and Ohsumi, Y. (2001). The pre-autophagosomal structure organized by concerted functions of APG genes is essential for autophagosome formation. EMBO J *20*, 5971-5981.

Svenning, S., Lamark, T., Krause, K., and Johansen, T. (2011). Plant NBR1 is a selective autophagy substrate and a functional hybrid of the mammalian autophagic adapters NBR1 and p62/SQSTM1. Autophagy *7*, 0--1.

Takayanagi, H., Kim, S., Koga, T., Nishina, H., Isshiki, M., Yoshida, H., Saiura, A., Isobe, M., Yokochi, T., Inoue, J.-i., *et al.* (2002). Induction and Activation of the Transcription Factor NFATc1 (NFAT2) Integrate RANKL Signaling in Terminal Differentiation of Osteoclasts. Developmental Cell *3*, 889-901.

Tan, J.M.M., Wong, E.S.P., Dawson, V.L., Dawson, T., and Lim, K.-L. (2008). Lysine 63-linked polyubiquitin potentially partners with p62 to promote the clearance of protein inclusions by autophagy. Autophagy *4*, 251-253.

Tanida, I. (2011). Autophagy basics. Microbiology and Immunology *55*, 1-11.
Tanida, I., Tanida-Miyake, E., Komatsu, M., Ueno, T., and Kominami, E. (2002). Human Apg3p/Aut1p Homologue Is an Authentic E2 Enzyme for Multiple Substrates, GATE-16, GABARAP, and MAP-LC3, and Facilitates the Conjugation of hApg12p to hApg5p. Journal of Biological Chemistry *277*, 13739-13744.

Tanida, I., Tanida-Miyake, E., Ueno, T., and Kominami, E. (2001). The Human Homolog of Saccharomyces cerevisiae Apg7p Is a Protein-activating Enzyme for Multiple Substrates Including Human Apg12p, GATE-16, GABARAP, and MAP-LC3. Journal of Biological Chemistry *276*, 1701-1706.

Tatsumi, S., Ishii, K., Amizuka, N., Li, M., Kobayashi, T., Kohno, K., Ito, M., Takeshita, S., and Ikeda, K. (2007). Targeted Ablation of Osteocytes Induces Osteoporosis with Defective Mechanotransduction. Cell Metabolism *5*, 464-475.

Teitelbaum, S.L. (2007). Osteoclasts: What Do They Do and How Do They Do It? The American Journal of Pathology *170*, 427-435.

Thrower, J.S., Hoffman, L., Rechsteiner, M., and Pickart, C.M. (2000). Recognition of the polyubiquitin proteolytic signal. EMBO J *19*, 94-102.

Thurston, T.L.M., Ryzhakov, G., Bloor, S., von Muhlinen, N., and Randow, F. (2009). The TBK1 adaptor and autophagy receptor NDP52 restricts the proliferation of ubiquitin-coated bacteria. Nat Immunol *10*, 1215-1221.

Timpson, N.J., Tobias, J.H., Richards, J.B., Soranzo, N., Duncan, E.L., Sims, A.-M., Whittaker, P., Kumanduri, V., Zhai, G., Glaser, B., *et al.* (2009). Common variants in the region around Osterix are associated with bone mineral density and growth in childhood. Human Molecular Genetics *18*, 1510-1517.

Tögel, M., Eichinger, R., Wiche, G., and Propst, F. (1999). A 45 amino acid residue domain necessary and sufficient for proteolytic cleavage of the MAP1B polyprotein precursor. FEBS Letters *451*, 15-18.

Tögel, M., Wiche, G., and Propst, F. (1998). Novel Features of the Light Chain of Microtubule-associated Protein MAP1B: Microtubule Stabilization, Self Interaction, Actin Filament Binding, and Regulation by the Heavy Chain. The Journal of Cell Biology *143*, 695-707.

Tondravi, M.M., McKercher, S.R., Anderson, K., Erdmann, J.M., Quiroz, M., Maki, R., and Teitelbaum, S.L. (1997). Osteopetrosis in mice lacking haematopoietic transcription factor PU.1. Nature *386*, 81-84.

Tooze, S.A., Jefferies, H.B.J., Kalie, E., Longatti, A., McAlpine, F.E., McKnight, N.C., Orsi, A., Polson, H.E.J., Razi, M., Robinson, D.J., *et al.* (2010). Trafficking and signaling in mammalian autophagy. IUBMB Life *62*, 503-508.

Tracy, K., Dibling, B.C., Spike, B.T., Knabb, J.R., Schumacker, P., and Macleod, K.F. (2007). BNIP3 Is an RB/E2F Target Gene Required for Hypoxia-Induced Autophagy. Mol Cell Biol *27*, 6229-6242.

Tskhovrebova, L., and Trinick, J. (2003). Titin: properties and family relationships. Nat Rev Mol Cell Biol *4*, 679-689.

Turner, G.C., and Varshavsky, A. (2000). Detecting and Measuring Cotranslational Protein Degradation in Vivo. Science *289*, 2117-2120.

Utting, J.C., Robins, S.P., Brandao-Burch, A., Orriss, I.R., Behar, J., and Arnett, T.R. (2006). Hypoxia inhibits the growth, differentiation and bone-forming capacity of rat osteoblasts. Experimental Cell Research *312*, 1693-1702.

Vadlamudi, R.K., Joung, I., Strominger, J.L., and Shin, J. (1996). p62, a Phosphotyrosine-independent Ligand of the SH2 Domain of p56lck, Belongs to a New Class of Ubiquitin-binding Proteins. Journal of Biological Chemistry *271*, 20235-20237.

van Bezooijen, R.L., Roelen, B.A.J., Visser, A., van der Wee-Pals, L., de Wilt, E., Karperien, M., Hamersma, H., Papapoulos, S.E., ten Dijke, P., and Löwik, C.W.G.M. (2004). Sclerostin Is an Osteocyte-expressed Negative Regulator of Bone Formation, But Not a Classical BMP Antagonist. The Journal of Experimental Medicine *199*, 805-814.

Van Criekinge, W., and Beyaert, R. (1999). Yeast two-hybrid: State of the art. Biological Procedures Online *2*, 1-38.

van Leeuwen, F.W., de Kleijn, D.P.V., van den Hurk, H.H., Neubauer, A., Sonnemans, M.A.F., Sluijs, J.A., Köycü, S., Ramdjielal, R.D.J., Salehi, A., Martens, G.J.M., *et al.* (1998). Frameshift Mutants of β Amyloid Precursor Protein and Ubiquitin-B in Alzheimer's and Down Patients. Science *279*, 242-247.

Van Wesenbeeck, L., Cleiren, E., Gram, J., Beals, R.K., Bénichou, O., Scopelliti, D., Key, L., Renton, T., Bartels, C., Gong, Y., *et al.* (2003). Six Novel Missense Mutations in the LDL Receptor-Related Protein 5 (LRP5) Gene in Different Conditions with an Increased Bone Density. The American Journal of Human Genetics *72*, 763-771.

Van Wesenbeeck, L., Odgren, P.R., Coxon, F.P., Frattini, A., Moens, P., Perdu, B., MacKay, C.A., Van Hul, E., Timmermans, J.-P., Vanhoenacker, F., *et al.* (2007). Involvement of PLEKHM1 in osteoclastic vesicular transport and osteopetrosis in incisors absent rats and humans. The Journal of Clinical Investigation *117*, 919-930.

Verborgt, O., Tatton, N.A., Majeska, R.J., and Schaffler, M.B. (2002). Spatial Distribution of Bax and Bcl-2 in Osteocytes After Bone Fatigue: Complementary Roles in Bone Remodeling Regulation? Journal of Bone and Mineral Research *17*, 907-914.

Viereck, C., Tucker, R., and Matus, A. (1989). The adult rat olfactory system expresses microtubule-associated proteins found in the developing brain. The Journal of Neuroscience *9*, 3547-3557.

Walker, D. (1975). Bone resorption restored in osteopetrotic mice by transplants of normal bone marrow and spleen cells. Science *190*, 784-785.

Wang, Q.J., Ding, Y., Kohtz, S., Mizushima, N., Cristea, I.M., Rout, M.P., Chait, B.T., Zhong, Y., Heintz, N., and Yue, Z. (2006). Induction of Autophagy in Axonal Dystrophy and Degeneration. The Journal of Neuroscience *26*, 8057-8068.

Wang, X., Goh, C.H., and Li, B. (2007). p38 Mitogen-Activated Protein Kinase Regulates Osteoblast Differentiation through Osterix. Endocrinology *148*, 1629-1637.

Wang, Z., Zhang, Y., Zhang, S., Guo, Q., Tan, Y., Wang, X., Xiong, R., Ding, J., and Chen, S. (2011). DJ-1 can inhibit microtubule associated protein 1 B formed aggregates. Mol Neurodegener *6*, 38.

Watanabe, Y., and Tanaka, M. (2011). p62/SQSTM1 in autophagic clearance of a non-ubiquitylated substrate. Journal of Cell Science *124*, 2692-2701.

Waters, S., Marchbank, K., Solomon, E., Whitehouse, C., and Gautel, M. (2009). Interactions with LC3 and polyubiquitin chains link nbr1 to autophagic protein turnover. FEBS Letters *583*, 1846-1852.

Waters, S.L. (2009). The role of Nbr1 in autophagosomal degradation of ubiquitinated proteins and M-band titin. In Cardiovascular division & Department of Medical & Molecular Genetics

School of Medicine (London, Kings College London).

Watts, G.D.J., Wymer, J., Kovach, M.J., Mehta, S.G., Mumm, S., Darvish, D., Pestronk, A., Whyte, M.P., and Kimonis, V.E. (2004). Inclusion body myopathy associated with Paget disease of bone and frontotemporal dementia is caused by mutant valosin-containing protein. Nat Genet *36*, 377-381.

Wefes, I., Mastrandrea, L.D., Haldeman, M., Koury, S.T., Tamburlin, J., Pickart, C.M., and Finley, D. (1995). Induction of ubiquitin-conjugating enzymes during terminal erythroid differentiation. Proceedings of the National Academy of Sciences *92*, 4982-4986.

Weidberg, H., Shvets, E., Shpilka, T., Shimron, F., Shinder, V., and Elazar, Z. (2010). LC3 and GATE-16/GABARAP subfamilies are both essential yet act differently in autophagosome biogenesis. EMBO J *29*, 1792-1802.

Whitehouse, C., Chambers, J., Catteau, A., and Solomon, E. (2004). Brca1 expression is regulated by a bidirectional promoter that is shared by the Nbr1 gene in mouse. Gene *326*, 87-96.

Whitehouse, C., Chambers, J., Howe, K., Cobourne, M., Sharpe, P., and Solomon, E. (2002). NBR1 interacts with fasciculation and elongation protein zeta-1 (FEZ1) and calcium and integrin binding protein (CIB) and shows developmentally restricted expression in the neural tube. European Journal of Biochemistry *269*, 538-545.

Whitehouse, C.A., Waters, S., Marchbank, K., Horner, A., McGowan, N.W.A., Jovanovic, J.V., Xavier, G.M., Kashima, T.G., Cobourne, M.T., Richards, G.O., *et al.* (2010). Neighbor of Brca1 gene (Nbr1) functions as a negative regulator of postnatal osteoblastic bone formation and p38 MAPK activity. Proceedings of the National Academy of Sciences *107*, 12913-12918.

Whyte, M.P., and Hughes, A.E. (2002). Expansile Skeletal Hyperphosphatasia Is Caused by a 15-Base Pair Tandem Duplication in TNFRSF11A Encoding RANK and Is Allelic to Familial Expansile Osteolysis. Journal of Bone and Mineral Research *17*, 26-29.

Whyte, M.P., Obrecht, S.E., Finnegan, P.M., Jones, J.L., Podgornik, M.N., McAlister, W.H., and Mumm, S. (2002). Osteoprotegerin Deficiency and Juvenile Paget's Disease. New England Journal of Medicine *347*, 175-184.

Wiktor-Jedrzejczak, W.W., Ahmed, A., Szczylik, C., and Skelly, R.R. (1982). Hematological characterization of congenital osteopetrosis in op/op mouse. Possible mechanism for abnormal macrophage differentiation. J Exp Med *156*, 1516-1527.

Wild, P., Farhan, H., McEwan, D.G., Wagner, S., Rogov, V.V., Brady, N.R., Richter, B., Korac, J., Waidmann, O., Choudhary, C., *et al.* (2011). Phosphorylation of the Autophagy Receptor Optineurin Restricts Salmonella Growth. Science *333*, 228-233.

Wilde, I.B., Brack, M., Winget, J.M., and Mayor, T. (2011). Proteomic Characterization of Aggregating Proteins after the Inhibition of the Ubiquitin Proteasome System. Journal of Proteome Research *10*, 1062-1072.

Wilkinson, K.D., Urban, M.K., and Haas, A.L. (1980). Ubiquitin is the ATP-dependent proteolysis factor I of rabbit reticulocytes. Journal of Biological Chemistry *255*, 7529-7532.

Williams, G.A., Callon, K.E., Watson, M., Costa, J.L., Ding, Y., Dickinson, M., Wang, Y., Naot, D., Reid, I.R., and Cornish, J. (2011). Skeletal phenotype of the leptin receptor–deficient db/db mouse. Journal of Bone and Mineral Research *26*, 1698-1709.

Wójcik, C., Yano, M., and DeMartino, G.N. (2004). RNA interference of valosin-containing protein (VCP/p97) reveals multiple cellular roles linked to ubiquitin/proteasome-dependent proteolysis. Journal of Cell Science *117*, 281-292.

Wooten, M.W., Geetha, T., Seibenhener, M.L., Babu, J.R., Diaz-Meco, M.T., and Moscat, J. (2005). The p62 Scaffold Regulates Nerve Growth Factor-induced NF-κB Activation by Influencing TRAF6 Polyubiquitination. Journal of Biological Chemistry *280*, 35625-35629.

Wooten, M.W., Hu, X., Babu, J.R., Seibenhener, M.L., Geetha, T., Paine, M.G., and Wooten, M.C. (2006). Signaling, Polyubiquitination, Trafficking, and Inclusions: Sequestosome 1/p62's Role in Neurodegenerative Disease. Journal of Biomedicine and Biotechnology *2006*.

Wooten, M.W., Seibenhener, M.L., Mamidipudi, V., Diaz-Meco, M.T., Barker, P.A., and Moscat, J. (2001). The Atypical Protein Kinase C-interacting Protein p62 Is a Scaffold for NF-κB Activation by Nerve Growth Factor. Journal of Biological Chemistry *276*, 7709-7712.

Xia, X., Kar, R., Gluhak-Heinrich, J., Yao, W., Lane, N.E., Bonewald, L.F., Biswas, S.K., Lo, W.-K., and Jiang, J.X. (2010). Glucocorticoid-induced autophagy in osteocytes. Journal of Bone and Mineral Research *25*, 2479-2488.

Xiao, G., Jiang, D., Ge, C., Zhao, Z., Lai, Y., Boules, H., Phimphilai, M., Yang, X., Karsenty, G., and Franceschi, R.T. (2005). Cooperative Interactions between Activating Transcription Factor 4 and Runx2/Cbfa1 Stimulate Osteoblast-specific Osteocalcin Gene Expression. Journal of Biological Chemistry *280*, 30689-30696.

Xie, R., Nguyen, S., McKeehan, K., Wang, F., McKeehan, W.L., and Liu, L. (2011). Microtubule-associated Protein 1S (MAP1S) Bridges Autophagic Components with Microtubules and Mitochondria to Affect Autophagosomal Biogenesis and Degradation. Journal of Biological Chemistry *286*, 10367-10377.

Xie, R., Nguyen, S., McKeehan, W., and Liu, L. (2010). Acetylated microtubules are required for fusion of autophagosomes with lysosomes. BMC Cell Biology *11*, 89.
Xie, Z., and Klionsky, D.J. (2007). Autophagosome formation: core machinery and adaptations. Nat Cell Biol *9*, 1102-1109.

Yagi, M., Miyamoto, T., Sawatani, Y., Iwamoto, K., Hosogane, N., Fujita, N., Morita, K., Ninomiya, K., Suzuki, T., Miyamoto, K., *et al.* (2005). DC-STAMP is essential for cell–cell fusion in osteoclasts and foreign body giant cells. The Journal of Experimental Medicine *202*, 345-351.

Yakar, S., Rosen, C.J., Beamer, W.G., Ackert-Bicknell, C.L., Wu, Y., Liu, J.L., Ooi, G.T., Setser, J., Frystyk, J., Boisclair, Y.R., *et al.* (2002). Circulating levels of IGF-1 directly regulate bone growth and density. J Clin Invest *110*, 771-781.

Yamaza, T., Tsuji, Y., Goto, T., Kido, M.A., Nishijima, K., Moroi, R., Akamine, A., and Tanaka, T. (2001). Comparison in localization between cystatin C and cathepsin K in osteoclasts and other cells in mouse tibia epiphysis by immunolight and immunoelectron microscopy. Bone *29*, 42-53.

Yang, J.-Q., Liu, H., Diaz-Meco, M.T., and Moscat, J. (2010). NBR1 is a new PB1 signalling adapter in Th2 differentiation and allergic airway inflammation in vivo. EMBO J *29*, 3421-3433.

Yang, X., and Karsenty, G. (2004). ATF4, the Osteoblast Accumulation of Which Is Determined Post-translationally, Can Induce Osteoblast-specific Gene Expression in Non-osteoblastic Cells. Journal of Biological Chemistry *279*, 47109-47114.

Yang, X., Matsuda, K., Bialek, P., Jacquot, S., Masuoka, H.C., Schinke, T., Li, L., Brancorsini, S., Sassone-Corsi, P., Townes, T.M., *et al.* (2004). ATF4 Is a Substrate of RSK2 and an Essential Regulator of Osteoblast Biology: Implication for Coffin-Lowry Syndrome. Cell *117*, 387-398.

Yao, T., and Cohen, R.E. (2002). A cryptic protease couples deubiquitination and degradation by the proteasome. Nature *419*, 403-407.

Yasuda, H., Shima, N., Nakagawa, N., Yamaguchi, K., Kinosaki, M., Mochizuki, S.-i., Tomoyasu, A., Yano, K., Goto, M., Murakami, A., *et al.* (1998). Osteoclast differentiation factor is a ligand for osteoprotegerin/osteoclastogenesis-inhibitory factor and is identical to TRANCE/RANKL. Proceedings of the National Academy of Sciences *95*, 3597-3602.

Yip, K.H.M., Feng, H., Pavlos, N.J., Zheng, M.H., and Xu, J. (2006). p62 Ubiquitin Binding-Associated Domain Mediated the Receptor Activator of Nuclear Factor-[kappa]B Ligand-Induced Osteoclast Formation: A New Insight into the Pathogenesis of Paget's Disease of Bone. The American Journal of Pathology *169*, 503-514.

Yokota, T., Nagai, H., Harada, H., Mine, N., Terada, Y., Fujiwara, H., Yabe, A., Miyazaki, K., and Emi, M. (2001). Identification, tissue expression, and chromosomal position of a novel gene encoding human ubiquitin-conjugating enzyme E2-230k. Gene *267*, 95-100.

Yoon, K.W., Cho, J.-H., Lee, J.K., Kang, Y.-H., Chae, J.S., Kim, Y.M., Kim, J., Kim, E.K., Kim, S.E., Baik, J.-H., *et al.* (2009). CIB1 functions as a Ca2+-sensitive

modulator of stress-induced signaling by targeting ASK1. Proceedings of the National Academy of Sciences *106*, 17389-17394.

Yoshida, H., Hayashi, S.-I., Kunisada, T., Ogawa, M., Nishikawa, S., Okamura, H., Sudo, T., Shultz, L.D., and Nishikawa, S.-I. (1990). The murine mutation osteopetrosis is in the coding region of the macrophage colony stimulating factor gene. Nature *345*, 442-444.

Yoshimori, T. (2004). Autophagy: a regulated bulk degradation process inside cells. Biochemical and Biophysical Research Communications *313*, 453-458.

Yu, X., Huang, Y., Collin-Osdoby, P., and Osdoby, P. (2003). Stromal Cell-Derived Factor-1 (SDF-1) Recruits Osteoclast Precursors by Inducing Chemotaxis, Matrix Metalloproteinase-9 (MMP-9) Activity, and Collagen Transmigration. Journal of Bone and Mineral Research *18*, 1404-1418.

Zahm, A.M., Bohensky, J., Adams, C.S., Shapiro, I.M., and Srinivas, V. (2011). Bone cell autophagy is regulated by environmental factors. Cells Tissues Organs *194*, 274-278.

Zahm, A.M., Bucaro, M.A., Srinivas, V., Shapiro, I.M., and Adams, C.S. (2008). Oxygen tension regulates preosteocyte maturation and mineralization. Bone *43*, 25-31.

Zhang, K., Barragan-Adjemian, C., Ye, L., Kotha, S., Dallas, M., Lu, Y., Zhao, S., Harris, M., Harris, S.E., Feng, J.Q., *et al.* (2006). E11/gp38 Selective Expression in Osteocytes: Regulation by Mechanical Strain and Role in Dendrite Elongation. Mol Cell Biol *26*, 4539-4552.

Zhang, L., Guo, Y.-F., Liu, Y.-Z., Liu, Y.-J., Xiong, D.-H., Liu, X.-G., Wang, L., Yang, T.-L., Lei, S.-F., Guo, Y., *et al.* (2010). Pathway-based genome-wide association analysis identified the importance of regulation-of-autophagy pathway for ultradistal radius BMD. Journal of Bone and Mineral Research *25*, 1572-1580.

Zhao, C., Irie, N., Takada, Y., Shimoda, K., Miyamoto, T., Nishiwaki, T., Suda, T., and Matsuo, K. (2006). Bidirectional ephrinB2-EphB4 signaling controls bone homeostasis. Cell Metabolism *4*, 111-121.

Zhao, G., Monier-Faugere, M.-C., Langub, M.C., Geng, Z., Nakayama, T., Pike, J.W., Chernausek, S.D., Rosen, C.J., Donahue, L.-R., Malluche, H.H., *et al.* (2000). Targeted Overexpression of Insulin-Like Growth Factor I to Osteoblasts of Transgenic Mice: Increased Trabecular Bone Volume without Increased Osteoblast Proliferation. Endocrinology *141*, 2674-2682.

Zhao, J., Brault, J.J., Schild, A., Cao, P., Sandri, M., Schiaffino, S., Lecker, S.H., and Goldberg, A.L. (2007). FoxO3 Coordinately Activates Protein Degradation by the Autophagic/Lysosomal and Proteasomal Pathways in Atrophying Muscle Cells. Cell Metabolism *6*, 472-483.

Zhao, M., Qiao, M., Harris, S.E., Oyajobi, B.O., Mundy, G.R., and Chen, D. (2004). Smurf1 Inhibits Osteoblast Differentiation and Bone Formation in Vitro and in Vivo. Journal of Biological Chemistry *279*, 12854-12859.

Zhao, M., Qiao, M., Oyajobi, B.O., Mundy, G.R., and Chen, D. (2003). E3 Ubiquitin Ligase Smurf1 Mediates Core-binding Factor α1/Runx2 Degradation and Plays A Specific Role in Osteoblast Differentiation. Journal of Biological Chemistry *278*, 27939-27944.

Zhao, S., Kato, Y., Zhang, Y., Harris, S., Ahuja, S.S., and Bonewald, L.F. (2002). MLO-Y4 Osteocyte-Like Cells Support Osteoclast Formation and Activation. Journal of Bone and Mineral Research *17*, 2068-2079.

Zheng, Y.T., Shahnazari, S., Brech, A., Lamark, T., Johansen, T., and Brumell, J.H. (2009). The Adaptor Protein p62/SQSTM1 Targets Invading Bacteria to the Autophagy Pathway. The Journal of Immunology *183*, 5909-5916.

Zolk, O., Schenke, C., and Sarikas, A. (2006). The ubiquitin–proteasome system: Focus on the heart. Cardiovascular Research *70*, 410-421.